Application of a Continuously Variable Transmission to Engine Boosting and Exhaust Energy Recovery Systems

Rose, Adam

Award date:
2013

Awarding institution:
University of Bath

Application of a Continuously Variable Transmission to Engine Boosting and Exhaust Energy Recovery Systems

Adam Thomas Joel Matthew Rose

A thesis submitted for the degree of Doctor of Philosophy
University of Bath
Department of Mechanical Engineering
September 2013

Summary

Governments across the world are implementing legislation for ever more strict limits for vehicle emissions; combined with customer expectations for growing levels of performance and equipment, automotive manufacturers face a significant challenge. With the aim of meeting this challenge, downsizing is an established trend in passenger car engine development. However, since downsizing is commonly achieved through pressure charging (turbocharging, for example), the associated benefits in improved fuel economy and emissions are often obtained at the expense of engine dynamic response, and, consequently, vehicle driveability.

This thesis presents predominantly simulation-based research into a novel combined charging system comprising a conventional turbocharger used in conjunction with a declutchable supercharger driven through a CVT. An initial investigation using this system in place of a variable geometry turbocharger on an already downsized passenger car diesel engine demonstrated greatly increased low speed torque as well as improved dynamic response. A downsizing project that involved replacing a naturally aspirated gasoline engine with a highly boosted engine with 40% of the original displacement formed the basis for more extensive investigations. Although it was unable to produce the low speed transient response of the naturally aspirated engine, in tip-in tests the CVT-supercharger system was shown to achieve the target torque much quicker than an equivalent system with a fixed supercharger drive ratio. However, balancing this with good fuel efficiency for the initial part load period was a complex trade-off. In vehicle acceleration simulations the CVT-supercharger system did not outperform the fixed drive ratio configuration, but on the CVT system the boost limit was reached at an early stage during the transients. Thus there may be potential to include an ‘over-boost’ facility, allowing boost pressure to temporarily exceed normal steady state limits in order to improve transient performance and bring it closer to that of the baseline vehicle. It is suggested that the CVT-supercharger provides the best flexibility for calibration and compromise between performance and fuel efficiency, perhaps incorporating different user-selectable modes (such as ‘economy’ and ‘sport’ modes).

Acknowledgements

I would like to thank the Engineering and Physical Sciences Research Council (EPSRC) for funding this research, and the UK Technology Strategy Board (TSB) for their funding and support for the Ultraboost project. I would also like to acknowledge the Ultraboost consortium partners: Jaguar Land Rover, Lotus Engineering, GE Precision Engineering, Imperial College London, the University of Leeds, CD-adapco, and Shell Fuels.

I would particularly like to thank my supervisors Dr Sam Akehurst and Dr Chris Brace for their direction, constructive feedback and support throughout this project.

I am also grateful to all of my colleagues who have provided camaraderie, advice and help during my time at the university: Andy Lewis, Karl Giles, Dom Parsons, Amyce Aurora-Smith, Harry Chu, Richard Burke, Apiwat Suyabodha, Sahand Malek, Adrian Hunt, Mitch Piddock, Peter Dowell, Joe Moyers, and Chris Ye.

Finally, I would like to thank all of my family and friends who have had faith in me and supported me during this testing time – especially my wife Catherine, whose continual love and encouragement have made it bearable.

Soli Deo gloria.

Contents

List of Figures

List of Tables

Notation

A_p	total piston area (m^2)
a	acceleration (m/s^2)
AFR	air-fuel ratio
ATDCF	after top dead centre firing
BDC	bottom dead centre
BMEP	brake mean effective pressure
BSFC	brake specific fuel consumption
CAD	crank angle degrees
CAGE	Calibration Generation
CAHU	charge air handling unit
CAN	controller area network
CO	carbon monoxide
CO_2	carbon dioxide
CR	compression ratio
CVT	continuously variable transmission
d	diameter (m)
DCE	differential compound engine
DI	direct injection
DoE	design of experiments
DPF	diesel particulate filter
EAT	electrically assisted turbocharger
ECU	engine control unit
EDC	electrically driven compressor
EGR	exhaust gas recirculation
EPA	Environmental Protection Agency
EU	European Union
(F/A)	fuel-air ratio
FCV	fuel cell vehicle
FEV	full electric vehicle
FMEP	friction mean effective pressure
GDI	gasoline direct injection
HC	hydrocarbon (emissions)
HP	high pressure
HSDI	high speed direct injection

I	inertia (kgm^2)
IDI	indirect injection
LP	low pressure
LTC	limiting torque curve
m	mass (kg)
$\dot{m}$	mass air flow (kg/s)
MAF	mass air flow
MBC	Model-Based Calibration Toolbox
MCVT	Milner continuously variable transmission
MOP	maximum opening point
n	speed (rad/s)
NEDC	New European Drive Cycle
NHTSA	National Highway Traffic Safety Administration
NO_x	oxides of nitrogen
p	pressure (N/m^2)
P	power (W)
PEV	prediction error variance
PFI	port fuel injection
PI	proportional-integral (control)
PID	proportional-integral-derivative (control)
PM	particulate matter
Q_{HV}	fuel heating value (J/kg)
RBF	radial basis function
RMSE	root mean squared error
$\overline{S_p}$	mean piston speed (m/s)
SC	supercharger compressor
SF	scaling factor
SGDI	spray guided direct injection
SOI	start of injection (fuel)
T	temperature (K)
t	time (s)
TC	turbocharger compressor
TDC	top dead centre
THC	total hydrocarbons
TT	turbocharger turbine
TVS	Twin Vortices Series
v	vehicle speed (m/s)
VCR	variable compression ratio
VGT	variable geometry turbocharger

VTES	Visteon Torque Enhancement System
WOT	wide open throttle
η_f	fuel conversion efficiency
η_v	volumetric efficiency
ρ	density (kg/m^3)
τ	torque (Nm)

Subscripts

a	air
act	actual
$comp$	compressor
$corr$	corrected
in	inlet
n	nth data point
$n-1$	n-1th data point
ref	reference
$turb$	turbine

Chapter 1 Introduction

Governments throughout the world are implementing legislation for ever more strict limits for vehicle emissions. In the European Union (EU), emissions standards are becoming increasingly demanding year on year, as the standards for passenger cars in Table 1.1 demonstrate.

Table 1.1 – EU emission standards for passenger cars [1] (values in g/km)

Stage	*Date*	*CO*	*HC*	*HC+NO_x*	*NO_x*	*PM*
Compression Ignition (Diesel)						
Euro 1	Jul 1992	2.72	-	0.97	-	0.14
Euro 2, IDI	Jan 1996	1.0	-	0.7	-	0.08
Euro 2, DI	Jan 1996	1.0	-	0.9	-	0.10
Euro 3	Jan 2000	0.64	-	0.56	0.50	0.05
Euro 4	Jan 2005	0.50	-	0.30	0.25	0.025
Euro 5a	Sep 2009	0.50	-	0.23	0.18	0.005
Euro 5b	Sep 2011	0.50	-	0.23	0.18	0.005
Euro 6	Sep 2014	0.50	-	0.17	0.08	0.005
Positive Ignition (Gasoline)						
Euro 1	Jul 1992	2.72	-	0.97	-	-
Euro 2	Jan 1996	2.2	-	0.5	-	-
Euro 3	Jan 2000	2.30	0.20	-	0.15	-
Euro 4	Jan 2005	1.0	0.10	-	0.08	-
Euro 5	Sep 2009	1.0	0.10	-	0.06	0.005
Euro 6	Sep 2014	1.0	0.10	-	0.06	0.005

Regarding carbon dioxide (CO_2) emissions – which directly relates to fuel consumption – UK annual vehicle road tax bands are based on a sliding scale, with vehicles producing high levels of CO_2 being taxed increasingly (Table 1.2).

Table 1.2 – UK vehicle tax rates for passenger cars [2]

Band	*CO_2 emission (g/km)*	*12 months rate*	*6 months rate*
A	Up to 100	£0.00	Not available
B	101-110	£20.00	Not available
C	111-120	£30.00	Not available
D	121-130	£105.00	£57.75
E	131-140	£125.00	£68.75
F	141-150	£140.00	£77.00
G	151-165	£175.00	£96.25
H	166-175	£200.00	£110.00
I	176-185	£220.00	£121.00
J	186-200	£260.00	£143.00
K	201-225	£280.00	£154.00
L	226-255	£475.00	£261.25
M	Over 255	£490.00	£269.50

Legislation is in place to ensure that by 2015 average CO_2 emissions for new passenger cars in the EU do not exceed 130 g CO_2/km, with a long term target of 95 g CO_2/km by 2020 [3]. Likewise in the United States, the Environmental Protection Agency (EPA) and National Highway Traffic Safety Administration (NHTSA) have introduced national standards with a target for combined average emissions for light-duty vehicles of 250 g CO_2/km by 2016 [4]. It is only a matter of time before financial penalties are introduced to help motivate manufacturers to reduce the levels of CO_2 produced by their vehicles [5]. These factors combined with the need to remain profitable in the current global economic climate present automotive manufacturers with a significant challenge.

A vast array of engine technologies are either currently available or being developed to help achieve these targets – such as hybridisation [6][7][8], full electric vehicles (FEV) [9], and fuel cell vehicles (FCV) [10][11]. However, according to Hancock et al. [12] engine downsizing 'has long been known as one of the most effective technologies for immediate implementation'. This is owing to a number of factors, such as downsizing being a development of conventional internal combustion

engine technology rather than shifting to relatively unproven new technologies, as well as its comparative cost effectiveness; consequently, downsizing is proving popular among vehicle manufacturers [13][14][15][16]. Furthermore, breakthroughs in technology are required, particularly in terms of effective energy storage, for these alternative powertrain systems to become feasible for widespread production. It is anticipated that internal combustion engines will remain dominant for years to come, as acknowledged by the UK Automotive Council [17] and illustrated in their passenger car low carbon technology roadmap (Figure 1.1). Further research in the field of engine downsizing is therefore fully justified.

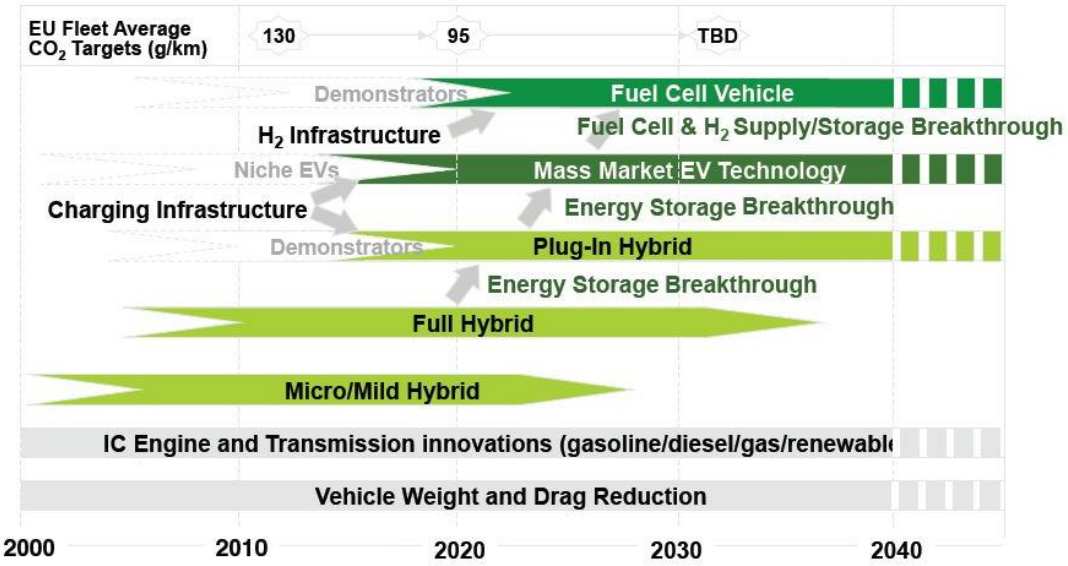

Figure 1.1 – Automotive Council passenger car low carbon technology roadmap [17]

1.1 Aim and Objectives

The aim of this research was to identify a potential application of continuously variable transmission (CVT) technology to engine boosting and exhaust energy recovery systems in the field of passenger car engine downsizing, and to quantify the potential benefits through engine simulations and experimental testing.

The specific objectives in order to achieve the research aim were:

1. To undertake an extensive review of current literature and research on the subject of engine boosting and exhaust energy recovery systems in the area of downsizing for passenger car engines; to consider how developing CVT technology may be applied to this field in order to maximise fuel efficiency, and thereby reduce emissions of CO_2 and other pollutants.

2. To conduct extensive simulations of the chosen system to assess it against three key performance criteria for downsized engines:

    a. Low-speed torque;

    b. Part-load fuel efficiency;

    c. Transient performance.

3. To evaluate model validity and simulation accuracy against relevant empirical data, where this was possible.

1.2 Overview of Chapters

Chapter 2 – Review of Existing Technology and Literature

A review of existing literature and research on the subject of engine downsizing for passenger car engines is given in this chapter. Focus is particularly placed on different pressure charging ('boosting') systems and their developments. The disadvantages of the various systems used in engine downsizing are discussed. Special consideration is made regarding how CVT technology may be applied to this field in order to mitigate these shortcomings, maximise fuel efficiency, and thereby reduce emissions of CO_2 and other pollutants.

Chapter 3 – HSDI Diesel Engine: Low-Speed Torque Investigation

This chapter details an initial simulation based investigation into the novel forced induction boosting system identified in the literature review as a possible solution to improving low speed engine torque and transient response of future downsized and existing turbocharged engines. This system comprises a centrifugal-type supercharger driven from the engine crankshaft via a CVT, which acts as a pre-boost to a traditional fixed geometry turbocharger. The concept was modelled around an existing baseline high speed direct injection (HSDI) diesel engine model featuring a variable geometry turbocharger (VGT).

Chapter 4 – Ultraboost Project Introduction and Validation of the Engine Model

The Ultraboost project (highly boosted downsized gasoline engine) is introduced in this chapter, along with a model of the Ultraboost engine that was created in GT-Power, the salient features of which are described. Details are given of the engine testing facilities at the University of Bath and the instrumentation and data acquisition methods used to collect performance data from a prototype of the Ultraboost engine. The GT-Power model is then compared with and validated against this recorded data.

Chapter 5 – Ultraboost Engine: Part Load Efficiency and Transient Performance Trade-off

This chapter gives details of a co-simulation based investigation into the trade-off between steady state part load fuel efficiency and resulting tip-in transient response for the Ultraboost engine. (The 2.0 litre in-line 4 cylinder gasoline engine is equipped

with a positive displacement supercharger in a sequential series arrangement with a fixed geometry turbocharger.) Three separate supercharger engagement regimes were investigated for part load operation, defined as: with the supercharger disengaged and bypassed; with the supercharger engaged with a fixed drive ratio; with the supercharger engaged using a variable ratio (i.e. through a CVT). For each of these supercharger engagement regimes, design of experiments and optimisation techniques were used to find the best settings for key engine control parameters. Using these calibrations as a starting point, transient performance was then assessed in fixed speed tip-in simulations.

Chapter 6 – Vehicle Model: In-Gear Acceleration Simulations

This chapter gives details of a vehicle model which was constructed to simulate the performance of the Ultraboost target vehicle. Logged empirical data of in-gear 'sawtooth' accelerations were used to calibrate a baseline model; this model was subsequently modified to incorporate the Ultraboost downsized engine. Simulations were performed from the respective starting points of the three supercharger engagement regimes described in Chapter 5, and the results are compared with the baseline.

Chapter 7 – Overall Conclusions

This chapter contains overall conclusions that are drawn from this thesis, and recommendations are given for further work to develop this research.

Chapter 2 Review of Existing Technology and Literature

This chapter contains a review of existing literature and research on the subject of engine downsizing for passenger car engines. Focus is particularly placed on different pressure charging (‘boosting’) systems and their developments. The disadvantages of the various systems used in engine downsizing are discussed. Special consideration is made regarding how CVT technology may be applied to this field in order to mitigate these shortcomings, maximise fuel efficiency, and thereby reduce emissions of CO_2 and other pollutants.

2.1 Engine Downsizing

Engine downsizing is generally defined by Thirouard et al. [18] as using a 'smaller capacity engine operating at higher specific engine loads in order to achieve lower fuel consumption'. The reduction in fuel consumption is achieved primarily through: reduced friction losses associated with the reduced engine size; and the inherently better efficiency of an engine when running at higher loads [18], owing to reduced pumping losses as less intake throttling is required. Petitjean et al. [19] describe the latter aspect as effectively 'moving the best fuel economy island [of the engine] closer to the steady state road load condition', which can alternatively be viewed as avoiding operation in the area of the map where pumping losses are greatest. With regards to the aspect of friction, sliding surface friction is typically reduced through decreased piston ring to cylinder contact area (associated with a reduced number of cylinders and/or decreased bore and stroke) and a reduction in the swept area of crankshaft journal bearings.

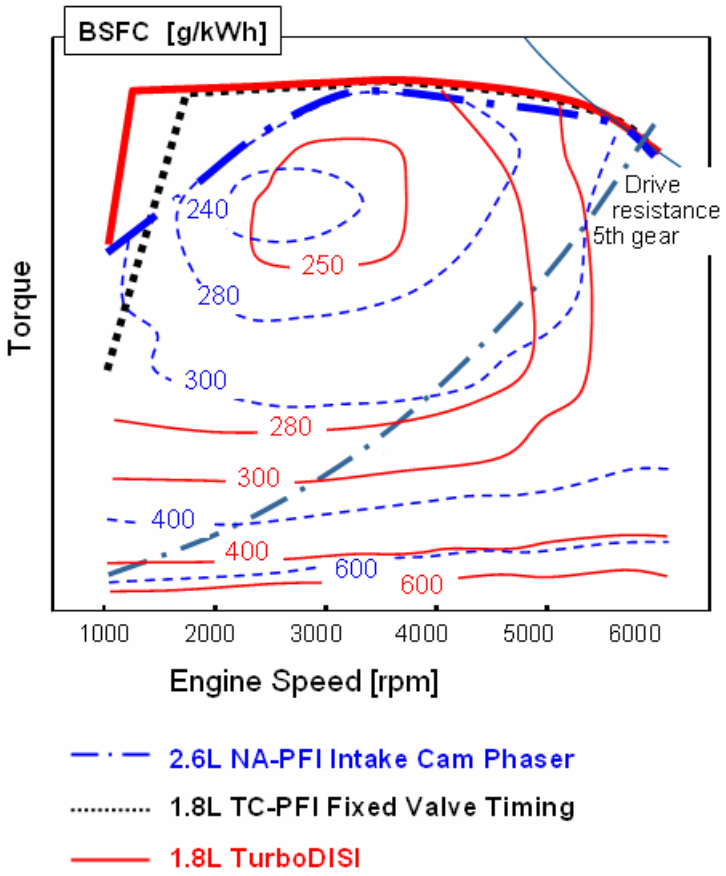

Figure 2.1 – Comparison of BSFC maps of naturally aspirated and turbocharged downsized engines [20]

This effect is also illustrated in Figure 2.1 (reproduced from Kleeberg et al. [20]), which compares the brake specific fuel consumption (BSFC) map of a 2.6 litre naturally aspirated gasoline engine with that of a 1.8 litre turbocharged downsized engine. The BSFC of the downsized engine is consistently lower along the steady state road load curve.

As is the case in this example, to facilitate downsizing, full load performance potential is typically maintained through pressure charging (supercharging) [12][20][21][22]. Particularly for gasoline engines, in conjunction with turbocharging, direct fuel injection and extreme variability of valve timing for both inlet and exhaust valves can also aid downsizing [12]. According to Turner et al. [23], gasoline direct injection (GDI), due to its charge cooling effects, allows higher compression ratios for improved thermal efficiency; and variable valve timing (both inlet and exhaust) allows for increased scavenging and reduced part-load throttling losses. These technologies have been combined and adopted by a number of manufacturers in search of reduced emissions through engine downsizing, including Ford [15] and Alfa Romeo [24]. Fiat have even removed the throttle (and therefore throttling losses) altogether with their 'MultiAir' electro-hydraulic valve actuation technology [25]. Other technologies synergistic with downsizing include spray guided direct injection (SGDI) [26] and variable compression ratio (VCR) [27][28], although neither have yet attained production.

The basis for increased specific engine output – which is critical to engine downsizing – can be traced back to the definition of fundamental engine performance parameters. Heywood [29] derives the following equation for specific power:

$$\frac{P}{A_p} = \frac{\eta_f \eta_v \overline{S_p} Q_{HV} \rho_{a,in} (F/A)}{4}$$

Equation 2.1

From this equation the author deduces a list of factors that directly affect the performance of an engine – stating that increasing any of these factors will increase engine performance (all else being equal):

1. Fuel conversion efficiency (which is inversely proportional to specific fuel consumption)

2. Volumetric efficiency

3. Inlet air density

4. Maximum fuel/air ratio that can be usefully burned in the engine

5. Mean piston speed.

Engine downsizing targets points 2 and 3 in this list, and point 1 – at least for 'real-world' (part load) driving conditions, if not full load conditions as well.

2.2 Supercharging

According to Watson and Janota [30], 'supercharging can be defined as the introduction of air (or air/fuel mixture) into an engine cylinder at a density greater than ambient', allowing a proportionally greater amount of fuel to be burned, and thus raising the potential power output of the engine. There are three basic methods of achieving this: turbocharging, pressure wave supercharging, and mechanical supercharging.

2.2.1 Turbocharging

A turbocharger is a device with a compressor and turbine on a single shaft – the turbine is powered by energy in the engine's exhaust gases; the turbine in turn drives the compressor, which provides the increase in intake pressure. A Sankey diagram for a typical 1.4 litre 4 cylinder spark ignition (gasoline) engine (reproduced from Stobart and Weerasinghe [31]) is shown in Figure 2.2. A maximum of a third of the fuel energy is converted into useful work, whereas up to nearly 50% of the fuel energy is wasted as exhaust heat. One major benefit of a turbocharger is that it utilises exhaust gas energy that would otherwise be wasted, and can thus lead to an overall improvement in thermal efficiency.

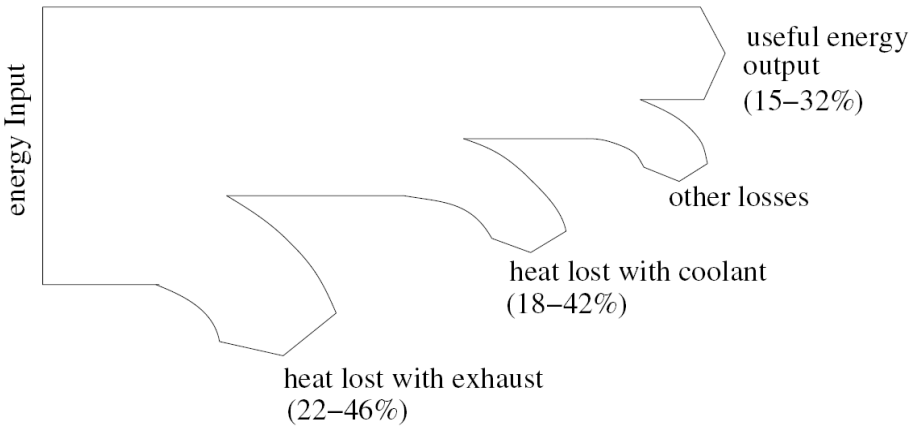

Figure 2.2 – Sankey diagram showing energy balance for typical naturally aspirated spark ignition engine [31]

For reasons discussed elsewhere (particularly in Watson and Janota [30] and Baines [32]), conventional automotive turbochargers use a centrifugal compressor and radial flow turbine. Due to the design and operating principles, such turbomachines have an optimum operating point and 'are not well suited for operation over a wide flow range' [30] – as is the case with an automotive engine.

Emissions reduction technologies such as exhaust gas recirculation (EGR) and diesel particulate filters (DPF) also make the matching of compressor to turbine problematic [33]. Several authors [21][30][32] highlight a fundamental compromise when matching a turbocharger to an engine: between torque at low speed and power at high engine speed. A large turbocharger offers the power at high speed, but would suffer from poor low speed performance and transient response due to the lack of exhaust gas flow rate to overcome the inertia of the system. On the other hand a small turbocharger provides improved low speed torque and transient response due to a reduced inertia, but at high engine speeds would require turbine bypassing to prevent excessive turbocharger speed, thus sacrificing efficiency; in addition, small turbochargers generally exhibit lower efficiency owing to increased leakage pressure losses between turbine and housing. With highly boosted engines this low speed performance impairment is compounded [21][34]. Ideally for a forced induction engine, the driveability characteristics of a comparable naturally aspirated unit are an aim and a number of solutions have been introduced to diminish the effects of this turbocharging compromise.

Mentioned above, a turbine bypass – or 'wastegate' – allows correct sizing of the turbocharger for low engine speed performance [32]. As speed increases, the wastegate is opened, allowing a proportion of the exhaust gas to bypass the turbine, which has the effect of limiting boost pressure and preventing over-speeding of the turbocharger. However, as previously stated, thermal efficiency is sacrificed as the bypassed exhaust gas energy is wasted.

The idea of variable turbine geometry, where the effective turbine area (or aspect ratio) can be matched to the changing exhaust gas flow rate, has been around for some time. The concepts designed to achieve this can be placed in two categories, depending on whether it is the geometry of the volute or the nozzle that is adjustable. A turbocharger with variable geometry volute, according to Matsura et al. [35], is a lower cost alternative to variable geometry nozzle arrangements, which are generally more complex. In spite of experimentally demonstrated improvements in transient response [35][36][37], few variable geometry volute designs have attained commercial production. Baines [32] proposes that this may be due to issues of aerodynamic inefficiency relative to fixed geometry counterparts, and questions over durability and performance deterioration in service. The author goes on to say that turbochargers with variable nozzle geometry have achieved much greater

commercial success. Variable nozzle devices are of two principal types, pivoting vanes and moving sidewall [32], and have been shown to provide (amongst other benefits) improved transient performance [35] and low speed boost [38]. With a variable nozzle turbocharger fitted to 1.8 litre direct injection diesel engine, Hawley et al. [39] achieved increased torque over the entire engine speed range compared with an equivalent fixed geometry unit. However, Wijetunge et al. [21] and Matsura et al. [35] argue that variable geometry turbochargers still rely on the build-up of exhaust gas energy and consequently do not completely solve the problem of transient response, particularly at low engine speeds. Due to the much greater proliferation of variable nozzle devices (as opposed to variable geometry volute), they shall hereafter be referred to by the more general term, 'variable geometry turbocharger' (VGT).

There are a number of arrangements involving multiple turbochargers, which can generally be separated into three categories: series, parallel, or sequential. These shall be considered in turn.

There are several factors that limit the pressure ratio that can be achieved by a single compressor – principally efficiency reductions at high pressure ratios, mass flow range requirements, and temperature limits [32]. As boost pressure (i.e. pressure ratio) requirements increase – as is the case with downsizing – a series turbocharged configuration may become viable. Considering a two-stage system, two turbochargers are placed in series, such that the exhaust gases undergo two stages of expansion, and the intake charge goes through two stages of compression. As Watson and Janota [30] point out, 'high overall pressure and expansion ratios may be developed using conventional turbochargers', without sacrificing efficiency or mass flow range. Series systems may include bypass valves (for turbines and/or compressors) for greater flexibility of operation – see Figure 2.3 (reproduced from Pflüger [40]). One such two-stage arrangement investigated by Pflüger [40] on a 12 litre commercial diesel engine, when compared with an equivalent single-stage system, showed: increased torque at all engine speeds; increased rated power; improved air supply; reduced BSFC and smoke; and potential to reduce NO_x emissions. Although transient tests were not performed, the author argues that transient response could potentially be improved with a two-stage system. However, both Baines [32] and Watson and Janota [30] highlight the disadvantages of series turbocharging of the cost of the extra turbocharger and

intercooler (which is usually required); increased bulk and complexity of the system; and additional pressure losses. Baines [32] also states that the transient performance of a two-stage system is generally worse than that of an equivalent single-stage unit, as the exhaust gas energy available to accelerate the two turbochargers is shared between them. In a computational investigation by Saulnier and Guilain [41], a 2.0 litre diesel engine is downsized to 1.5 litres by moving from single-stage to two-stage turbocharging; equivalent steady state performance was easily achieved, but low speed transient response was worsened.

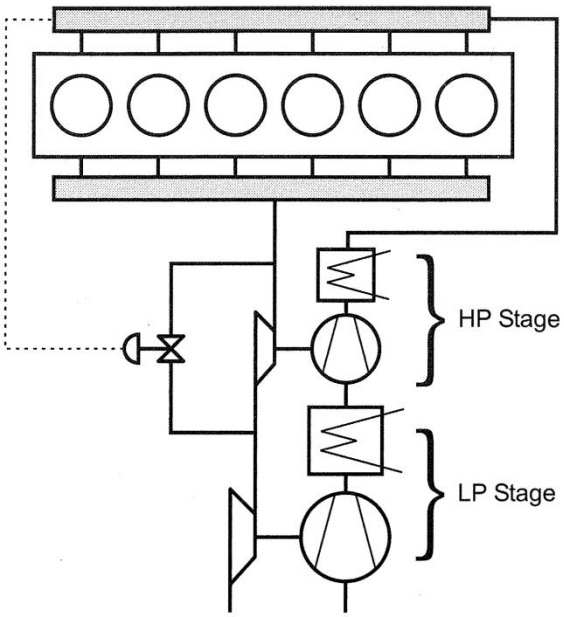

Figure 2.3 – Schematic diagram of regulated series (two-stage) turbocharging system [40]

In a parallel turbocharged arrangement, two (or four) turbochargers of equal size are used to replace a larger single unit. Parallel turbocharging is typically used on engines with six or more cylinders, dividing the exhaust pipes from the cylinders into groups which are most favourable for utilising exhaust pulse effects (pulse turbocharging is comprehensively dealt with in Watson and Janota [30], and hence shall not be covered here). In a system with two turbochargers, each turbine receives exhaust gases from half the cylinders from the engine; on the intake side, the compressors generally feed into a common intake plenum – see Figure 2.4, reproduced from Luttermann and Mährle [42]. As well as the aforementioned exhaust pulse effects, further benefits of parallel turbocharging are: reduced (combined) turbocharger inertia for improved transient response [42][43]; and simplified packaging, particularly for V-type engines [30][43]. However, as

discovered by Sommerhoff [43], compared with a single turbocharger setup, the net gain of a parallel system can be debatable, due to factors such as the higher efficiency of larger turbomachinery and an associated reduction in back pressure.

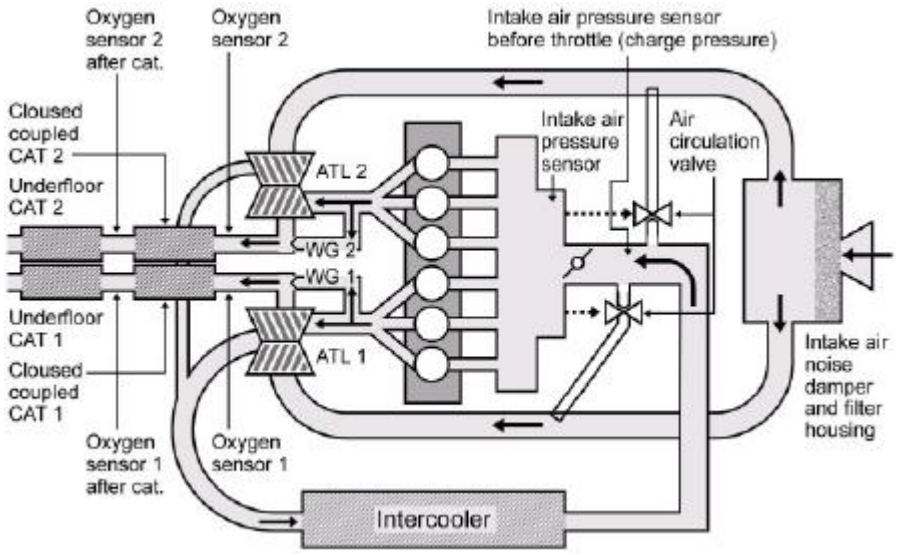

Figure 2.4 – Schematic diagram of a parallel twin turbocharging system (fitted to a 6 cylinder SI engine) [42]

In a sequential system two (or more) turbochargers are arranged in parallel and supply charge air to a common intake manifold, similar to parallel turbocharging. Unlike a purely parallel configuration, the turbines are driven by exhaust gases from a common exhaust manifold and, through the systematic use of flow control valves, the number of turbochargers in operation can be varied. The turbochargers employed may be of equal (or similar) size; in which case, for a twin-turbo system, during the first sequence (at low engine speeds) only one turbocharger is in operation; during the second sequence (high engine speeds) both turbochargers are used. One such system was developed by Tashima et al. [44] for a 1.3 litre gasoline rotary (Wankel) engine, a schematic of which is shown in Figure 2.5. Alternatively, a small turbocharger may be used for low engine speed operation, switching solely to a large turbocharger at high engine speeds. Hancock et al. [12] use a system of this type – but with the turbochargers arranged in series – on a highly downsized 1.2 litre 3 cylinder GDI engine. In both cases the purpose and result is the same: changing the effective turbine area to match it to engine speed and exhaust gas flow, in order to improve low speed boost, torque and transient response. Baines [32] likens the effect to ‘a stepwise variable geometry scheme’. In the aforementioned work of Tashima et al. [44], boost pressure and torque were substantially improved (by

200% and 36%, respectively) at low engine speeds when compared with a conventional turbocharger. As demonstrated in vehicle acceleration tests, transient response was also markedly superior, with the time taken to reach maximum boost reduced by 43%. Similar improvements are exhibited in computational simulations of a 2.5 litre 4 cylinder gasoline engine carried out by Brüstle et al. [45]. As for disadvantages of sequential turbocharging, Tashima et al. [44] and Baines [32] stress the need for careful matching both of the turbochargers and the engine speed at which the sequence transition occurs – these are critical in avoiding a drop in torque prior to the switch as well as compressor surge (and choking) issues. As with other multi-turbocharger schemes, additional plumbing and associated potential pressure losses must also be factored in. Furthermore, as previously mentioned in relation to VGTs, Wijetunge et al. [21] assert that the transient response of any of these turbocharged systems is still ultimately limited by the available exhaust gas energy, and any transient response issues are multiplied in highly boosted (e.g. highly downsized) applications.

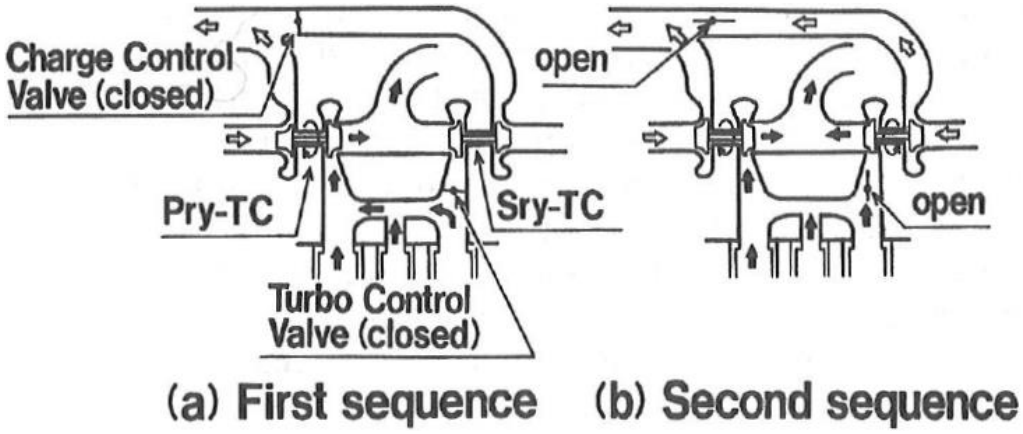

Figure 2.5 – Schematic diagram of a sequential twin turbocharging system [44]

2.2.2 Pressure Wave Supercharging

In pressure wave supercharging, as the name suggests, pressure waves in the intake and exhaust manifolds are used to compress the intake charge. Heywood [29] describes the working principle thus: 'if two fluids having different pressures are brought into direct contact in long narrow channels, equalisation of pressure occurs faster than mixing'. By far the most well-known pressure wave device for automotive use is the Comprex system, developed by Brown Boveri [46]. The main component of the Comprex supercharger is a cylindrical rotor with a number of the requisite long narrow channels around the circumference – see Figure 2.6, reproduced from

Baines [32]. The rotor is belt driven from the engine crankshaft to keep the rotor speed proportional to engine speed – the rotor itself provides no compression work so the power consumption is minimal. As the rotor is rotated, individual cells in turn are opened and closed as they pass the exhaust and intake inlet and outlet ports. When the cell reaches the exhaust inlet port, high pressure exhaust gas flows in, creating a pressure wave which compresses the intake air already present. The opposite end of the cell is then opened to the intake manifold; the pressure wave continues, forcing high pressure air out towards the cylinders. The aperture is closed before the exhaust gases are allowed to flow out, and the gases become stationary as both ends of the cell are closed. However, the cell pressure is higher than in the exhaust outlet, so when the cell is opened to this port the exhaust gases expand out, drawing fresh air in from the subsequently opened inlet port. Both apertures are closed and the system returns to the initial state. This process is explained in more detail by Gyarmathy [46] (as well as Heywood [29] and Baines [32]).

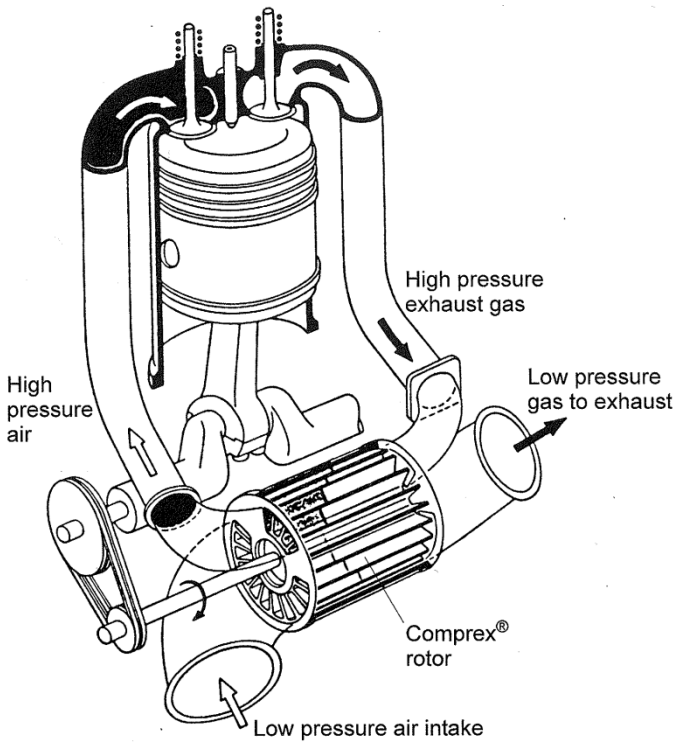

Figure 2.6 – The Comprex pressure wave supercharger [32]

A number of groups have performed comparative studies of Comprex devices versus conventional turbochargers, and on the most part the conclusions are consistent. Performing tests on a 6 cylinder diesel tractor engine, Schwarzbauer [47] achieved increased torque at all engine speeds, particularly at low and medium

speeds – with some 90% of maximum torque available at idle. Smoke levels were reduced in the lower half of the speed range. Fuel consumption, however, was worse with the Comprex system at high speed and load; part load BSFC was similar with both devices. These steady state results are corroborated by Summerauer et al. [48] when testing a 12 litre 6 cylinder diesel truck engine. The transient tests also performed by the authors showed much improved response and lower smoke levels with the Comprex. They state that the improved driveability would allow a simpler gearbox to be fitted, yielding further benefits. Wallace and Aldis [49], testing a similar engine to the previous authors, (perhaps unsurprisingly) obtain corresponding results. As Baines [32] points out, in spite of the potential gains available with the Comprex system, it has achieved limited commercial success. The author attributes this to issues such as noise during operation, even with later design improvements; the bulk and weight of the device; and high system cost caused by the required manufacturing precision.

2.2.3 Mechanical Supercharging

Mechanical supercharging is where the increased charge air density is provided by a pump or compressor, which is usually driven from the engine crankshaft via a gear train or belt and pulley system. As the term ‘supercharger’ is usually reserved for mechanically driven systems [50], this precedent will be maintained from here onwards. Superchargers can be categorised according to the method of compression: positive displacement, or dynamic compressor.

A positive displacement pump – in general terms – displaces fluid in a pipe system by cyclically trapping and discharging a fixed amount of the fluid. In an automotive context, increased charge density is accomplished by pumping the air into the intake at a faster rate than the engine would normally ingest. Since this is at a fixed rate relative to engine speed (if the drive ratio is fixed), positive displacement superchargers are capable of producing almost constant boost pressure. The mechanical drive results in good transient response, but the downside is that power is drawn from the useful output of the engine instead of utilising ‘free’ exhaust gas energy as with turbocharging. On the other hand, some of the energy used by the supercharger is recovered as positive pumping work on the pistons [50], whereas a turbocharger also raises exhaust backpressure and thus increases pumping losses and trapped residuals [51]. Considering positive displacement superchargers specifically, Bhinder [50] highlights a major disadvantage, namely their size and

weight relative to the boost provided. There are many different designs of positive displacement supercharger, with varying degrees of commercial success – these types include Roots, screw (such as the Lysholm compressor), sliding vane, and scroll. Roots-type superchargers do not provide internal compression, unlike the other types listed here; as a result they have a relatively low efficiency (see Stone [52] for details) – although recent developments such as Eaton's Twin Vortices Series (TVS) [53], with reduced clearances and improved flow characteristics, are a big improvement. Devices with internal compression, such as the Lysholm compressor, offer greater volumetric and isentropic efficiencies [54], but these benefits come at the cost of increased manufacturing precision requirements [50]. Furthermore, as discovered in analysis by Stone [52], these efficiency improvements are rapidly eroded when the internal compression ratio of the device does not match the overall required pressure ratio – i.e. when external compression (or expansion) occurs. A Roots-type supercharger was used by Joyce [55] on a 4.0 litre 6 cylinder gasoline engine to increase torque and power by 35-50%, exceeding the output of a naturally aspirated 6.0 litre V12. At part load (equal torque), BSFC is greater for the supercharged engine than the naturally aspirated unit it is based on, due to parasitic losses and a reduced compression ratio; however, for the same conditions BSFC is substantially lower for the supercharged engine than the larger capacity V12. Transient performance was not tested against the naturally aspirated engines, but it was expected to be slightly diminished. As Joyce [55] explains, 'there is a finite time taken to compress the air in the volume between the blower and the engine. As a result, when the engine's speed is changing, the mass of air delivered by the supercharger is different to that being received by the engine'. There is thus a reduction in engine performance from the steady state maximum. Although the author does not explicitly state it, this forms the basis of an argument for employing a variable supercharger drive ratio, such as through a CVT. Stone [56] also addresses the point of a continuously variable drive ratio, but in relation to reducing part load throttling losses. Considering the performance differences between supercharging and turbocharging, Richter and Hemmerlein [57] have performed a comparative study on a 2.5 litre 4 cylinder gasoline engine. The supercharged version shows a torque advantage of 50-70% at low to medium engine speeds; torque is nearly identical at high engine speeds. Vehicle acceleration from low engine speeds is correspondingly superior with the supercharged engine. Conversely, the BSFC of the supercharged engine is 13% higher than the turbocharged version at low engine speeds, and 10% higher at high engine speeds

– in the middle speed range, the BSFC values of both engines are very similar. The authors also demonstrate the efficiency advantage of superchargers with internal compression over those without. It is worth nothing that both Joyce [55] and Richter and Hemmerlein [57] employed a bypass valve around the respective superchargers for part load operation.

Dynamic compressors comprise centrifugal (radial flow) and axial compressors; but for automotive supercharger use, the centrifugal type is by far the more common of the two. A centrifugal compressor works by accelerating the intake air to a high velocity, and then this velocity is converted to pressure by way of diffusion [30]; consequently, the pressure ratio produced increases with compressor speed. Thus with a fixed ratio mechanically driven centrifugal supercharger boost increases with engine speed, which, as Bhinder [50] points out, makes it a less than ideal match to automotive engines. The author goes on to state that this characteristic of centrifugal compressors is not a problem when used in a turbocharger, as turbocharger speed is free to vary independently of engine speed. Centrifugal superchargers do have benefits in that they are typically smaller, lighter, and capable of producing higher pressure ratios than their positive displacement counterparts. In addition, while the increasing boost with engine speed attribute may be rightly seen as a drawback, in the case of gasoline engines it may allow a higher compression ratio to be used. In this case air flow can be improved at high engine speeds where volumetric efficiency would usually drop off, without significantly increasing cylinder pressures at low to medium engine speeds, thus avoiding auto-ignition (knock). This benefit is perhaps more relevant to applications where performance at high engine speeds is of particular importance, for instance with specialist high performance car manufacturers Koenigsegg and Caterham [58]. Following on from his earlier line of reasoning, Bhinder [50] suggests that driving a centrifugal supercharger through a variable transmission would allow the boost to be matched to the engine requirements at any given speed and load. This idea is currently being developed by Rotrak [51], a joint venture between centrifugal supercharger manufacturer Rotrex and variable transmission specialist Torotrak. The Rotrak device combines a full-toroidal variator with a centrifugal supercharger – the latter already incorporates a compact, innovative epicyclic traction drive patented by Rotrex, which has a single stage step up ratio of nearly 13:1 to achieve the high speeds required by the compressor. As yet there are no published results for performance simulations or engine testing, but taken individually the

technologies are mature and proven. Listing the potential benefits of the Rotrak concept for gasoline engines, Stone [51] states that controlling the engine load via the boost pressure (i.e. by controlling compressor speed) is a possibility, which would allow reduced throttling of the engine and therefore reduced pumping losses.

2.2.4 Combined Charging Systems

Ideally, a pressure charging system would incorporate the transient response and torque at low engine speeds that a mechanical supercharger offers with the greater efficiency and part load flexibility of a turbocharger. One solution to this dilemma is to simply combine a declutchable supercharger with a conventional turbocharger in a sequential series arrangement – such systems have been researched, particularly for heavy duty diesel applications [34][35][59]. (This configuration shall hereafter be referred to as a 'combined charging system'.) Schmitz et al. [34] investigated a combined charging system for a 10.9 litre V6 commercial diesel engine, with a positive displacement supercharger (Wankel-type, which has internal compression) upstream of a fixed geometry turbocharger. An electro-magnetic clutch was fitted to the supercharger drive pulley so that the supercharger could be disengaged (in conjunction with an intake bypass valve) at high engine speeds or low loads in order to maintain efficiency. The system configuration is shown in Figure 2.7 (reproduced from Schmitz [34]). Compared to the purely turbocharged engine, the combined charging system gave significantly increased low speed boost and torque with only a small BSFC penalty; available engine braking power was also vastly improved. As for transient performance, in simulations of loaded vehicle acceleration, the time taken to reach maximum engine speed from idle was reduced by more than 30%.

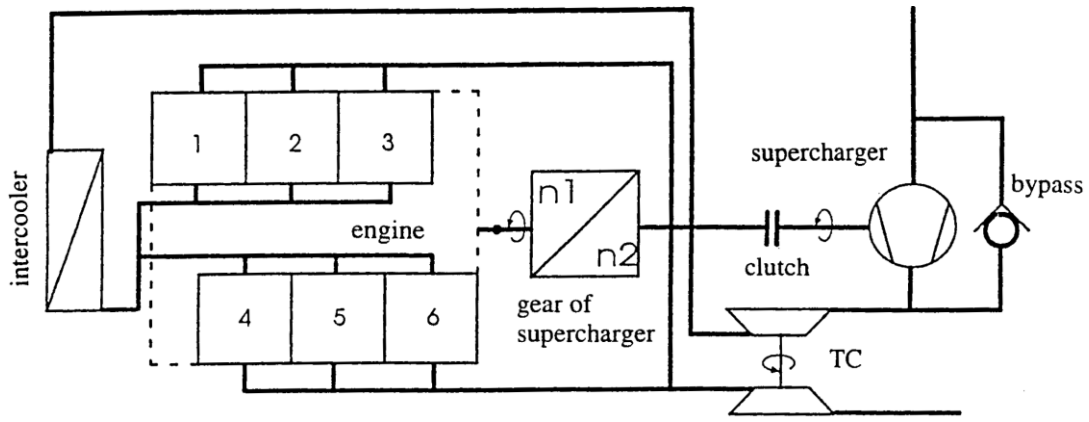

Figure 2.7 – Schematic diagram of a combined charging system (fitted to a V6 engine) [34]

Matsura et al. [35] have tested a similar system – also with a Wankel-type supercharger – on an 11 litre 6 cylinder commercial diesel engine. In this case the base engine was fitted with a VGT, and the supercharger was downstream of the turbocharger and intercooler. Low speed torque was increased by some 50-60%, and loaded vehicle acceleration was reduced by a remarkable 65%. Due to the improved air supply, smoke and BSFC could be reduced while achieving the same torque curve. Tomita et al. [59] investigated a combined charging system – much the same as the two previous – on an 8.8 litre 6 cylinder heavy duty diesel engine. In this case, a Lysholm screw-type supercharger (positive displacement, with internal compression) was fitted downstream of the turbocharger and prior to the intercooler, and the turbocharger featured a wastegate. The addition of the supercharger allowed low speed torque to be substantially increased while at the same time improving the air-fuel ratio (AFR), thereby reducing smoke levels; BSFC was comparable with the two systems, with some improvement at very low engine speed. The authors calculated that 20-55% of the power used to drive the supercharger was recovered as positive pumping work – the amount recovered decreasing with increasing engine speed. As for transient response, loaded vehicle acceleration tests showed that acceleration times were reduced whilst simultaneously improving transient boost pressure and thus AFR.

The idea of the combined charging system has not been explored solely by the heavy duty diesel sector; Volkswagen has successfully implemented this technology on a 1.4 litre GDI engine [60]. Here a Roots-type supercharger is used in conjunction with a fixed geometry turbocharger. As reported by Whitworth [13] at the time the 'twincharged' engine was released to market, Volkswagen claims that it 'delivers the equivalent performance of a naturally aspirated 2.3 litre 4 cylinder engine, but with a significant drop in fuel consumption', costs less to produce than a modern turbocharged HSDI diesel engine, and is equally reliable. As for passenger car diesel engines, Cantore et al. [61] have – by way of a computer model – downsized a 2.5 litre 4 cylinder turbocharged HSDI diesel engine to 1.8 litres by adopting a combined charging system, with no reduction in steady state or transient performance. The authors calculate that around a third of the power consumed by the supercharger is recovered as pumping work, and the downsized engine delivers significantly better part load fuel consumption than the baseline for points along a typical driving cycle. One of the authors of the previous work, Mattarelli [62], has carried out a further computational study for a 2.8 litre 4 cylinder HSDI diesel

engine, comparing the performance of a combined charging system with a series sequential turbocharged arrangement – as well as a baseline engine, which is fitted with a VGT. Here the turbocharger of the combined system was a VGT, as was the high-pressure turbocharger of the sequential system. Both configurations provided increased steady state torque (up to 14%) and slightly reduced BSFC over the baseline. In simulated vehicle accelerations from 70 to 120 km/h, the sequential and combined systems were around 14% and 25% quicker than the baseline, respectively. For reference, a sequential system with fixed geometry for both turbochargers offered very little improvement over the baseline single VGT system in steady state performance, and performed only marginally better than the baseline (~3%) in the acceleration test.

It is worth noting that in each of these examples of combined charging systems a positive displacement supercharger is used.

2.2.5 Electrical Systems

Up until this point only purely mechanical boosting systems have been discussed; there are also several electrical boosting systems that are worthy of review. On the one hand there are electrically driven compressors (EDC) such as the Visteon Torque Enhancement System (VTES). According to its manufacturer, using a standard 12 V vehicle electrical system, the VTES centrifugal EDC is capable of producing a pressure ratio of 1.45:1 and has a time to maximum boost of less than 350 ms [63]. Pallotti et al. [64] have downsized a 1.6 litre gasoline engine to 1.4 litres by using an EDC to compensate for the deficit in full load performance. Standing start vehicle acceleration from 0 to 100 km/h was increased by some 14% with the downsized engine, but in-gear acceleration was improved by around 9%. Fuel consumption was reduced by 12% over the New European Driving Cycle (NEDC), as the EDC was not required throughout. Adopting a larger alternator accounted somewhat for the additional electrical demand caused by the EDC, but a noticeable drop in engine performance resulted when other electrical loads (such as lights, heater, and radio) were applied, or when full performance was requested for sustained periods. The authors note that battery condition would also have to be monitored. Wijetunge et al. [21] have carried out computer simulations comparing a series sequential turbocharging system with a combined charging system that uses an EDC (in this case the VTES) in place of the mechanical supercharger – see Figure 2.8b, reproduced from Baines [32]. The series system used a VGT for the

low-pressure stage, as was the turbocharger in the combined system. The purpose of both systems was to downsize a typical 2.0 litre HSDI turbocharged diesel engine to 1.4 litres. In both fixed speed tip-in transient tests and vehicle accelerations, the response of the system with the EDC was significantly better than the conventional two-stage system. The authors acknowledge that using an EDC would have an impact on the vehicle electrical system. On the other hand, they argue that the EDC is much easier to match to the engine than the combination of turbochargers in a two-stage system, as it avoids exhaust backpressure issues and compressor speed is not dependent on exhaust conditions. Fuel consumption is not discussed.

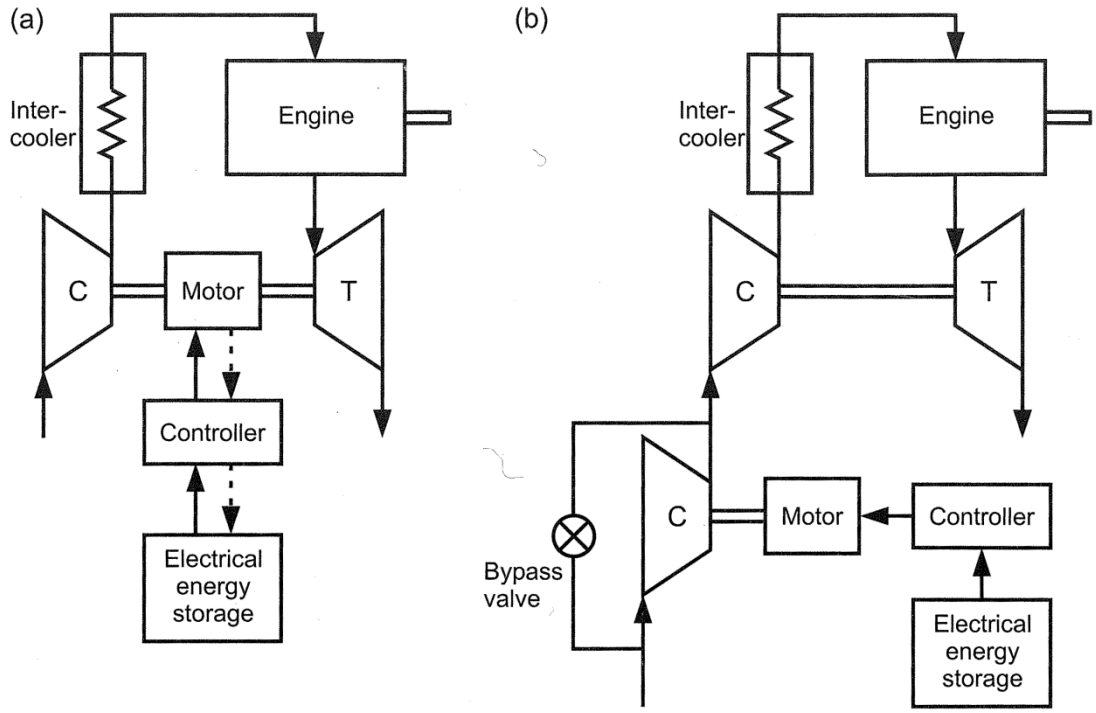

Figure 2.8 – Electrical turbocharging systems – a) electrically assisted turbocharger; b) electrically driven compressor (in a combined charging system) [32]

Another type of electrical boosting system is the electrically assisted turbocharger (EAT), such as evaluated by Katrašnik et al. [65]. With this type of device, torque is applied to the turbocharger shaft by a high speed electric motor – the motor may be integrated into the turbocharger bearing housing (see Figure 2.8a), or as an extension to the turbocharger shaft on the compressor side. As Baines [32] discusses, the former configuration is attractive from a packaging point of view, but the motor would have to be able to withstand high temperatures and thermal gradients resulting from the proximity to the turbine and exhaust system; whereas the latter arrangement would be a less severe working environment for the motor,

increased unit size and effects on shaft dynamics may be problematic. On a general note, the motor will add weight (which in turn will affect bearing loads) and increase the base inertia of the turbocharger, which must be taken into account when the motor is not used. However, as an additional feature, the motor may also be operated as a generator in order to recover exhaust energy as electrical power – the benefits of exploiting this capability will be assessed under the following section on turbocompounding. In the aforementioned work by Katrašnik et al. [65], the transient response and load acceptance of a 6.9 litre 6 cylinder commercial diesel engine were simulated with the original fixed geometry turbocharger installed and also with two electrically assisted variants. The engine model was calibrated and validated with experimental data, as were the operating characteristics of the two different electric motors. The transient response of the engine during a fixed speed tip-in was reduced by up to 55% with an EAT, and load acceptance was also substantially improved. It should be noted, however, that these results were achieved by applying higher than standard voltage to the turbocharger motor (42 V). The authors address the previously mentioned increase in rotational inertia of the turbocharger caused by the motor, recommending that a motor with as low a moment of inertia as possible be used to mitigate any detrimental effects on turbocharger dynamic performance. In a computational study by Panting et al. [66], a theoretical 5.3 litre 4 cylinder diesel engine was configured to provide a baseline for acceptable transient response by installing a small conventional turbocharger with a wastegate. By replacing the turbocharger with an EAT with a larger turbine and no wastegate (as well as modifying injection and valve timings), the thermal efficiency of the engine was improved by some 10%, predominantly through reduced pumping losses. Although the EAT allowed the transient performance to be maintained, this was achieved by using considerable motor power – in the region of 100 kW. The authors acknowledge that this would likely be unfeasible for typical vehicle electrical systems.

Considering the relative merits of EDCs and EATs, Fieweger et al. [67] have performed computer simulations to assess both types of electrical device on a passenger car V6 HSDI diesel engine against a baseline setup using a VGT. The EDC was incorporated in a combined charging system (as with Wijetunge et al. [21]), with a conventional fixed geometry turbocharger downstream of the EDC. Both electrical systems were limited to 2.5 kW of electrical power input, assumed to be provided solely by the vehicle battery. In fixed engine speed tip-in tests, both

electrical systems produced significantly improved transient response than the baseline. The authors state that at low engine speeds the potential improvement with the EAT would be limited by compressor surge (which was not simulated), whereas the EDC is not affected in the same way. As engine speed increases, however, the EAT gains the upper hand, as the EDC becomes limited by its maximum motor speed. The improvements in transient response shown in these tests are reflected in simulated vehicle accelerations, with both electrical systems reducing acceleration time from engine idle speed by some 18%. The authors also claim that the transient BMEP characteristic with the electrical systems is similar to a comparably powerful naturally aspirated engine. Whether the EDC or EAT is superior overall is left open to debate.

2.3 Turbocompounding

As discussed earlier, a turbocharger uses an exhaust-driven turbine to power a compressor, which in turn increases the density of the air entering the engine. Alternatively, it may be beneficial to harness the power produced by the turbine in a different manner; namely by directly adding to the useful output of the engine. Watson and Janota [30] define a turbocompounded engine as one where there is 'some mechanical linkage and power transmission between the exhaust-gas driven turbine and crankshaft of the engine'. However, the same term may be used also to describe a system where the turbine drives an electrical generator and the exhaust energy is thus recovered as electrical power. Both mechanical and electrical turbocompounding arrangements will be considered in turn.

2.3.1 Mechanical Turbocompounding

There are four basic mechanical turbocompounding arrangements, each with particular advantages and disadvantages – see Figure 2.9, reproduced from Baines [32].

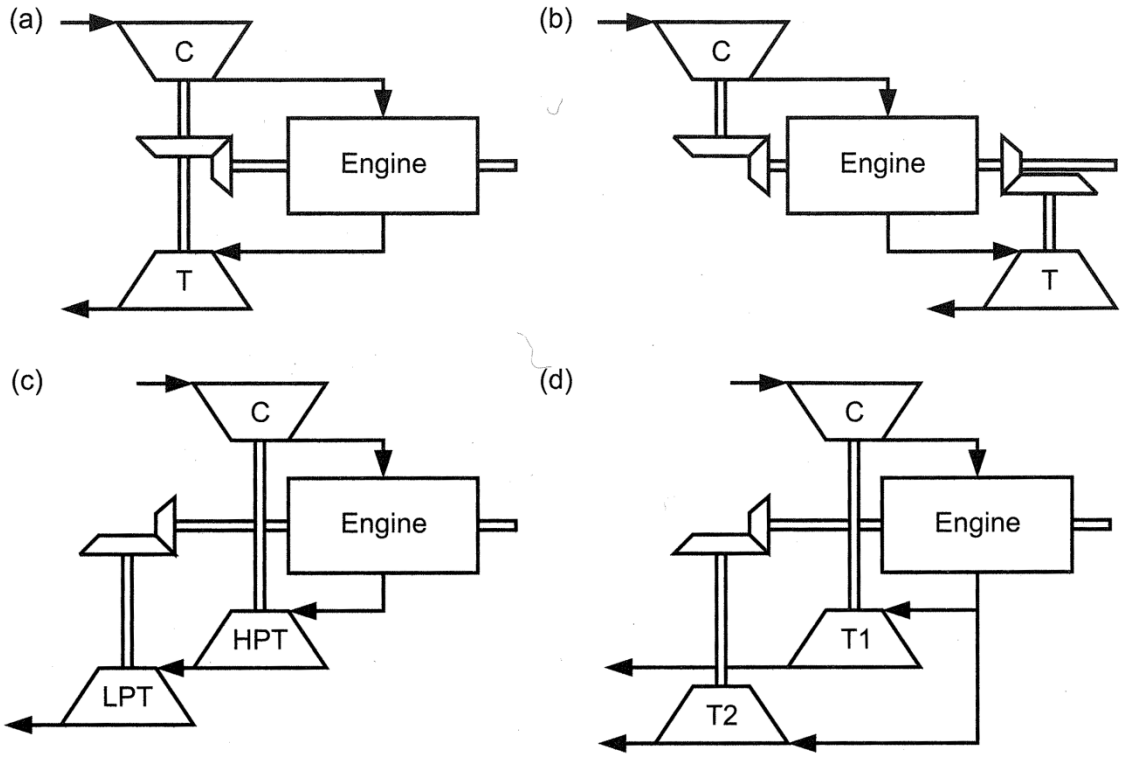

Figure 2.9 – Turbocompounding schemes – a) directly coupled turbocharger; b) separately coupled turbocharger; c) separate power turbine, series arrangement; d) separate power turbine, parallel arrangement [32]

In the first type, the shafts of the engine and turbocharger are directly linked (Figure 2.9a); however, (as with the centrifugal supercharger) the difficulty comes in selecting a fixed transmission ratio to match engine and turbocharger speeds at all speed and load conditions, with particular problems at part load [30][32]. Brockbank [68] discusses the possibility of using a CVT with this arrangement, which would allow the level of turbocompounding to be controlled independently of engine speed. Furthermore, by manipulating the CVT ratio, the turbocharger could intentionally be driven by the engine when there would normally be insufficient boost – the turbocharger effectively acting as a supercharger. A system of this type (with a CVT) was used on the well-known Napier Nomad aircraft engine of the 1950s [30][32] – as Baines [32] points out, although it (and other contemporary turbocompounded engines) showed promise, it was a notoriously complex machine, and was soon superseded by the advancing development of gas turbine engines. Chadwell and Walls [22] have investigated a modern counterpart for the automotive sector – the VanDyne SuperTurbocharger – which claims to offer supercharging, turbocharging and turbocompounding in one device. The SuperTurbocharger comprises a turbocharger which transmits power to and from the engine crankshaft via a high speed traction drive with an integral reduction ratio, a further set of reduction gears, a traction drive CVT, and finally a belt and pulley system – see Figure 2.10, reproduced from VanDyne et al. [69]. In the computational study performed by Chadwell and Walls [22], the SuperTurbocharger was used to downsize a typical 3.2 litre V6 naturally aspirated gasoline engine to a 2 litre 4 cylinder unit. Steady state torque was superior with the downsized engine, but full load BSFC was worse, which the authors attribute to the fuel enrichment and retarded ignition timing that was necessary to maintain the turbine inlet temperature limit of 950°C. However, part load fuel efficiency was increased, leading to a 17% reduction in fuel consumption over the NEDC. Simulated transient tip-in tests suggest the downsized engine has good transient response, but no comparison was drawn with the baseline engine. As a progression from these results, a compressor map width enhancement technique was used to facilitate even greater downsizing. Bypassing some of the compressed intake air to upstream of the turbine increased mass flow through the compressor at low engine speeds, simultaneously avoiding surge and allowing higher boost. Using the intake air bypass at high engine loads also removed the need for fuel cooling. Thus a torque curve comparable to a 4.2 litre V8 was attained from the 2.0 litre engine, achieving a better full load BSFC curve at the same time. As would be expected, part load fuel economy was also vastly superior,

with a 36% improvement over the NEDC. During full load operation up to 10 kW of power was transmitted to the device (for supercharging) at low engine speeds; up to 12 kW was recovered by turbocompounding at high engine speeds. However, the potential of turbocompounding during part load conditions was not discussed, and again, transient performance was not compared.

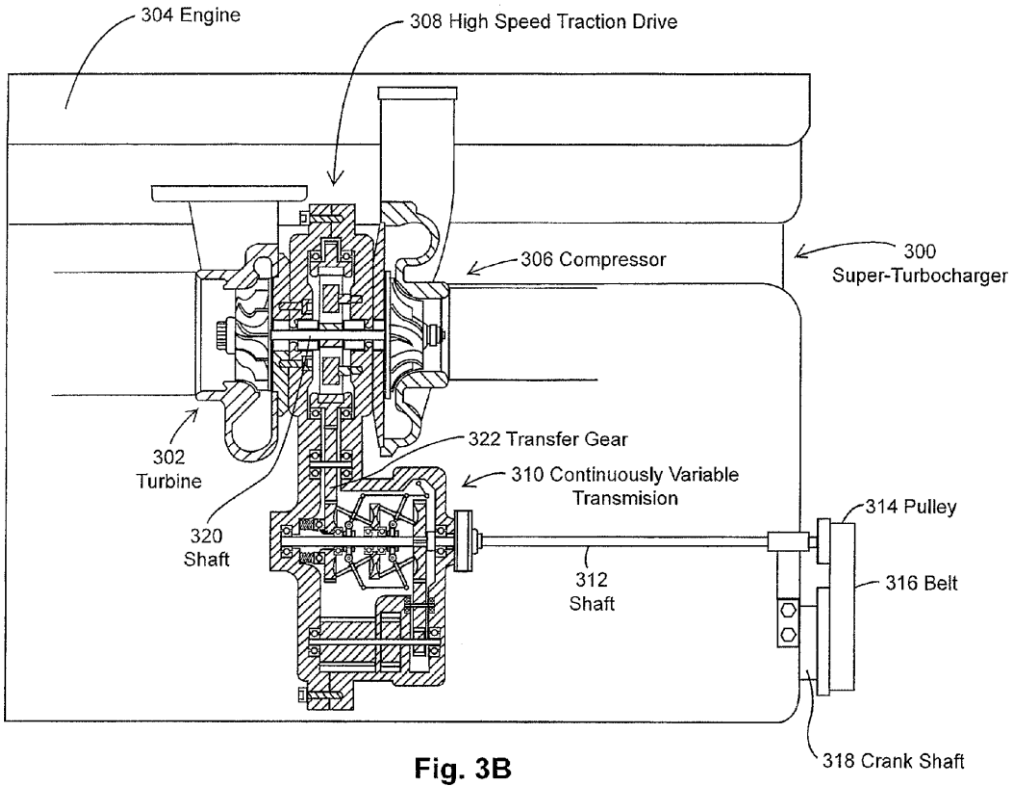

Figure 2.10 – The VanDyne SuperTurbocharger [69]

Connecting the compressor and turbine to the engine via separate transmissions forms a second type of mechanical turbocompounding (Figure 2.9b). The advantage of this is that the compressor and turbine can run at different speeds, and the turbomachinery can be matched separately. However, unless variable speed drives are used, the same problems apply as faced by the previous system. It has been suggested that a positive displacement compressor (and possibly expander as well) be used to overcome the low speed performance deficit, but the problem of part load operation remains [30], and the relative inefficiency of such devices renders the potential gains negligible [32]. Over a number of years, Wallace [70] developed the concept of a 'differential compound engine' (DCE), where the compressor was driven by the engine through an epicyclic gear system, and the turbine transmitted power to the engine via a fixed speed ratio. Initially this was for two-stroke diesel

engines; later iterations [71] were adapted for heavy duty four-stroke engines and used a variable geometry turbine transmitting power through a CVT to ensure optimum turbine efficiency – see the schematic in Figure 2.11, reproduced from Wallace et al. [71]. Although the DCE was shown to offer many benefits over conventional turbocharged diesel engines – particularly in terms of steady state and transient performance, fuel economy, and refinement [72] – commercial production has not been attained; Baines [32] reasonably attributes this to the great complexity of the system.

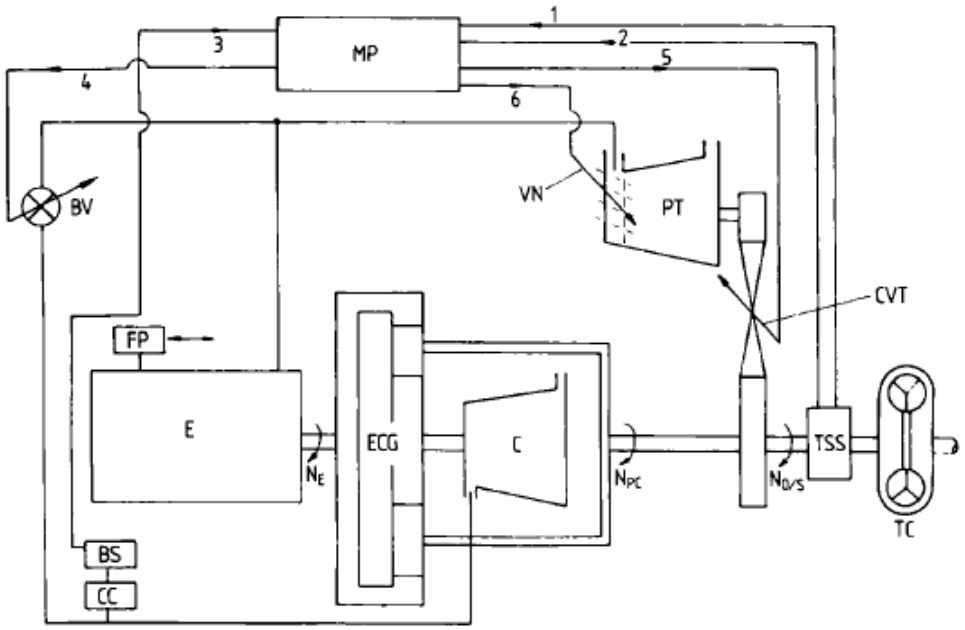

DCE layout: final version
BV bypass valve; BS boost sensor; C compressor; CC charge cooler; E semi-adiabatic engine; ECG epicyclic gear train; FP fuel pump; PT power turbine; TC torque converter; VN variable turbine nozzles; TSS output torque and speed sensor; N_E engine speed; $N_{o/s}$ output shaft speed; N_{pc} planet carrier speed; MP micropressor;
Input signals: 1 torque transducer; 2 speed transducer; 3 boost transducer
Output signals: 4 bypass valve control; 5 CVT control; 6 nozzle control

Figure 2.11 – Differential compound engine schematic [71]

A third type of mechanical turbocompounding uses a conventional turbocharger, with a second turbine mounted in series with and downstream of the turbocharger turbine. Power from the second turbine – known as a 'power turbine' – is mechanically transmitted to the crankshaft (Figure 2.9c). According to Baines [32] and Patterson et al. [73], this is the most common form of turbocompounding, with commercial production first being attained in the heavy duty vehicle sector by Scania and turbocharger manufacturer Cummins Turbo Technologies (formerly

Holset) [74]. Baines [32] points out that 'the power turbine, because it is dealing with a gas of lower density, can be larger and rotate more slowly than the turbocharger, and this eases the transmission problem'. However, as Watson and Janota [30] argue, the additional turbine in the exhaust stream increases backpressure, both increasing the outlet pressure (and thus reducing power) of the turbocharger and increasing the engine pumping losses – these effects partly offset the benefit from turbocompounding on overall engine efficiency. Nevertheless, in a study by Walsham [75] where various turbocharging technologies were tested and compared, the author argues that the modified exhaust flow characteristics caused by the power turbine result in the turbocharger behaving like it has a small turbine at low engine speeds (i.e. low mass flows) and a large turbine at high engine speeds. This has the effect of increased boost and transient torque over a conventionally turbocharged engine, as well as improved full load BSFC. On the other hand, the transient response does not match that of a comparable VGT system – whereas the effective turbine area of the VGT can be actively controlled, the apparent turbine size of the turbocharger in a turbocompound system is a passive effect dependent on engine speed and load. The turbocompound system does, however, maintain the superiority in terms of BSFC. Wallace [76] has conducted a computational study in order to ascertain the ultimate performance potential of turbocompounded heavy duty diesel engines, comparing single- and two-stage turbocharging systems, with and without an additional power turbine, for a nominal 8 litre 6 cylinder diesel engine. Similar limiting torque curves are achieved with and without turbocompounding for both the single- and two-stage systems – the two-stage systems having higher BMEP levels corresponding with the greater boost. The single-stage systems both have similar full load BSFC values, but the greatest efficiency of the turbocompounded engine is skewed towards high engine speeds, where the power turbine recovers the most energy. At low loads, the turbocompounded engine loses in a comparison of efficiency – in these conditions the engine has to drive the power turbine at a loss, as recoverable exhaust energy is minimal, and pumping losses are greater due to the increased backpressure caused by the power turbine. As for the two-stage systems, the turbocompounded engine has a more favourable full load BSFC curve, but the best values are even more skewed towards high engine speeds than with the single-stage system. Again, the non-turbocompounded engine has the advantage in terms of part load BSFC, for the same reasons as above. The author concludes that turbocompounding 'becomes technically and economically viable only in units operating at very high levels of

boost and BMEP'. This conclusion is affirmed by Baines [32], who asserts that turbocompounding 'is not really suitable for application to passenger car engines, for example, which spend most of their time at part load'.

The fourth type of mechanical turbocompounding is similar to the previous, the difference being that the power turbine is arranged in parallel with the turbocharger instead of series (Figure 2.9d). Baines [32] argues that this configuration may be preferable for large diesel engines where the power turbine necessary for an equivalent series system would be prohibitively large and expensive.

2.3.2 Electrical Turbocompounding

The various arrangements of electrical turbocompounding systems essentially mirror the four types detailed under the previous section on mechanical turbocompounding. Hence, the first type is fundamentally the same as the electrically assisted turbocharger (EAT) described under the section on electrical pressure charging systems; with an appropriate control scheme the integrated motor of an EAT can function as a generator to recover exhaust gas energy as electrical power. In the previously mentioned work by Panting et al. [66], the authors assert that this eliminates the need for a wastegate, as turbocharger speed can be controlled by adjusting the level of power generation – this is corroborated by Katrašnik et al. [65]. Hopmann and Algrain [77] have developed an EAT of this type, with a focus on maximising the fuel efficiency of a 14.6 litre 6 cylinder heavy duty diesel engine. Modifications to the turbocharger included redesigning the bearing housing and turbine housing interface in order to insulate the shaft-mounted motor from extreme thermal gradients. A second motor-generator was mounted on the engine crankshaft to provide the two-way energy transfer between the EAT and the engine. Engine performance was simulated at a number of steady state operating points – the overall efficiency of the electrical system was assumed to be 85% for the purpose of the simulation. Fuel consumption reductions of 2.5 to 10% were predicted, with the maximum potential benefit at rated power (i.e. high speed and load). The authors also state that this device offers more efficient and flexible operation compared with fixed ratio mechanical turbocompounding systems. Millo et al. [78] have investigated the possibility of replacing a VGT with an EAT with turbocompounding capability for an 8 litre 6 cylinder diesel engine in an urban bus application. The authors identify the driving cycle of the application as being critical to the potential benefit of turbocompounding systems – that is, the proportion of time

during which energy can be recovered. This was especially pertinent for the system investigated here, as recovered energy was stored in supercapacitors, which could hold sufficient energy for up to six assisted accelerations only. However, the supercapacitors could also be charged from – and discharged to – the 24 V vehicle electrical system. Thus, the potential efficiency benefit of this particular system is manifested through reduced alternator load. A number of driving cycles were simulated, with a maximum reduction in fuel consumption with the EAT system of some 6% during free-flowing highway (extra-urban) driving conditions. However, the efficiency benefit decreased down to around 1% as the proportion of congested traffic conditions increased, due to progressively more power being required for accelerating the EAT and fewer opportunities for energy recovery. Predicted improvements in transient response were more substantial; the EAT achieved the boost target 30% faster than the VGT during simulated tip-in tests. Hountalas et al. [79] have performed a computational study comparing a mechanical turbocompounding system (with a series power turbine) with an EAT with turbocompounding capability for a nominal 10.3 litre 6 cylinder heavy duty diesel engine. Both systems were found to reduce primary engine output as a result of increased exhaust backpressure and pumping losses; however, both systems also resulted in a net increase in output, as the power recovered through turbocompounding was greater than these reductions – this is in line with previously reported findings. With an assumed power turbine efficiency of 80%, the mechanical system provided a maximum BSFC reduction of 4.5% at full load; the corresponding value for the electrical system was 2%. However, these values decreased to 0.5% and 0.2%, respectively, at 25% engine load. Using higher efficiency turbomachinery had a large effect on the recovery potential of the EAT, increasing the BSFC reductions to 6.5% at full load and 3.3% at part load. The considerable sensitivity of turbocompounding effectiveness to EAT turbine efficiency was also explored by Millo et al. [78].

The second type of electrical turbocompounding system comprises an electrically driven compressor (EDC) – as described under the section on electrical pressure charging systems – and an exhaust gas turbine driving a separate electrical generator. This allows the speeds of the separate turbomachines to be independently controlled, with the potential for each to be optimally matched to engine speed and load. Aeristech [80] have developed an example of this concept, but, unfortunately, no results of performance testing are currently available.

The third type of electrical turbocompounding is similar to the series power turbine system detailed under the section on mechanical turbocompounding, but instead of the power turbine mechanically transmitting power to the crankshaft, it drives an electrical generator. Patterson et al. [73] have performed computer simulations to compare a system of this type with an equivalent mechanical power turbine system for a typical heavy duty diesel engine. In this case, the energy recovered by the electrical power turbine could either be used directly to power a flywheel-mounted motor, or stored in the vehicle electrical system. The authors acknowledge the trade-off between work done by the power turbine and the resulting increase in exhaust backpressure – which is unfavourable both to turbocharger and engine efficiency – as well as the necessity for high turbomachinery efficiency to maximise the benefit offered by turbocompounding. Results from the simulation show that both turbocompounding systems improve fuel efficiency, but the electrical power turbine offers greater fuel efficiency benefits at all load points – particularly at part load, where the speed of the mechanical power turbine is constrained by its fixed transmission ratio. The authors also state that the electrical power turbine will consume no power at low loads and engine idle, unlike the mechanical unit – this issue is discussed above, with reference to work done by Wallace et al. [76].

The fourth and final type of electrical turbocompounding is the equivalent of the parallel power turbine arrangement listed under the section on mechanical turbocompounding, but again, the power turbine drives an electrical generator. However, unlike the counterpart mechanical system, the electrical power turbine does not have to be constantly in operation. Odaka et al. [81] have made use of this functionality by using the exhaust gases from the turbocharger wastegate valve to drive the power turbine. Thus the base performance of the engine is not affected, and the exhaust backpressure is not increased, but exhaust energy is recovered that would otherwise be wasted. The parallel power turbine was evaluated on an 8 litre 6 cylinder commercial diesel engine in both steady state and transient conditions. As with all the other turbocompounding arrangements that have been reviewed, the greatest benefit was achieved at high load and high engine speeds – a region in which a typical vehicle engine may seldom operate; energy recovery at low speed and load was negligible. The overall effect on fuel efficiency was not predicted.

2.4 Other Technologies

2.4.1 Hyperbar

Several further technological developments are worthy of review. Firstly, the Hyperbar turbocharging system, which comprises a compressed air bypass (similar to the VanDyne SuperTurbocharger [22]) together with an auxiliary combustion chamber in the exhaust system upstream of the turbocharger turbine – see Figure 2.12, reproduced from Baines [32]. This combustion chamber allows high turbocharger speed to be maintained regardless of engine speed and load, overcoming the problem of low boost pressure at low engine speed; the air bypass complements this by increasing compressor mass flow and thus avoiding surge, particularly during transient conditions. In principle, then, the Hyperbar system provides solutions to two of the critical factors that hinder engines with high levels of boost. As Watson and Janota [30] highlight, the two major disadvantages are the complexity of the system, and the penalty to fuel consumption – the latter exacerbated by the need to maintain a continuous fuel supply to the combustor, even at low load [32]. Consequently, although the Hyperbar system may facilitate high specific output, it is clearly unsuitable for engine downsizing, where fuel efficiency at part load is crucial.

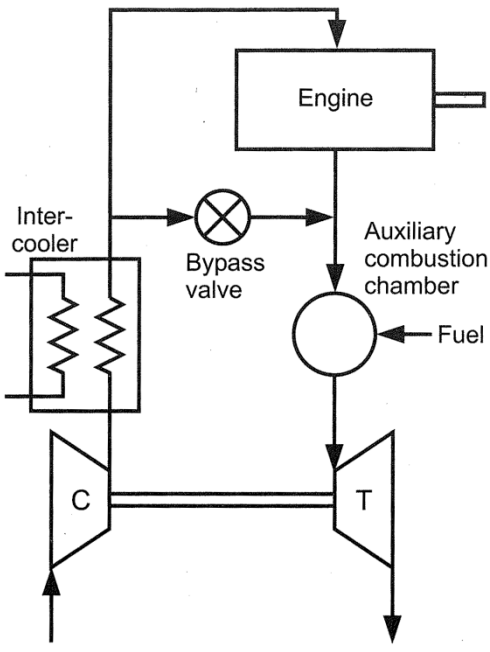

Figure 2.12 – Schematic diagram of the Hyperbar turbocharging system [32]

2.4.2 Rankine Cycle Systems

Turbocompounding is just one of a number of means of recovering exhaust heat energy as useful work; others include Brayton bottoming cycles, Stirling bottoming cycles, and thermoelectric generators [82]. Rankine bottoming cycles also come under this category, and have received sustained interest from the automotive industry over recent years. As Stobart and Weerasinghe [31] put it, 'heat recovery in the automobile internal combustion engine has been an overlooked area until recently due to the complications and the loss in power to weight ratios that would be the inevitable result. Pressure on fuel economy has led to a renewed interest'. Considering the working principle of a typical Rankine cycle system (see Figure 2.13, reproduced from Arias et al. [83]), the pressurised working fluid is brought to a superheated state from a subcooled liquid state in the evaporator – which, in this case, is a heat exchanger with the exhaust system. The high pressure superheated vapour is then expanded to the condensation pressure by the turbine – during which mechanical work is extracted – and subsequently condensed to saturated or subcooled liquid in the condenser. The condensate is then re-pressurised by a pump, thus completing the thermodynamic cycle. A reciprocating expander (a piston, for example) may be used in place of the turbine, and there are a variety of possible working fluids – see Teng et al. [84] for discussion on both of these subjects. Using a Rankine cycle system in conjunction with a conventional automotive engine, Ringler et al. [85] and Teng et al. [84][86] have predicted potential improvements in overall engine power of up to 10% and 20%, respectively, with no increase in fuel consumption; other researchers have also reported favourable results with regards to fuel efficiency [83][87]. However, although improvements in overall engine efficiency are attainable, the aforementioned additional bulk, weight and complexity of Rankine cycle systems would be prohibitive for incorporation with downsizing.

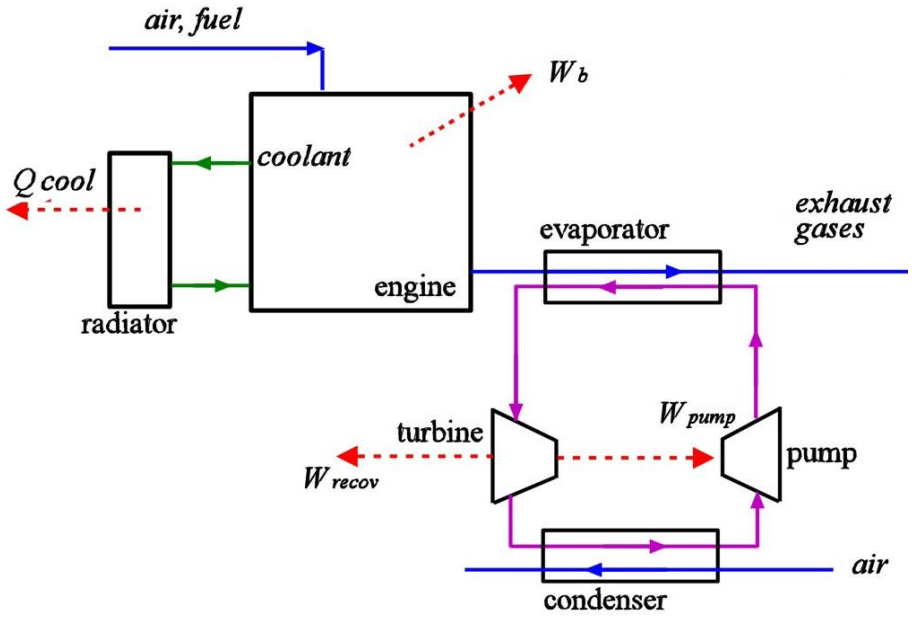

Figure 2.13 – Schematic of a typical Rankine cycle exhaust heat recovery system [83]

2.5 Discussion and Conclusions

Engine downsizing, according to Wijetunge et al. [21], 'has been identified as a viable, cost-effective method for the automotive industry to meet the increasingly stringent emissions and fuel economy targets stipulated by legislation throughout the world'. Full load performance potential is usually maintained through pressure charging – typically turbocharging or supercharging. The following factors were subsequently established as critical for a pressure charged and downsized engine to be effective:

- Increased specific power;
- Transient performance as close to a naturally aspirated characteristic as possible;
- Improved part load BSFC.

(Efficiency at full load is also somewhat important, but for 'real-world' operation – that is, the operating conditions of a typical drive cycle – part load efficiency is of much greater significance.)

Various turbocharging systems and configurations were considered, including VGTs and several arrangements with multiple turbochargers. Compared with conventional turbocharging, most of these systems offered improved specific engine power and fuel efficiency, and faster transient response. Nevertheless, a number of authors maintain that the low speed torque and transient response of such systems is ultimately limited by the available exhaust gas energy, and these problems are compounded in highly boosted (i.e. highly downsized) applications [12][21][35][67]. Mechanical supercharging avoids both of these drawbacks, but is considerably less efficient than turbocharging due to the parasitic power losses incurred. Proponents of supercharging, however, argue that it provides positive pumping work, whereas turbocharging incurs pumping losses due to the exhaust backpressure caused by the turbine – thus turbocharging is not 'free' energy recovery [50][51]. Combined charging systems, featuring both a declutchable supercharger and a turbocharger, were found to offer the transient response and low speed torque of supercharging with the overall efficiency and part load flexibility of turbocharging. Each of the

combined charging systems reviewed used a positive displacement supercharger; using a more efficient centrifugal supercharger instead may yield additional benefits. Furthermore, driving the supercharger through a CVT would offer greater flexibility of operation.

Electrical boosting systems – namely electrically driven compressors (EDCs) and electrically assisted turbochargers (EATs) – were also explored. Combined charging systems involving an electrically driven compressor in place of the mechanical supercharger have been investigated by some authors, yielding similar performance benefits. It is proposed, however, that a mechanical arrangement has significant advantages over electrical boosting systems, as the latter are generally limited by issues such as electrical heating and battery depletion, or require upgrading of the standard vehicle electrical architecture.

A number of turbocompounding arrangements, both mechanical and electrical, were considered. The general consensus of the authors is that turbocompounding is viable only for applications which operate consistently at high load [76], as the potential for energy recovery at low speed and load is minimal. Correspondingly, Baines [32] asserts that turbocompounding 'is not really suitable for application to passenger car engines, for example, which spend most of their time at part load'. One particular turbocompounding configuration displayed significant promise, however: the VanDyne SuperTurbocharger. This is a device where the turbocharger shaft and engine crankshaft are mechanically linked via a CVT, and depending on the CVT ratio used, offers turbocharging, supercharging, or turbocompounding. Significant levels of downsizing are apparently obtainable, whilst fulfilling the three critical factors listed at the beginning of this section.

Other systems – namely pressure wave supercharging, Hyperbar, and Rankine bottoming cycles – were also reviewed, but ruled out for the purposes of downsizing for a combination of reasons: cost; complexity; added bulk and weight; limited benefit to performance; and limited (or negative) effect on fuel efficiency.

In conclusion, then, two pressure charging concepts stand out as viable for offering substantial levels of effective downsizing, and as such are deemed worthy of further research:

- A combined charging system comprising a conventional turbocharger in conjunction with a declutchable supercharger driven through a CVT;

- A turbocharger which is mechanically linked to the engine crankshaft via a CVT, thereby offering potential for turbocharging, supercharging, and turbocompounding.

The latter concept of CVT-turbocompounding is intriguing, but the potential energy recovery benefits of turbocompounding in passenger car applications (which predominantly operate at low engine speeds and part load) are considered to be negligible – this technology is more suitable for heavy duty applications. The combined charging system also offers greater mass flow range and pressure ratio capabilities. For these reasons in particular, the combined charging system with CVT-supercharger will be taken forward for further investigation in this thesis.

Chapter 3 HSDI Diesel Engine: Low-Speed Torque Investigation

This chapter details an initial simulation based investigation into the novel forced induction boosting system identified in the literature review as a possible solution to improving low speed engine torque and transient response of future downsized and existing turbocharged engines. This system comprises a centrifugal-type supercharger driven from the engine crankshaft via a CVT, which acts as a pre-boost to a traditional fixed geometry turbocharger. The concept was modelled around an existing baseline high speed direct injection (HSDI) diesel engine model featuring a variable geometry turbocharger (VGT).

Conclusions are drawn comparing the potential of the proposed system to the baseline engine in terms of brake specific fuel consumption (BSFC), and both steady state and transient performance. A design of experiments approach is applied to investigate the effect of supercharger compressor size, turbocharger compressor and turbine size, CVT ratio and engine compression ratio on the system performance. Optimisation techniques are then applied to identify the best settings for these parameters in the proposed system. Transient simulation was undertaken in a Matlab/Simulink Ricardo WAVE co-simulation environment to develop the required control strategies for the CVT supercharger.

3.1 Methodology

From a review of literature, it is apparent that combined charging arrangements involving a centrifugal supercharger have not yet been reported – and certainly not with drive transmitted through a CVT. It is this concept – as shown in the schematic diagram in Figure 3.1 – that has been investigated at this point.

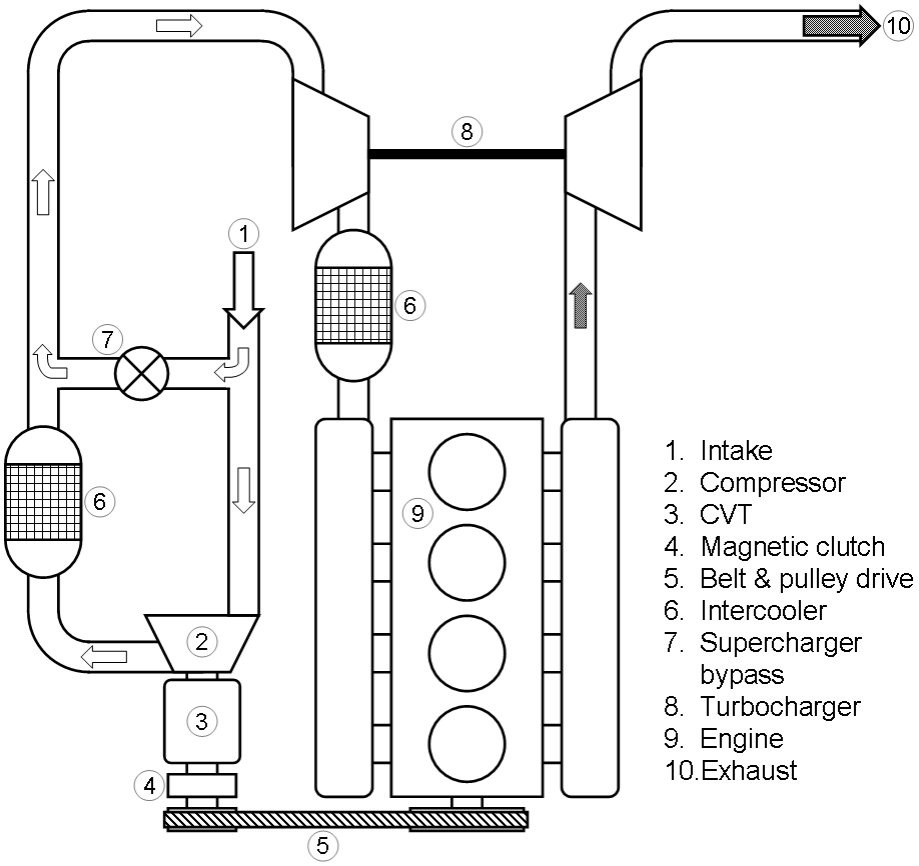

Figure 3.1 – Schematic diagram of the proposed twincharged engine

3.1.1 Ricardo WAVE Engine Model

The primary tool for analysis was Ricardo WAVE – an ISO approved 1D engine and gas dynamics simulation software package capable of complete engine performance prediction and optimisation, and as such ideally suited to the task. The analysis was based on a previously validated [88] Ricardo WAVE engine model of a 2.0 litre in-line 4 cylinder HSDI diesel engine, employing common rail fuel injection and a variable geometry turbocharger – see Table 3.1. The combustion process was described using a correlational compression ignition Wiebe model, whereby ignition delay and premixed burn fraction are computed using the fuel cetane number and in-cylinder temperature and pressure; heat transfer was represented by a Woschni

model [89]; blow-by effects were ignored. These assumptions and simplifications account for the differences between the resulting model and the experimental data (Figure 3.2). However, the level of correlation of these bulk parameters was considered adequate for the purposes of this study. (Please note that the level of experimental uncertainty in the results presented in Figure 3.2 is unknown.)

Table 3.1 – Baseline engine parameters

Parameter	*Value*
Bore (mm)	86
Stroke (mm)	86
Displacement (cc)	1998
Con Rod Length (mm)	152
Compression Ratio	19:1
Max Power (kW) @ Rated Speed (rpm)	96, 4000
Max Torque (Nm) @ Rated Speed (rpm)	330, 1900

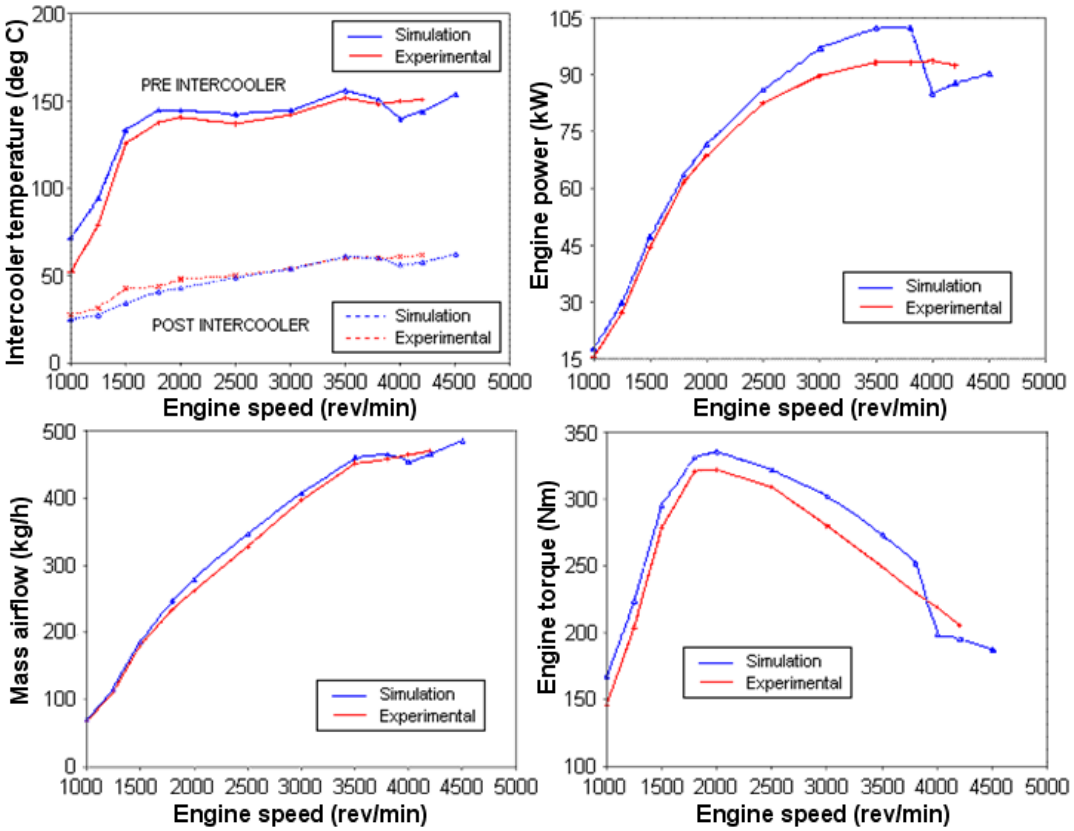

Figure 3.2 – Comparison of experimental data and simulation results for baseline engine

The standard engine model was run at a range of engine speeds along the limited torque curve (LTC) to provide a baseline for the performance characteristics. The twincharged concept was modelled by modifying the baseline model in the following ways. The standard intercooler was duplicated and placed between the two compressors to account for the increase in charge temperature caused by the additional compressor. To avoid the complexities of adapting the control of the variable geometry rack position to the new configuration, the turbine was made pseudo-fixed geometry by setting the mechanism to fully open.

A bypass valve arrangement was implemented around the supercharger, the purpose of which is to allow the supercharger to be disengaged once it has reached the limits of its speed and mass flow range, and the intake air flow to be uninterrupted. By this stage – around 3000 rpm at full load – the turbocharger provides sufficient boost unaided. A magnetic clutch, similar to those used on automotive air-conditioning compressors, would allow the supercharger to be engaged and disengaged depending upon engine speed and load requirements. This type of arrangement has been previously explored by various groups [34][35][59], and is also in place on the Volkswagen TSI engine mentioned previously [13]. The changes implemented in the model can be seen in Figure 3.3 and Figure 3.4.

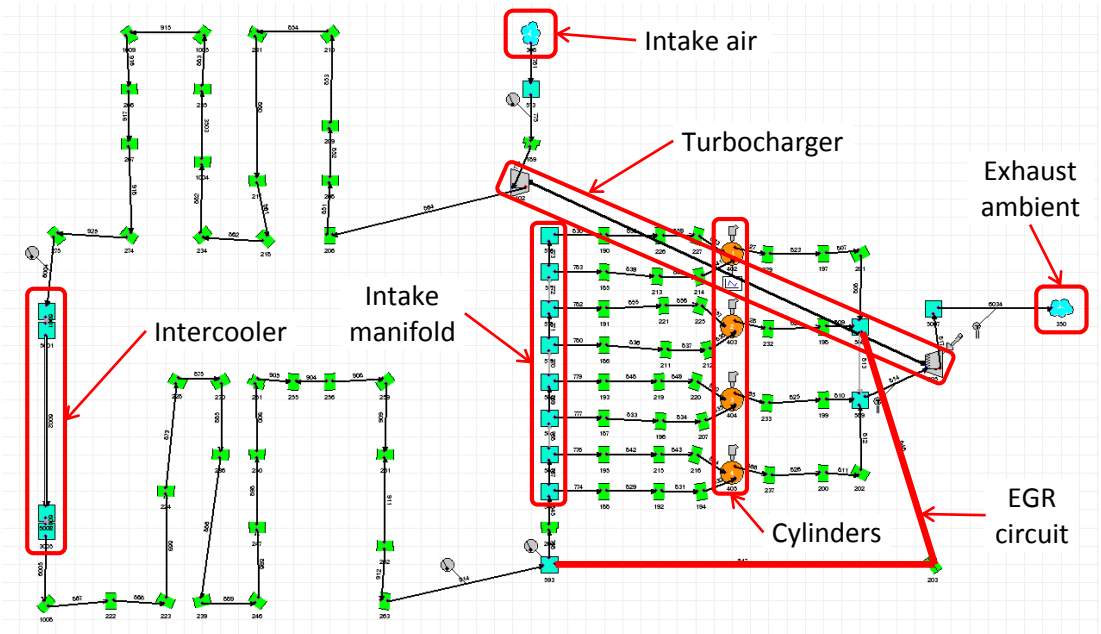

Figure 3.3 – Baseline engine WAVE model

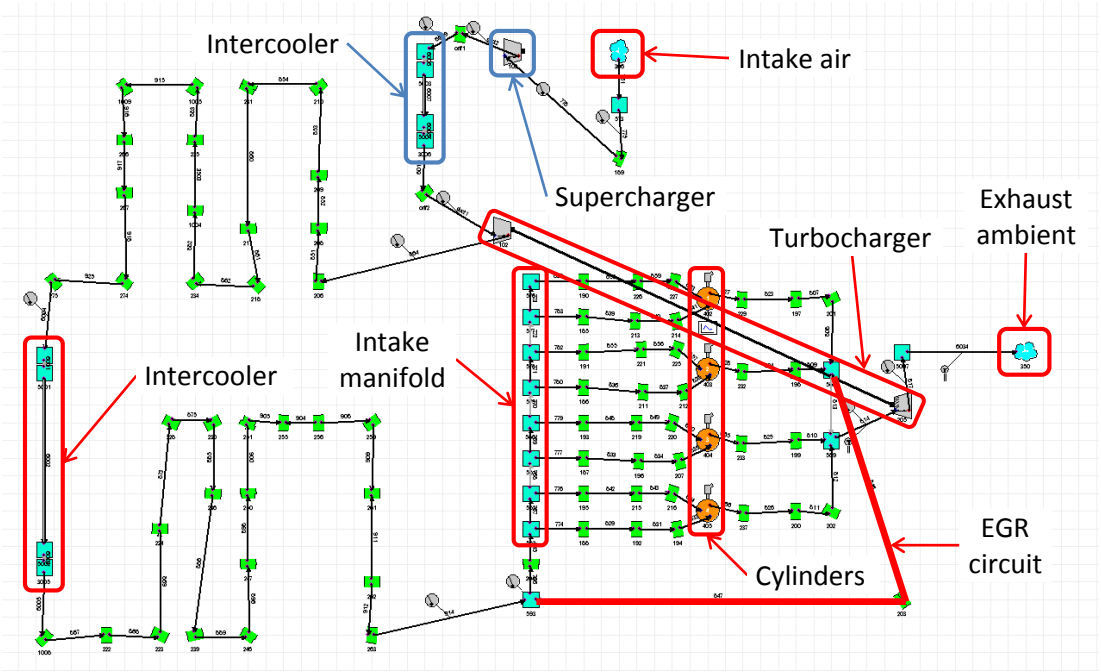

Figure 3.4 – Twincharged engine WAVE model

As this investigation was to assess the potential of the concept, the original turbomachinery was retained (with the supercharger compressor a duplication of the original turbocharger compressor) – this was done to avoid the complexities of matching completely new turbomachinery, and sourcing a suitable commercially available supercharger. Instead, the existing turbomachinery components were 'scaled' – the WAVE software has this functionality, producing the effect of having a different size of compressor or turbine, but with similar flow characteristics. Scaling has the following effects:

For mass flow:

$$\dot{m}_{corr} = \dot{m}_{act} \sqrt{\frac{T_{in,act}}{T_{in,ref}}} \frac{p_{in,ref}}{p_{in,act}} \left(\frac{d_{ref}}{d_{act}}\right)^2$$

Equation 3.1

For speed:

$$n_{corr} = n_{act} \frac{d_{act}}{d_{ref}} \sqrt{\frac{T_{in,ref}}{T_{in,act}}}$$

Equation 3.2

For torque:

$$\tau_{corr} = \tau_{act}\left(\frac{d_{ref}}{d_{act}}\right)^3 \frac{p_{in,ref}}{p_{in,act}}$$

Equation 3.3

In which $\frac{d_{act}}{d_{ref}}$ is defined as the scale factor (SF).

For inertia:

$$I_{turb,act} \propto m_{turb,ref}\left(\frac{d_{turb,act}}{d_{turb,ref}}\right)^5$$

Equation 3.4

$$I_{comp,act} \propto m_{comp,ref}\left(\frac{d_{comp,act}}{d_{comp,ref}}\right)^5$$

Equation 3.5

It is assumed that isentropic efficiency is unaffected by the scaling process – although there would likely be a reduction in efficiency with reduced component size, due to effects such as increased tip leakage.

3.1.2 Performance Constraints

The following constraints were imposed upon the analysis and during the optimisation process in order to provide realistic and reasonable results:

- Maximum cylinder pressure < 160 bar
- Air-fuel ratio (AFR) > 17:1

160 bar peak cylinder pressure was deemed an acceptable limit given that much higher pressures (180-200 bar) have been demonstrated on both standard production and research engines [18][30]. The 17:1 AFR limit was imposed as a smoke limitation measure and was based on the lowest value of the baseline engine. Together with these absolute limits, at each stage the CVT ratios were evaluated to ensure they were within a feasible range. Furthermore, a torque limit of 400 Nm was applied to avoid excessive transmission loads.

3.1.3 Design of Experiment Construction and Evaluation

The Model Based Calibration Toolbox (MBC) is a set of design tools for design of experiment (DoE), statistical modelling and calibration of complex systems, based in the Matlab environment. Following the initial model set up, the next stage was to apply DoE techniques to optimise the scaling factors of the turbomachinery, as well as reducing the geometric compression ratio of the engine to account for the increased boost pressures. The complex interdependence of each of the parameters to be optimised necessitated a formal approach. The ranges for the eight input parameters are specified in Table 3.2.

Table 3.2 – Design of Experiments factors

Parameter	*Min*	*Max*
SC factor	0.8	1.1
TC factor	0.9	1.2
TT factor	0.9	1.2
CR	16	19
Supercharger drive ratio (incorporates CVT ratio)	0	250
Engine speed	1000 rpm	4500 rpm
AFR	17	22
SOI	-30	0

The MBC toolbox was used to develop the experimental test plan and to fit response models to the acquired WAVE model data. An initial simulation screening experiment of 500 points of a grid-type 'optimal' design was used to fill the corners and outer edges of the design space; these were then augmented with 1500 points determined using a Halton Sequence 'space-filling' design to maximise coverage of the variables' ranges in the most efficient way. Within the global maximum and minimum values for the supercharger drive ratio, possible test points were constrained in relation to engine speed in order to avoid over-speeding the supercharger. Also, assuming that the supercharger would be engaged from 1000 rpm to at least 2500 rpm in order for the engine to provide adequate low speed torque, the region of low speed and low drive ratio was avoided. This was done to maximise the system knowledge and resulting predictive capability in the operating

region that was of greatest interest. The constrained region is shown in Figure 3.5 – the blue area represents the allowable values of supercharger drive ratio.

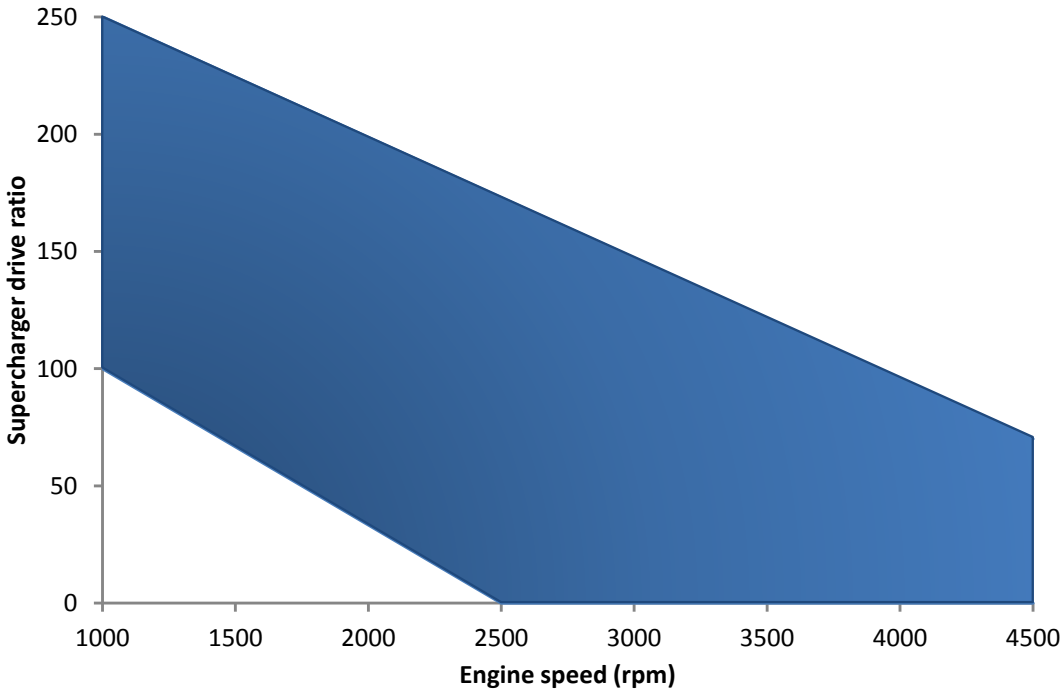

Figure 3.5 – Supercharger drive ratio constrained region

The effectiveness of coverage of the design space can be seen in Figure 3.6 – it is particularly worth noting the even distribution along the edges and corners. This diagram shows the coverage of four of the design parameters: engine speed (x-axis); compression ratio (y-axis); AFR (z-axis); and fuel injection timing (colour gradient). The remaining four parameters span their respective ranges within the displayed points.

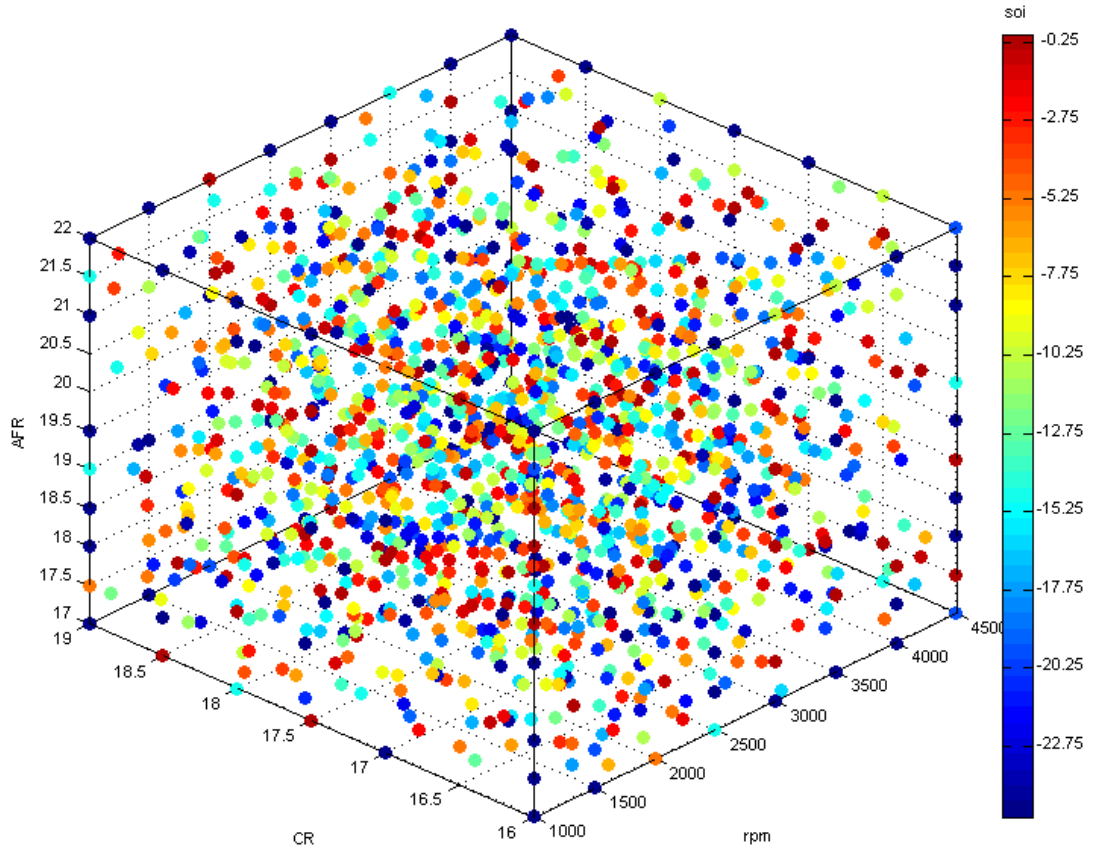

Figure 3.6 – Four-parameter DoE design projection: engine speed (x-axis); compression ratio (y-axis); AFR (z-axis); and fuel injection timing (colour gradient)

Beyond the visual inspection of the experiment design, a quantitative assessment tool – Prediction Error Variance (PEV) – was used to evaluate the effectiveness of the experimental design. This also gives some indication of the resulting predictive capability of the response models that will be fitted to the results (although the accuracy of these model predictions is also dependent on any errors in the data). For PEV>1, then any errors in the data are multiplied; conversely, PEV<1 reduces the effects of errors during the model fitting process. PEV values tending to zero indicate that the model should provide good predictions at that point. Details of the mathematical derivation for PEV can be found in [90].

Using only a 'space-filling' design it is relatively simple to produce low values of PEV in the middle of the design space; but the mathematical sequences in this case do not cover the outer limits of the variable ranges sufficiently, resulting in increased PEV figures in these outer regions. The grid-type 'optimal' design, on the other hand, does cover these extremes more satisfactorily, but is less capable of

producing an overall coverage of the variable ranges due to its more structured generation method. Consequently, the combination of the two design methods yields good PEV throughout the design space – as shown in Figure 3.7. Even though the combination of parameter values used here give a 'worst case', the PEV is low throughout the design space, which was reflected in the quality of the response models fitted to the results (as discussed below).

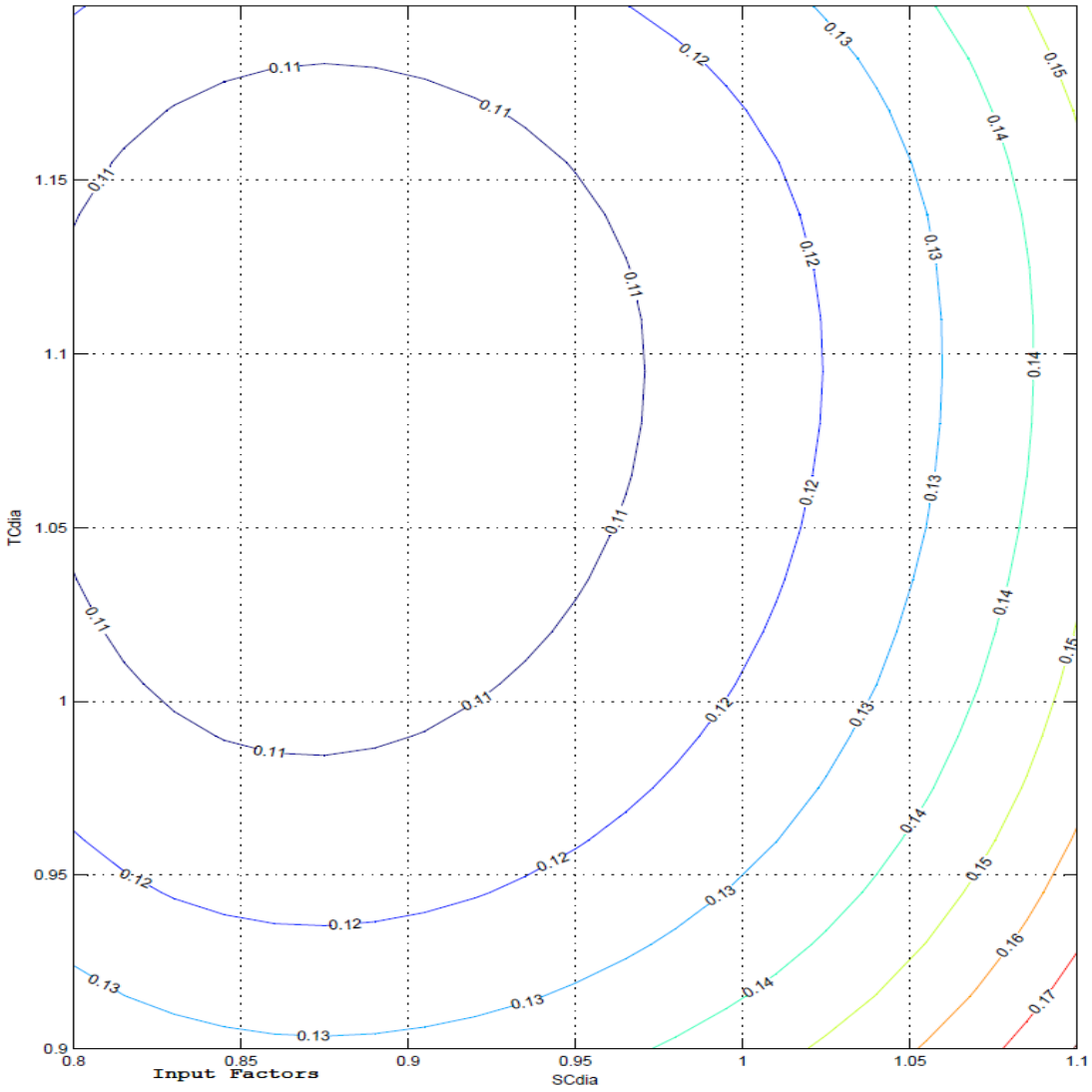

Figure 3.7 – PEV contour plot of 2000 point experimental design. TC scaling factor against SC scaling factor, remaining parameters held constant (rpm: 1000, CR: 19, AFR: 22, SOI: -25, CVT ratio: 250)

3.1.4 Response Models

The responses of significant engine variables (such as brake torque and peak cylinder pressure) were subsequently modelled within MBC. The quality of each response model was assessed using a number of criteria:

- Root Mean Squared Error (RMSE) – a basic measure of how closely the model fits the data, giving the average difference between the raw data and the model. A low RMSE value indicates a good fit. (Note that RMSE values are proportional to the order of the data values.)

- Coefficient of determination (R^2) – a value between zero and one denoting how closely a regression line fits the data set; an R^2 value of one means a perfect fit, and values approaching one indicate a good fit.

- Visual inspection of the response model when plotted as surface, and cross sections of this surface. Although this is a subjective assessment, it was important to include this to avoid 'over-fitting' the data, and the response model exhibiting unrealistic behaviour.

Although a number of different types of response model are available for use – such as polynomial, radial basis function (RBF), hybrid RBF, and neural networks – for the majority of the variables a neural network modelling approach was required. This was due to the high complexity of the system, resulting from the relatively high number of input parameters. Simple response models did not fit the data adequately, but judgement was required to avoid over-fitting the data. Improving the RMSE and R^2 values is simply a matter of increasing the complexity (number of layers) of the neural network model, but visual inspection often revealed the model to be unrealistic.

For example, Figure 3.8 shows a neural network model fitted to a complex BSFC response, which has RMSE and R^2 values of 3.62 and 0.996 respectively, both indicating a very good fit to the data. (Please note that the data shown in Figure 3.8, Figure 3.9 and Figure 3.10 are from a model not used in this thesis, and are purely intended to illustrate the described process.) The upper graph shows the standardised residuals of the model – which are defined as the difference between the observed value and the value estimated by the model (residual) divided by an

estimate of its standard deviation. Again, low standardised residual values are desirable, and suggest a good model fit; in MBC values greater than 3 are classed as outliers (circled in red). The lower graph shows the values predicted by the model plotted against the observed values, and the fit is clearly very good, with only a small number of outliers.

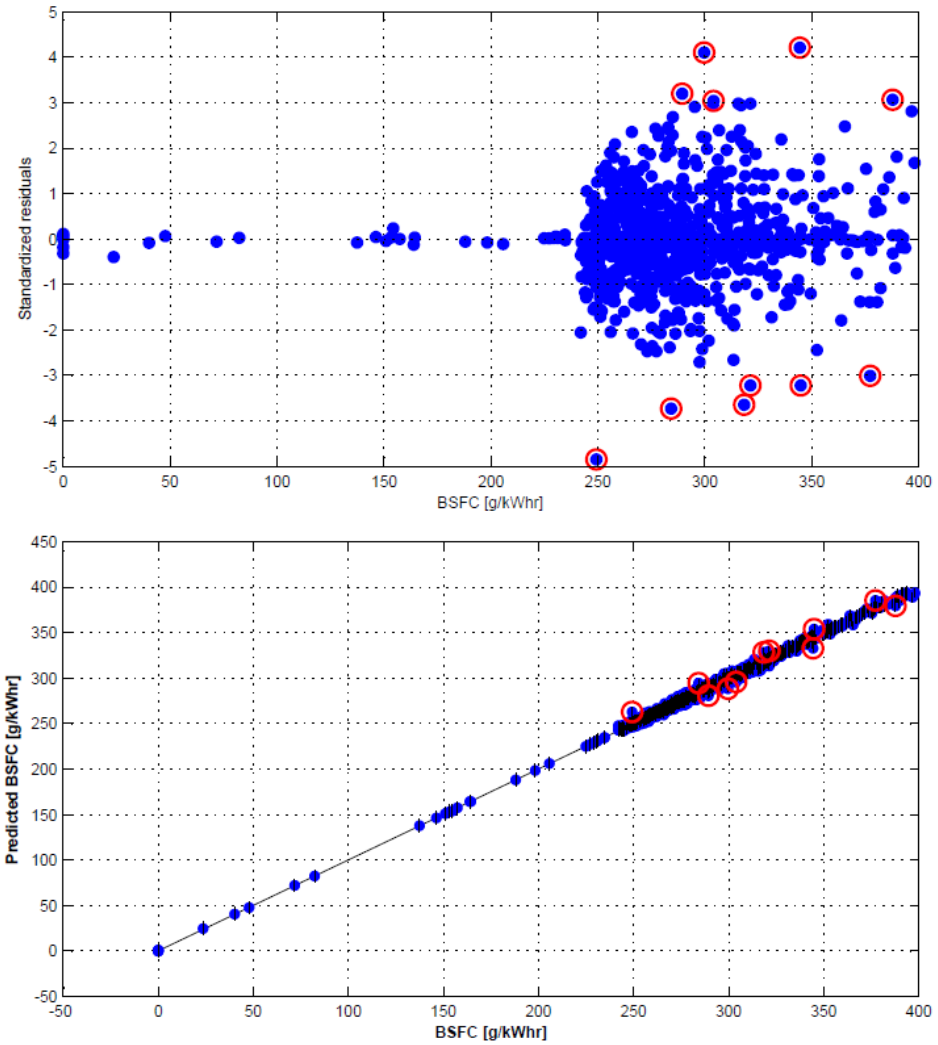

Figure 3.8 – Example response model viewer: a) standardised residuals; b) predicted vs. observed results

However, when upon evaluating a corresponding surface plot of the response model, it is clear that the model is over-fitted and not representative of the expected actual behaviour (Figure 3.9). In this case, a less complex model would be used; although likely to be less well fitted, statistically speaking, it would be more representative of actual behaviour expected to be observed, which is of great importance when subsequently used in optimisation algorithms.

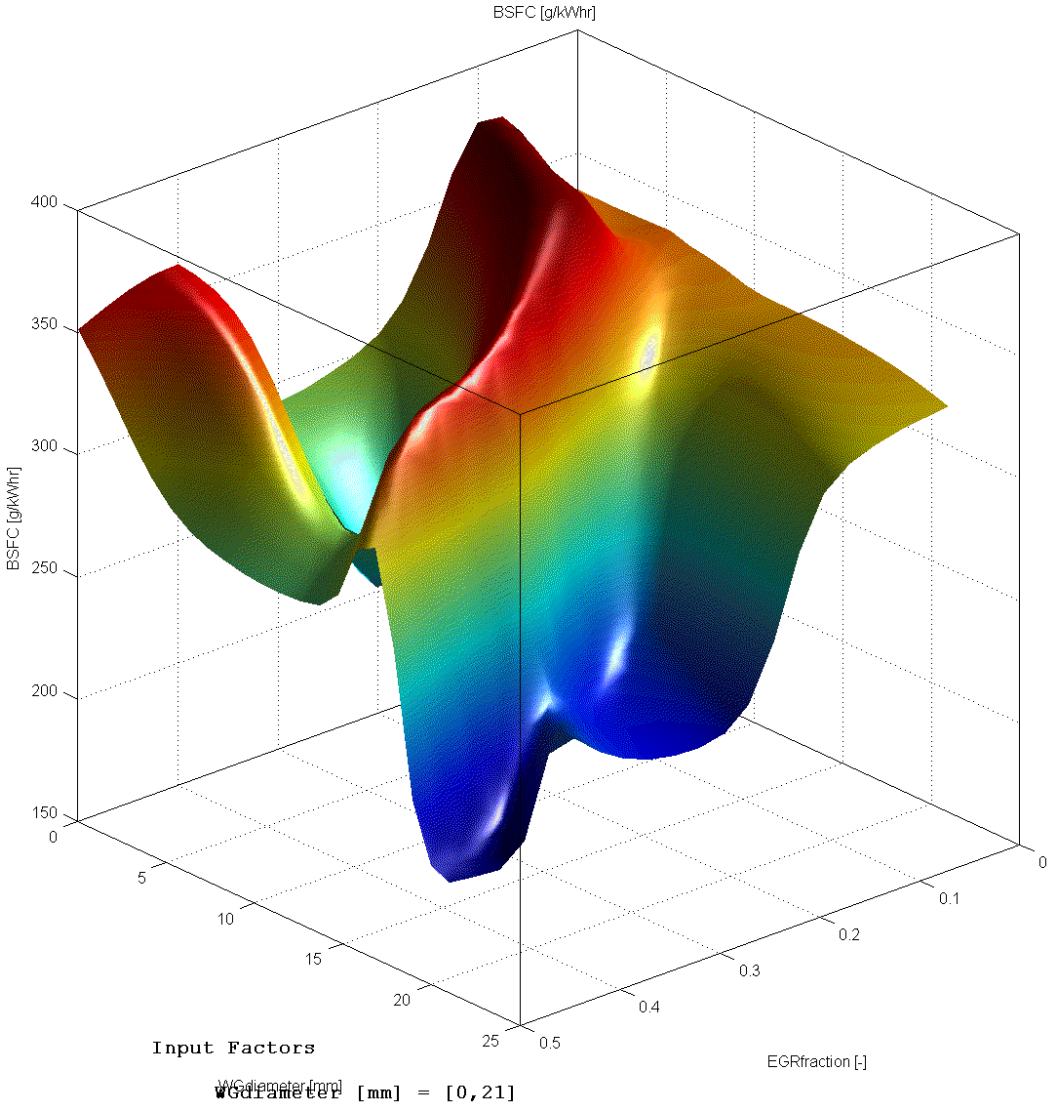

Figure 3.9 – Example response model 3D surface plot, showing unrealistic behaviour of the over-fitted response model

In conjunction with the 3D surface plots, cross-sections of the response model were also considered. This essentially isolates the effects of individual parameters (with confidence intervals), displayed in graphs corresponding to each parameter. For example, Figure 3.10 shows response model cross-section plots of predicted BSFC response to four separate parameters: intake valve timing, exhaust valve timing, CVT ratio, and compressor bypass orifice diameter. For significant sections of the displayed trends the confidence bands are very close, signifying a high level and consistency of input data and a well-fitted model. However, there are regions where the behaviour is clearly erratic and the confidence bands are wide. This may not be a problem, if the combination of parameter values in question will not be used in practice. Therefore, a certain level of consideration and judgement must be used.

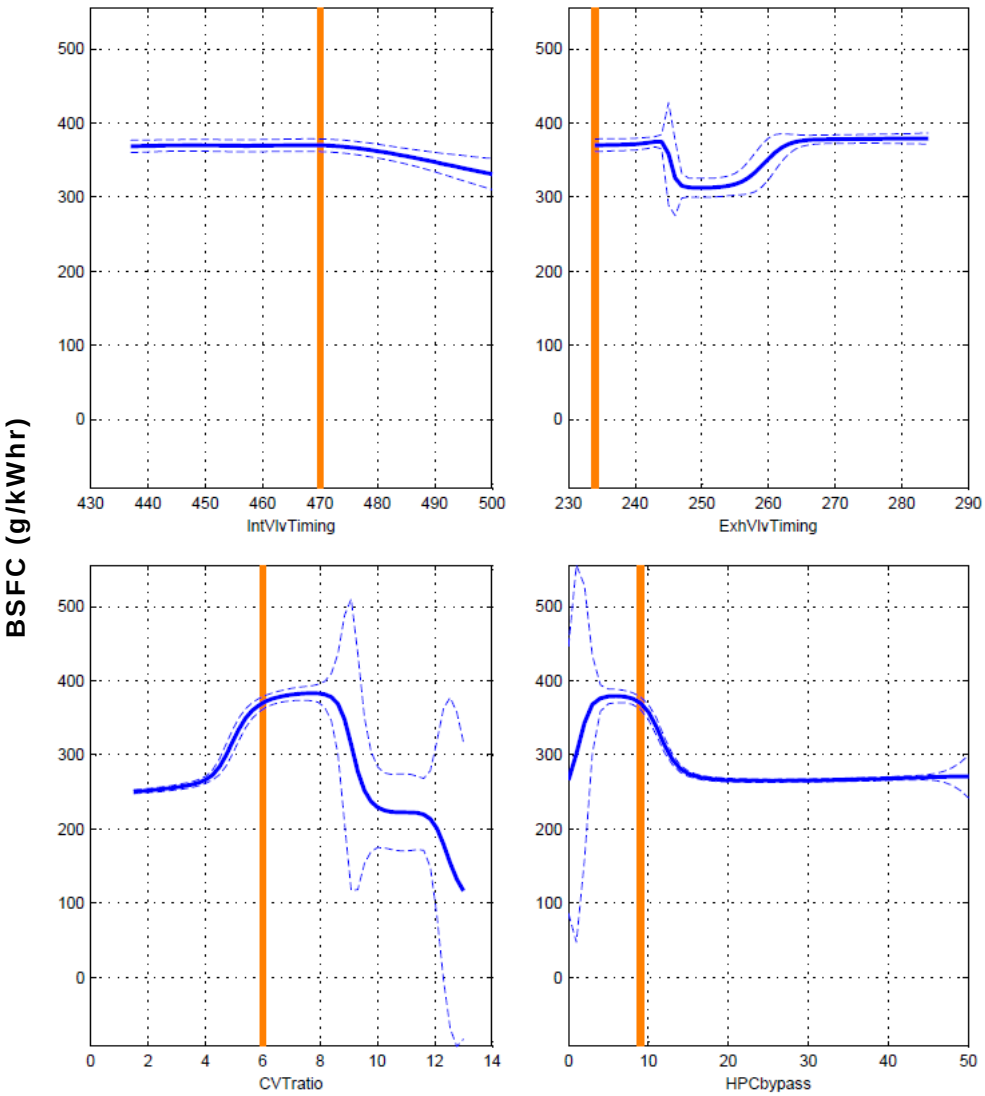

Figure 3.10 – Example response model cross-section plots, showing predicted BSFC response (g/kWhr) to four parameters at specific values: a) intake valve timing (470 CAD ATDCF); b) exhaust valve timing (234 CAD ATDCF); c) CVT ratio; d) compressor bypass orifice diameter (mm). The dashed blue lines are confidence bands.

3.1.5 Parameter Optimisation

Once the response models had been evaluated satisfactorily they were imported into the calibration generation (CAGE) element of MBC, to form the plant model for the subsequent optimisation process. A single-objective gradient search optimisation algorithm was chosen for the task – 'foptcon', which is based on the Matlab algorithm 'fmincon' (find minimum of constrained nonlinear multivariable function). A relatively large number of start points (20) were also used to prevent false (i.e. local instead of global) minima and maxima being obtained.

Although the primary aim of this section of the investigation was to assess the low-speed torque augmentation potential of the CVT-supercharger, of secondary interest was seeing whether increased power density could be achieved due to the sequential arrangement allowing a larger turbocharger. Hence, initially, a sum optimisation method was applied to maximise the sum total of the modelled torque response over the engine speed range. The torque response was evaluated at 250 rpm intervals over the range (1000-4500 rpm) – using the engine speed as a fixed variable and the remaining parameters as free variables. Using a sum optimisation (as opposed to a point-to-point optimisation, where torque would be maximised for each operating point individually) allowed the constraints of constant turbomachinery scaling factors and compression ratio to be applied across the speed range; otherwise these variables would be allowed to fluctuate with each operating point. However, maximising for torque in this manner made it difficult to simultaneously constrain the optimisation for good fuel efficiency. The optimisation objective was therefore revised to minimise the sum of fuel consumption (BSFC) across the engine speed range. In order to achieve a minimum (arbitrary) target torque curve, a constraint for minimum torque at each engine speed was added. This constraint and the others applied during the optimisation process are summarised in Table 3.3.

Table 3.3 – Constraints applied to CAGE optimisation

Constrained parameter	*Purpose*	*Type of constraint*	*Min allowed value*	*Max allowed value*
Torque	Achieve target torque curve	1D table	300 Nm @ 1000 rpm 350 Nm @ 1500-2000 rpm 275 Nm @ 3500 rpm 200 Nm @ 4500 rpm	-
SC scaling factor	↑ Keep parameter value constant across engine speed range ↓	Gradient	-	-
TC scaling factor		Gradient	-	-
Compression Ratio		Gradient	-	-
Max cylinder pressure	↑ Limit max value ↓	Value limit	-	160 bar
Turbine inlet temperature		Value limit	-	1250 K
Compressor pressure ratio (both compressors)	Avoid compressor surge region	1D table	Dependent on (normalised) mass flow	
Supercharger drive ratio (incorporates CVT ratio)	Prevent SC over-speeding	1D table	-	250 @ 1000 rpm 70 @ 4500 rpm

3.1.6 Simulink–WAVE Co-Simulation

A further aspect of air handling system performance is its capability to respond during transient events. The aim of this part of the investigation was to predict the response to a fixed speed 'tip-in' transient – i.e. a step in fuel quantity from a low to high value. This is designed to simulate the driver depressing the accelerator pedal – or 'tipping-in' – at light load and demanding full load from the engine [21].

To undertake this work the WAVE engine models were integrated in to a co-simulation environment with Simulink to control the engine actuators in response to sensors defined in the engine model. A block diagram was constructed around the twincharged engine architecture (with original supercharger compressor) with engine speed and fuel demand as the main user input parameters. From the mass air flow (MAF) sensor, an AFR/smoke limit feedback loop was created. Boost demand and CVT ratio maps were developed based on the respective values from the full load steady state results. These were included as lookup tables as part of a boost demand feedback loop in the block diagram – a proportional-integral (PI) controller was used to convert the boost error into a CVT ratio, which was then added to the value from the CVT ratio lookup table (essentially providing a basic 'feed-forward' action). A function was also included to limit the rate of change of CVT ratio, since it cannot realistically change instantaneously. Turbocharger speed, peak cylinder pressure, and turbine inlet temperature were also monitored. Figure 3.11 shows the complete block diagram for the twincharged engine simulation.

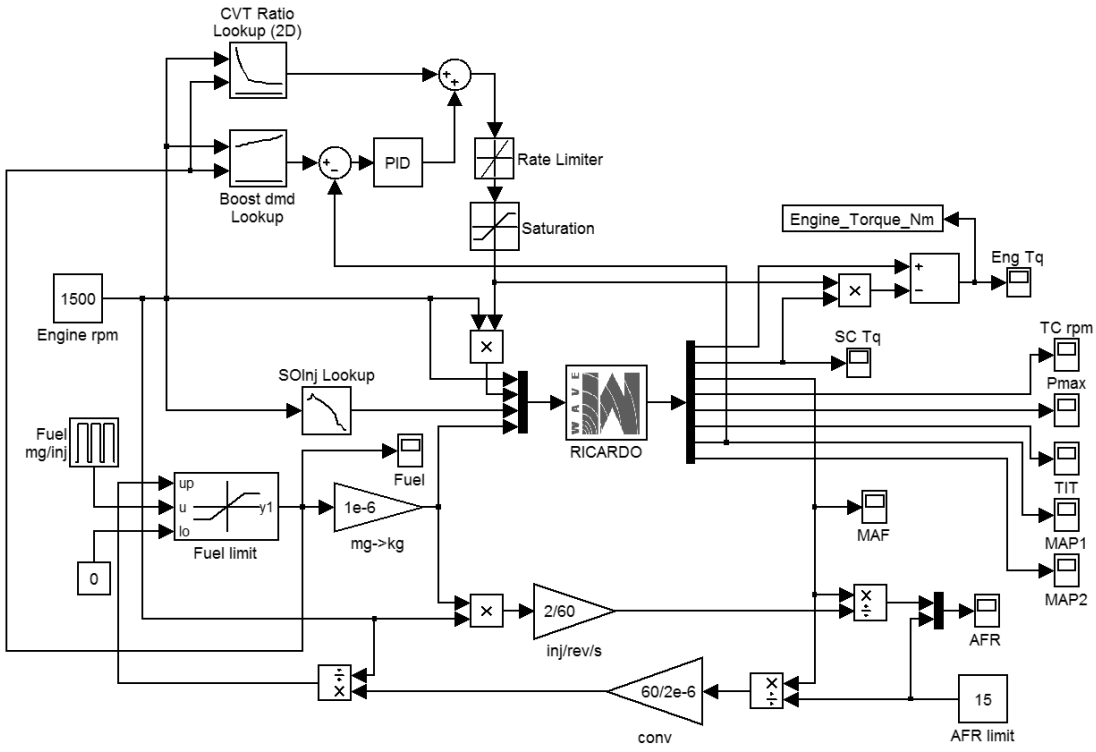

Figure 3.11 – Simulink block diagram – twincharged engine

A similar model was developed for the baseline engine (Figure 3.12). The boost demand lookup table was updated with the relevant full load steady state data, and a PI controller was developed to drive the VGT rack position actuator. (The gains for

the PI controllers for both the VGT rack and the CVT were empirically determined to give a good balance between rise time and stability.)

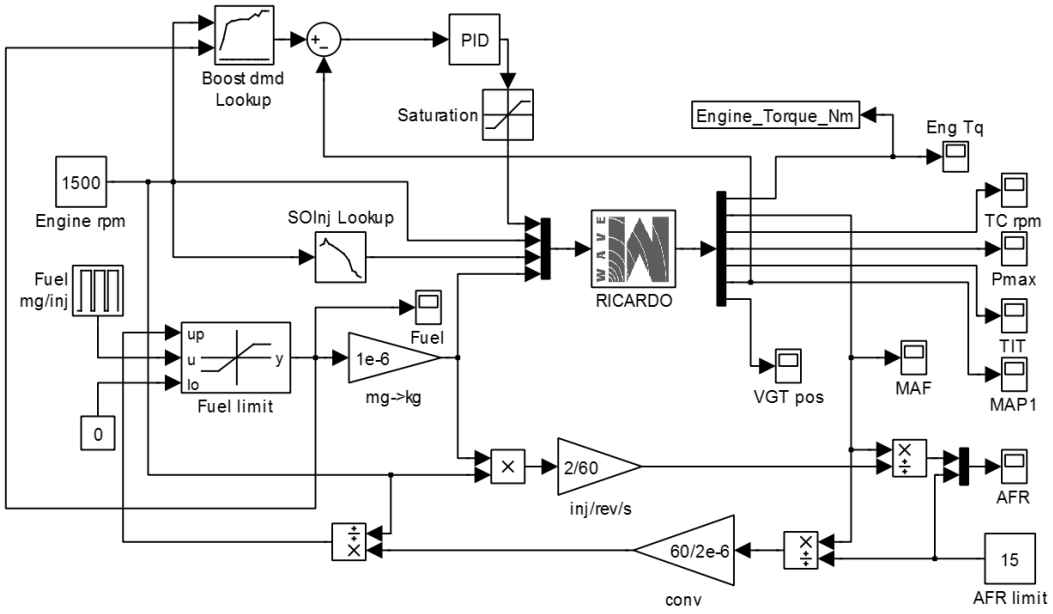

Figure 3.12 – Simulink block diagram – baseline engine

Both the baseline and optimised twincharged models were then tested using a step in fuel demand from 10 mg/injection to an upper value which was dependent on engine speed. For the baseline engine, these upper values were determined from the steady state LTC. As for the twincharged engine, the following logic was applied to allow a more direct comparison: where equal or greater torque was produced, the same fuel values as the baseline were used; otherwise, the fuelling was increased to produce the same torque as the baseline (this was only required at the 1750 and 2000 rpm test points). In all cases the fuel demand was set to a constant 10 mg/injection for the first two seconds to allow the simulation to stabilise prior to commencing the tip-in. Tests were performed at 250 rpm intervals from 1000-2000 rpm inclusive.

3.1.7 CVT Ratio Control

The linearly interpolated lookup tables that were constructed for boost demand and CVT ratio 'feed-forward' action were perhaps a little simplistic, as was the tuning of the PI controllers – although their performance was deemed satisfactory for the purpose of this investigation. Improved transient response may be achieved if more

effort were spent on this task; however, it is likely that this would best be done with physical hardware.

A more crucial feature was the simplified rate of change of CVT ratio. This was modelled by a simple linear rate limit block, with an allowable rate-of-change of +/-320 per second. This value was reached from the assumption that the ratio change of 200:1-40:1 could be achieved in 0.5 seconds, and hence this ratio gap could be traversed twice in one second. From experience of the MCVT this is a realistic target and adequately demonstrates the concept.

3.2 Design of Experiments and Optimisation Results

3.2.1 Response Models

A summary of the response models produced from the DoE simulations is given in Table 3.4. The range of each variable is given in order to provide context for the RMSE values, since these are scale-dependent. In terms of statistical quality, all of the response models are excellent, with close to perfect R^2 values; relative to their respective ranges, the RMSE values are also suitably low. This good statistical accuracy is a benefit of the large number of data points provided by the simulation environment. The visual model quality and trends are discussed below.

Table 3.4 – Summary of response models

Response variable	*Response model used*	*R^2 value*	*RMSE*	*Variable range*
Torque (Nm)	Neural network	0.999	4.271	70-700
Max cylinder pressure (bar)	Neural network	0.998	2.574	50-300
Turbine inlet temperature (K)	5th order polynomial	1	3.476	550-1500
SC normalised mass flow rate (kg/hr)	Neural network	0.999	4.810	5-500
TC normalised mass flow rate (kg/hr)	Neural network	0.998	6.765	50-700
SC pressure ratio	Neural network	1	0.012	1-3.5
TC pressure ratio	Neural network	0.998	0.027	1-3
SC normalised compressor speed (rpm)	3rd order polynomial (cubic)	1	0.221	0-450000
Fuel mass flow rate (kg/hr)	Neural network	1	0.160	3.5-35

It is worth noting that a response for BSFC is conspicuously absent from this list – although an adequate (in terms of the statistical measurements) response model could be produced, BSFC was instead calculated from the response models of torque and fuel flow rate, as this was found to give more accurate and reliable results when used as the basis for the optimisation objective.

In order to calculate BSFC, a function for brake power was first created from the torque response model and the engine speed variable:

$$Power[kW] = \frac{Torque[Nm] \times EngineSpeed[rpm] \times (2\pi/60)}{1000}$$

Equation 3.6

Then BSFC could be calculated from engine power and the fuel flow rate response model:

$$BSFC[kg/kWhr] = \frac{FuelFlow[kg/hr]}{Power[kW]}$$

Equation 3.7

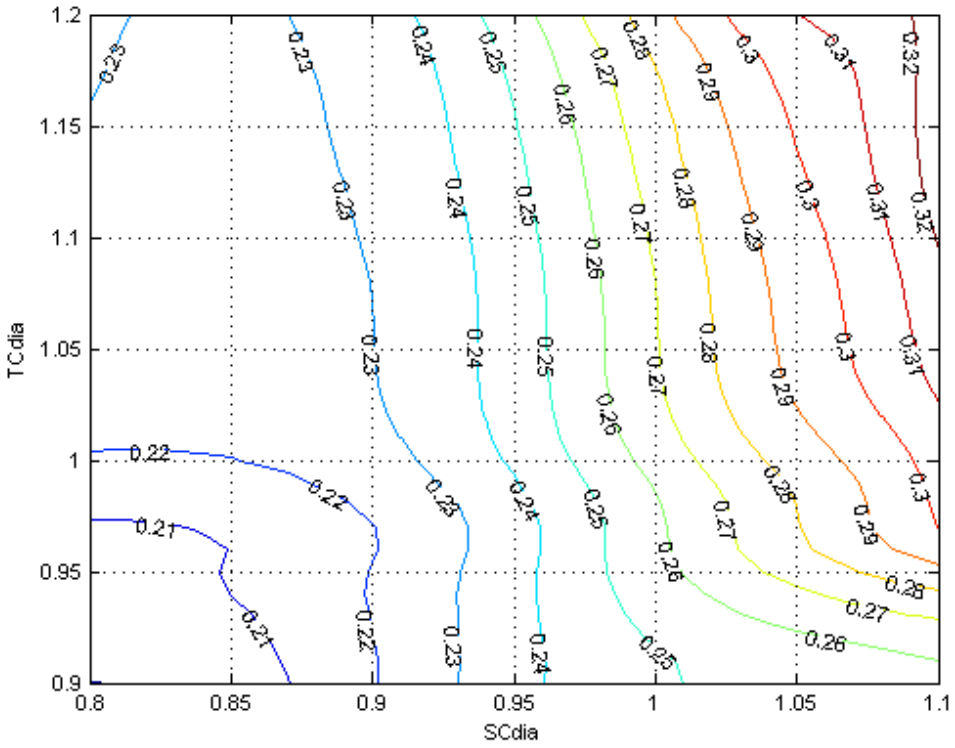

Figure 3.13 – Cross-section through calculated BSFC (kg/kWhr) function. TC scaling factor against SC scaling factor, remaining parameters held constant (rpm: 1250, CR: 18, AFR: 18, SOI: -5, CVT ratio: 150)

Sections through the resulting BSFC function are shown in Figure 3.13 and Figure 3.14. It is worth noting that great care must be taken when evaluating multi-parameter functions and response models in this way, since a single plot is only a 'snapshot' view of the system, with a single set of fixed parameter values; multiple combinations of parameter values must be considered, as well as the corresponding

effects on other key responses, in order to gain the overall picture. An example of this is when evaluating the function at a low engine speed a higher supercharger scaling factor is shown to result in increased fuel consumption (Figure 3.13). However, taking into account the fixed drive ratio, although the actual compressor speed is the same, due to the effects of the scaling factor the relative compressor speed is higher (see Equation 3.2) – hence the parasitic power required by the supercharger is higher. As a side issue, the overall brake torque would be increased due to the higher boost pressure. There is also a slight efficiency advantage to reducing the turbocharger scaling factor.

The situation is more straightforward at higher engine speeds when the supercharger is effectively removed from the system (zero drive ratio) and bypassed. Here the benefit to efficiency of increased turbocharger size is clear (Figure 3.14). The trade-off of efficiency and performance across the speed range shows the necessity for the formal optimisation process.

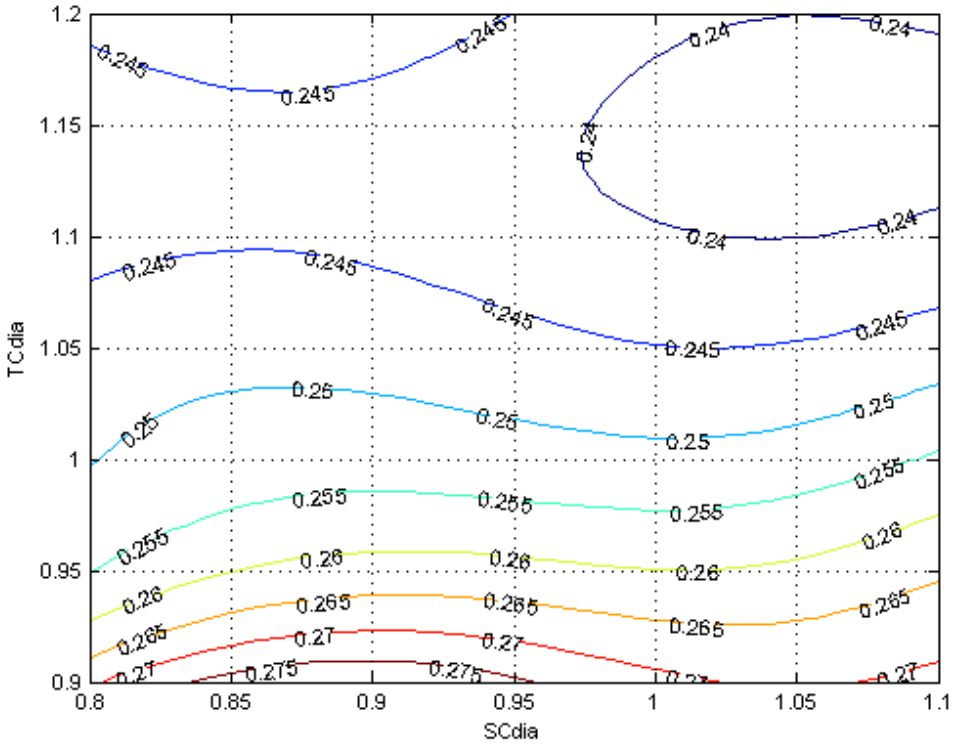

Figure 3.14 – Cross-section through calculated BSFC (kg/kWhr) function. TC scaling factor against SC scaling factor, remaining parameters held constant (rpm: 4000, CR: 18, AFR: 19, SOI: -20, CVT ratio: 0)

Figure 3.15 and Figure 3.16 give cross-sections through the torque response model. With the exception of at low supercharger drive ratios, very narrow confidence bands are displayed throughout – as mentioned above, this is a benefit of the large number of data points. The reason for the wide confidence bands at low supercharger drive ratios is the constraint placed on the range of values of this variable when creating the experiment test plan – no data was collected in this region, hence the model is heavily extrapolated. As would be expected, AFR has a linear effect on torque, as increasing fuelling results in a corresponding proportional increase in torque.

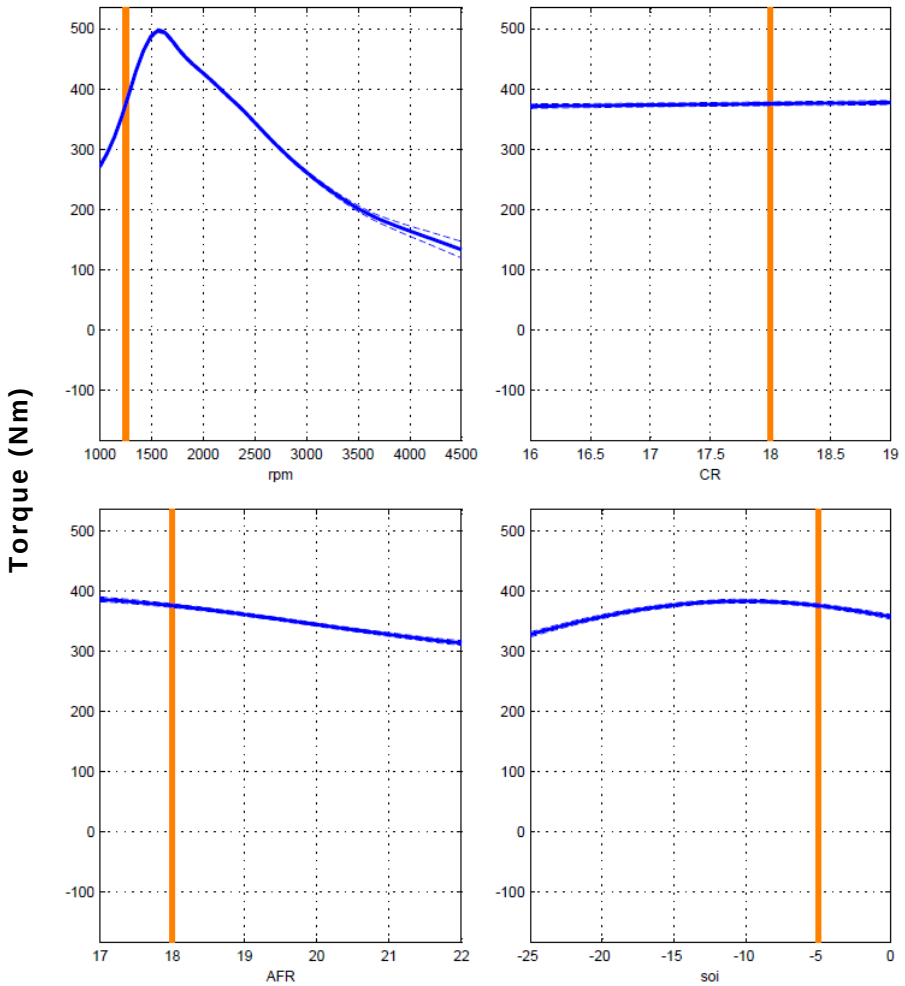

Figure 3.15 – Cross-section through Torque (Nm) response model at 1250 rpm, showing effects of engine speed (rpm), compression ratio, AFR, and fuel injection timing (CAD ATDCF)

As Figure 3.16 shows, the supercharger drive ratio also has a largely linear effect on torque, with the exception of at high ratios where the curve hits a plateau as the supercharger begins to choke. Theoretically speaking, decreasing the turbocharger size would effectively reduce the turbine area, increasing its speed, and resulting in increased intake pressure and thus engine torque – this effect is seen in the response model. Increasing the supercharger size would also increase the torque (up to a point), as the compressor would be running at a relatively higher speed (and pressure ratio), taking into account the effects of the scaling factor on map speed. It is worth noting, however, that these response models are incapable of accounting for such aspects as the compressor surge region and maximum cylinder pressure; such limitations are taken into account in the subsequent optimisation process.

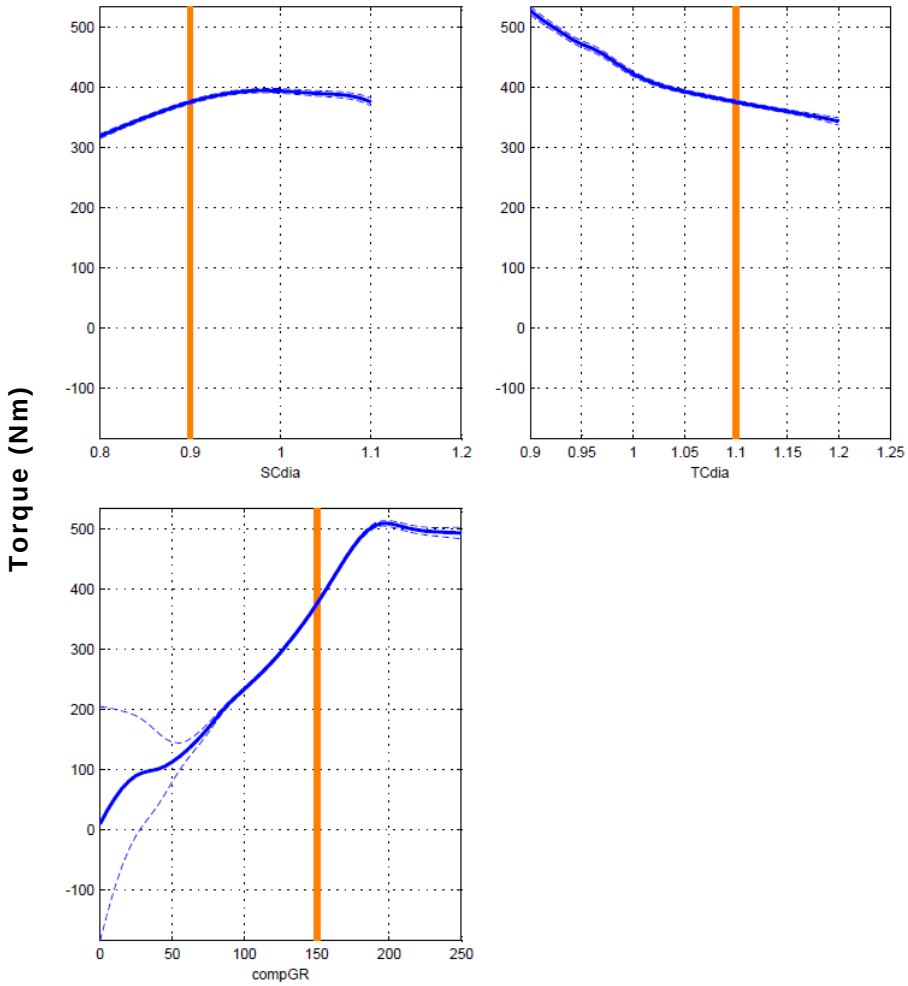

Figure 3.16 – Cross-section through Torque (Nm) response model at 1250 rpm, showing effects of SC scaling factor, TC scaling factor, and supercharger drive ratio ('compGR')

Considering the torque response model at high engine speeds, here the supercharger is no longer required – in fact torque benefits from the supercharger being disengaged, as Figure 3.17 shows. This is because the supercharger would be running up against the choke line at these speeds, and having a net loss effect on the engine brake torque due to the power required to drive the compressor. At high engine speeds the benefits of increased turbocharger size are clear, as it would be capable of passing greater mass flows. However, a peak in torque is achieved with a 5-10% larger turbocharger; this would be considered a good match to the flow requirements of the engine, as any further increase in size results in torque decreasing again.

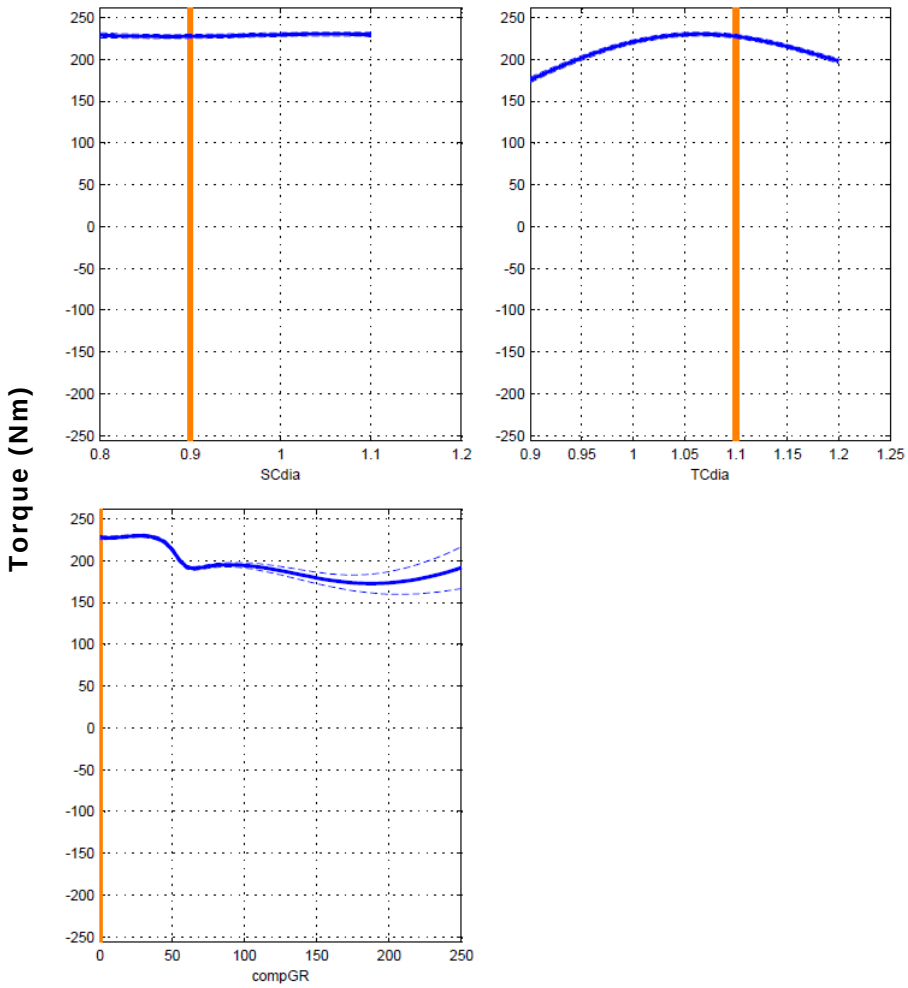

Figure 3.17 – Cross-section through Torque (Nm) response model at 4000 rpm, showing effects of SC scaling factor, TC scaling factor, and supercharger drive ratio ('compGR')

With the increased turbocharger size (and its fixed geometry), the necessity of the supercharger at low engine speeds is clear, as torque quickly drops off below 3000 rpm with the supercharger disengaged (Figure 3.18). As with the lower engine speeds (Figure 3.15 and Figure 3.16), the confidence bands are very narrow throughout, with the exception of the regions outside of the permitted supercharger drive ratio and engine speed combinations (Figure 3.5). Overall, the trends displayed in the torque response model are sensible and logical.

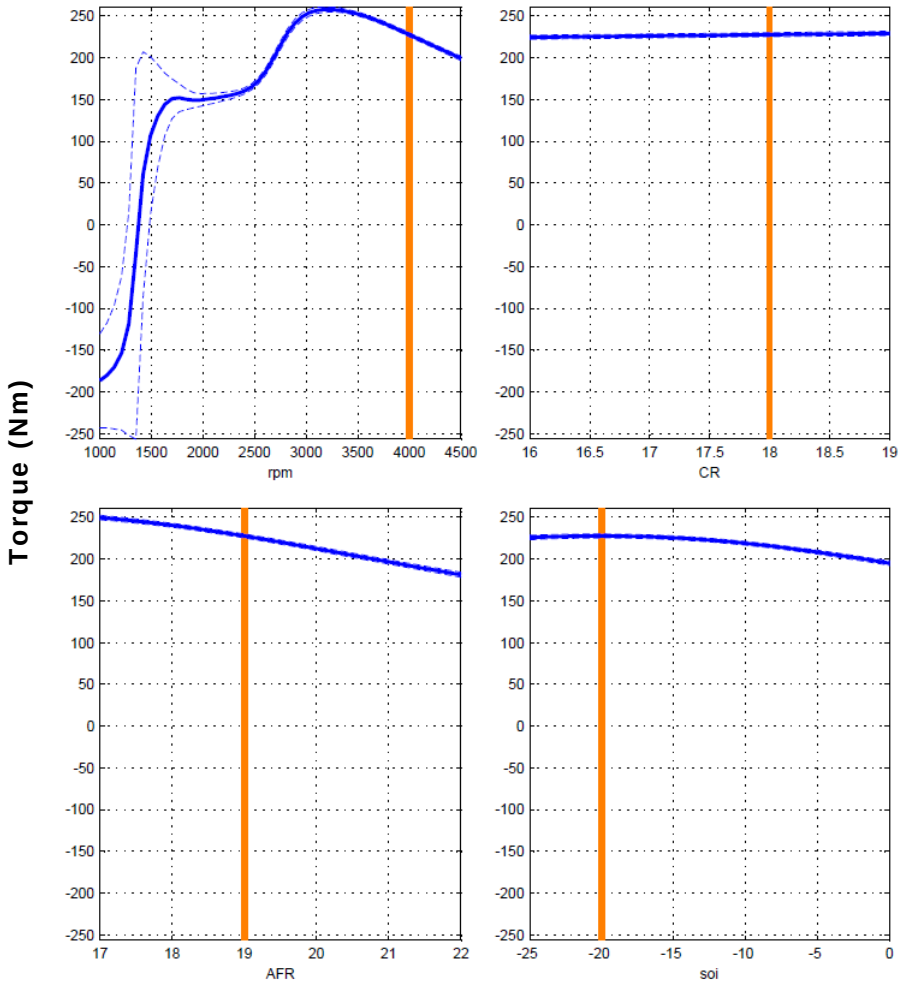

Figure 3.18 – Cross-section through Torque (Nm) response model at 4000 rpm, showing effects of engine speed (rpm), compression ratio, AFR, and fuel injection timing (CAD ATDCF)

Considering the maximum cylinder pressure response model, desirable narrow confidence bands are again displayed (Figure 3.19 and Figure 3.20). The trends displayed are also reasonable and logical, such as the increasing compression ratio causing a corresponding linear increase in cylinder pressure (assuming that boost pressure is approximately constant). Fuel injection timing clearly has a significant effect, as advanced injection would allow for a more complete combustion, which would be hotter, and therefore result in higher cylinder pressure. (Effects of injection timing on aspects such as ignition delay and emissions will be discussed later.)

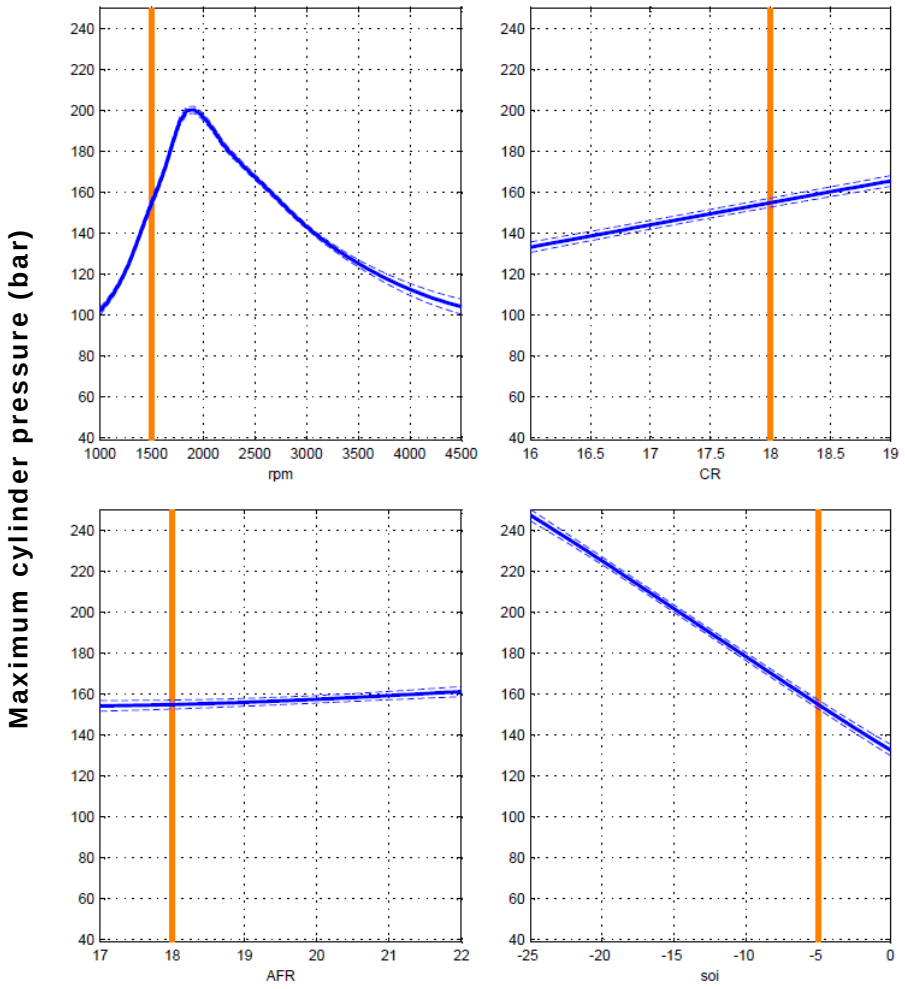

Figure 3.19 – Cross-section through Maximum cylinder pressure (bar) response model at 1500 rpm, showing effects of engine speed (rpm), compression ratio, AFR, and fuel injection timing (CAD ATDCF)

As discussed above, the turbomachinery scaling factors and supercharger drive ratio have significant effects on engine torque; Figure 3.20 clearly shows corresponding relationships with maximum cylinder pressure. At low engine speeds, increasing the supercharger scaling factor and decreasing the turbocharger scaling factor would result in the turbomachinery spinning faster and thus compressing more air into the cylinder; with more air, more fuel is injected (for a constant AFR) and thus higher cylinder pressures would be seen, along with more power and torque being produced (all else being equal). Similarly, increasing the supercharger drive ratio increases both torque and cylinder pressure, up to the plateau when the supercharger compressor chokes. These figures clearly show the need for the maximum cylinder pressure limit imposed during the optimisation process.

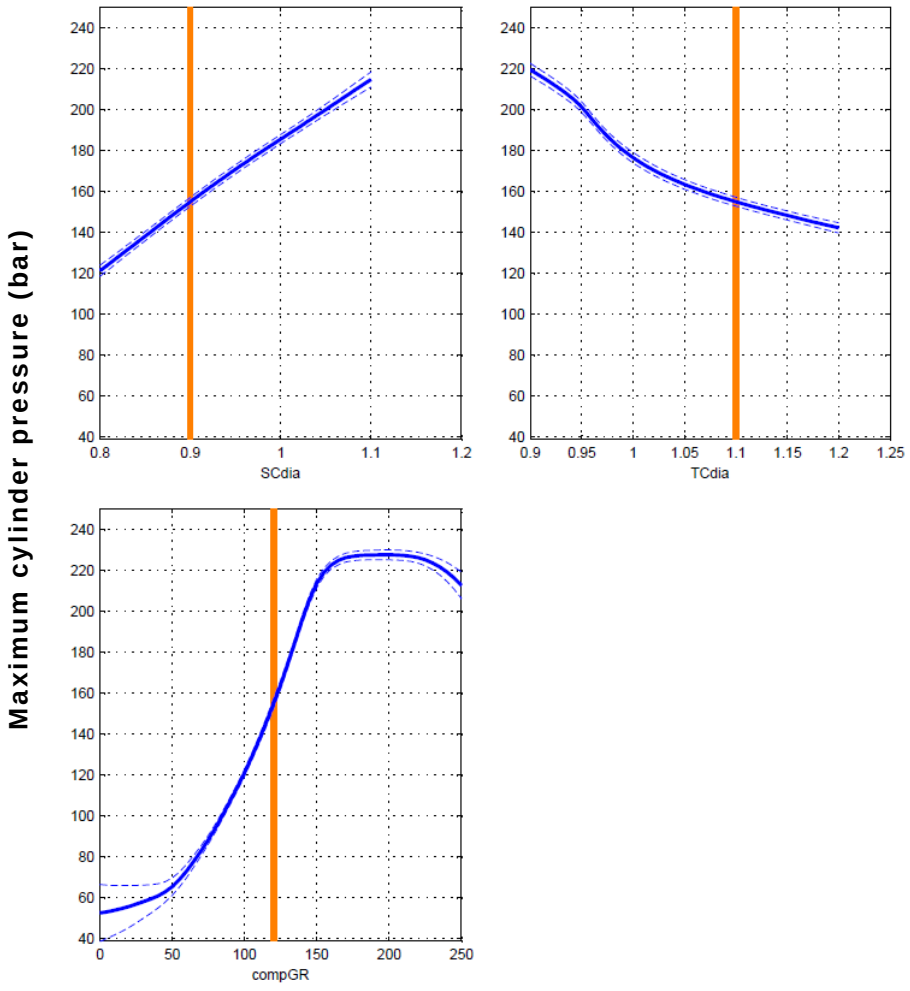

Figure 3.20 – Cross-section through Maximum cylinder pressure (bar) response model at 1500 rpm, showing effects of SC scaling factor, TC scaling factor, and supercharger drive ratio ('compGR')

The response model for turbine inlet temperature was most sensitive to the fuelling parameters (as well as engine speed), as shown in Figure 3.21. Increasing the fuelling rate (by decreasing the AFR at constant air mass flow) would result in higher engine torque, but more importantly increased levels of unburned fuel in the exhaust – this would increase the exhaust enthalpy, and thus the temperature at the turbine. Likewise, retarding the fuel injection would increase the amount of fuel in the exhaust, with the same result. The difference in exhaust gas temperature is significant across the ranges of these two parameters (around 250K), and must be taken into account with the maximum temperature constraint used during the optimisation process.

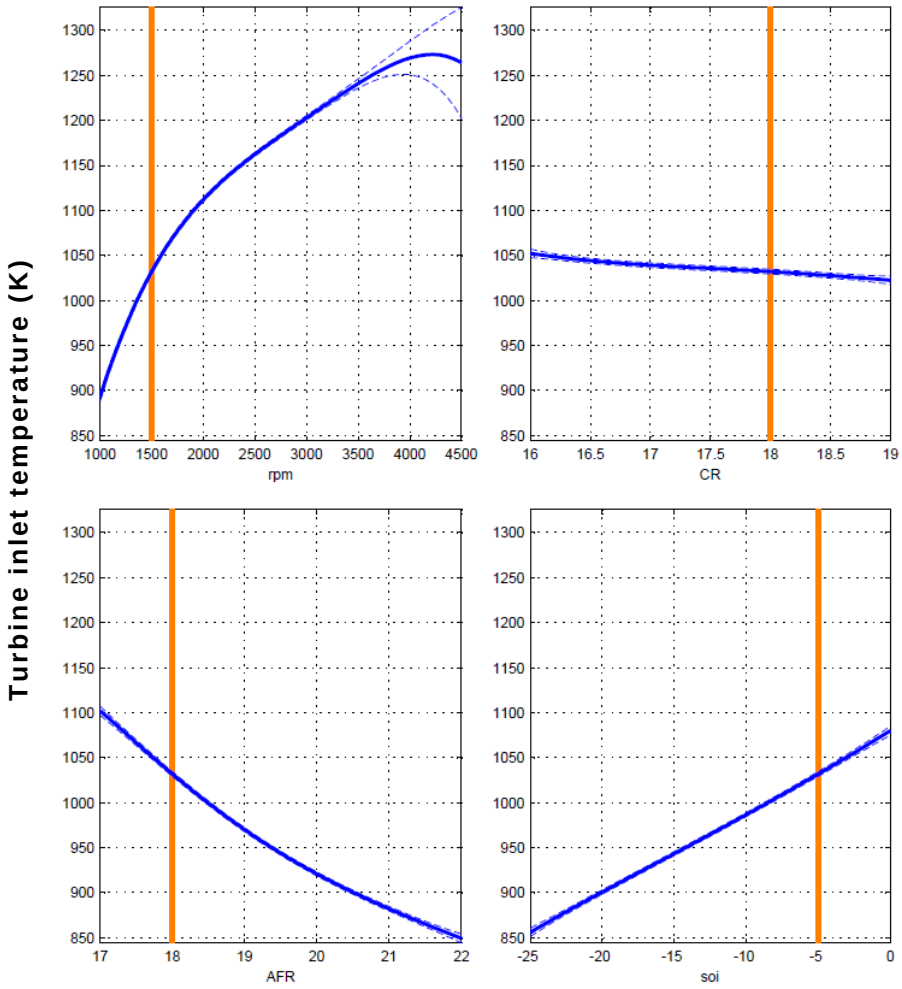

Figure 3.21 – Cross-section through Turbine inlet temperature (K) response model at 1500 rpm, showing effects of engine speed (rpm), compression ratio, AFR, and fuel injection timing (CAD ATDCF)

Turbomachinery parameters had little effect on turbine inlet temperature (Figure 3.22) – although slight increases are seen with increasing supercharger scaling factor and decreasing turbocharger scaling factor (at low engine speeds), which would result from the corresponding increased engine load (Figure 3.16).

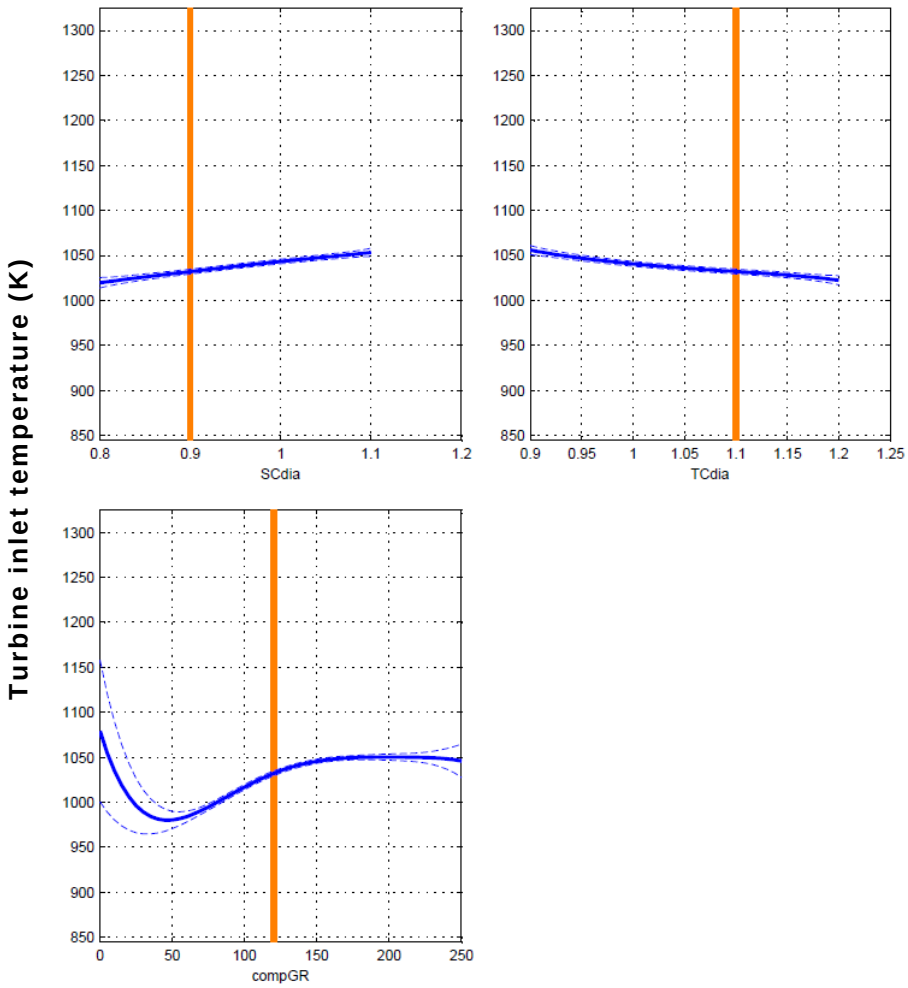

Figure 3.22 – Cross-section through Turbine inlet temperature (K) response model at 1500 rpm, showing effects of SC scaling factor, TC scaling factor, and supercharger drive ratio ('compGR')

Considering the supercharger normalised mass flow rate response model (Figure 3.23), the only parameters to have an effect on this variable are the supercharger drive ratio and turbocharger scaling factor (other than engine speed). Increasing the supercharger drive ratio produces a corresponding increase in mass flow, up to the now familiar plateau. Reducing the turbocharger size (i.e. scaling factor) causes mass flow through the supercharger to increase, as the turbocharger itself would be spinning faster due to the reduced turbine area and therefore passing more mass flow at these low engine speeds. It is perhaps surprising that the supercharger scaling factor has little to no effect on its mass flow rate; however, this is logical, provided the pressure ratio varies to compensate for the relative change in normalised compressor speed (i.e. the operating point travels in a vertical plane through the compressor map).

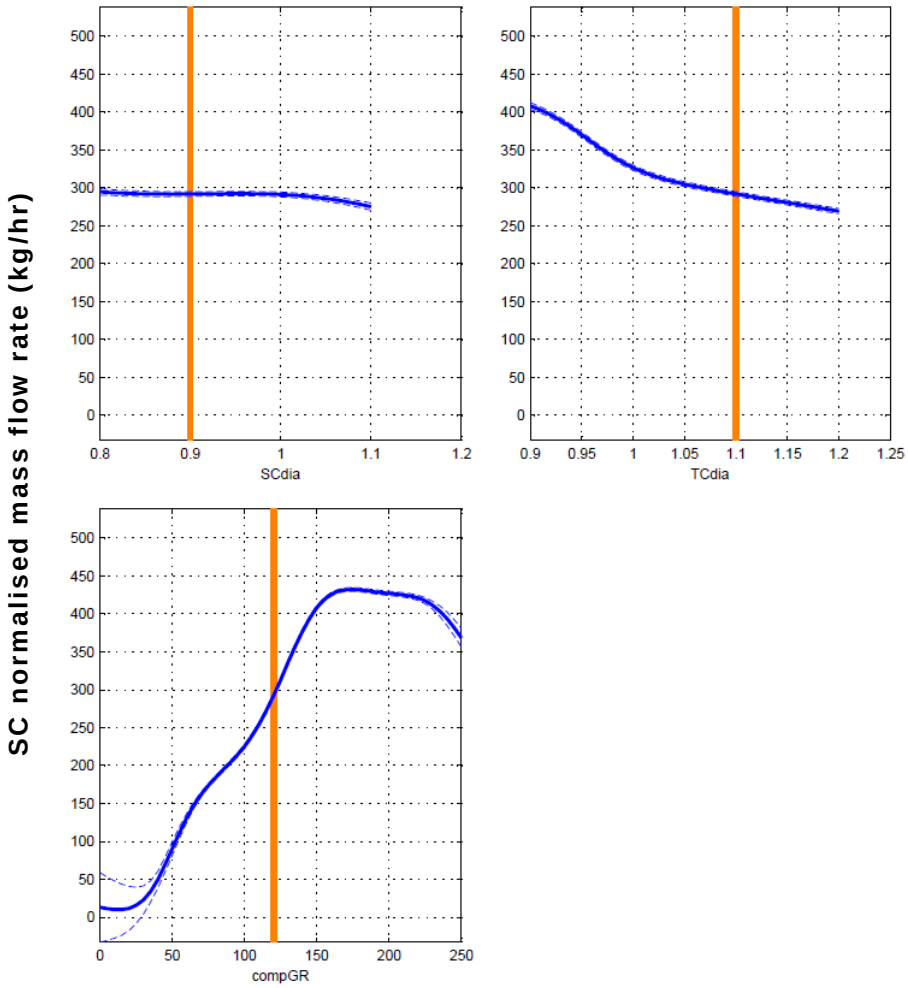

Figure 3.23 – Cross-section through Supercharger normalised mass flow rate (kg/hr) response model at 1500 rpm, showing effects of SC scaling factor, TC scaling factor, and supercharger drive ratio ('compGR')

This is seen to be the case, as shown in the corresponding supercharger pressure ratio response model in Figure 3.24. Keeping a constant drive ratio – and therefore compressor speed – but increasing the supercharger scaling factor increases the normalised speed, and the system responds with an equivalent increase in pressure ratio, while the mass flow remains relatively stable (Figure 3.23). Also note the appropriate pressure ratio response to supercharger drive ratio, which approximates a second order polynomial (up to the plateau) – since the pressure ratio of a centrifugal compressor increases with the square of its speed.

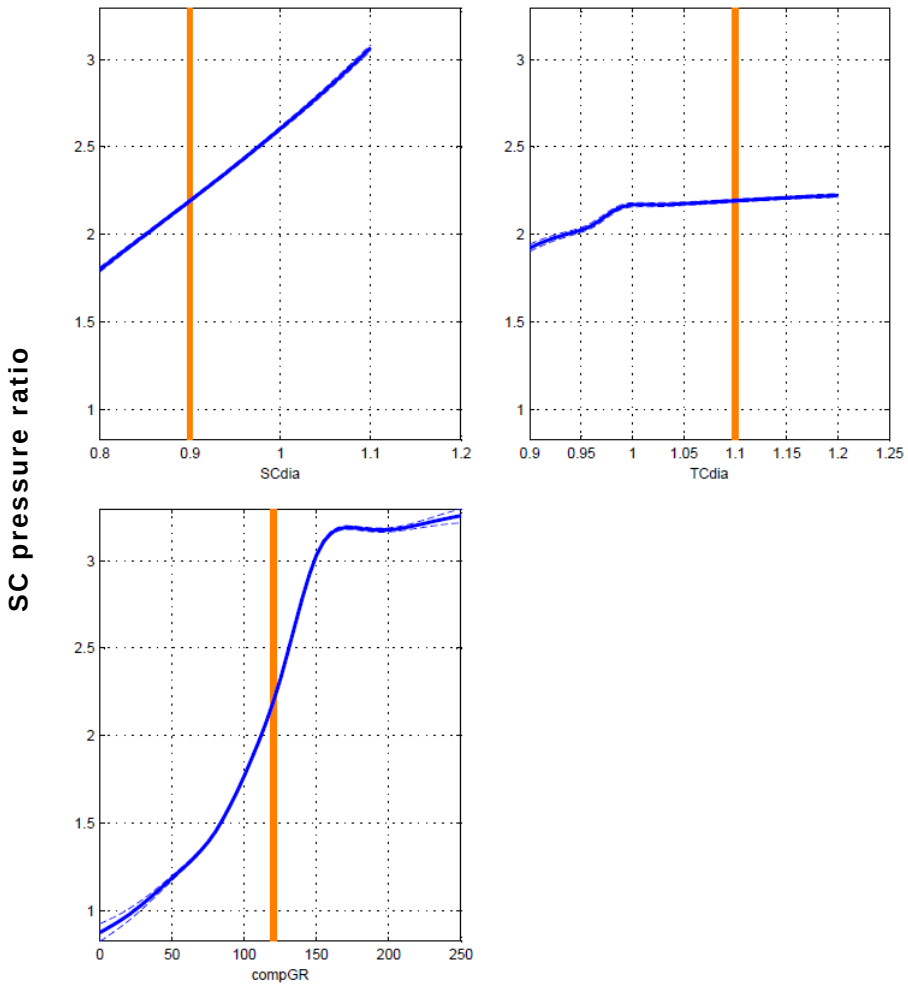

Figure 3.24 – Cross-section through Supercharger pressure ratio response model at 1500 rpm, showing effects of SC scaling factor, TC scaling factor, and supercharger drive ratio ('compGR')

The only parameters to have an effect on the turbocharger compressor normalised mass flow rate are the supercharger drive ratio and turbocharger and supercharger scaling factors (other than engine speed) (Figure 3.25). As with the supercharger mass flow rate, reducing the turbocharger size (i.e. scaling factor) causes system mass flow to increase, as the turbocharger would be spinning faster due to the reduced turbine area. Increasing either the supercharger scaling factor or drive ratio have the effect of drawing more air into the engine, which must also pass through the turbocharger compressor, hence increase its mass flow rate; this has the secondary effect of causing mass flow through the turbine to increase, further increasing its speed and thus mass flow through the compressor.

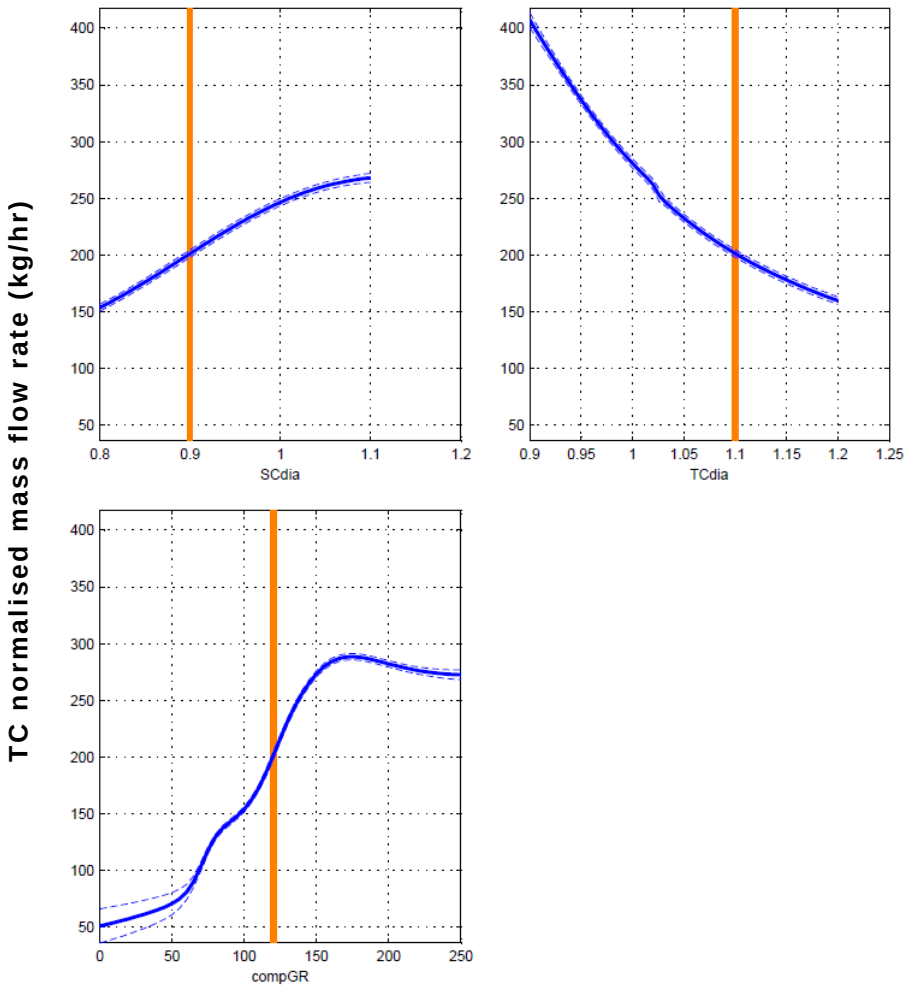

Figure 3.25 – Cross-section through Turbocharger compressor normalised mass flow rate (kg/hr) response model at 1500 rpm, showing effects of SC scaling factor, TC scaling factor, and supercharger drive ratio ('compGR')

At low engine speeds, the only parameter to have a significant effect on the turbocharger compressor pressure ratio is the turbocharger scaling factor (other than engine speed) (Figure 3.26). As with mass flow, decreasing the turbocharger size causes an increase in turbine speed (following the reduction in turbine area), resulting in increased compressor speed and thus pressure ratio. It is interesting to note that – unlike the equivalent supercharger variables – the turbocharger scaling factor has an effect on both mass flow and pressure ratio. This can be attributed to the complex relationship between compressor and turbine performance – particularly the need for speed and torque to be balanced at these steady state conditions.

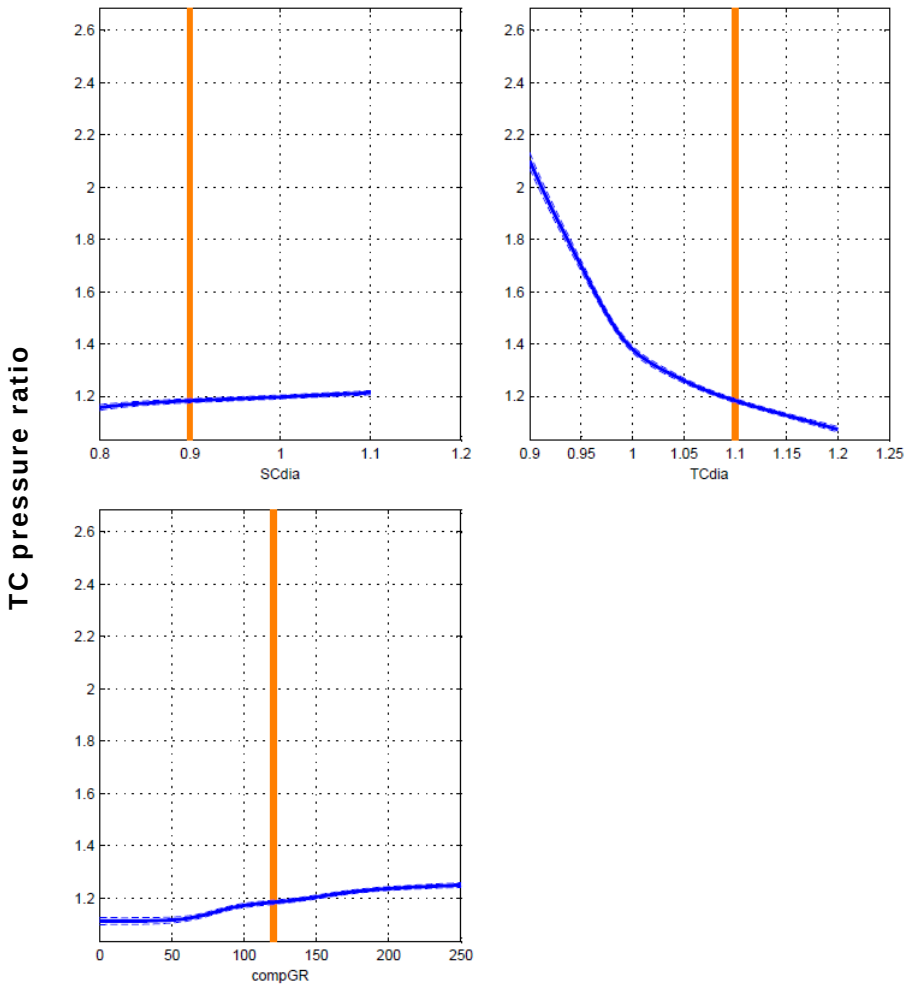

Figure 3.26 – Cross-section through Turbocharger compressor pressure ratio response model at 1500 rpm, showing effects of SC scaling factor, TC scaling factor, and supercharger drive ratio ('compGR')

At higher engine speeds, the fuelling parameters begin to have a large influence on turbocharger compressor pressure ratio, as shown in Figure 3.27. The relationships shown here with regards to AFR and injection timing reflect those shown with turbine inlet temperature in Figure 3.21. Essentially, reducing the AFR (for a constant quantity of air) or retarding the fuel injection timing both result in increased levels of fuel in the exhaust; more fuel leads to increased exhaust enthalpy, which is subsequently available for extraction by the turbine. This means power transferred to the compressor is greater, and its speed and pressure ratio increase.

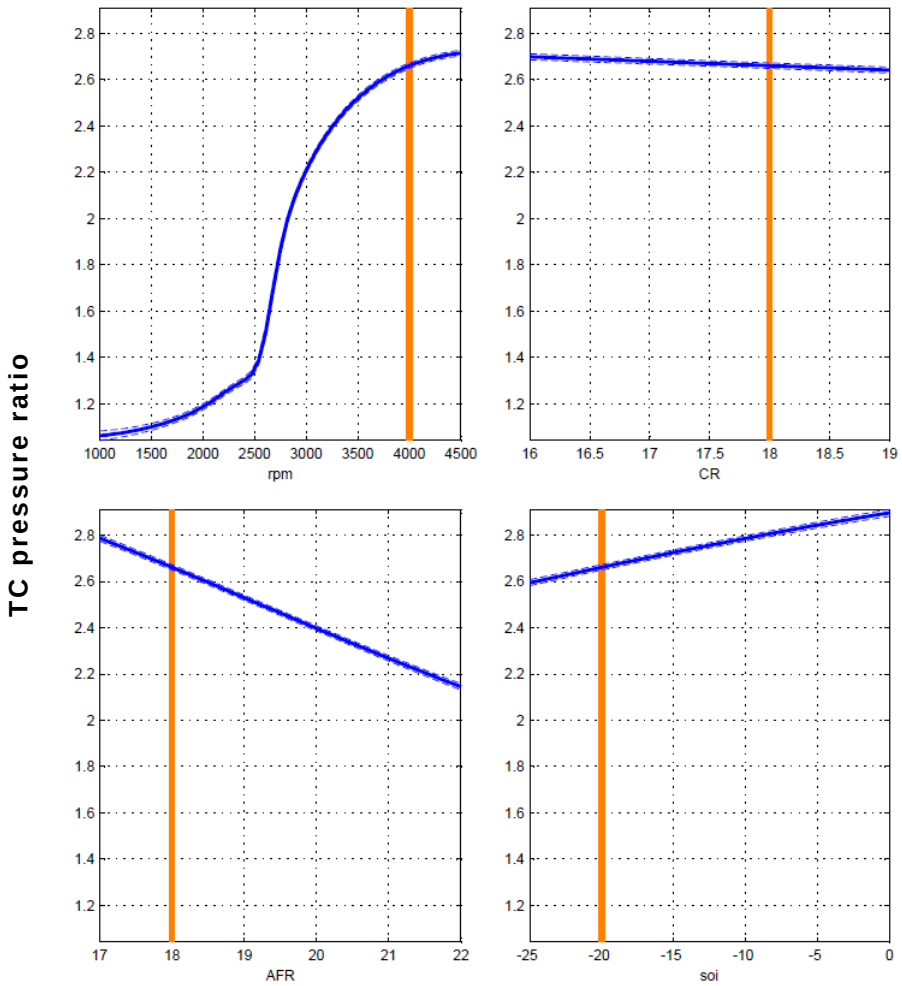

Figure 3.27 – Cross-section through Turbocharger compressor pressure ratio response model at 4000 rpm, showing effects of engine speed (rpm), compression ratio, AFR, and fuel injection timing (CAD ATDCF)

Figure 3.28 shows how the peak turbocharger pressure ratio has shifted from the lowest scaling factor at low engine speeds to a higher scaling factor at high engine speed. Here the increased mass flow requirement of the engine at high speeds is evident, and a larger turbocharger is beneficial. Note that this peak coincides with the peak torque of the corresponding Figure 3.17, although in this instance it is more pronounced.

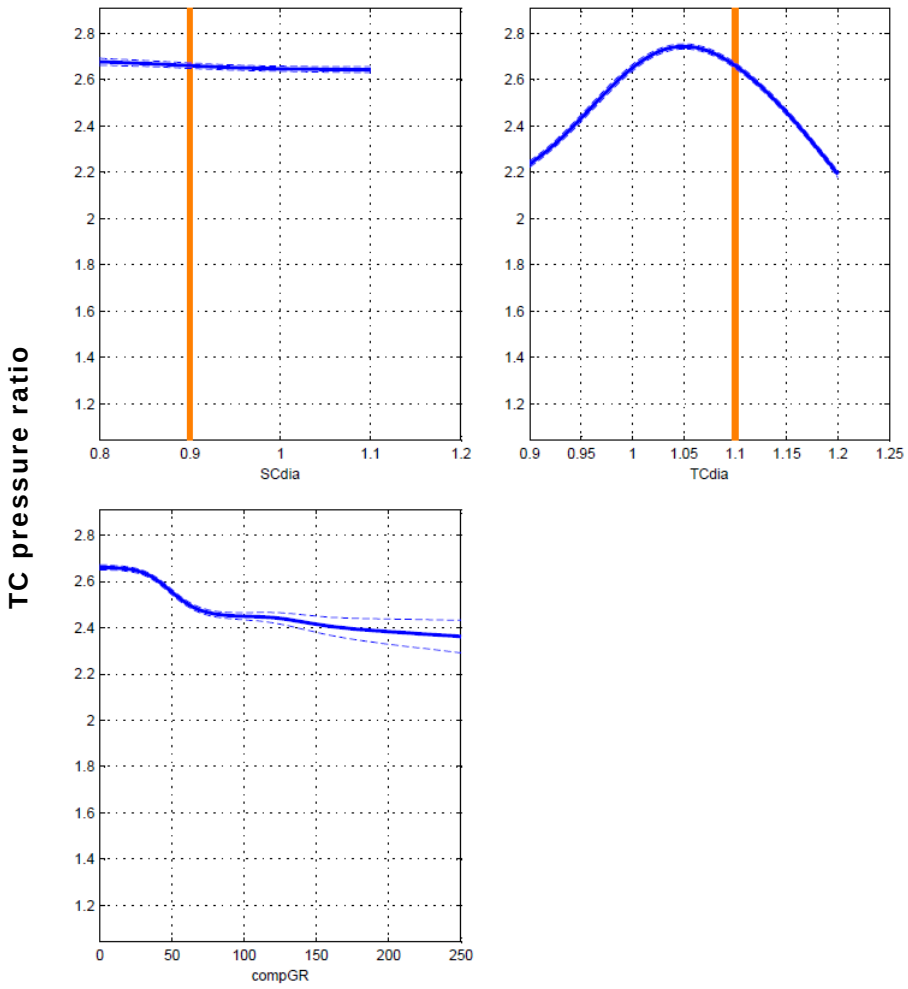

Figure 3.28 – Cross-section through Turbocharger compressor pressure ratio response model at 4000 rpm, showing effects of SC scaling factor, TC scaling factor, and supercharger drive ratio ('compGR')

The supercharger speed response is a straightforward product of supercharger scaling factor (in line with Equation 3.2), drive ratio, and engine speed, and hence requires only a relatively simple cubic response model – shown in Figure 3.29.

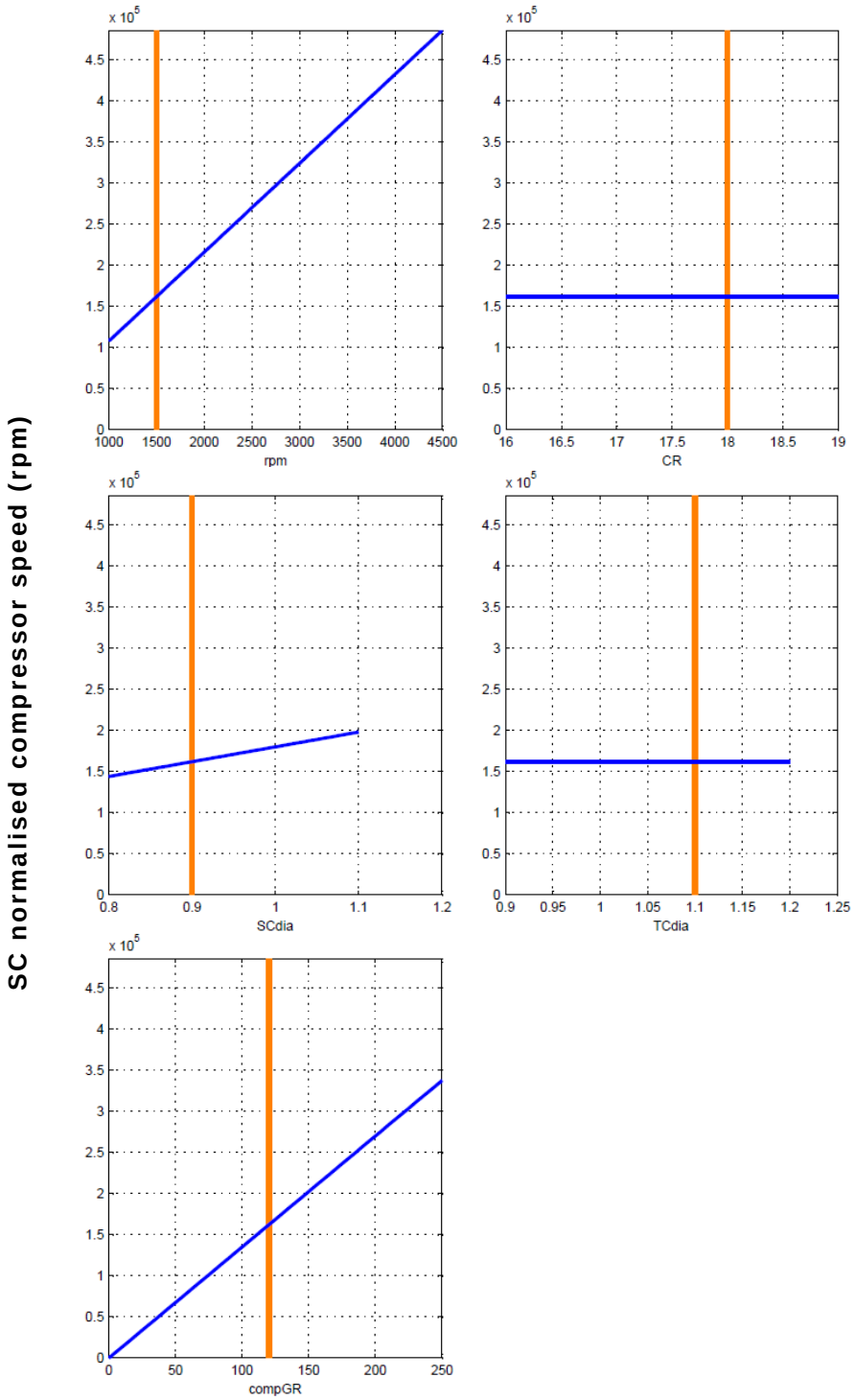

Figure 3.29 – Cross-section through Supercharger speed (rpm) response model at 1500 rpm, showing effects of engine speed (rpm), compression ratio, SC scaling factor, TC scaling factor, and supercharger drive ratio ('compGR')

The fuelling rate is a function of engine air mass flow and AFR, and hence the response model should reflect the trends shown in the respective turbocharger and supercharger mass flow rate response models, which it does faithfully (Figure 3.30 and Figure 3.31).

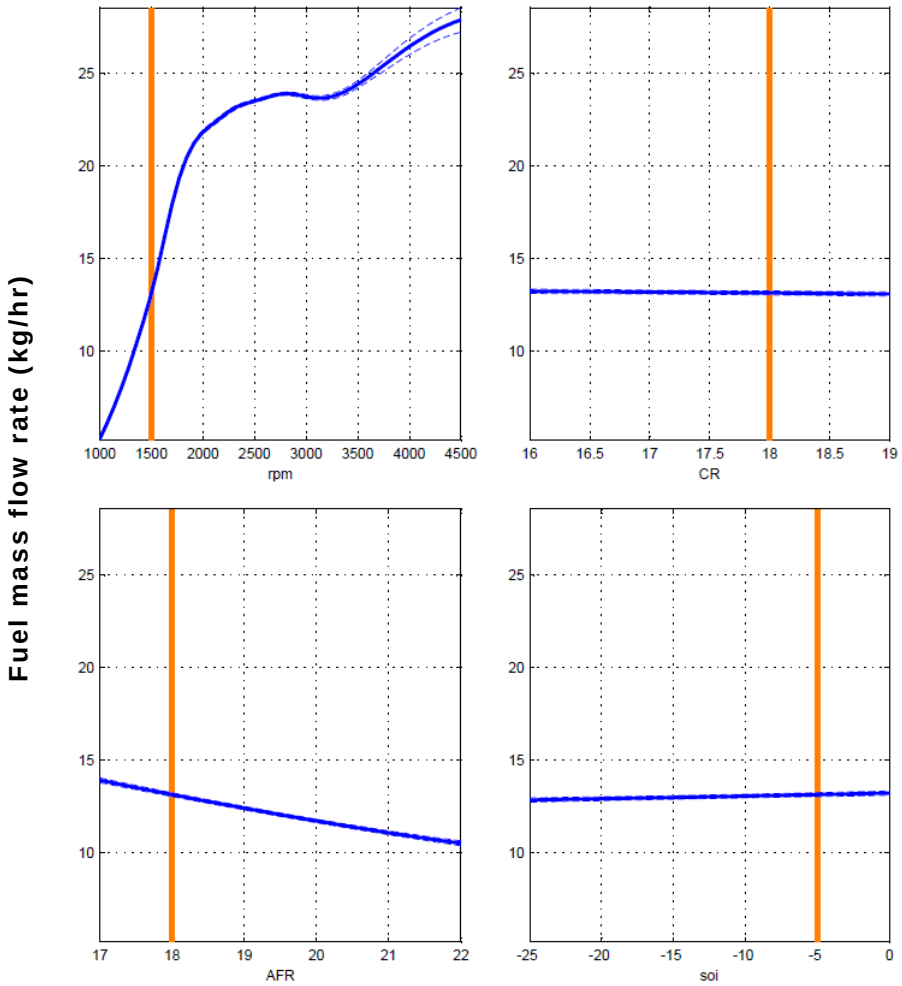

Figure 3.30 – Cross-section through Fuelling rate (kg/hr) response model at 4000 rpm, showing effects of engine speed (rpm), compression ratio, AFR, and fuel injection timing (CAD ATDCF)

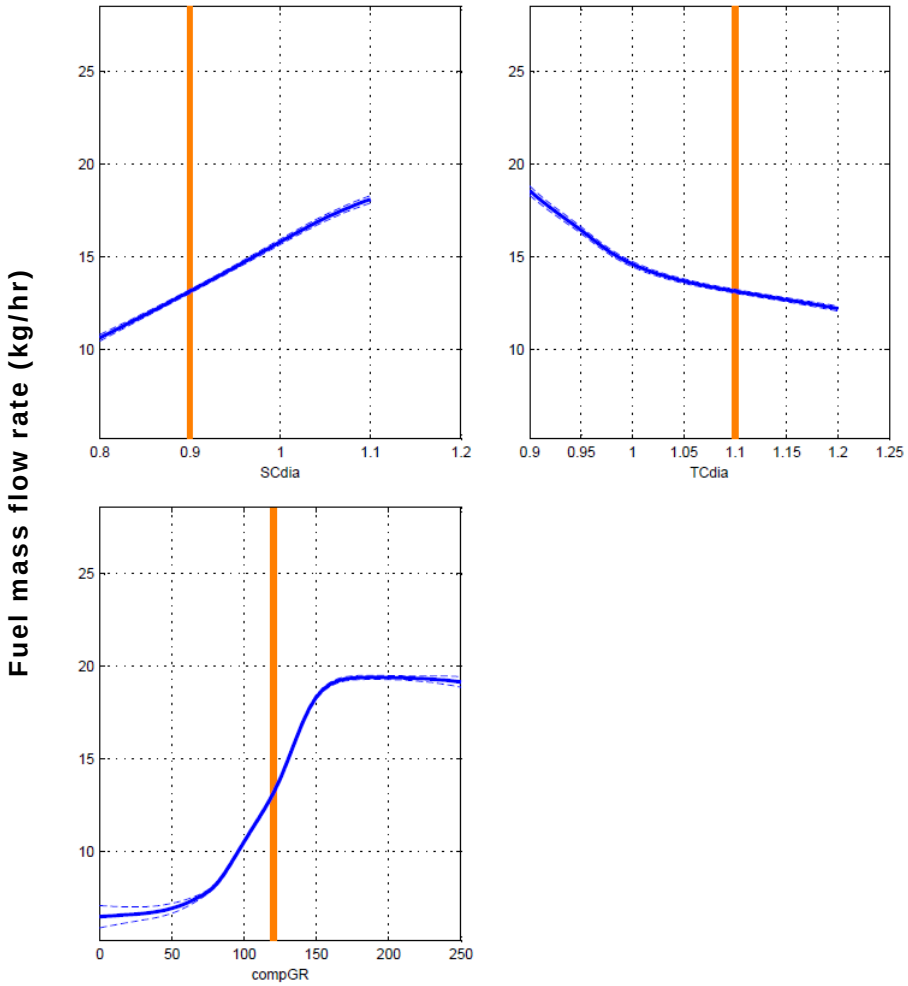

Figure 3.31 – Cross-section through Fuelling rate (kg/hr) response model at 4000 rpm, showing effects of SC scaling factor, TC scaling factor, and supercharger drive ratio ('compGR')

Overall, the response models that were fitted to the key variables showed logical trends and realistic behaviour in the regions of interest, together with narrow confidence bands throughout; it was concluded that they would form a good basis for the following optimisation process.

3.2.2 Optimised Design Parameters

Using these response models in the CAGE optimisation process discussed in Section 3.1.5 resulted in the parameter values shown in Table 3.5. The supercharger has been reduced in size by some 10%, relative to the original compressor, while the turbocharger compressor has increased by 7.5% and the turbine reduced by 7%. The reduction in supercharger size was in order to provide the required pressure ratios at low mass flow (i.e. low engine speed) within surge limits. The turbocharger compressor has increased in size to take advantage of the

potential to increase mass flow at high engine speeds without having to accommodate for the pressure ratios normally required at low speed. These results correlate with the trends found in the torque response model (Figure 3.15 to Figure 3.18). A slightly reduced compression ratio of 18:1 was required to maintain the engine within the maximum cylinder pressure constraint. (The optimised values for AFR, injection timing and supercharger drive ratio vary with engine speed, and are addressed in the following section.)

Table 3.5 – Optimised design parameters

Parameter	*Optimised Value*
SC scaling factor	0.90
TC scaling factor	1.075
TT scaling factor	0.93
CR	18

3.3 Steady State Simulation Results

Running the twincharged WAVE model with the optimised parameters produces a torque curve significantly enhanced over the baseline – up until 3000 rpm, the point of supercharger disengagement (Figure 3.32a). Peak torque has been increased by 15% and is produced at a lower engine speed – down from 2000 rpm to 1500 rpm. More crucially, up to 90% of the peak value is available at 1000 rpm, compared with 50% for the baseline engine. However, the twincharged system is virtually identical to the original model past the point of supercharger disengagement. This is predominantly due to the rudimentary way in which the original turbocharger was adapted for this purpose – using a turbine and housing combination designed for a VGT as a fixed geometry unit is less than ideal. This is primarily manifested in the isentropic efficiencies of the turbine: the maximum efficiency is 65%, occurring when the variable geometry mechanism is around 30-70% open; maximum efficiency is just 55% when fully open. (A similar problem is encountered in a computational study by Millo et al. [78], albeit when modelling an electrical turbocompounding system.) At full load, the VGT of the baseline engine operates in the region of greatest efficiency (as shown in Figure 3.32b), whereas the twincharged engine is always operating in the off-design, fully open condition.

As a result of these shortcomings, the modified turbocharger was unable to produce the same mass flow (and pressure ratio) as the original VGT, as Figure 3.32c shows. However, maintaining the fuelling rate of the baseline engine past 3000 rpm – thereby reducing the AFR in the process (Figure 3.32d) – and advancing the injection timing maintained the rated power of the baseline engine (Figure 3.32e and Figure 3.32f). It is worth noting that the dip in torque of the baseline engine at 4000 rpm is purely due to the fuelling rate (see Figure 3.32c); the reason for this is unknown, and it is rectified in the calibration of the twincharged engine.

The injection timing of the twincharged engine was determined with the objective of minimising brake specific fuel consumption (BSFC). With the fuel injection advanced to this extent, NO_x emissions would be expected to increase; however, due to the limitations of the model and software, any such effect could not be predicted in the simulation. The same applies to any adverse effects the generally low AFR of the twincharged engine may potentially have on exhaust smoke. Nevertheless, in a typical driving cycle during which emissions levels are officially assessed, engine

speed and load would not approach the operating points considered in this investigation. Furthermore, in practice an appropriately matched turbocharger – that is, more efficient and designed for purpose – would be expected to alleviate the problems of mass flow capability, and negate the need for injection timing advancement.

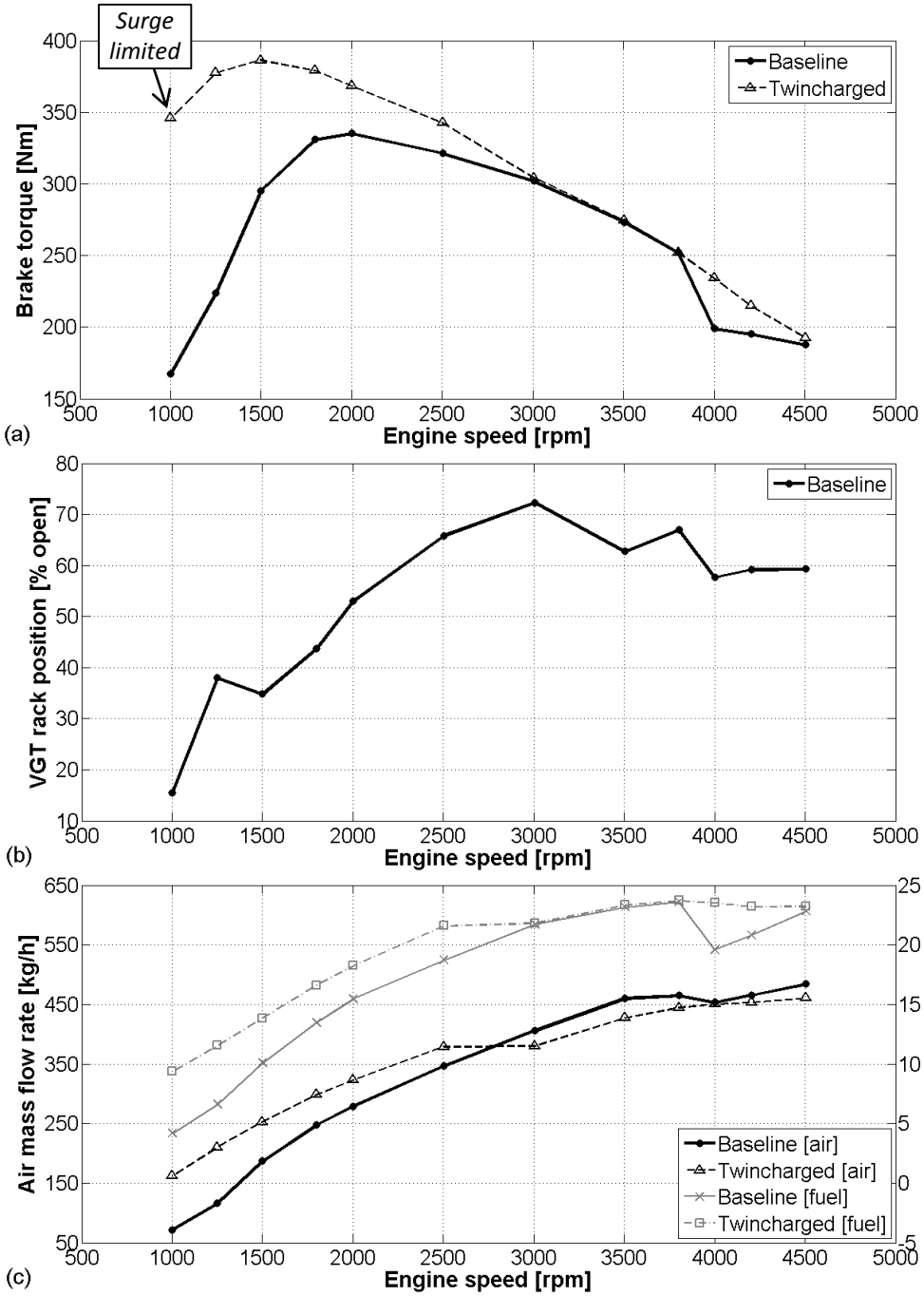

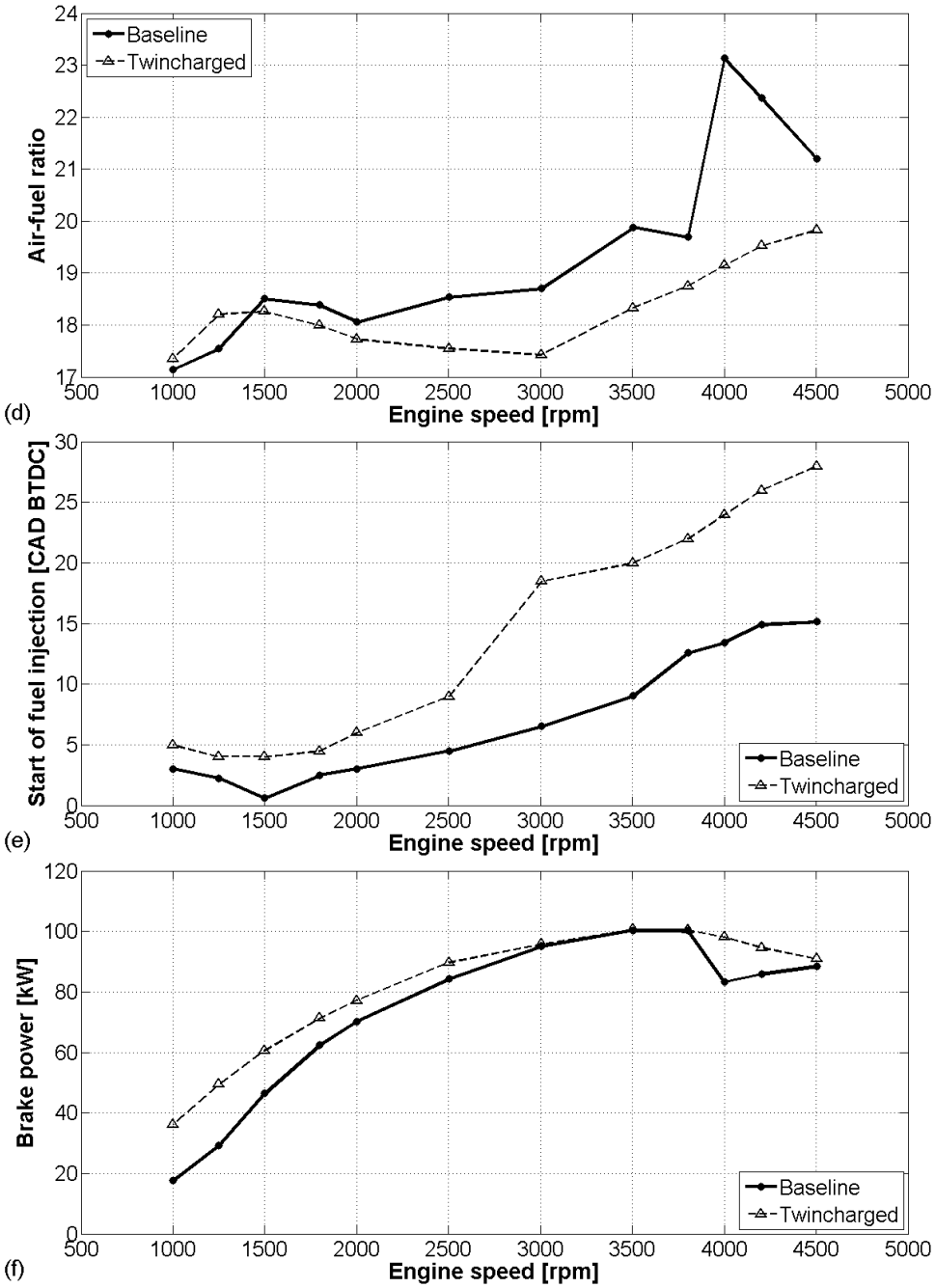

Figure 3.32 – Steady state results – a) torque; b) baseline VGT rack position; c) air and fuel mass flow; d) AFR; e) fuel injection timing; f) power

The continuously variable supercharger thus shows considerable potential as a pre-boost system to aid downsizing; however, the process of matching further turbomachinery (such as an efficient, high pressure ratio, narrow mass flow range turbocharger – fixed or variable turbine geometry) to achieve the required increase in rated power (and power density) is beyond the scope of this particular investigation. Nevertheless, the current results offer the opportunity to use a smaller

engine in a given application where low speed driveability is the limiting factor rather than maximum power.

3.3.1 Fuel Consumption

The twincharged system performance improvement came at the cost of deterioration in BSFC while the supercharger was engaged, which is an obvious consequence of the parasitic losses associated with supercharging. As Figure 3.33 shows, full load BSFC has increased by 4-9% throughout this range. However, since the loads are much higher than those of the baseline engine, it is anticipated that there would be benefits at part load when compared with a conventional engine (of greater displacement) capable of producing similar low speed torque.

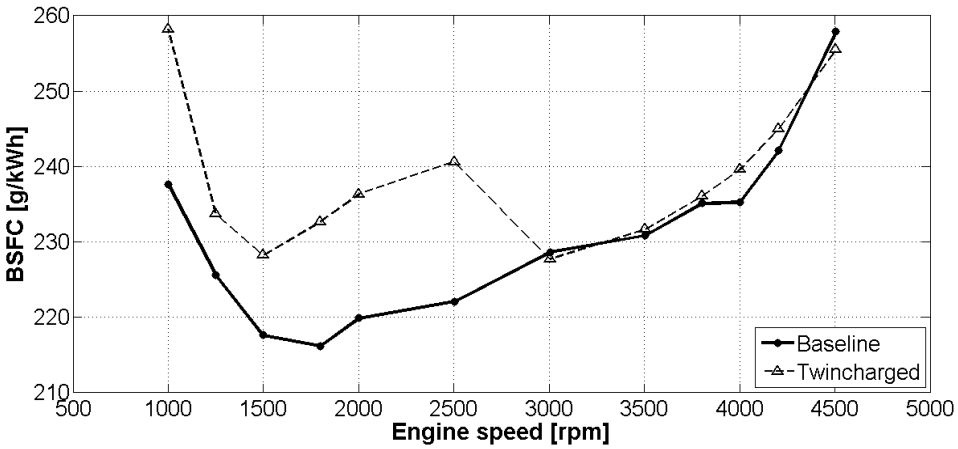

Figure 3.33 – Steady state results – BSFC

3.3.2 Gas Temperatures

Intake air temperatures are shown in Figure 3.34. The supercharger does have an appreciable effect while it is engaged on the twincharged engine (below 3000 rpm), even with the second intercooler. Above 3000 rpm, when purely turbocharged, intake temperatures return to baseline levels, as would be expected. Exhaust temperatures in the twincharged engine are comparable to the baseline, as shown in Figure 3.35. The peak temperature of 884°C at 2500 rpm is well within the temperature limits of current turbine and housing materials [32].

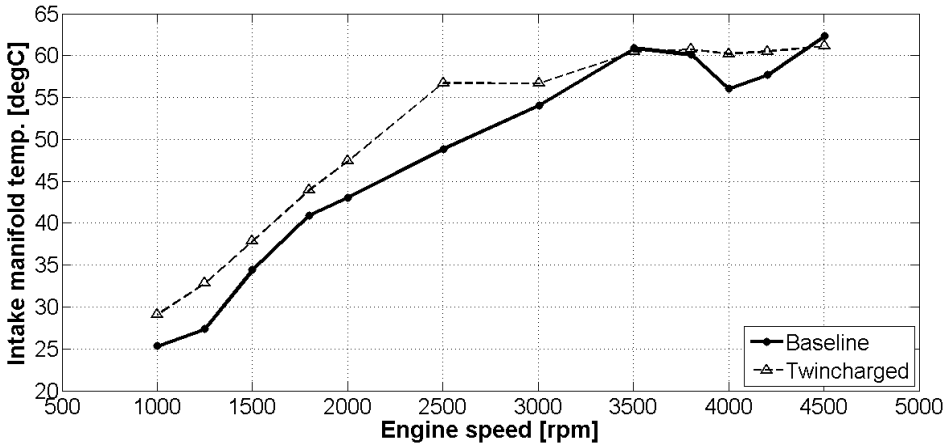

Figure 3.34 – Steady state results – intake manifold temperature

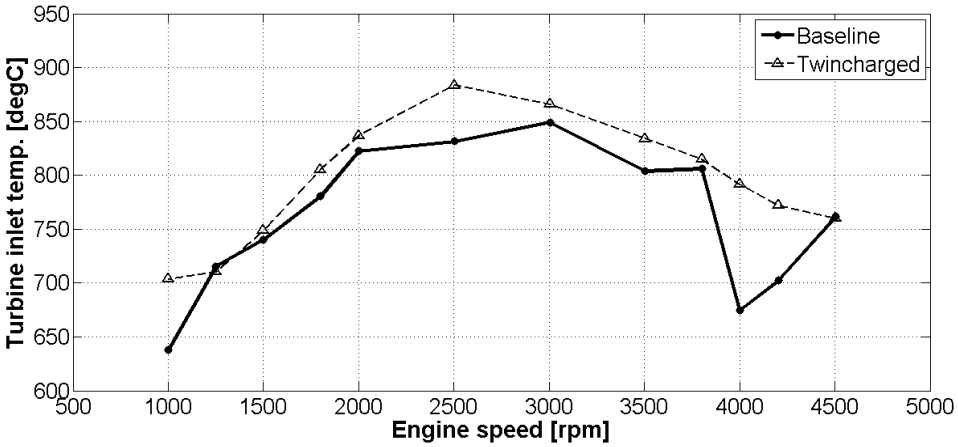

Figure 3.35 – Steady state results – turbine inlet temperature

3.3.3 Turbomachinery Operating Points

The operating points of the supercharger and turbocharger compressors are shown on the respective compressor maps in Figure 3.36 and Figure 3.37. The supercharger is run at a fairly uniform speed across the range it is used, with the majority of the operating points occurring in the regions of highest isentropic efficiency. The first operating point (at 1000 rpm engine speed) is up against the surge line of the compressor – in practice, this may not be possible, depending on the necessary surge margin. To avoid this, either the supercharger scaling factor could be reduced, but this would have implications across the whole operating range; alternatively, the supercharger speed would have to be reduced, which would reduce engine torque in the process, but only at this point. The final discrete operating point at which the supercharger is used (2500 rpm) is at low efficiency (<40%); although this is not ideal, it is necessary to use the supercharger up until

this point in order to maintain a smooth torque curve (see Figure 3.32a), since the resized fixed geometry turbocharger cannot provide sufficient boost alone.

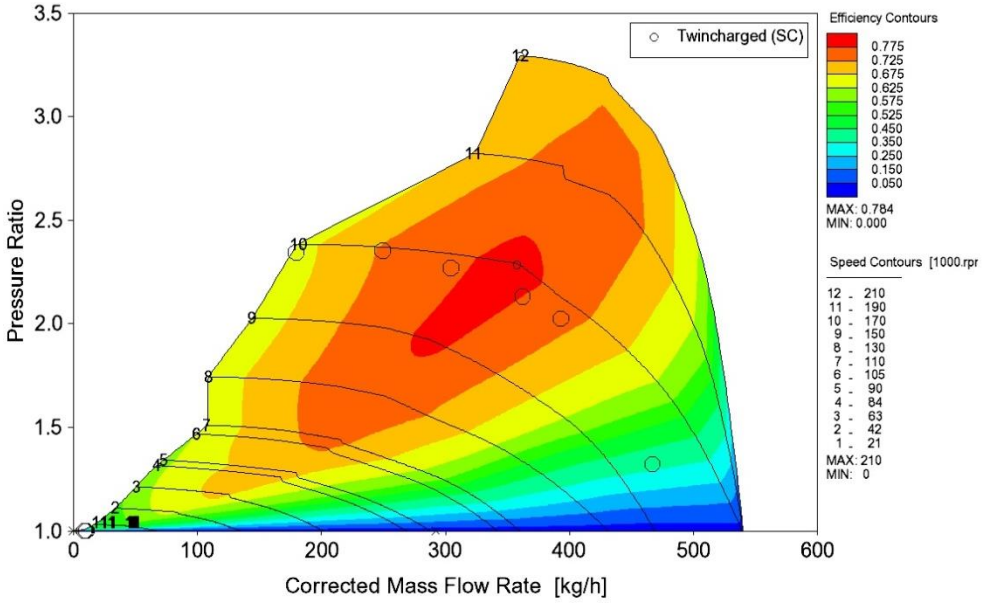

Figure 3.36 – Steady state results – supercharger operating points

It is interesting to note the narrower range of turbocharger compressor mass flows used by the twincharged engine (Figure 3.37). This is due to the supercharger effectively providing the majority of the mass flow at low engine speeds, allowing the turbocharger to be optimised for higher engine speeds – hence why the operating points of the twincharged engine inhabit the most efficient region of the map.

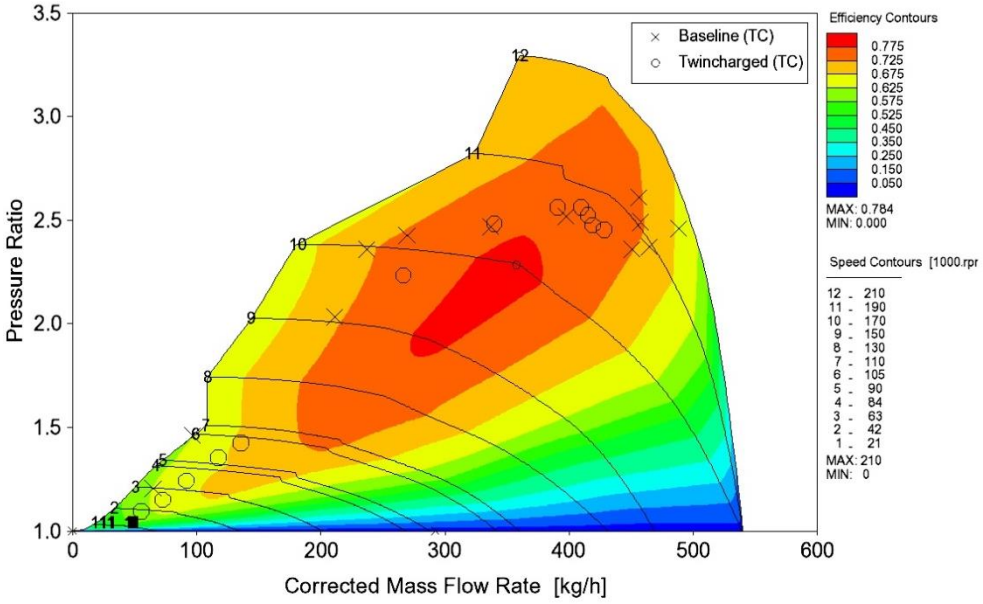

Figure 3.37 – Steady state results – turbocharger operating points

3.3.4 Exhaust Gas Recirculation

The baseline engine has a high pressure (HP) external exhaust gas recirculation (EGR) system, driven by the pressure gradient from exhaust manifold (pre-turbine) to intake manifold (post-compressor). For the sake of simplicity, the EGR rate was set to zero throughout the modelling process, as would be expected on the LTC. As Figure 3.38 shows, although beneficial in terms of volumetric efficiency, the increase in intake manifold pressure caused by the supercharger would prevent this type of EGR from being used below 2500 rpm.

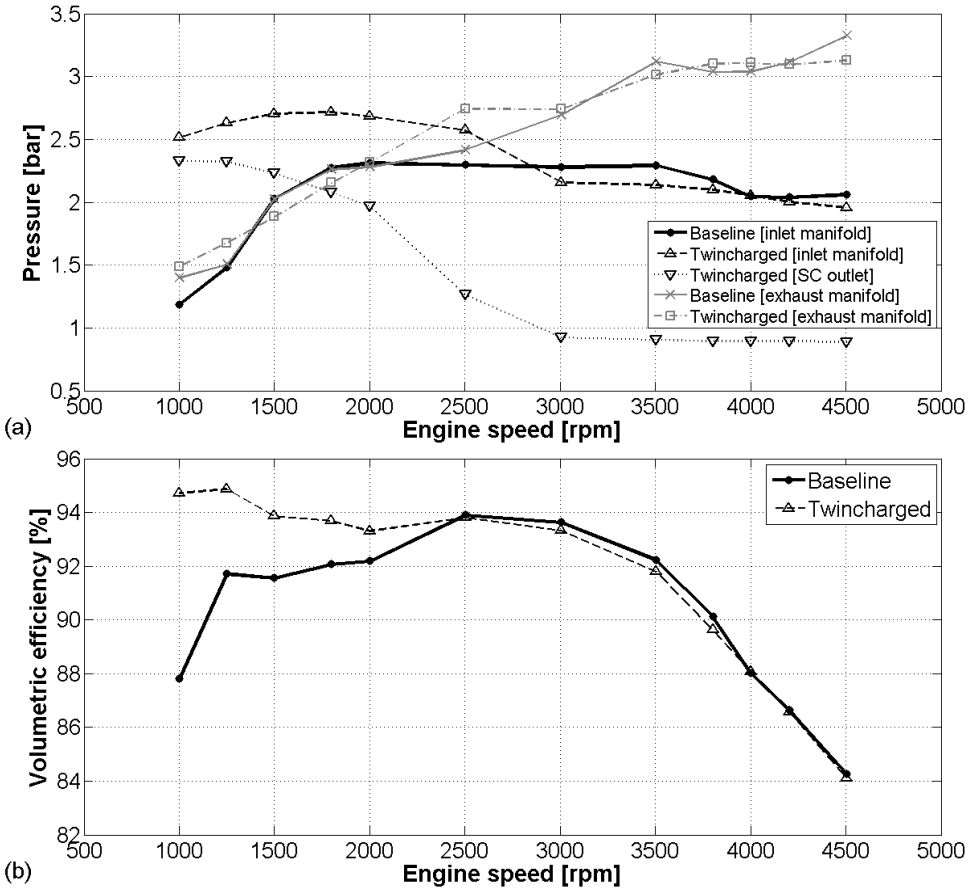

Figure 3.38 – Steady state results – a) inlet and exhaust manifold pressures; b) volumetric efficiency (relative to inlet manifold conditions)

However, depending upon the EGR and supercharger engagement schedules, the original HP EGR system may still be useable at part load. In some circumstances it may be possible to use the supercharger essentially as an EGR pump, in order to improve the trade-off between fuel efficiency and emissions. Furthermore, replacing the fixed geometry turbocharger used in the twincharged system with a VGT and closing the turbine vanes would increase the exhaust back pressure and thus

improve the pressure gradient from exhaust to intake manifold. Alternatively, if this pressure gradient is still problematic, a low pressure (LP) EGR system (post-turbine to pre-compressor) could be adopted, which would circumvent the issue. LP EGR is currently the focus of considerable research efforts as it offers a number of benefits over conventional HP systems (albeit with its own disadvantages) [91][92].

Considering the predicted combustion temperatures (since this is a primary factor in the formation rate of NO_x), the profile of the twincharged model matches that of the baseline fairly well at low engine speeds, as Figure 3.39 shows – importantly, the peak temperatures are very similar. Of course, these results must be assessed in the light of the predictive combustion model used, and the fact that it is not experimentally validated for the twincharged engine model. Figure 3.40 shows the combustion temperature profile of the twincharged engine at high engine speed – the magnitude of the peak remains high, but not extreme, staying below 1750°C. The baseline results, however, must be considered with caution since the data corresponds with the operating point with a dip in fuelling evident in the model, 4000 rpm (see Figure 3.32a).

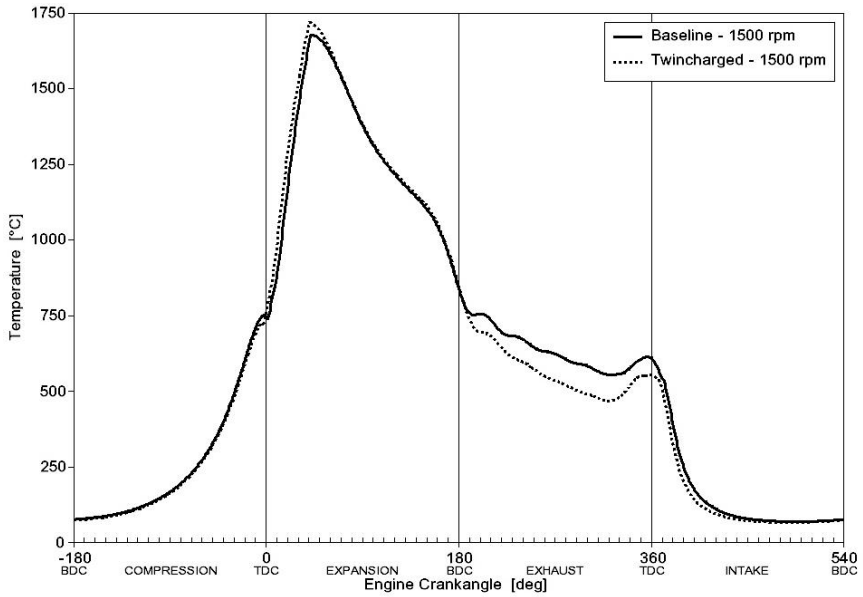

Figure 3.39 – Steady state results – combustion temperature vs. crank angle at 1500 rpm

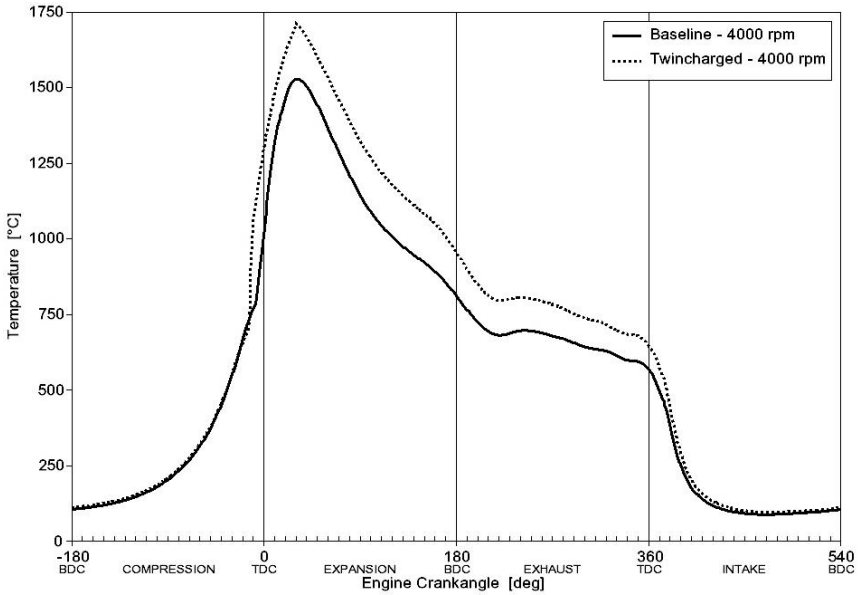

Figure 3.40 – Steady state results – combustion temperature vs. crank angle at 4000 rpm

3.3.5 CVT Ratio Range

The range of combined gear ratios of the CVT and drive pulley that were applied in the engine model is shown in Figure 3.41. A ratio range of 2.64:1 was required for the twincharged system, which is well within the capacity of most CVT systems; including traction drives [93] such as the Milner CVT (MCVT) [94][95], the Torotrak full toroidal variator [96], the half toroidal variator [97], and the belt drive CVT [98]. However, this ratio range is only taking into account full load conditions; at part load air mass delivery requirements would be proportionally less than these, implying a further required reduction in supercharger drive ratio. The necessary extension to the ratio range would depend on the control strategy employed for engaging the supercharger. In an earlier study by Schmitz et al. [34] a positive displacement-type supercharger was driven via an electromagnetic clutch and bypass arrangement to boost the performance of a turbocharged heavy duty diesel engine. In this instance the supercharger was engaged during all transient and steady state conditions below a set speed threshold, and was also engaged in transient conditions above the threshold when boost pressure was less than the demanded value, Table 3.6 shows the rules used to implement this scheme.

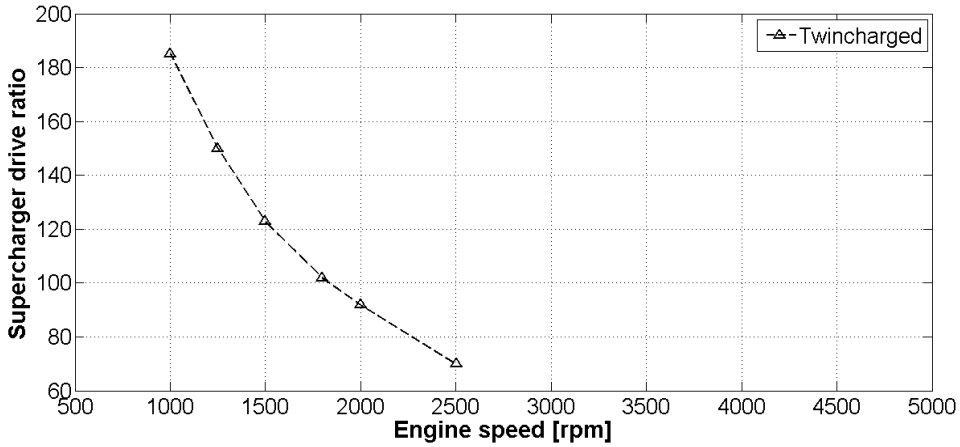

Figure 3.41 – Steady state results – CVT ratio range

Table 3.6 – Decision map for supercharger engagement (data reproduced from Schmitz et al. [34])

Operating Condition	*Criteria*	*Magnetic Clutch*
Engine start	Engine speed = 0; ignition on	Disengaged
Vehicle stand still	Vehicle speed = 0; engine idling; gearbox in neutral	Disengaged
Vehicle start	Vehicle speed = 0; engine idling; gear engaged	Engaged
Engine speed < 1100 rpm steady state and transient	Engine speed	Engaged
Engine speed > 1100 rpm steady state	Boost pressure = rated value of accelerator position	Disengaged
Engine speed > 1100 rpm transient	Boost pressure ≤ rated value of accelerator position	Engaged
Engine braking operation	Switch on	Engaged

The overall ratio required to drive the supercharger is significant. Table 3.7 summarises how these ratios might be achieved for typical existing CVT systems, using a speed up pulley drive, and an intermediate step up between the CVT and the turbomachinery. Experience suggests that most traction drive CVTs are capable of being driven at up to 10000 rpm, indicating a drive pulley ratio up to 3.5 as being appropriate, depending on engine disengagement speed. The belt drive CVT is typically limited to 6000 rpm, due to centripetal belt forces. The requirement for the step up ratio between the CVT output and supercharger input will then be a function of the CVT ratio. This ratio will be dependent on the turbomachinery design speed

and the ratio of the CVT. For example most traction drives and the belt drive ratio spread is symmetrical through unity (1:1) ratio, while the MCVT range is biased to typically below 1.6~2:1.

Table 3.7 – CVT ratio ranges to match turbomachinery

Parameter	*Milner CVT*	*Full Toroidal CVT Half Toroidal CVT*	*Belt Drive CVT*
Input speed limit (rpm)	10000	10000	6000
Input drive ratio	3.5	3.5	2
CVT ratio range	4.5	6	6
Min CVT ratio	2	0.41	0.4
Max CVT ratio	9	2.45	2.5
Step up ratio	5.6	20.5	35
Min overall ratio	39.2	29.3	28
Max overall ratio	176.4	175.8	175

From Table 3.7 it can be seen that the ratio requirement for the step up system is significantly less for the MCVT compared to the full and half toroidal drives, and significantly higher again for the belt drive. This may have considerable implications for transient performance, where the acceleration torque (due to supercharger inertia) will be factored by the square of the step up. However, the full and half toroid designs and the belt drive typically have a higher ratio range, although work has been undertaken to derive MCVT concepts with greater ratio range [99][100]. Increased ratio range is likely to be beneficial in lower load operating conditions where turbomachinery speeds will be reduced.

3.3.6 CVT Efficiency

During the initial model development the CVT efficiency was assumed to be 100% to simplify analysis – the object of this project was to investigate the potential of the general concept rather than constrain the concept to a specific type of CVT at this stage. Figure 3.42 shows the influence of CVT efficiency on the torque curve of the twincharged system, indicating that for typical efficiency values [94] there is little impact on overall performance – a CVT efficiency of 85% resulting in a reduction in peak torque of 2%.

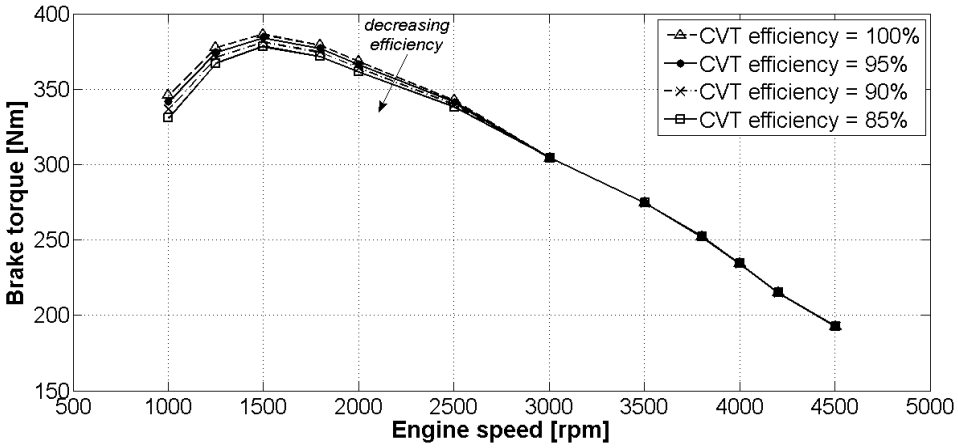

Figure 3.42 – Effect of CVT efficiency

3.4 Transient Simulation Results

As mentioned above, the aim of this part of the investigation was to predict the response to a fixed speed 'tip-in' transient – i.e. a step in fuel quantity from a low to high value. This is designed to simulate the driver depressing the accelerator pedal – or 'tipping-in' – at light load and demanding full load from the engine [21].

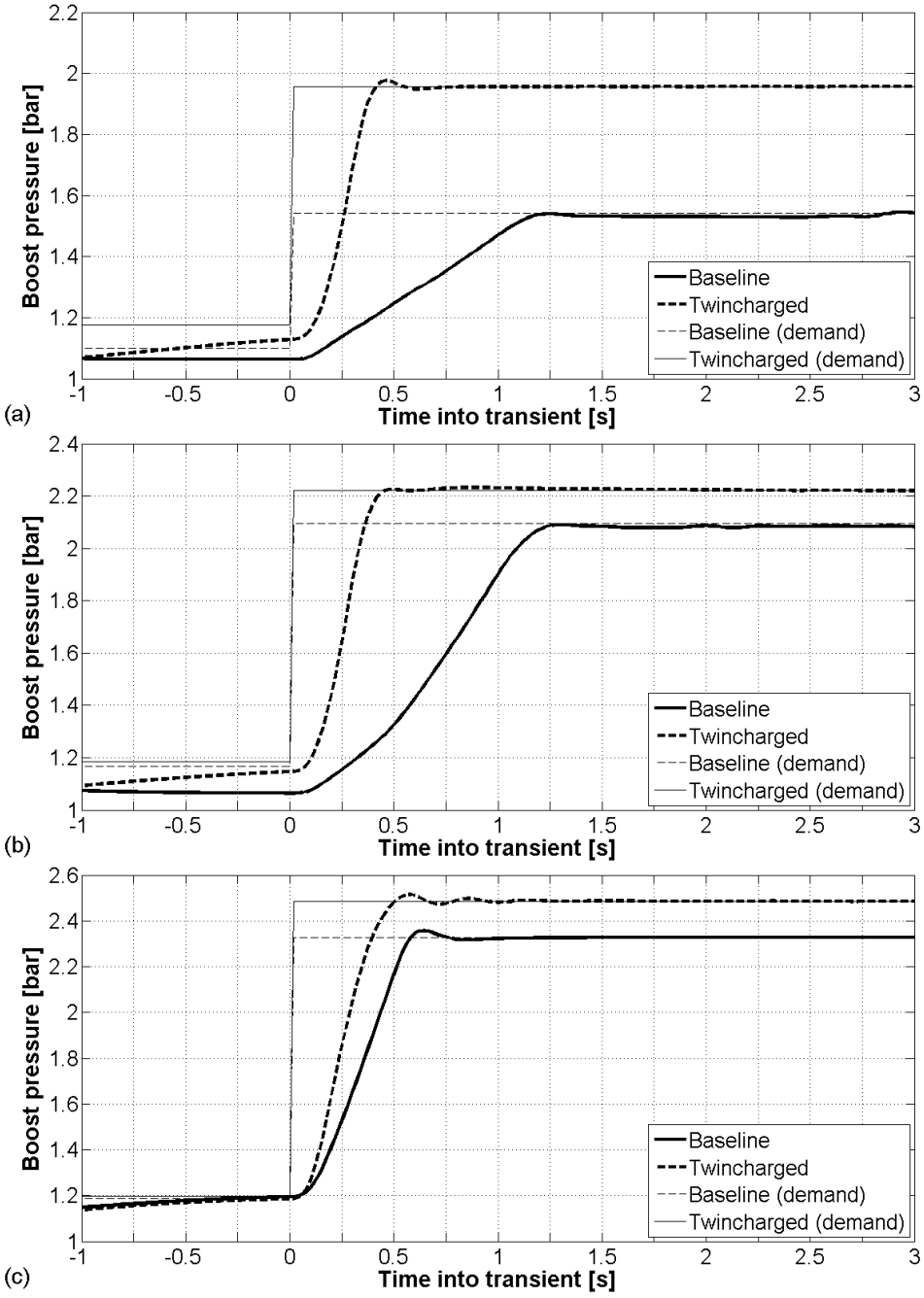

Figure 3.43 – Transient boost response – a) 1250 rpm; b) 1500 rpm; c) 2000 rpm

At the lower engine speeds the difference in boost response between the baseline and twincharged engines was clearly evident; at 1250 rpm the twincharged engine achieving the boost demand in less than 0.5 seconds compared with around 1.25 seconds for the baseline engine (Figure 3.43a), despite the demanded boost being significantly higher. As engine speed increased, the performance deficit between the models gradually decreased, with the response time reduced to 0.6 seconds at 2000 rpm for the baseline engine (Figure 3.43c).

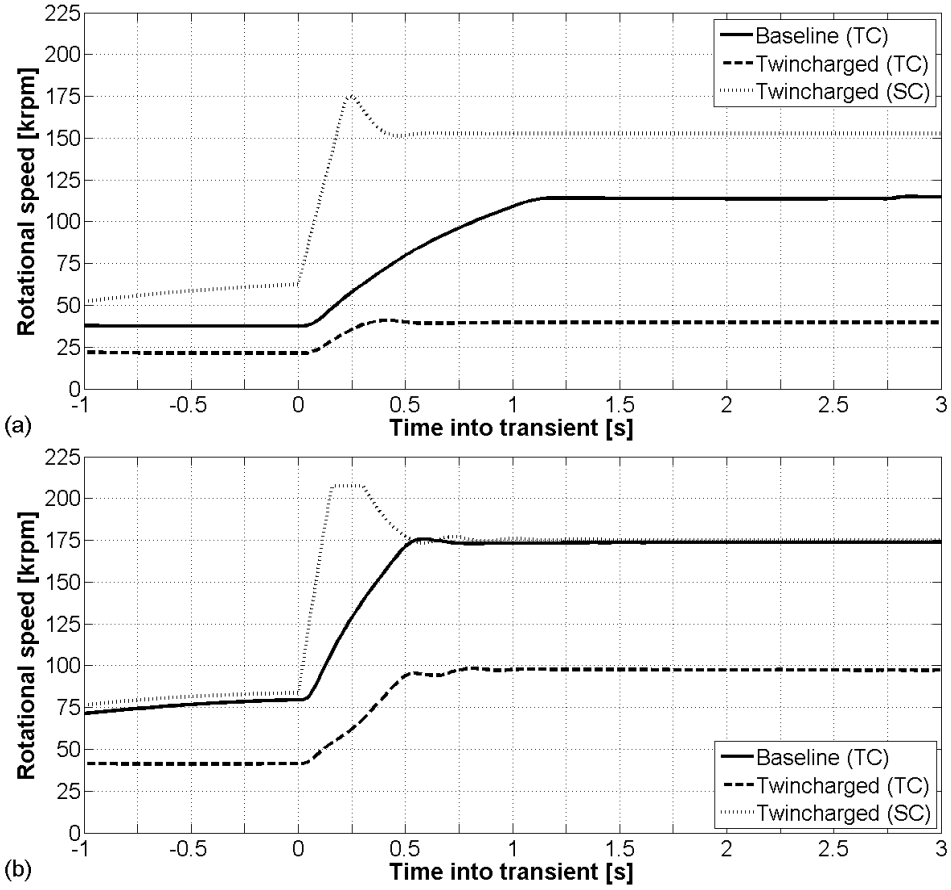

Figure 3.44 – Transient turbocharger and supercharger speeds – a) 1250 rpm; b) 2000 rpm

The difference in transient response between the two systems is also demonstrated in the turbomachinery speeds, shown in Figure 3.44. Despite the VGT system, the turbocharger of the baseline engine accelerates at a much lower rate than the supercharger of the twincharged engine, Figure 3.44a.

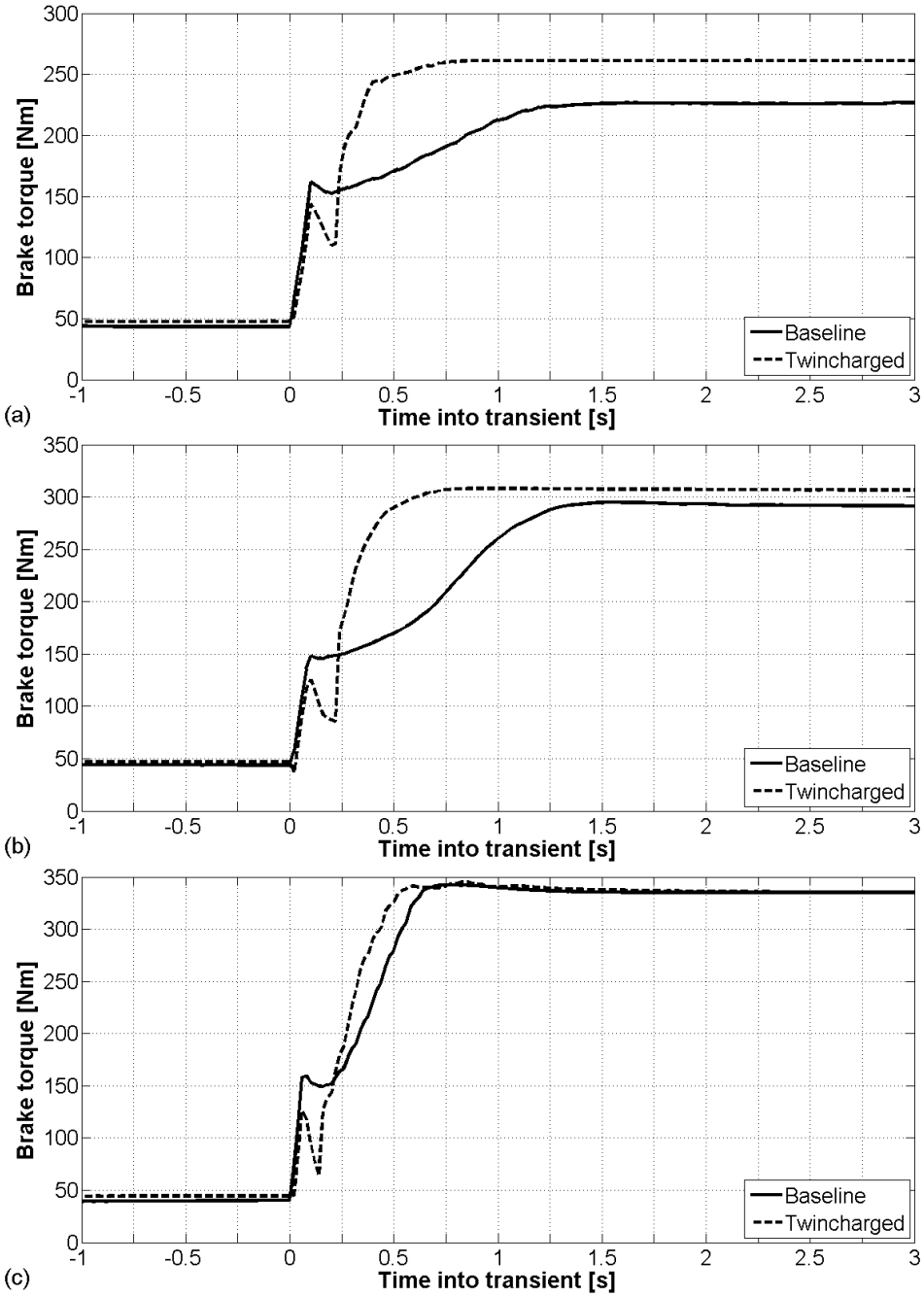

Figure 3.45 – Transient torque response – a) 1250 rpm; b) 1500 rpm; c) 2000 rpm

Considering the torque response of the two systems at 1250 rpm (Figure 3.45a), not only does the twincharged engine reach its peak torque in less than half the time of the baseline engine, but its final magnitude is also greater. This would present clear benefits in driveability of the vehicle through enhanced acceleration response. As engine speed is increased, the twincharged system retains its superiority in terms of transient torque response, although this is significantly reduced as engine speed reaches 2000 rpm (Figure 3.45c). Since the VGT mechanism was disabled in the

twincharged model in order to simulate the behaviour of a fixed geometry turbocharger, the speed (and thus boost pressure) of the turbocharger in the twincharged system is negligible at these engine speeds (Figure 3.44). It is expected that greater performance could be extracted from the twincharged scheme if the VGT system was incorporated and appropriately calibrated.

The phenomenon in torque response around 0.2 seconds into the transient as shown in Figure 3.45 is due to the slight delay in boost response to the instantaneous step in fuel demand – this can be seen to a lesser extent in Figure 3.43, where there is a slight lag in boost response in each test case. For the twincharged engine, the fluctuating supercharger power requirement is also a major factor in this uneven behaviour, as shown in Figure 3.46.

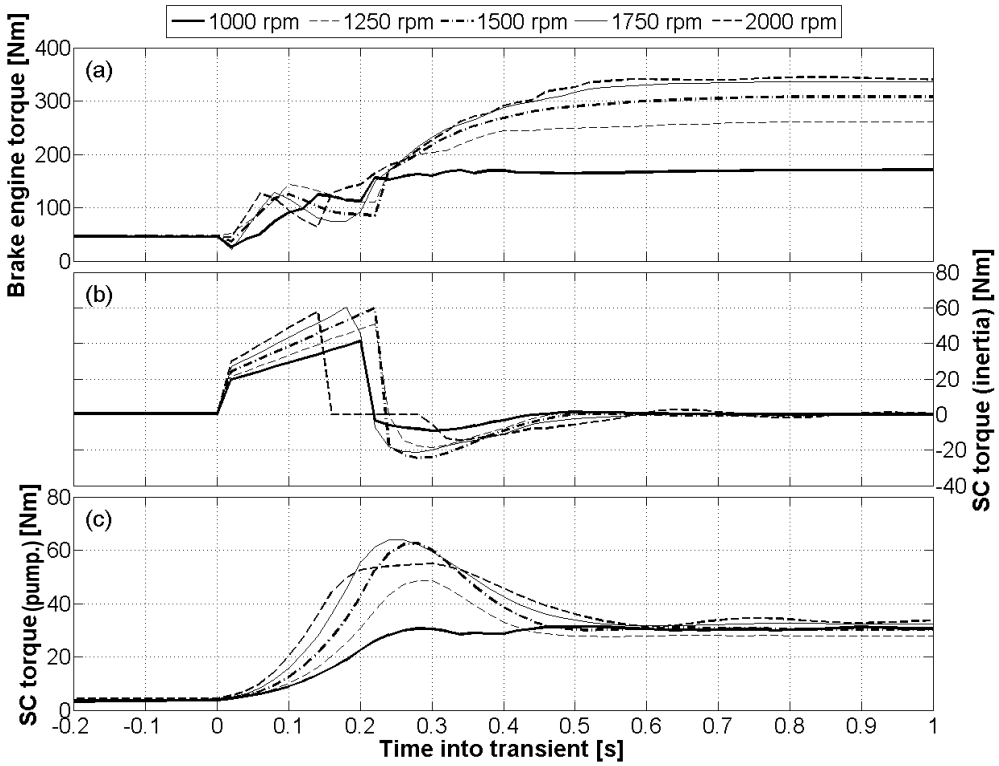

Figure 3.46 – Twincharged engine transient torque – a) brake engine torque; b) supercharger inertia torque demand; c) supercharger pumping torque demand

Figure 3.46a is the engine brake torque response for each of the engine speeds tested, displayed at a higher resolution in time than Figure 3.45; Figure 3.46b is the torque (at the crankshaft) required to accelerate the supercharger, proportional to the inertia of the supercharger system rotating mass; Figure 3.46c is the crankshaft torque required to overcome the aerodynamic pumping load on the supercharger

compressor, which relates to supercharger speed. Supercharger inertia was assumed to be the same as the original turbocharger, but scaled according the aforementioned relationship in Equation 3.2 using the supercharger scaling factor (given in Table 3.5). The total turbocharger inertia was used in order to account for the inertia of the drive system – i.e. shafts, belts and pulleys – as well as the compressor itself. The inertia of the CVT was ignored, as this would depend both on the particular CVT system used, and on the varying transmission ratio. Consequently, the magnitude of the inertia torque would in reality be higher than in Figure 3.46b. Nevertheless, even factoring in an increase in system inertia, the input torque demand on the CVT (with an input drive ratio such as those listed in Table 3.7) would be within the capacity of most systems, and it is anticipated that the torque response of the engine would not be significantly diminished. Regarding the aforementioned uneven torque behaviour at the beginning of the transient, appropriate calibration of the control and fuelling systems would be expected to rectify this.

For all of the test speeds the CVT ratio ranges were within the operational limits proposed earlier (Figure 3.47). Figure 3.48 shows the transient AFR during the tip in processes at 1000 rpm and 2000 rpm. The twincharged engine tended to operate at higher AFRs and avoided running into the limit, which is likely to be beneficial in terms of improved transient smoke emissions, as well as showing potential for increasing the fuelling to bring the performance in line with the steady state LTC. The spike in the twincharged AFR around 0.25 seconds into the transient in Figure 3.48a is due to slight overshoot of the supercharger – see Figure 3.44a.

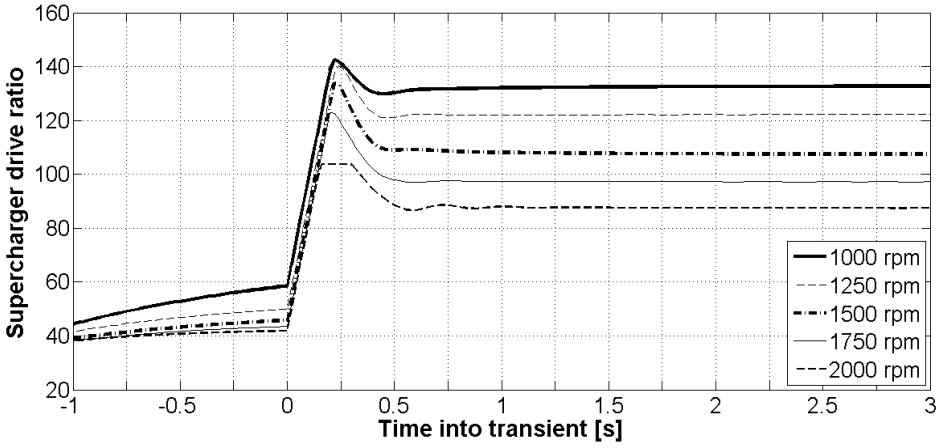

Figure 3.47 – Twincharged engine CVT ratio range

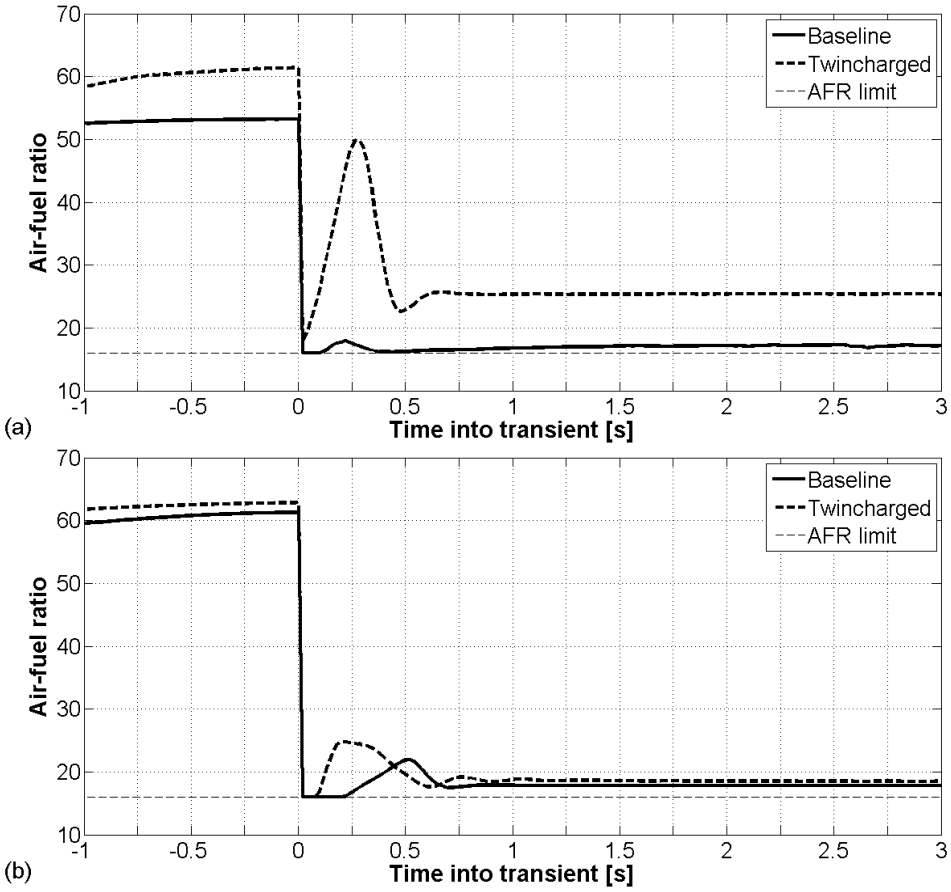

Figure 3.48 – Transient AFR – a) 1000 rpm; b) 2000 rpm

3.5 Conclusions

The potential for the augmentation of the low speed torque of a VGT-equipped high speed diesel engine has been demonstrated by employing a compound charging system (twincharged) using a combination of CVT driven supercharger and fixed geometry turbocharger. The original turbomachinery was used as the foundation for the twincharged scheme, and scaled in simulation. Design of experiments and optimisation techniques were used to find optimal settings for the size of the turbomachinery. It was found that the addition of a supercharger bypass arrangement avoided the flow range limitations (and parasitic losses) of the supercharger at high engine speeds (above 3000 rpm). This arrangement enabled the turbocharger performance to be fully exploited at higher engine speeds. Peak torque was improved by 15%, with up to 90% of the peak value available at 1000 rpm, compared with 50% for the baseline engine. Rated power, however, was not increased – a result of effectively using the original VGT as an inefficient fixed geometry unit away from the turbine design conditions. Using an appropriately matched turbocharger would be expected to rectify this. Brake specific fuel consumption increased by up to 9% while the supercharger was engaged, a result of the parasitic losses associated with mechanical supercharging. However, baseline levels were restored beyond the supercharger disengagement speed. Gas temperatures throughout the twincharged engine were comparable to baseline levels.

The supercharger drive ratio range required for the twincharged engine was investigated and found to be well within the capability of a range of CVT systems; a number of drive combinations were proposed to achieve the required overall drive ratio. CVT mechanical efficiencies were ignored throughout the investigation, but for typical values they were shown to have little overall impact on performance.

Transient performance of the proposed twincharged system was compared to the baseline engine in a Simulink co-simulation environment with the engine models. The twincharged system displayed significant improvement in transient response with improved boost response and an associated improvement in transient torque response, which would result in significantly improved vehicle acceleration and driveability. Transient AFR was also improved, which is likely to be demonstrated by reduced visible smoke during tip-in manoeuvres, as well as showing potential for

increasing the fuelling to bring the transient torque in line with the improved steady state LTC.

3.5.1 Further Work

Since the potential performance benefits of the twincharged system were established using scaled versions of the original turbomachinery, commercially available units will be investigated to explore whether further gains are achievable. In particular, Chapter 5 will cover this aspect as well as using a more efficient turbocharger capable of high pressure ratios to achieve the increased rated power (and high power density) required for downsizing. Part load efficiency benefits will also be assessed, and with the by-product of establishing and validating the required CVT ratio range.

Chapter 4 Ultraboost Project Introduction and Validation of the Engine Model

The Ultraboost project and its downsizing objectives are introduced in this chapter, along with the 'Minimap' points used to simplify the process of evaluating the predicted NEDC fuel consumption. A model of the Ultraboost engine was created in GT-Power, and its salient features and controls are described. Details are given of the engine testing facilities at the University of Bath and the instrumentation and data acquisition methods used to collect performance data from a prototype of the Ultraboost engine. Particular attention is given to the novel charge air handling unit (CAHU), which was used to emulate performance of the turbocharger and supercharger, since the boosting system hardware was unavailable at the time of testing. The GT-Power model is then compared with and validated against this empirically recorded data.

4.1 Ultraboost Project Introduction

The 'Ultraboost' project is a collaborative venture led by Jaguar Land Rover, consisting of a number of technical partners, within both industry and academia. The work reported in this and the following chapters comprises a small part of this overall project, further details of which can be found in [101]. The engine used for this investigation is a 2.0 litre in-line 4 cylinder highly boosted gasoline engine, which has been conceived as a downsized replacement for a 5.0 litre naturally aspirated V8. The full load torque and power objectives are shown in Figure 4.1, along with the corresponding air mass flow requirements for the downsized engine.

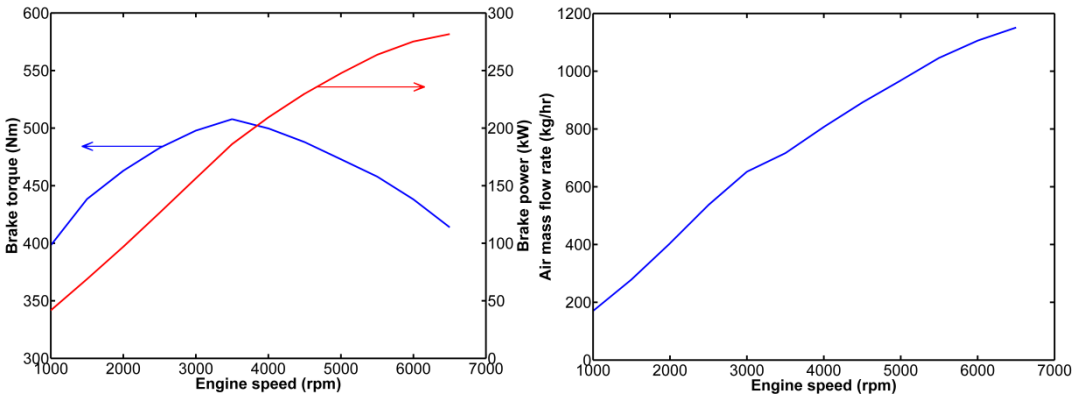

Figure 4.1 – Downsized engine performance requirements – a) torque and power; b) air mass flow

The downsized engine features a pre-turbine to pre-compressor EGR circuit and both gasoline direct injection (GDI) and port fuel injection (PFI); its air charging system consists of a fixed geometry turbocharger (Honeywell GT30 with external wastegate) in a sequential series arrangement with a positive displacement supercharger (Eaton R410 Roots-type); the supercharger can be declutched and bypassed depending on engine speed and load. This arrangement was selected as a balance between its ability to meet the performance demands, its availability for implementation, and other aspects such as the potential fuel efficiency improvements [102][103]. A schematic of the engine is shown in Figure 4.2; engine geometry and other details are given in Table 4.1.

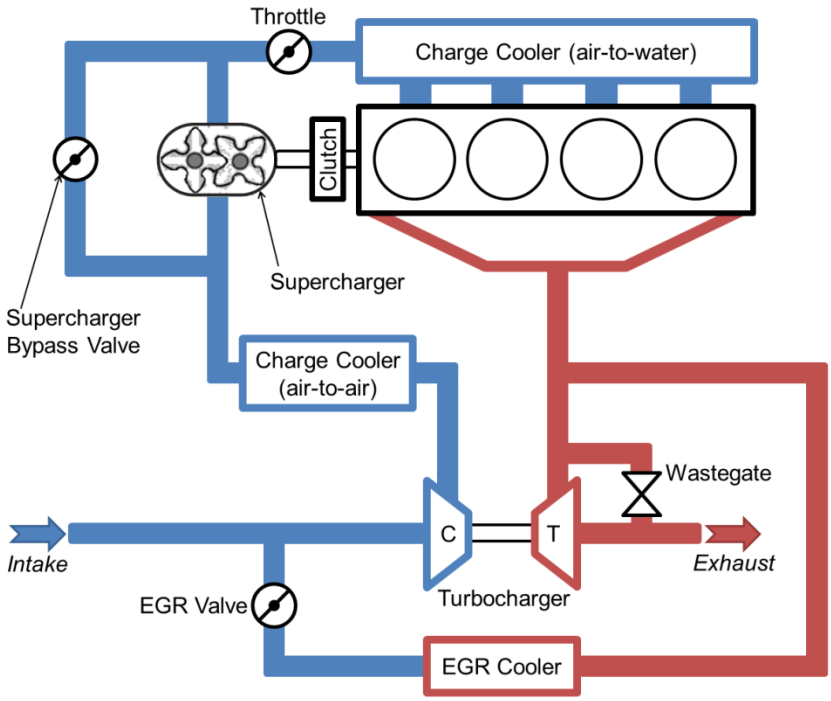

Figure 4.2 – Downsized engine schematic

Table 4.1 – Downsized engine parameters

Parameter	*Value*
Bore (mm)	83
Stroke (mm)	92
Displacement (cc)	1991
Con Rod Length (mm)	150
Compression Ratio	9:1
Max Power (kW) @ Rated Speed (rpm)	283, 6500
Max Torque (Nm) @ Rated Speed (rpm)	515, 3500

4.1.1 Minimap Points

The overall aim of this particular downsizing project is a 35% reduction in fuel consumption (and corresponding reduction in CO_2) over the New European Drive Cycle (NEDC). For ease of analysis and comparison, the performance of the baseline V8 engine (as mounted in the target vehicle) over the NEDC has been discretized into a number of steady state 'Minimap' operating points – these are listed in Table 4.2, and the process for defining them is described in [101]. Each of these points represents a portion of the drive cycle and holds a weighting equivalent

to the proportion of time the engine is run at this speed and load during the NEDC. Thus, applying the weighting to the corresponding fuel flow rate measured at each Minimap point, summing these values and multiplying by the drive cycle time gives a mass of fuel equivalent to that used over the NEDC – in this case, 1016 g. Using this method, drive cycle economy improvements can be estimated much more quickly than running a full drive cycle itself.

Table 4.2 – Baseline engine NEDC 'Minimap' points

Minimap no.	*Engine Speed (rpm)*	*Brake Torque (Nm)*	*NEDC Weighting (%)*	*Fuel Flow (g/s)*	*BSFC (g/kWhr)*	*NEDC Total (g/s)*
1	600	27.9	0.291	0.3614	742.2	0.1052
2	1500	39.8	0.013	0.8689	500.3	0.0114
3	1500	104.2	0.098	1.3570	298.5	0.1337
4	1500	198.9	0.024	2.1586	248.7	0.0537
5	2000	79.6	0.001	1.5700	339.0	0.0015
6	2000	198.6	0.008	2.8975	250.4	0.0244
7	1250	15.9	0.108	0.5744	992.6	0.0623
8	1000	15.9	0.079	0.4491	970.1	0.0355
9	1000	79.6	0.088	0.7783	336.2	0.0689
10	1250	159.2	0.022	1.5206	262.8	0.0344
11	1350	238.7	0.022	2.2958	244.9	0.0525
12	1500	298.4	0.014	3.1081	238.7	0.0448
13	1250	119.4	0.042	1.2370	285.0	0.0528
14	1250	59.7	0.124	0.8494	391.4	0.1054
15	1500	139.3	0.045	1.6419	270.2	0.0748
					Total fuel (g)	*1016*

4.1.2 GT-Power Engine Model

Engine performance was simulated using a 1D model implemented in the GT-Power engine simulation software package [104], using the engine schematic shown in Figure 4.2 as the basis for the model. Combustion was represented using a spark

ignition Wiebe model; the Wiebe parameters used are typical of a naturally aspirated, 4-valve, port-injected, gasoline engine. Combustion effects such as knock and auto-ignition were ignored throughout since the operating points selected had been demonstrated experimentally to be achievable. The air-fuel ratio (AFR) control in the model was implemented by using direct injection only, the injectors being of an AFR-targeting type, set to achieve stoichiometry at all operating conditions. This was in accordance with the project target (defined in [101]), the purpose of which is to maintain exhaust emissions and after-treatment performance.

The primary load control mechanisms of the engine were thus as follows: the throttle valve; engagement of the supercharger, and its drive ratio; the turbocharger wastegate; the supercharger bypass valve; inlet and exhaust valve timing; and the EGR circuit valve. It is worth noting that spark timing would have been included in this list, but the Wiebe combustion model precludes this.

4.2 Engine Testing Facilities

4.2.1 Engine Dynamometer

A prototype of the Ultraboost engine – described in Section 4.1 – was developed based on a current production version of the baseline 5.0 litre V8 engine. An open-source ECU made by EFI Technology was used, which was initially coded and calibrated by Lotus Engineering. The engine was installed on a specially developed transient dynamometer at the University of Bath. The dynamometer is in a tandem AC motor drive configuration, with a base AVL unit (providing motoring capability) in series with an eddy-current dynamometer to give a combined capacity of 400 kW.

4.2.2 Charge Air Handling Unit (CAHU)

Since the boosting hardware was still in the initial stages of selection and development when the experimental work started, the engine was run as naturally aspirated to collect data for the Minimap points (see Section 4.1.1) – this was sufficient for the mass air flow requirements of these relatively low load operating points. For investigations into high load operation the engine was connected to a charge air handling unit (CAHU) – a novel testing system developed at the University of Bath, which can be used in place of the boosting hardware to emulate the effects of charge temperature and pressure, as well as exhaust back pressure [88]. A schematic of the CAHU is given in Figure 4.3. Note that the geometric compression ratio and other major design features were the same for both naturally aspirated and boosted versions of the engine.

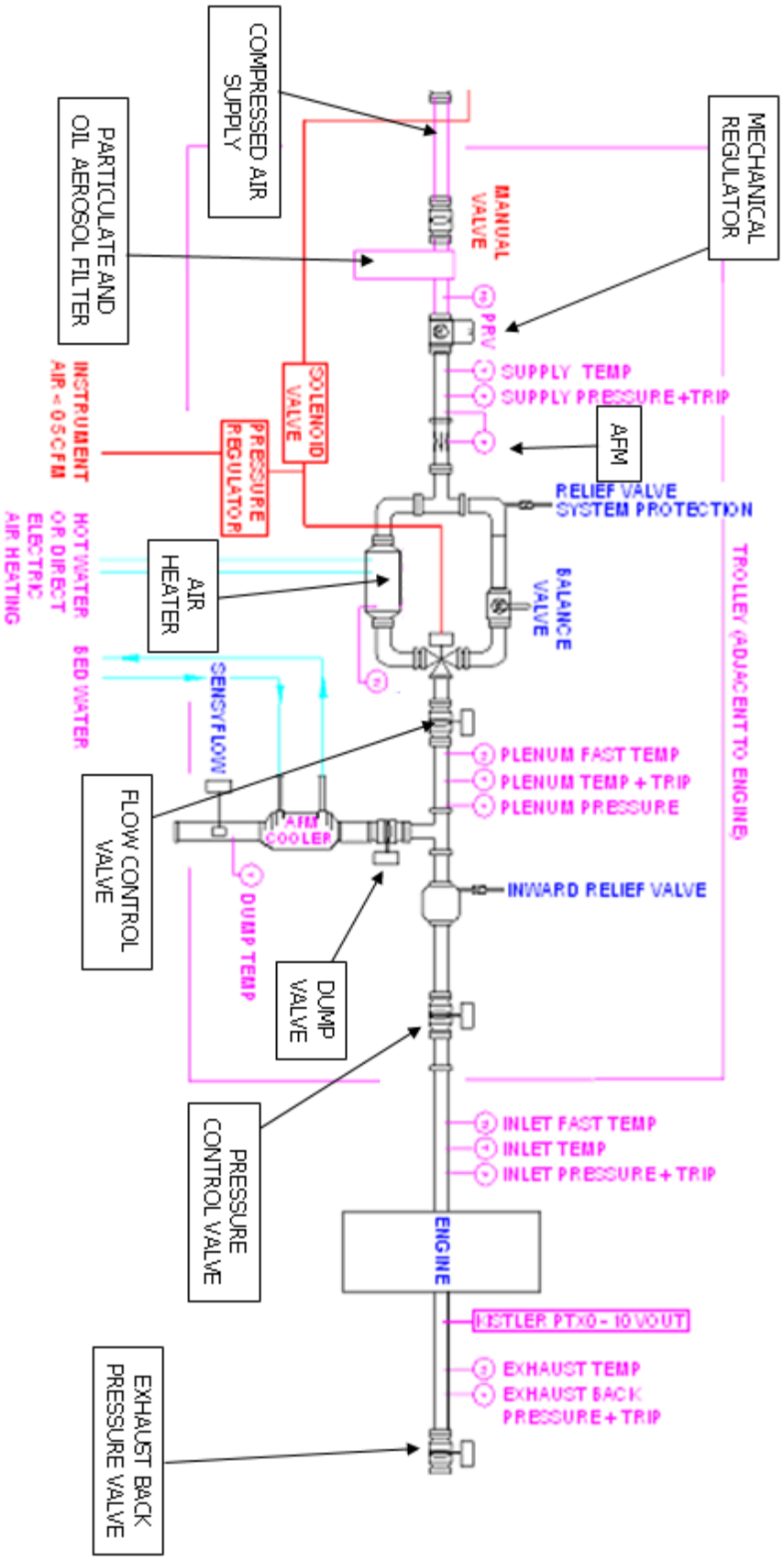

Figure 4.3 – Charge Air Handling Unit (CAHU) system schematic [88]

In order to emulate intake manifold conditions, an industrial compressor system is used to supply compressed air at 7 bar absolute pressure and 25°C, with flow rate capacity of up to 1500 kg/hr – well above the requirements of the Ultraboost engine (see Figure 4.1). The compressed air is passed through a particulate and oil filter in order to ensure a clean air supply, and a mechanical regulator is used to reduce the pressure to 5 bar. At this stage, total air flow into the CAHU is determined using a differential pressure transducer to measure the pressure drop over an orifice plate.

The flow is then split into two paths, one passing over a 15 kW electrical heating element, the other path unheated. The hot air path is maintained at 600°C using a PID controller acting on the heating element, with feedback provided by an infra-red sensor measuring the surface temperature. By modulating the proportion of air channelled down the heated path, the resulting charge temperature can be regulated – a PID controller on an upstream mixing valve is used to achieve the temperature demand. Intake pressure supplied to the engine is regulated using a butterfly valve, which introduces a pressure drop, in turn controlled by a closed loop PID controller. At this stage, excess air flow is then dumped to the atmosphere. The (cooled) dump flow is measured using an ABB Sensyflow air mass flow meter, and thus engine mass air flow can be calculated by the difference between total supplied flow and this dumped flow.

On the exhaust side, manifold back pressure caused by any turbocharger turbines is achieved by a fast-response butterfly valve in the exhaust system. The capacity of the back pressure valve is 4 bar absolute.

4.3 Instrumentation and Data Acquisition

The engine and dynamometer were controlled using CP Engineering CADET V14 software installed on the dynamometer host PC. This was also used to remotely control the CAHU operating point via a CAN bus connection to a second workstation (also using CP CADET software) which was specific to the CAHU. ECU input variables were also controlled by the main CADET system via an ASAP3 interface – ECU output channels were likewise recorded via this interface.

Dynamometer load was measured using an HBM torque flange, and speed was measured using a 1024 pulse encoder. The Sensyflow mass flow meter at the inlet to the CAHU was principally used for engine MAF measurement. Pressure transducers and K-type thermocouples were installed in key locations on the engine (e.g. intake and exhaust manifolds), and the main CADET system was used for recording time-averaged data from these components (at an 80Hz sampling rate). In order to record pulsed exhaust flow data for more detailed turbocharger performance analysis, Kistler 6041B water-cooled pressure transducers were fitted in the exhaust ports.

Crank angle based measurements for combustion analysis were recorded using an AVL IndiSet Advanced system, with data produced from in-cylinder mounted Kistler 6054 pressure transducers. Crank timing was determined using an AVL crank angle encoder (with a resolution of 0.1°) which was installed on the front of the engine.

Fuel flow was primarily measured using an Emerson CMF010 coriolis flow meter, which has a mass flow accuracy of +/-0.1% for liquids (including the combined effects of repeatability, linearity, and hysteresis). As a secondary measure, a gravimetric fuel meter was also used – although not as accurate as the coriolis flow meter, this was useful as a back-up and checking device.

4.3.1 Emissions Measurement

Emissions concentrations were measured using a Horiba MEXA-7000 series analyser, taking single point raw exhaust gas samples for CO_2, CO, THC and NO/NO_x dry exhaust gas fractions. (Although there is the facility for measuring both pre- and post-catalyst samples, only pre-catalyst was used in this case, since an exhaust catalyst was not fitted to the prototype engine.) EGR rate was calculated by

comparing measurements of CO_2 in the intake and exhaust manifolds. An AVL 439 opacimeter was used to measure exhaust smoke opacity (which was largely unnecessary, due to operating at or near lambda 1 in all cases for this project). In terms of air-fuel ratio, although the ECU performs closed-loop lambda control, an ETAS LA4 lambda sensor was used for verification purposes.

4.4 Part Load Test Points

The Ultraboost engine was initially run as naturally aspirated (i.e. without the CAHU) to characterise the maximum performance without the boosting hardware. In this configuration, a number of the Minimap points given in Table 4.2 were explored, including the three points that are to be more thoroughly investigated in simulation in the following chapter: 3, 9 and 14. The corresponding simulation and experimental results are compared below. (For the simulations, the supercharger was disengaged and bypassed in order to replicate as closely as possible the naturally aspirated experimental set-up.)

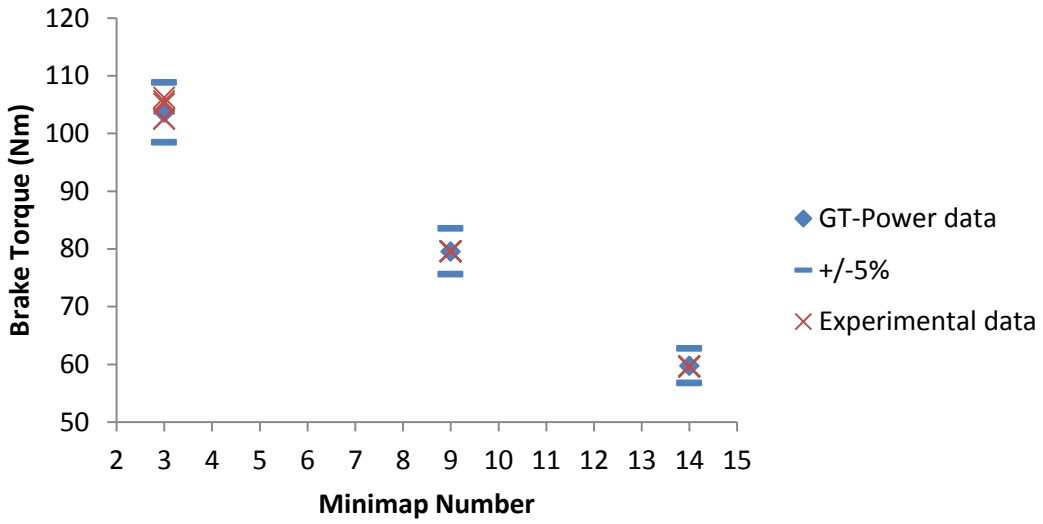

Figure 4.4 – Comparison of GT-Power simulation and empirical results at Minimap points 3, 9 and 14 – brake torque (Nm)

Figure 4.4 shows the experimental data and simulation results for engine torque correlate very well, with only some slight drift at Minimap point 3 – but the magnitude of this is only 2-3%. Considering the results for mass air flow (Figure 4.5), Minimap point 3 is this time the most consistent. Point 14 also correlates fairly well, but with some of the experimental points requiring slightly lower flow rates for the same engine output. The simulation for point 9 shows a tendency to under-predict the required air flow, but this is still largely within a 5% margin of error.

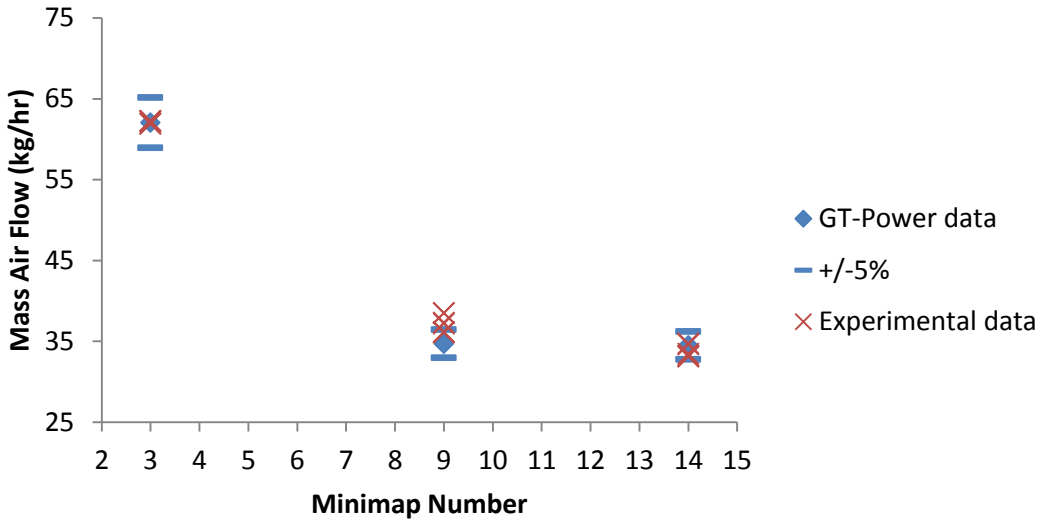

Figure 4.5 – Comparison of GT-Power simulation and empirical results at Minimap points 3, 9 and 14 – mass air flow (kg/hr)

The equivalent results for fuel flow reveal a similar trend of under-prediction for the simulation result for point 9; points 3 and 14 also display this tendency. Since the exhaust lambda measurements for these data points were within 1% of the target (lambda 1), this trend can be at least partially attributed to the difference between the in-cylinder lambda control used in the model and the exhaust lambda control used on the hardware. However, since these variations are within an acceptable margin of error, the discrepancy can be neglected.

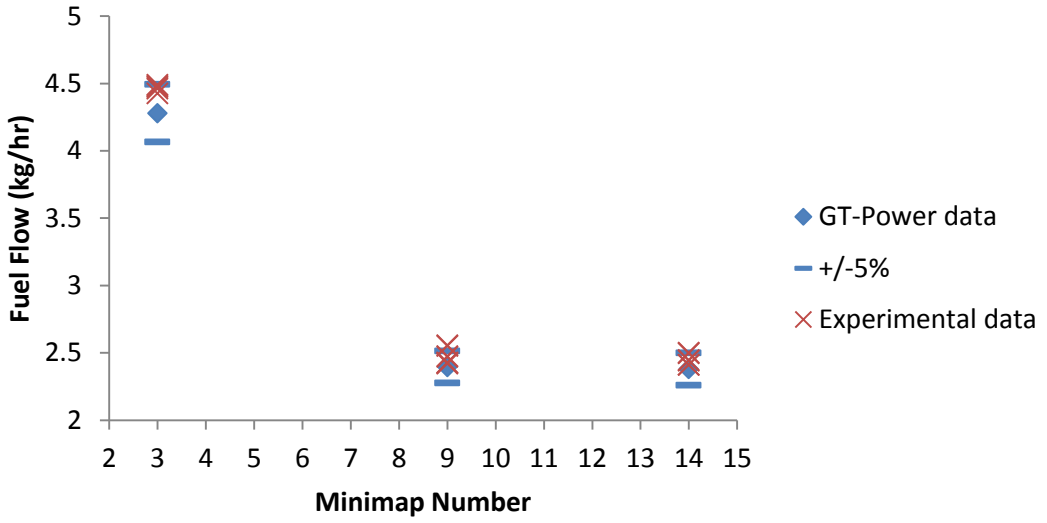

Figure 4.6 – Comparison of GT-Power simulation and empirical results at Minimap points 3, 9 and 14 – fuel flow (kg/hr)

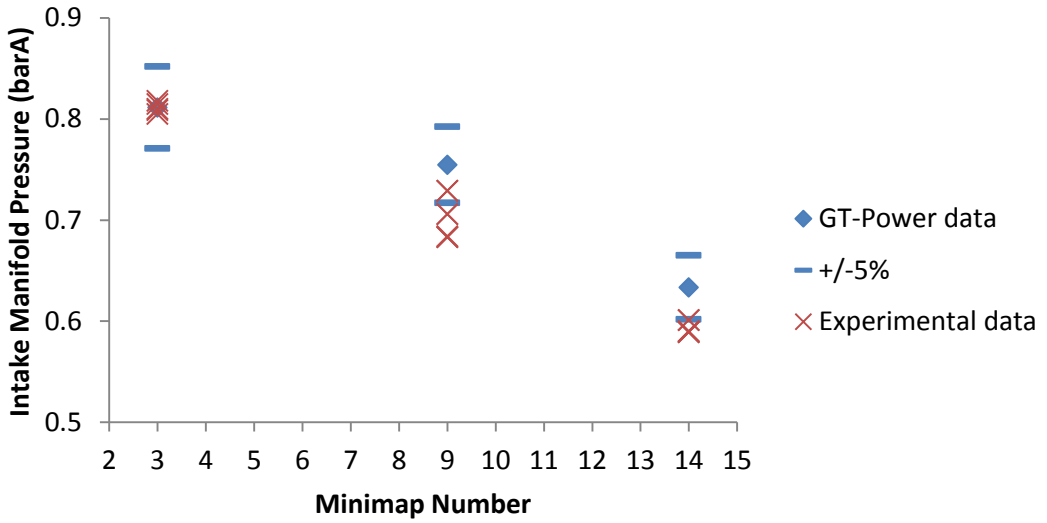

Figure 4.7 – Comparison of GT-Power simulation and empirical results at Minimap points 3, 9 and 14 – intake manifold pressure (bar)

For Minimap point 3, experimental and simulation results match extremely well for intake manifold pressure, as shown in Figure 4.7. For points 9 and 14, the model tends to over-predict; but these variations are only of the order of 30-50 mbar. Since the corresponding gas temperatures were reasonably consistent between measured and simulated data, these conflicting relationships between mass flow and pressure must either be due to differences in gas properties, or (more likely) slight discrepancies in the volumes of the modelled and real-life intake systems.

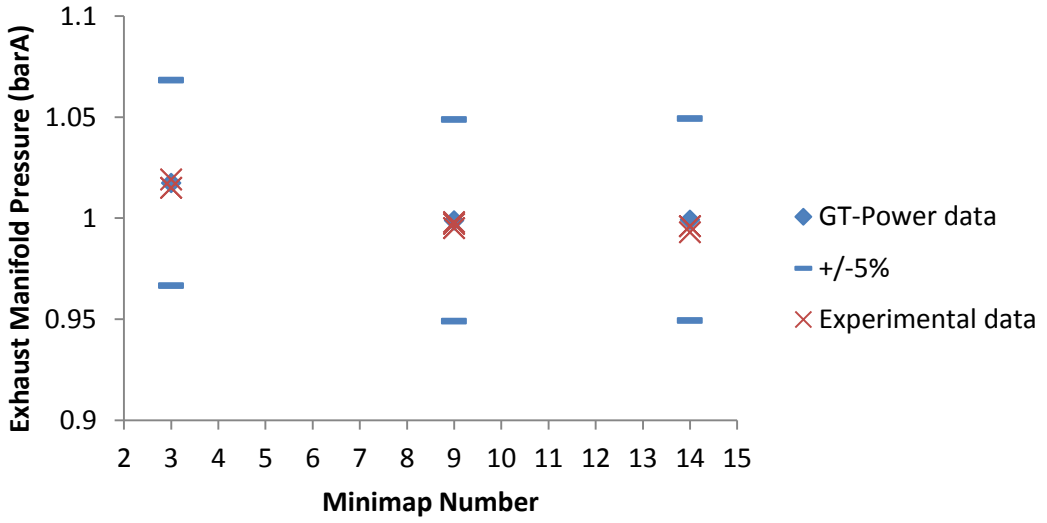

Figure 4.8 – Comparison of GT-Power simulation and empirical results at Minimap points 3, 9 and 14 – exhaust manifold pressure (bar)

Exhaust manifold pressures hold no cause for concern, as the simulation and experimental data were entirely consistent (Figure 4.8). However, this may be largely circumstantial, since the prototype engine was exhausting to atmospheric pressure, there were no features in the exhaust that would cause any back pressure, and at these relatively low loads there would not be significant exhaust pressure anyway. On the other hand, the corresponding results for exhaust manifold temperature give more confidence, with the simulation output matching up well with the experimental data (Figure 4.9).

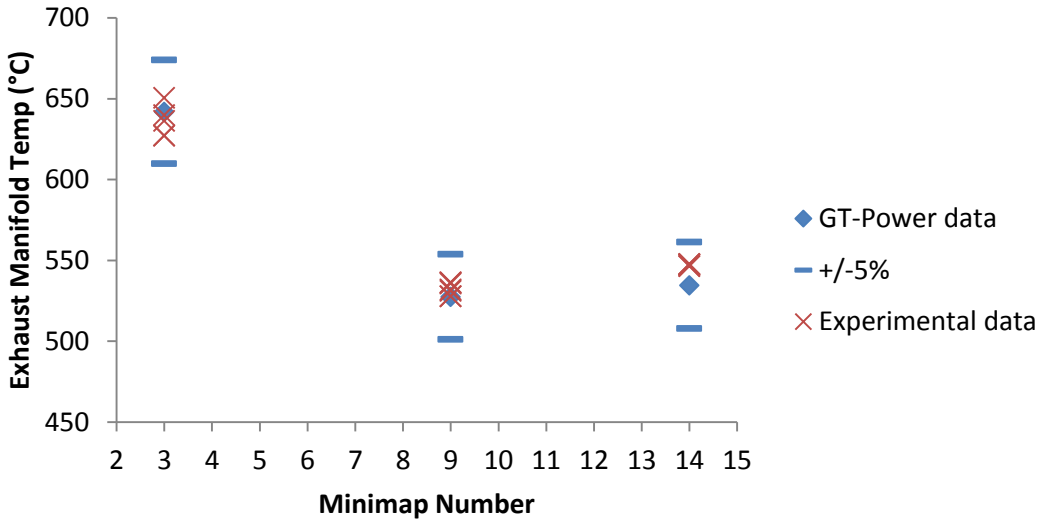

Figure 4.9 – Comparison of GT-Power simulation and empirical results at Minimap points 3, 9 and 14 – exhaust manifold temperature (°C)

Considering fuel consumption, as a result of the under-predicted values of fuel flow that the engine model produces (Figure 4.6), simulated values of BSFC are generally below the equivalent experimental data too, as shown in Figure 4.10. The level of under-prediction is not extreme, however, and this trend can be taken into account in the analysis of any subsequent modelling results.

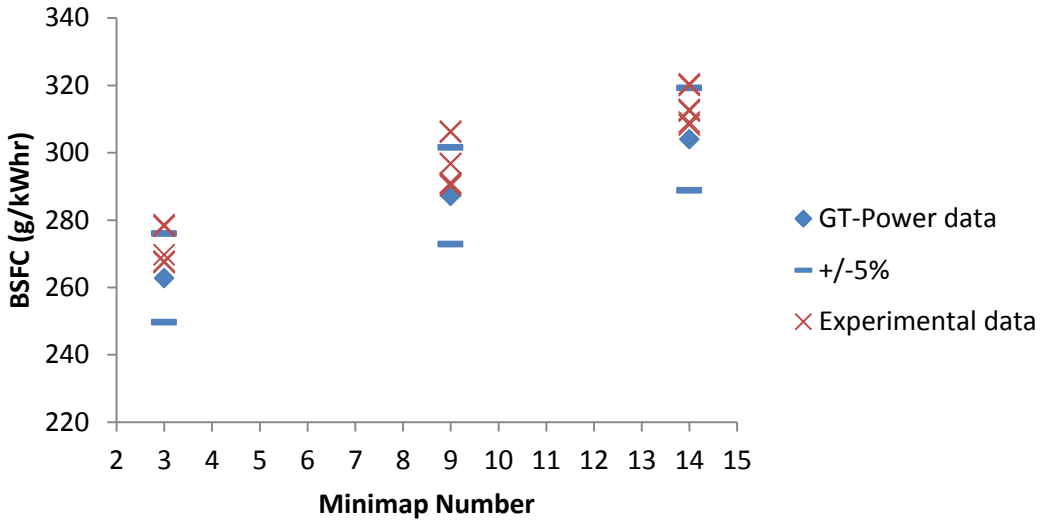

Figure 4.10 – Comparison of GT-Power simulation and empirical results at Minimap points 3, 9 and 14 – BSFC (g/kWhr)

Overall, there is a reasonably good correlation of these important bulk flow parameters between the recorded experimental data and the simulation results for the part load points considered.

4.5 Full Load Test Points

With the CAHU installed, the engine was run at various points along the target torque curve. On the whole, the torque achieved on the dynamometer matches up fairly well with the results obtained in simulation, as can be seen in Figure 4.11. (Note that the experimental torque values at 3000 rpm and below have been adjusted for the parasitic torque requirement of the supercharger.)

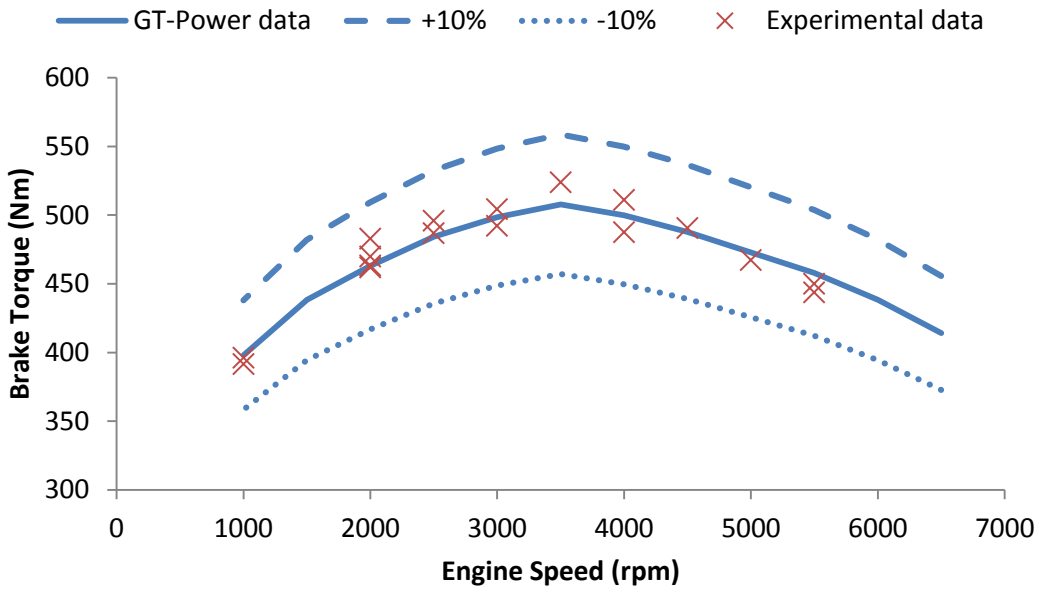

Figure 4.11 – Comparison of GT-Power simulation and empirical results at full load – brake torque (Nm)

Recorded air mass flow data was generally within a 10% margin of the simulation results, with the model slightly over-predicting at lower engine speeds (i.e. when the supercharger is engaged, at 3000 rpm and below), and under-predicting at higher engine speeds (when operating purely with the turbocharger) – see Figure 4.12. Corresponding fuel flow measurements also exhibit this trend at high engine speeds (Figure 4.13) – although there is some clear fuel enrichment occurring at the 5500 rpm points, which is confirmed in the recorded lambda values of approximately 0.9. Since subsequent simulation-based investigations are concerned only with operation at lower engine speeds (where the data is better matched), these discrepancies are acceptable.

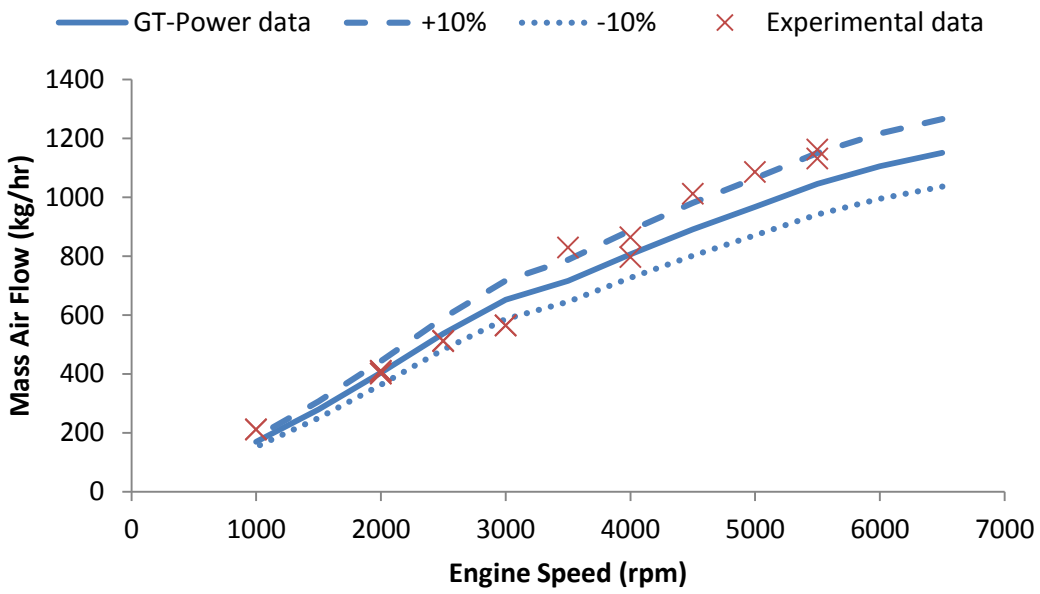

Figure 4.12 – Comparison of GT-Power simulation and empirical results at full load – mass air flow (kg/hr)

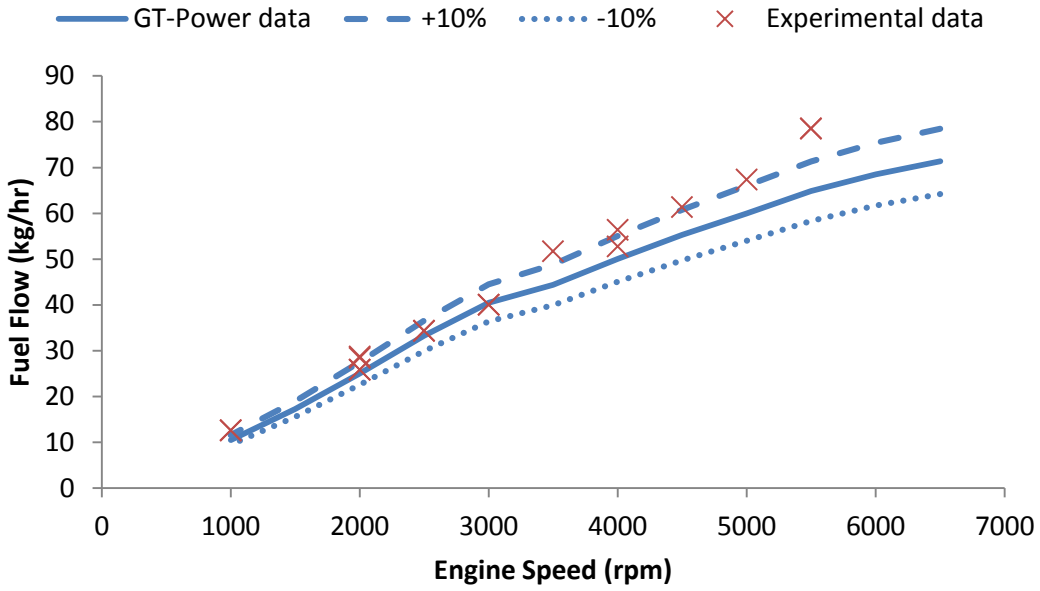

Figure 4.13 – Comparison of GT-Power simulation and empirical results at full load – fuel flow (kg/hr)

The differences in recorded and simulated manifold pressures are more of a problem. The CAHU set points used for intake pressure were significantly lower than those produced in the model, particularly in the region where the supercharger was engaged (Figure 4.14) – the difference is as much as 0.5 bar at 3000 rpm and

below. At higher engine speeds, the model still uses higher boost pressure, but the differences are mostly within acceptable margins.

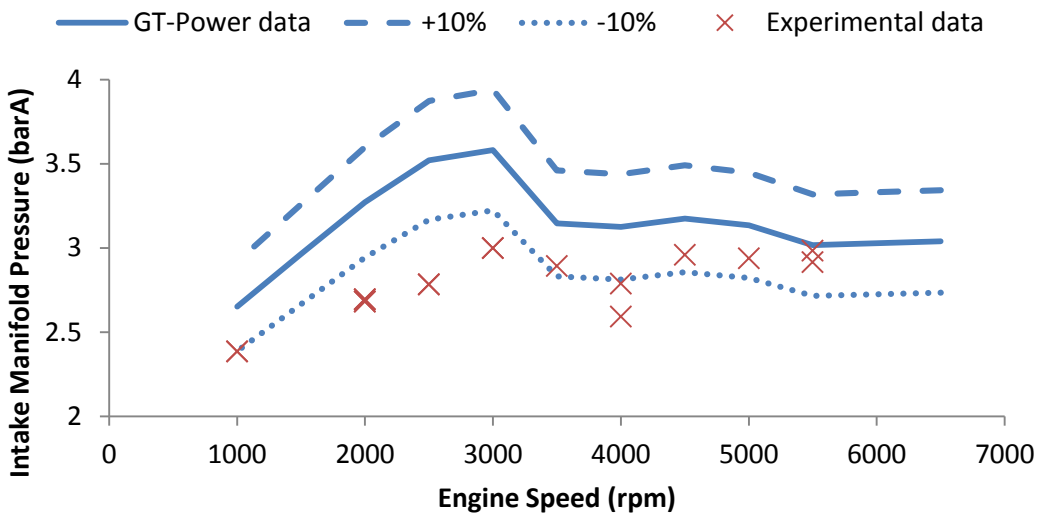

Figure 4.14 – Comparison of GT-Power simulation and empirical results at full load – intake manifold pressure (bar)

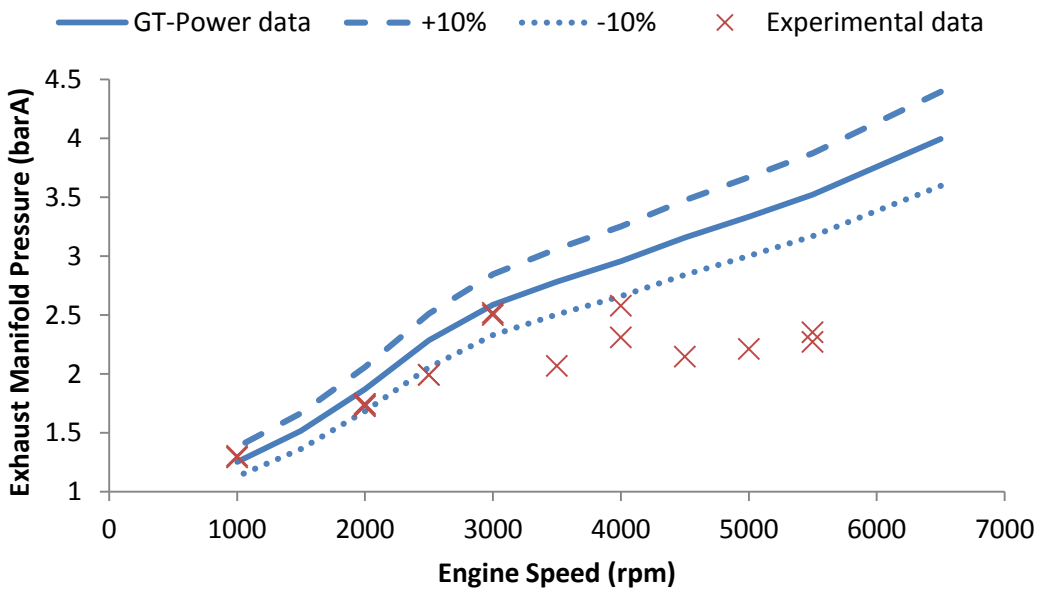

Figure 4.15 – Comparison of GT-Power simulation and empirical results at full load – exhaust manifold pressure (bar)

Comparing exhaust manifold pressures shows a similar trend of over-prediction in the model, but within acceptable margins at low speeds in this case, and much more significant divergence at high engine speeds (Figure 4.15). There are a number of

factors contributing to the differences in manifold pressures. Firstly, since mass flows roughly correlate between the simulations and the experimental data, there must be some differences in the geometry of the intake system – at least where pressure is being measured. Secondly, valve timings differed between simulation and the hardware for these test points. Thirdly, slight fuel enrichment was apparent throughout the experimental data. Fourthly, the increased exhaust back-pressure would increase residuals and thus necessitate a corresponding increase in boost pressure to achieve the required torque. However, perhaps the most significant factor causing the discrepancies was the overly conservative combustion model used in the simulations. This can be clearly seen in the comparison of recorded and predicted maximum cylinder pressures in Figure 4.16, where the model significantly under-predicts at all but the 1000 and 4000 rpm points. (The combustion model and cylinder pressure data will be discussed further in the next section.)

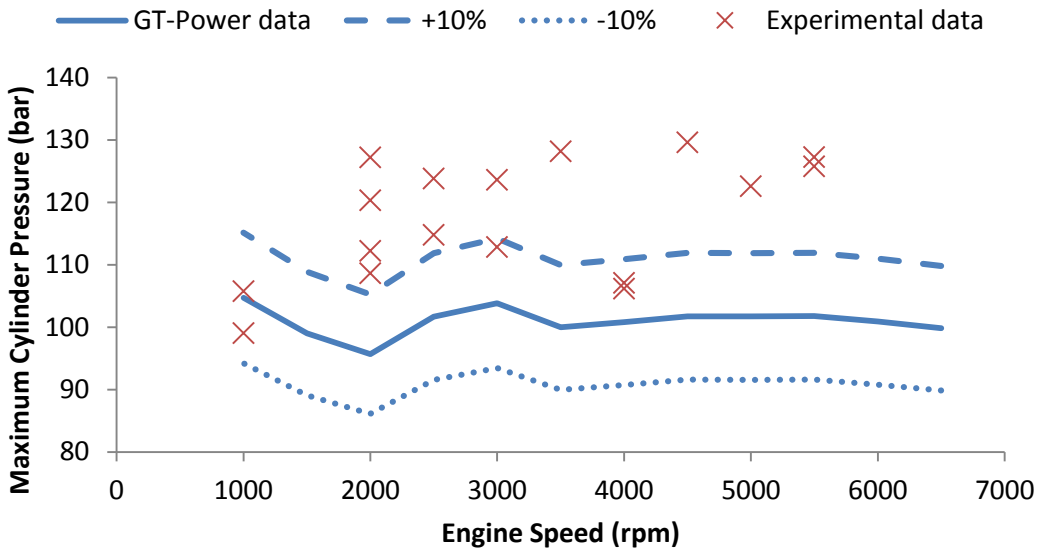

Figure 4.16 – Comparison of GT-Power simulation and empirical results at full load – maximum cylinder pressure (bar)

The generally higher fuel flows of the experimental data (i.e. fuel enrichment) are reflected in the BSFC results (shown in Figure 4.17). As with the part load simulation points considered above (Figure 4.10), the predicted BSFC results are somewhat optimistic. However, with the exception of the points at 1000 rpm and some at 2000 rpm (which have relatively low lambda readings of 0.97 and 0.96 respectively), in the region with the supercharger engaged the results display a reasonably good fit.

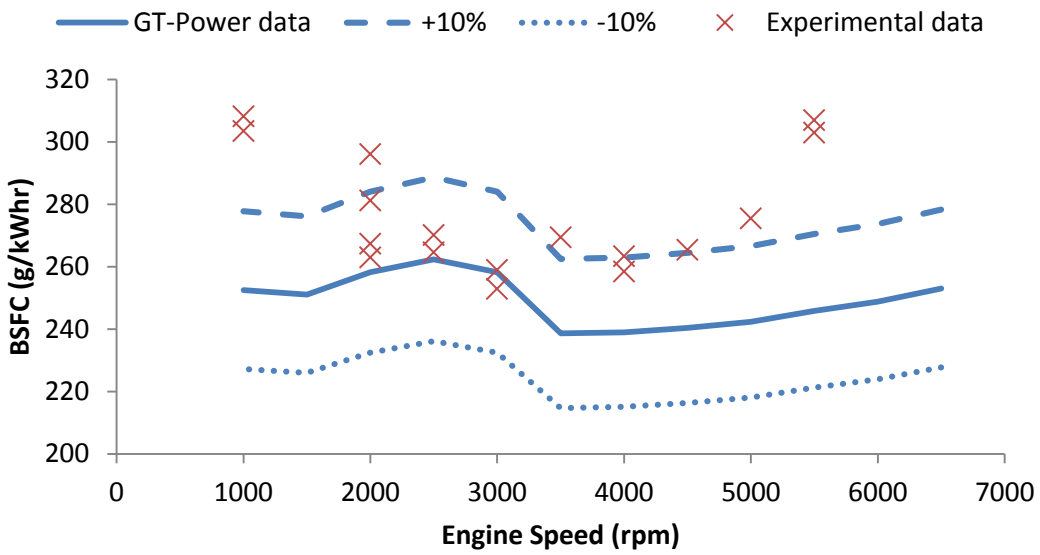

Figure 4.17 – Comparison of GT-Power simulation and empirical results at full load – BSFC (g/kWhr)

On the whole there is good correlation between predicted and recorded exhaust temperatures, as Figure 4.18 shows. The 4000 rpm test points are at particularly high temperature due to retarded spark timing, in turn resulting in late combustion, which is demonstrated in low maximum cylinder pressures (Figure 4.16), hence higher exhaust temperature and pressure (Figure 4.15). The low temperatures of the points at 2000 rpm are a result of the aforementioned rich fuelling used.

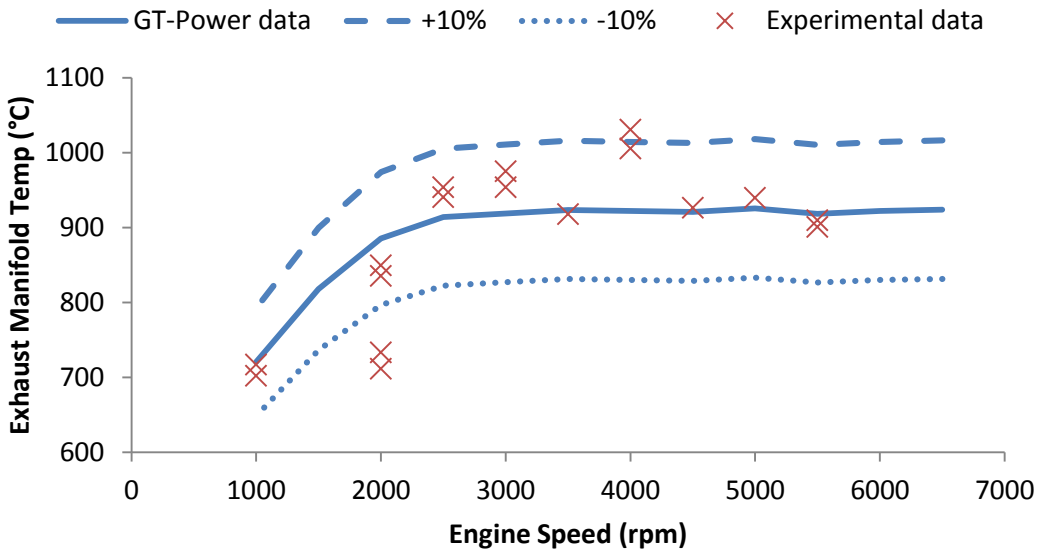

Figure 4.18 – Comparison of GT-Power simulation and empirical results at full load – exhaust manifold temperature (°C)

4.5.1 In-Cylinder Pressure Measurements

In cylinder pressure data was only recorded at some of the full load points – the instrumentation was not fitted for the initial part load (naturally aspirated) investigation. The empirical results shown below are the average of 300 recorded cycles at the relevant test point, and then averaged across the four cylinders. It should be stated that these experimental results must be treated with some caution, since effects such as potential thermal shock on the pressure transducer and the fact that blow-by was ignored in simulation may distort the displayed trends.

Firstly, considering the results at 1000 rpm (Figure 4.19), the peak pressures are well matched (reflecting those shown in Figure 4.16). The traces show excellent correlation throughout the power and exhaust strokes. Although the earlier exhaust valve timing used on the physical hardware is evident, the pressure changes during the blow-down phase are roughly equivalent. However, the higher intake pressure necessary in the simulation can be clearly seen in the compression phase, with a significant difference in pressure between the results at TDCF.

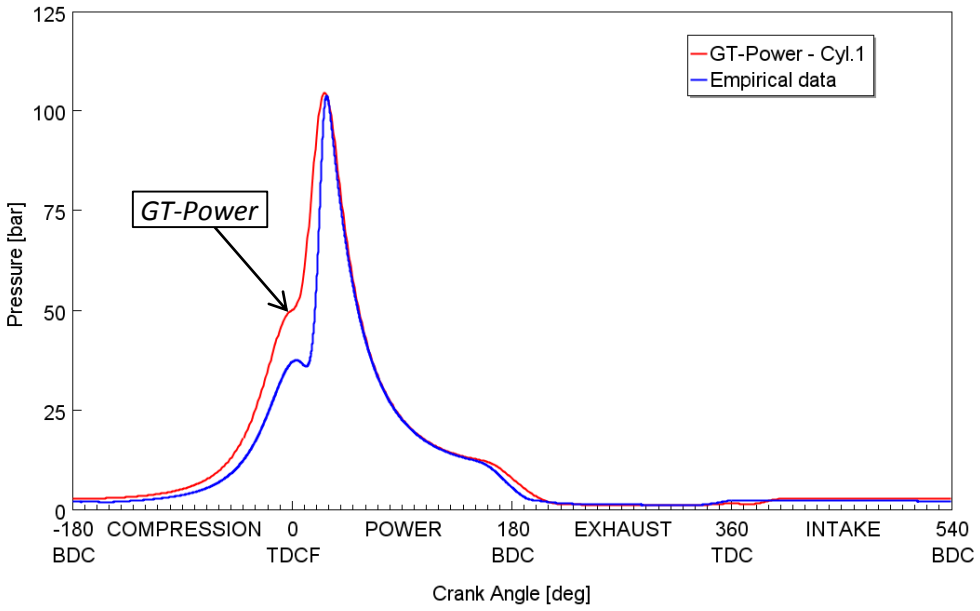

Figure 4.19 – Comparison of GT-Power simulation and empirical results at full load – cylinder pressure at 1000 rpm

At 2000 and 3000 rpm the results are not so well matched, as Figure 4.20 and Figure 4.21 show (note that the two sets of empirical data represent different spark timings, with the green traces having greater spark advance). Again, the higher intake pressures of the simulation are evident in the compression stroke, but the

conservative combustion model produces substantially lower peak pressures compared with the experimental results. The advanced spark timing of the hardware results in higher peak pressures which occur closer to TDC, whereas the delayed predicted combustion also causes higher pressures throughout the power stroke. On a positive note, the pressures at the end of the blow-down phase are well matched between simulation and experimental results.

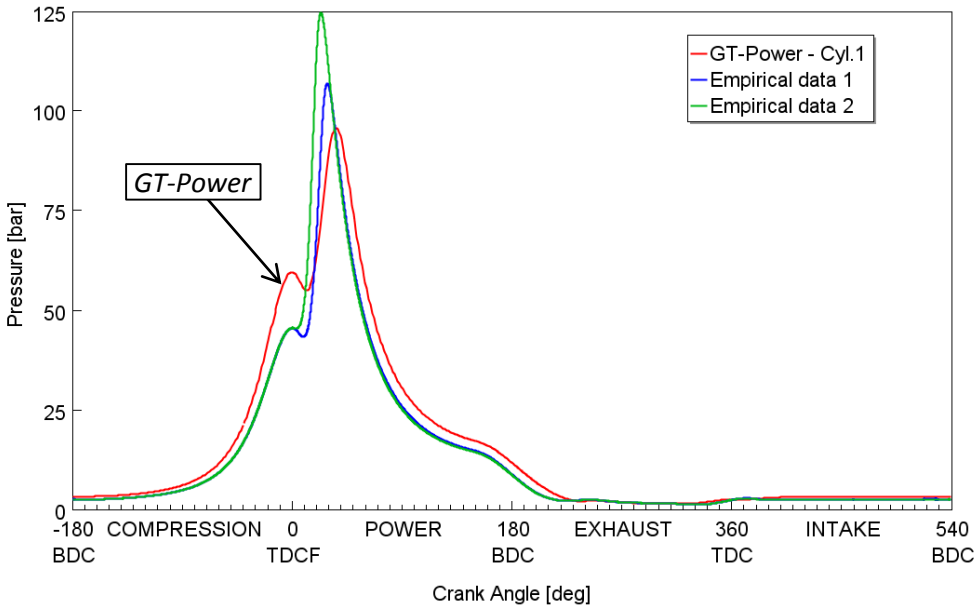

Figure 4.20 – Comparison of GT-Power simulation and empirical results at full load – cylinder pressure at 2000 rpm

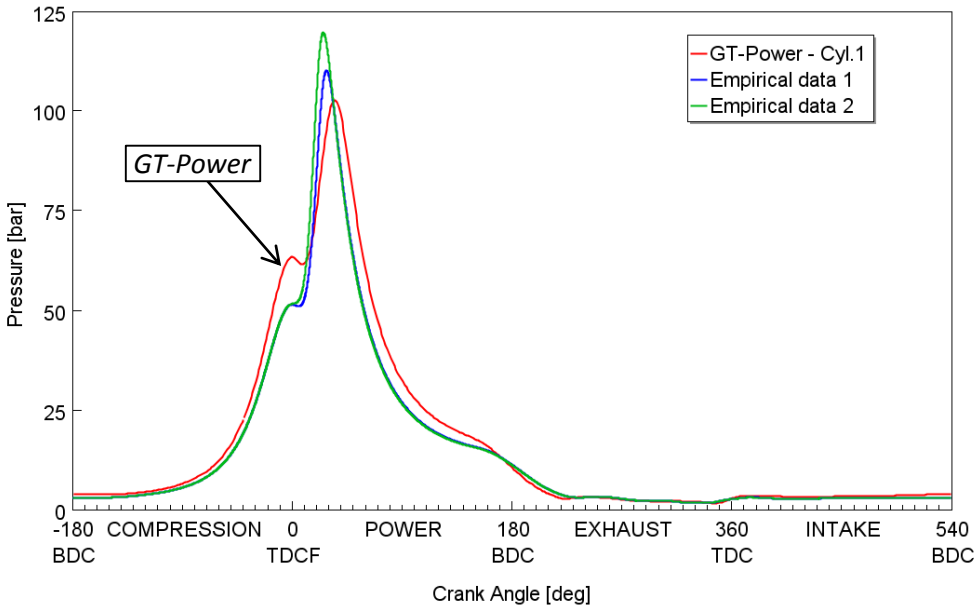

Figure 4.21 – Comparison of GT-Power simulation and empirical results at full load – cylinder pressure at 3000 rpm

At higher engine speeds, the closer fit of predicted intake pressures (seen in Figure 4.14) is reflected in the better matched compression phases of the simulation and experimental results – see Figure 4.22, Figure 4.23, and Figure 4.24, showing results at 4500, 5000, and 5500 rpm respectively. The combustion model still appears overly cautious, however, in terms of the resulting low peak pressures that are produced. A greater level of spark advance is again possible in practice, illustrated in the peak pressures of the experimental data being closer to TDC. The relative timings of the peak pressures happen to result in well matched power strokes; but this is only until the exhaust valves open, at which point the empirical data shows that the blow-down phase is more limited than predicted. However, the pressures are approximately the same by the end of the exhaust strokes. The fact that in reality greater pressure is retained within the cylinders explains why the measured exhaust manifold pressures are lower than those of the simulation at these engine speeds (see Figure 4.15).

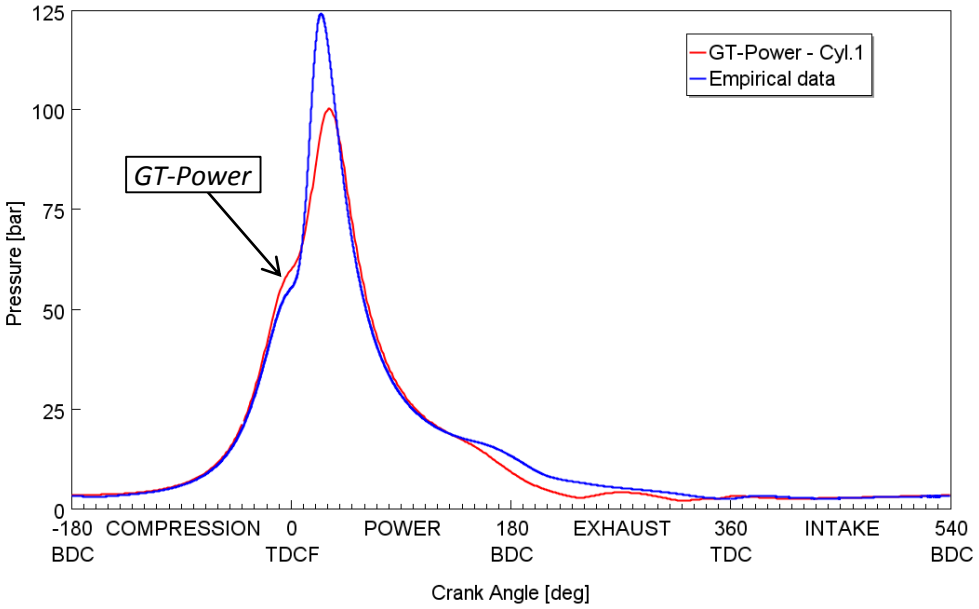

Figure 4.22 – Comparison of GT-Power simulation and empirical results at full load – cylinder pressure at 4500 rpm

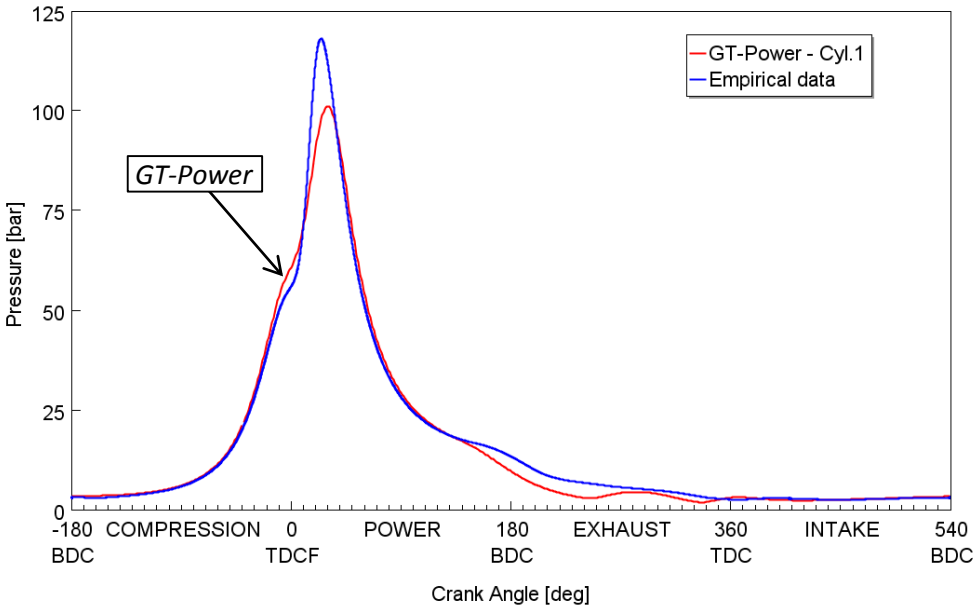

Figure 4.23 – Comparison of GT-Power simulation and empirical results at full load – cylinder pressure at 5000 rpm

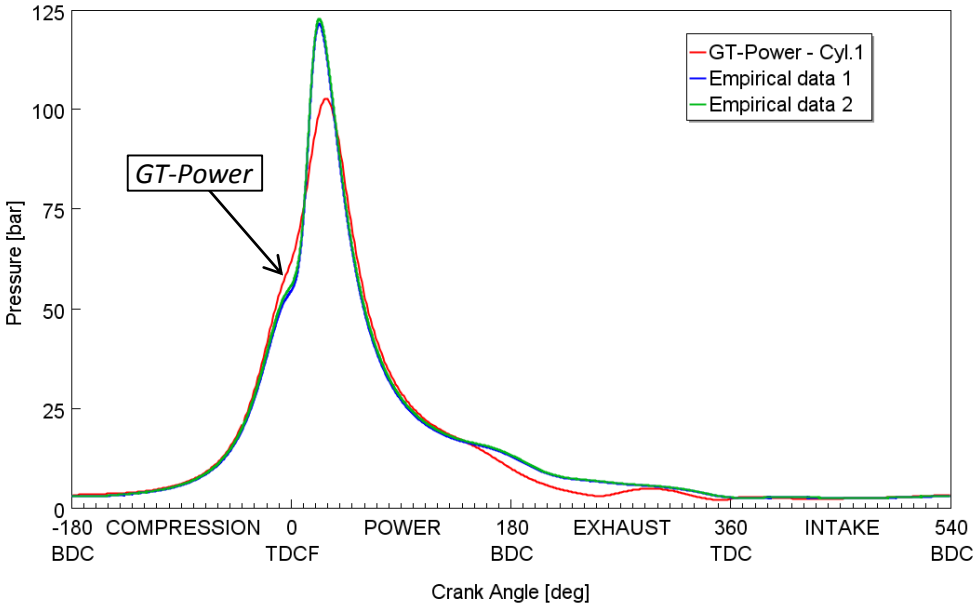

Figure 4.24 – Comparison of GT-Power simulation and empirical results at full load – cylinder pressure at 5500 rpm

Overall, the assumptions and errors applied in defining the combustion model used in simulation have been shown to produce rather conservative results, in terms of both timing and magnitude of peak cylinder pressures. The reliability of the combustion model is dependent on accurate mass upon ignition, combustion efficiency, and combustion duration – all of which are dependent on experimental

input. The model is also influenced by wall heat transfer and blow-by, the latter of which should be accurately estimated in future work. Although the current pressure traces are not perfectly matched as a consequence, this does provide a layer of pessimism to any further simulation results, which can certainly be regarded positively in helping to avoid overstatement of performance claims.

4.6 Conclusions

Empirical data obtained from a prototype of the Ultraboost engine installed in the testing facilities at the University of Bath was compared with an equivalent GT-Power engine model. In naturally aspirated form, the prototype engine was used to log data at key Minimap points which are to be used in subsequent simulation-based investigations. In general, simulation results closely matched the empirical data for the significant bulk flow parameters that were assessed – such as torque, air mass flow rate, and intake and exhaust pressures and temperatures. The exceptions to this were the tendency of the model to over-predict the required intake manifold pressure, and under-predict the resulting BSFC. However, these discrepancies were within acceptable margins of error, and could also be taken into account in interpreting subsequent simulation results.

Points along the full load torque curve were achieved on the prototype engine using the CAHU, and results were again compared with those obtained in simulation. Torque, air mass flow, and fuel flow results showed a generally adequate fit, but intake and exhaust manifold pressures were significantly over-predicted in simulation. Comparing cylinder pressure data revealed that this was due to the assumptions made in defining the combustion model producing conservative results, in terms of both timing and magnitude of peak cylinder pressures. This was in contrast to the tendency of the model to under-predict BSFC. Again, these trends can be taken into account in the analysis and interpreting of subsequent simulation results.

Chapter 5 Ultraboost Engine: Part Load Efficiency and Transient Performance Trade-off

This chapter gives details of a co-simulation based investigation into the trade-off between steady state part load fuel efficiency and resulting tip-in transient response for a highly boosted downsized gasoline engine. The engine was a 2.0 litre in-line 4 cylinder unit, designed to replace a 5.0 litre naturally aspirated V8, equipped with a positive displacement supercharger in a sequential series arrangement with a fixed geometry turbocharger with external wastegate. The supercharger can be declutched and bypassed, and therefore three separate supercharger engagement regimes were investigated for part load operation – defined as: with the supercharger disengaged and bypassed; with the supercharger engaged with a fixed drive ratio; with the supercharger engaged using a variable ratio (i.e. through a CVT). For each of these supercharger engagement regimes, design of experiments and optimisation techniques were used to find the best settings for key engine control parameters such as intake and exhaust valve timing and EGR rate. Using these calibrations as a starting point, transient performance was then assessed in fixed speed tip-in simulations.

5.1 Methodology

The potential for low speed torque augmentation of a boosted downsized engine by using a CVT-driven supercharger (in a sequential charging arrangement) was demonstrated in Chapter 3. The purpose of this section of work was to address the next research aim: the part-load fuel efficiency benefits of using this technology in downsizing. This aim was expanded and slightly redefined to investigating the trade-off between steady state part load efficiency – namely BSFC – and resulting tip-in transient response for a highly boosted downsized engine. The Ultraboost project (introduced in the previous chapter) was found to have a similar alignment of aims and objectives, hence why the association was formed at this stage.

5.1.1 GT-Power Engine Model and Supercharger Engagement Regimes

The Ultraboost engine and its corresponding GT-Power model were introduced and described in Chapter 4. The model was adapted for use in this trade-off investigation, and three distinct supercharger engagement regimes were used for the regions of part load operation – these are defined as:

- with the supercharger disengaged and bypassed;
- with the supercharger engaged with a fixed drive ratio;
- with the supercharger engaged using a variable ratio (i.e. through a CVT).

5.1.2 Selection of Part Load Operating Points

Figure 5.1 shows the distribution on a speed-load map of the Minimap points listed in Table 4.2. For each point the size (i.e. area) of the blue 'bubbles' is proportional to the drive cycle weighting percentage in terms of residency time, and the size of the overlaid red circles signifies the corresponding measured BSFC values. Points 3, 9 and 14 stand out as candidates for investigation due to their high NEDC weighting values (as defined above) and reasonable load requirements – it is highly unlikely that the supercharger would be need to be engaged at loads lower than this. As a starting point for the investigation, Minimap point 3 (1500 rpm, 104 Nm, equating to 6.58 bar BMEP for the downsized engine) was selected; once the analytical process was fully developed, points 9 and 14 were similarly investigated.

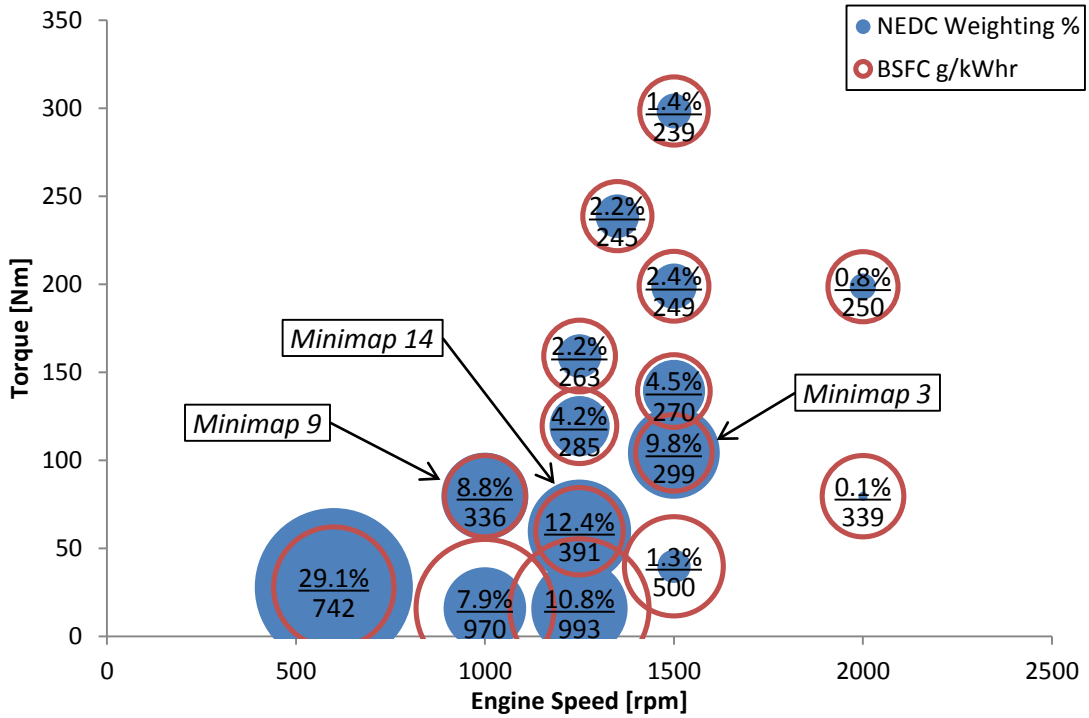

Figure 5.1 – Bubble plot of baseline engine NEDC 'Minimap' points – distribution, residency time weighting (%), and BSFC (g/kWhr)

5.1.3 Design of Experiment Construction and Evaluation

In order to find the optimal settings for the aforementioned load control mechanisms (valve timing, wastegate, etc.), a formal design of experiments (DoE) approach was adopted. The work was split into the three supercharger engagement regimes to allow a comparison of the optimal settings for each. The ranges of the seven input parameters are shown in Table 5.1.

Table 5.1 – Design of Experiments factors

Parameter	*SC disengaged*	*SC engaged*	*SC CVT*
Wastegate diameter (mm)	0 – 21	0 – 21	0 – 21
Target EGR rate (%)	0 – 50	0 – 50	0 – 50
Intake valve MOP (CAD ATDCF)	437 – 500	437 – 500	437 – 500
Exhaust valve MOP (CAD ATDCF)	234 – 284	234 – 284	234 – 284
SC bypass diameter (mm)	50	0 – 50	0 – 50
SC drive ratio	0	5.9	1.5 – 13
Throttle angle (deg)	PID controlled (BMEP target)		

The EGR rate in Table 5.1 was the target used in the EGR PID controller acting on a butterfly valve in the EGR circuit in the GT-Power model – defined as:

$$EGR\ Rate = \frac{MAF_{EGRvlv}}{MAF_{Throttle} + MAF_{EGRvlv}}$$

Equation 5.1

where $MAF_{Throttle}$ and MAF_{EGRvlv} are the mass airflows through the intake throttle and EGR valve, respectively. A high upper EGR target limit was used in order to test the boundaries of what is achievable with the system configuration used – in reality, lower values (<30%) would need to be used to retain combustion stability (which the simulations do not take into account) and to limit hydrocarbon emissions [29]. The combustion model was kept the same for both EGR and non-EGR simulations, hence the effects of spark timing were not taken into account. From an initial model review, it was evident that the maximum achievable EGR rate was around 11%, due to the low pressure gradient across the EGR circuit. Consequently, the EGR circuit was modified to a 'medium loop' arrangement – namely the inlet was moved from downstream to upstream of the turbocharger turbine to utilise the higher gas pressure at this point, enabling upwards of 30% EGR. In some cases this resulted in inhibited turbocharger performance due to the reduction in available exhaust gas energy. However, for the most part this could be compensated for by reduced intake throttling.

The wastegate and supercharger bypass diameters, for simplicity, were represented by variable orifice sections in the GT-Power model; in reality, flow control would likely be achieved by poppet and butterfly valves respectively. The supercharger bypass diameter was set to fully open when the supercharger was disengaged, and allowed to vary between its limits in the other instances. Valve timing limits were defined by the physical hardware used on the baseline engine. At this engine speed, standard intake valve maximum opening point (MOP) timing is 500 crank angle degrees (CAD) after top dead centre firing (ATDCF), with the ability to advance up to 63 degrees; standard exhaust valve MOP is 234 CAD ATDCF, with the ability to retard up to 50 degrees. Valve opening durations (fully closed to fully closed) around these MOPs are 202 and 216 degrees for inlet and exhaust respectively, giving a maximum possible overlap of 56 degrees – as shown in Figure 5.2.

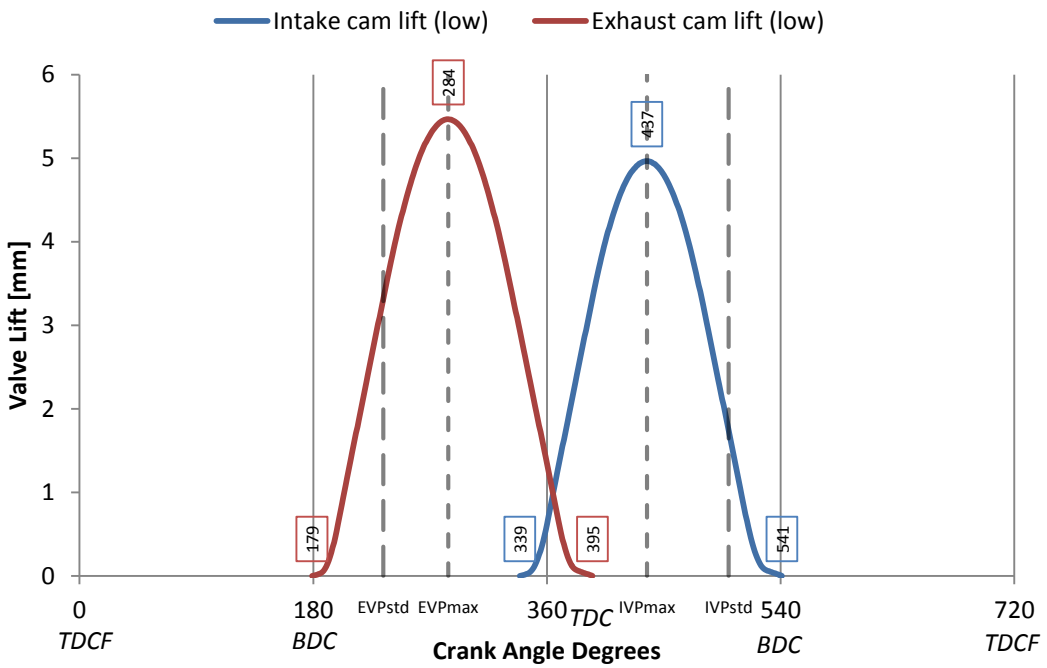

Figure 5.2 – Valve lift profiles at maximum overlap

The fixed supercharger drive ratio was determined by the full load (WOT) requirements (Figure 4.1a); as for the range of CVT ratios, the upper value was set by the supercharger maximum speed (20000 rpm), and the lower value was selected to test the lower boundaries of operation and based on an extreme ratio range of 9:1. With all the other parameter values defined, a throttle PID controller was used within GT-Power to target the operating load of the chosen Minimap point.

Consistent with the method developed in Chapter 3, the Matlab Model Based Calibration (MBC) toolbox was used to create the experimental test plan and to fit response models to the resulting data. For the supercharger disengaged regime, an initial simulation screening experiment of 100 points of a grid-type 'optimal' design was used to fill the corners and outer edges of the design space; these were then augmented with 400 points determined using a Halton Sequence 'space-filling' design to maximise coverage of the variables' ranges in the most efficient way. As can be seen in Figure 5.3, this approach thoroughly covers the design space. For both the supercharger engaged and CVT regimes, the total number of experimental points was increased to 1000 to account for the additional variables used.

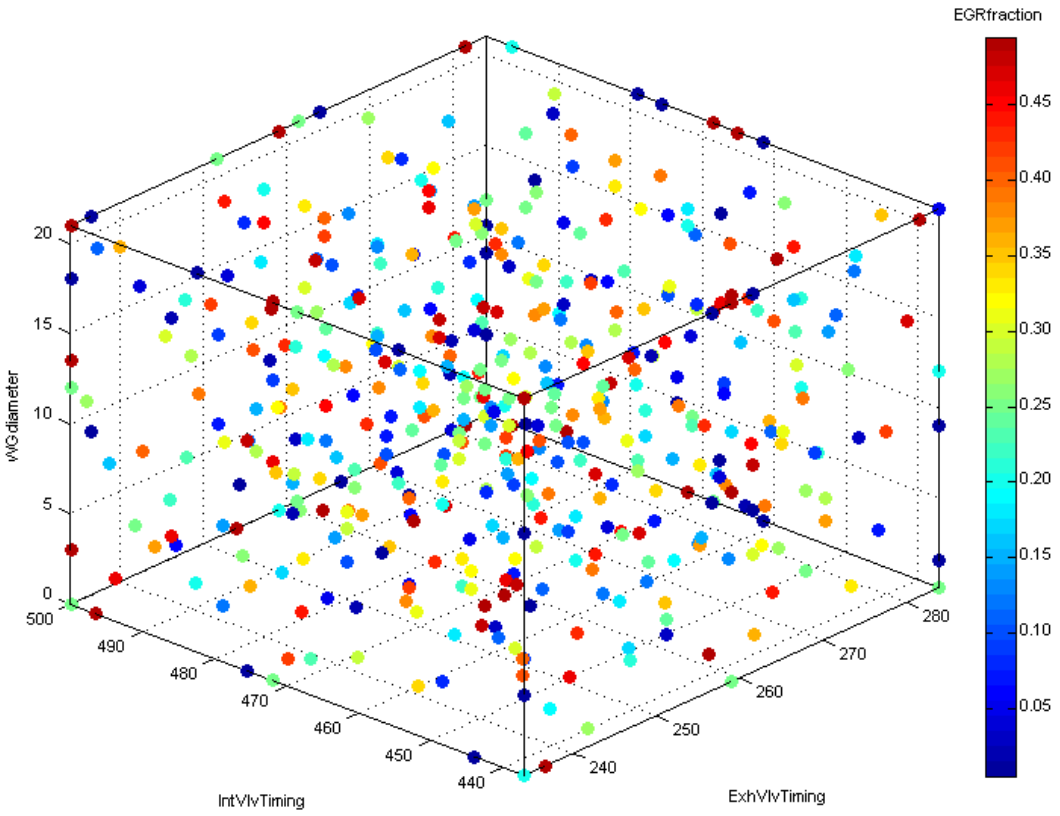

Figure 5.3 – Four-parameter DoE design projection: exhaust valve timing (x-axis); intake valve timing (y-axis); wastegate diameter (z-axis); and target EGR rate (colour gradient)

As with Chapter 3, Prediction Error Variance (PEV) was used as a quantitative evaluation tool of the effectiveness of each experimental design. PEV values tending to zero indicate that the model should provide good predictions at that point. Figure 5.4 is representative of the low PEV values seen throughout the experimental designs for all three supercharger engagement regimes, indicating that the response models resulting from the DoE should have a good predictive capability.

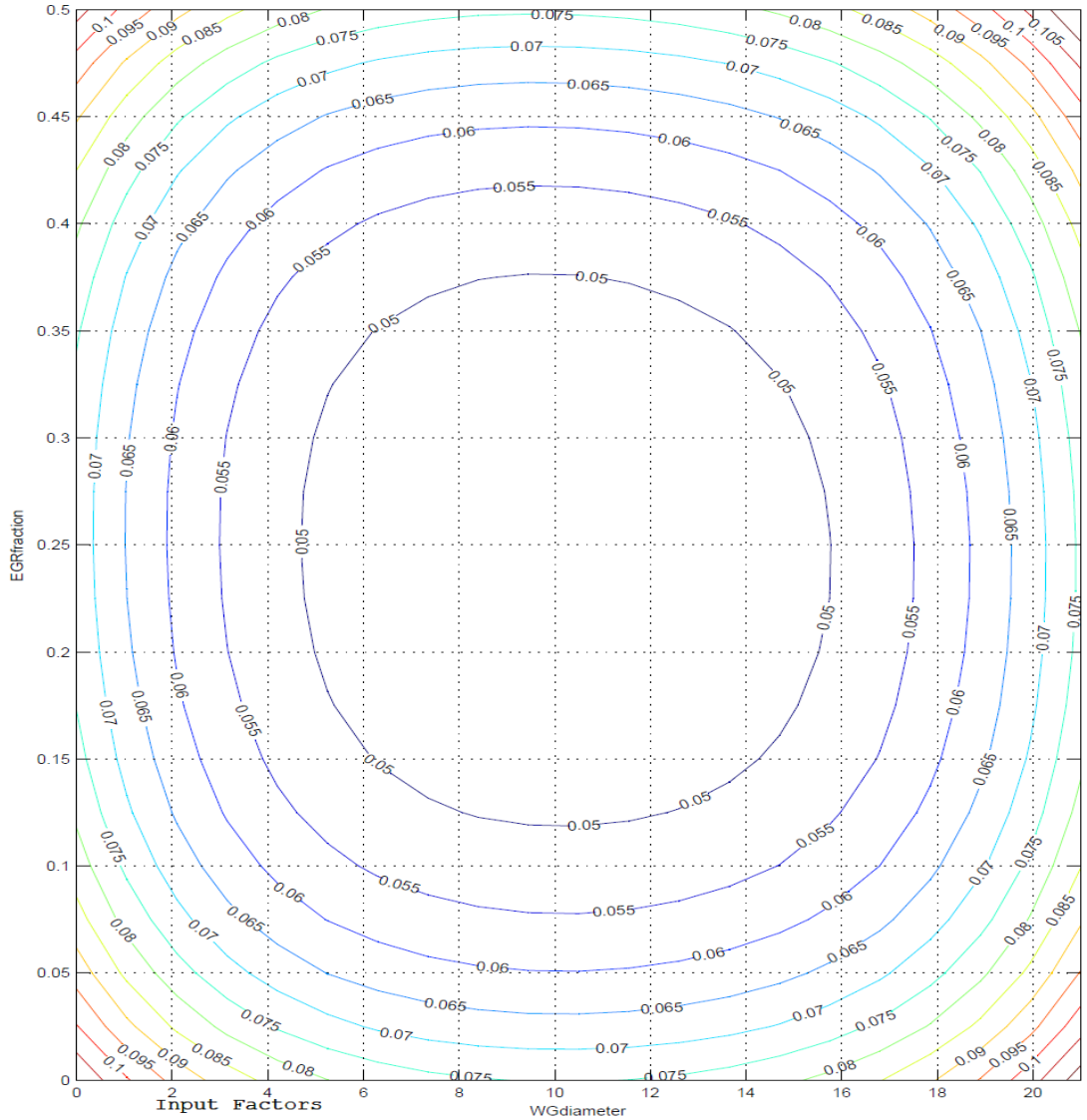

Figure 5.4 – PEV contour plot of 500 point supercharger disengaged experimental design. Target EGR fraction against wastegate diameter, remaining parameters held constant (intake valve timing: 500, exhaust valve timing: 284)

With extreme and unrealistic values filtered out, the responses of significant engine variables (such as BMEP and BSFC) were subsequently modelled. For the majority of the variables a neural network modelling approach was required due to the high complexity of the system – in part a result of the number of input parameters. Root Mean Squared Error (RMSE) and coefficient of determination (R^2) statistical values, as well as visual inspection, were used to evaluate the quality of the response models (for a more detailed explanation of this, see Section 3.1.4).

5.1.4 Parameter Optimisation

Once the response models had been evaluated satisfactorily they were imported into the calibration generation (CAGE) element of MBC, to form the plant model for the subsequent optimisation process. Initially, the 'foptcon' single-objective gradient search optimisation algorithm was used to find the optimum point for the various engine input parameters. The target was to minimise BSFC while achieving the specific Minimap engine load – the BMEP response model was used in a range constraint, with the limits being the relevant Minimap value +/-0.03 bar. A relatively large number of start points (10) were also used to prevent false (i.e. local instead of global) minima and maxima being obtained.

Of greater interest than the specific optimum settings, however, was exploring the trends and effects of each input parameter – and their combinations – on part load efficiency. Hence, the result of the optimisation was then used as the basis for populating lookup tables for the various input parameters (with reference to the response models) within the trade-off calibration feature of CAGE. Different tables (for example, intake against exhaust valve timing, supercharger drive ratio against bypass diameter) were completed and compared to see which parameters had the greatest effect on engine performance – particularly BSFC – and to collate the optimal settings that were found for each.

5.1.5 Transient Simulation Model Setup

The aim of this part of the investigation was to predict the response of the engine to a fixed speed tip-in transient – i.e. a step change in pedal demand from a low to a high value. This was to compare the transient performance commencing from each of the part load calibrations detailed above with that of the baseline engine. Experimental data of a number of tip-in transient tests were available for the baseline engine, which were used in the assessment of the performance of the downsized engine in the transient simulations. Full load was used as the target for the tip-in – at 1500 rpm: 438 Nm, equivalent to 27.7 bar BMEP for the downsized engine – with the step taking place over 0.15 seconds.

The GT-Power engine model used for the steady state simulations above was modified to perform a tip-in pedal event. The actual engine architecture was left largely unchanged from the arrangement described above. The EGR PID controller

used for the various steady state EGR targets was removed and replaced with a time-dependent lookup table for the EGR throttle. For the three calibrations using EGR, this was set to fully open for the initial steady state period, then closed (with immediate response assumed) at the same rate as the 0.15 second step demand in BMEP; for the non-EGR calibrations, the EGR throttle was fully closed throughout. Time-dependent lookup tables were also put in place for the intake and exhaust timing values, the supercharger bypass diameter, and the turbocharger wastegate. For the latter two parameters the respective optimised steady state values were used initially, adjusting (at the same rate as above) to fully closed when full load was demanded (but then opening again – being used as the load control mechanism – when full load was achieved, as explained below). Similarly for the valve timings, the respective optimised steady state values were used initially, ramping linearly to the predetermined full load values at the start of the tip-in.

Regarding the supercharger, for the steady state regime with it engaged, the drive ratio was kept constant throughout the simulation, at the value of 5.9:1 determined by the full load torque curve requirements. For the supercharger disengaged regime, the drive ratio was set to zero initially, ramping up to 5.9:1 over the same 0.15 second period to represent the supercharger being clutched in. As with the other dynamic parameter adjustments, the actuator response was assumed to be instantaneous with respect to the step in pedal demand. Supercharger transmission efficiency was assumed to be 94%. For the steady state simulations of the configuration with variable supercharger drive, the drive ratio of the supercharger was simply manipulated to represent the CVT; for the transient simulations, however, a CVT element was incorporated into the GT-Power model to adequately represent the dynamic behaviour of the transmission. Mechanical efficiency of the CVT was assumed to be 95%, which combined with the aforementioned value for the supercharger drive (94%) gave an overall efficiency of 89%. Input and output shaft inertias were both assumed to be 5×10^{-4} kgm^2 (for comparison, the supercharger shaft inertia was 4.9×10^{-4} kgm^2), and a 20 ms time delay in the response of the CVT was used.

5.1.6 Simulink–GT-Power Co-Simulation

Although the internal throttle controller in GT Power was (on the most part) adequate for achieving the steady state BMEP targets for the part load simulations above, it was found to be inadequate for the tighter control requirements of the

dynamic simulations. Consequently, the GT-Power model was set up to run in a co-simulation environment with Matlab Simulink, to utilise the more sophisticated dynamic control structures available. With the aforementioned lookup tables set for the other parameters, the sole control mechanism for the models without variable supercharger drive was the throttle, which was initially set to achieve the BMEP target (as with the steady state simulations). However – as explained below – this was found to be incapable of giving acceptable response behaviour when approaching the high BMEP target, with extremely unstable oscillation. The controller was subsequently modified to target manifold pressure, which was mapped to the required BMEP. This eliminated the oscillatory behaviour, but there was still a problem with overshoot. A solution was discovered in setting the throttle to fully open at the start of the tip-in (using a similar lookup table as for the other optimised parameters), and using a common PID controller for the supercharger bypass valve and turbocharger wastegate. This was found to be a much more effective method of regulating the mass air flow (MAF) load (and thus the engine BMEP). For the CVT-driven supercharger the difficulties described above were compounded by the added control requirements of the CVT; however, the latter control scheme (supercharger bypass valve and turbocharger wastegate) in conjunction with a similar manifold pressure-targeting PID controller for the CVT was found to be effective at providing acceptable transient behaviour. As with the parameter lookup tables, all controllers used were assumed to respond instantaneously to the step change in BMEP demand.

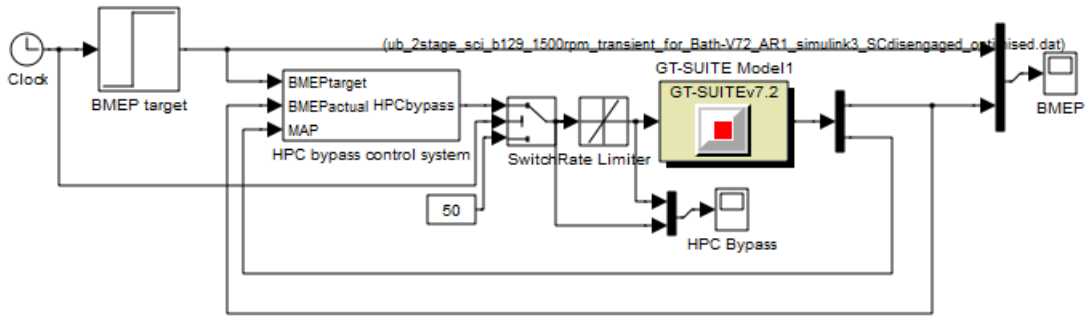

Figure 5.5 – Supercharger engaged/disengaged – Simulink model for transient simulations

The Simulink model configuration for the supercharger engaged and disengaged regimes is shown in Figure 5.5. The simulation was set to run for seven seconds, with the tip-in occurring after four seconds to allow the model to achieve a steady

state. A fixed value (corresponding to the respective optimised value – see Table 5.4) was used for supercharger bypass valve during the initial steady state period of the simulation, to ensure the correct setting was applied and to avoid unnecessary controller action and calibration. As both the supercharger bypass valve and turbocharger wastegate were controlled by the same signal, the signal was split within GT-Power and an appropriate gain applied to the branch leading to the wastegate, again to ensure the correct steady state setting. At the start of the tip-in the actuator signal was then switched within Simulink to the dynamic controller output, and the wastegate signal gain set to unity. The controller was of a proportional-integral (PI) type with anti-windup, and the PI values were manually calibrated for a satisfactory balance between speed of response and stability. The rate of actuator signal change was limited to an arbitrarily assumed value of +/-350 mm/s, equivalent to going from fully open to fully closed in approximately 0.14 seconds. The same basic structure was used for the CVT-driven supercharger Simulink model, with a similar control loop used for the CVT as for the supercharger bypass valve and wastegate – see Figure 5.6. Lower and upper limits for the CVT ratio were set at 2:1 and 13.3:1 (i.e. 20000 rpm supercharger speed limit divided by 1500 rpm engine speed) respectively. The rate of change was also limited to +/-40 per second, equivalent to traversing the ratio range twice in one second. The various control inputs and settings used for the initial steady state and transient sections of the simulation are summarised in Table 5.2.

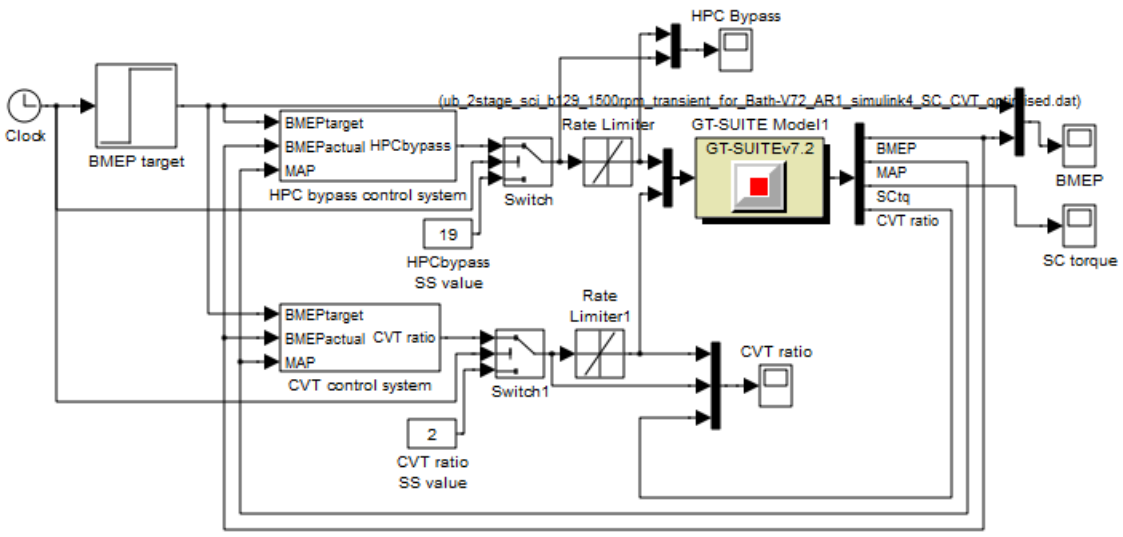

Figure 5.6 – Supercharger with CVT – Simulink model for transient simulations

Table 5.2 – Summary of parameter control settings during steady state and transient portions of tip-in test

Parameter	*SC disengaged*		*SC engaged*		*SC CVT*	
	Steady State	*Transient*	*Steady State*	*Transient*	*Steady State*	*Transient*
Wastegate diameter	Fixed (optimised)	PI control	Fixed (optimised)	PI control	Fixed (optimised)	PI control
EGR valve	Fully open / closed[1]	Fully closed	Fully open / closed[1]	Fully closed	Fully open / closed[1]	Fully closed
Intake valve MOP	Fixed (optimised)	Fixed (full load value)	Fixed (optimised)	Fixed (full load value)	Fixed (optimised)	Fixed (full load value)
Exhaust valve MOP	Fixed (optimised)	Fixed (full load value)	Fixed (optimised)	Fixed (full load value)	Fixed (optimised)	Fixed (full load value)
SC bypass diameter	Fully open	PI control	Fixed (optimised)	PI control	Fixed (optimised)	PI control
SC drive ratio	-	5.9 (clutched in)	5.9	5.9	Fixed (optimised)	PI control
Throttle	Fixed (optimised)	Fully open	Fixed (optimised)	Fully open	Fixed (optimised)	Fully open

[1] Depending on EGR / non-EGR calibration

5.2 Design of Experiments and Optimisation Results

Considering the results from the GT Power simulations, for both the supercharger engaged and disengaged around 70% of the experimental points were within +/-10% of the target load. The majority of the remaining 30% of the results were running at wide open throttle (WOT) and achieving less than the target load due to insufficient fresh air entering the cylinders resulting from high target EGR rates. Additionally, instability in the throttle controller action accounts for some of the outliers. Regarding the variable ratio supercharger simulations, 60% of the experimental points were within +/-10% of the target load. A large proportion of the rest failed to achieve the target load for the same reasons as above. Around 10% of the experiments were some way above the target load due to a combination of high supercharger drive ratio and low supercharger bypass diameter requiring the throttle controller to demonstrate fine control at low throttle openings, at which it failed.

5.2.1 Response Models

A summary of the response models produced from the DoE simulations for the three supercharger engagement regimes is given in Table 5.3. The range of each variable is given in order to provide context for the RMSE values, since these are scale-dependent. In terms of statistical quality, the majority of the response models are excellent, with close to perfect R^2 values; relative to their respective ranges, the RMSE values are also suitably low. This good statistical accuracy is a benefit of the large number of data points provided by the simulation environment. The BSFC response model for the CVT supercharger regime, though, was very difficult to fit, and the resulting model was a compromise between statistical data fitting and physically realistic behaviour. The visual model quality and trends of key response models are discussed below.

Table 5.3 – Summary of response models for each supercharger engagement regime

	Response variable	*Response model used*	*R^2 value*	*RMSE*	*Variable range*
SC disengaged	BSFC (g/kWhr)	Neural network	0.998	0.953	230-280
	BMEP (bar)	Neural network	0.996	0.036	4.5-8
	Throttle angle (deg)	Neural network	1	0.299	5-90
	Actual EGR rate	Hybrid RBF (5^{th} order)	0.998	4.7e-3	0-0.32
	EGR throttle angle (deg)	Neural network	1	0.151	0-90
	Turbocharger speed (rpm)	Hybrid RBF (5^{th} order)	0.984	521	9000-30000
SC engaged	BSFC (g/kWhr)	Neural network	0.997	1.815	150-600
	BMEP (bar)	Neural network	0.997	0.041	2.8-13
	Throttle angle (deg)	Neural network	1	0.396	0-90
	Actual EGR rate	Neural network	1	1.9e-3	0-0.5
	EGR throttle angle (deg)	Neural network	1	0.162	0-90
	Turbocharger speed (rpm)	Hybrid RBF (5^{th} order)	0.982	808	9000-50000
SC CVT	BSFC (g/kWhr)	Neural network	0.958	10.351	0-1500
	BMEP (bar)	Neural network	0.997	0.064	0.2-15
	Throttle angle (deg)	Neural network	0.995	2.958	0-90
	Actual EGR rate	Neural network	0.999	2.5e-3	0-0.5
	EGR throttle angle (deg)	Neural network	1	0.114	0-90
	Turbocharger speed (rpm)	Hybrid RBF (4^{th} order)	0.953	1502	9000-60000

Firstly, considering the throttle response model for the supercharger engaged regime (Figure 5.7), target EGR rate clearly has the greatest effect on the throttle angle required to achieve the target BMEP. With a low target EGR rate, the throttle angle is largely insensitive to the other input parameters – although a greater level of throttling is required to limit BMEP when the supercharger bypass valve diameter is reduced below a certain threshold (with this specific combination of input values, below 20 mm).

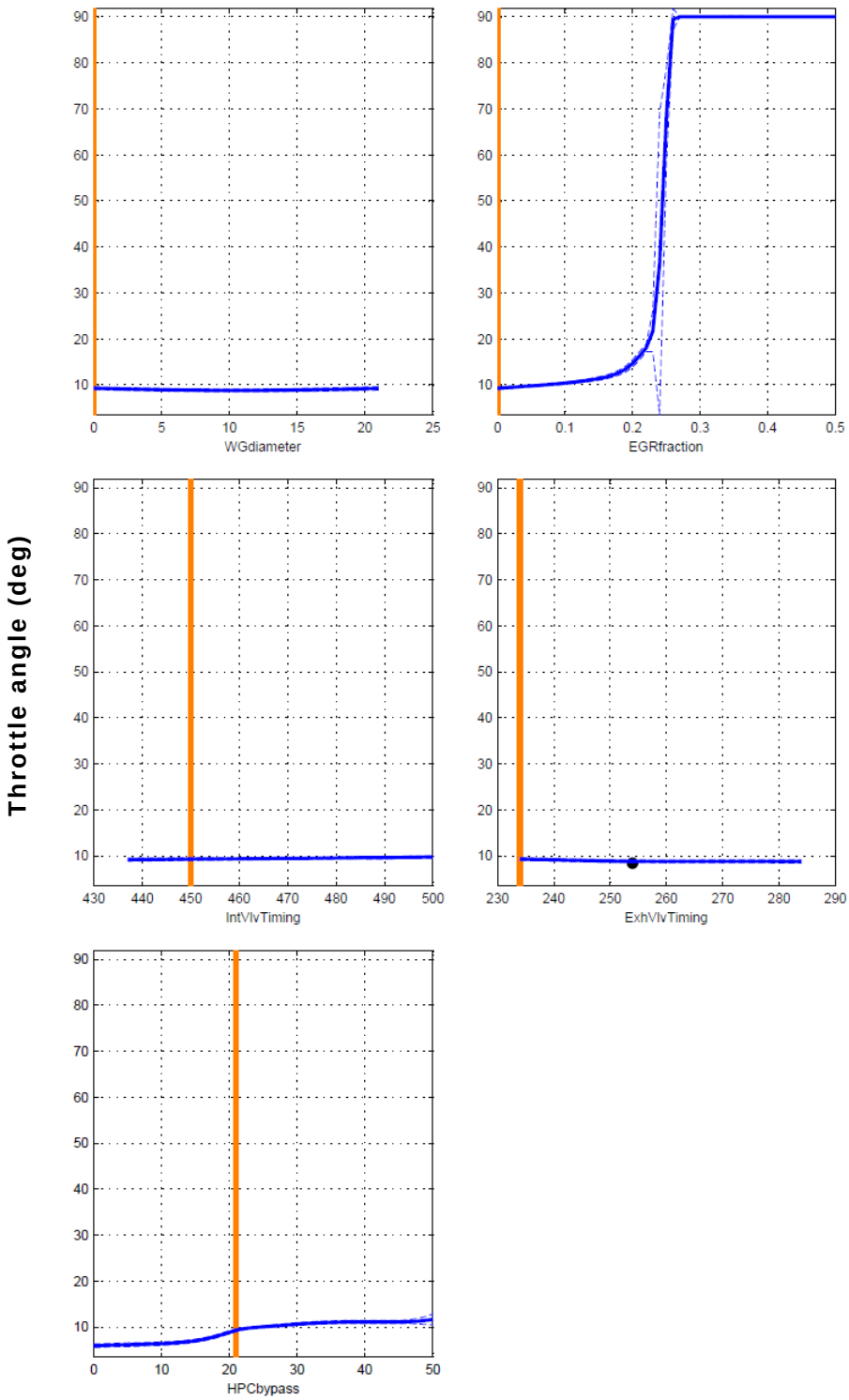

Figure 5.7 – Cross-section through SC engaged Throttle Angle (deg) response model, showing effects of wastegate diameter (mm), target EGR rate, intake valve MOP (CAD ATDCF), exhaust valve MOP (CAD ATDCF), and supercharger bypass valve diameter (mm)

As the desired level of EGR is increased, a greater amount of fresh intake air is also required in order to maintain BMEP; hence the throttle angle ramps up. Above a

certain threshold EGR target, the necessary throttle angle increases rapidly, as full throttle is now required in an attempt to achieve the BMEP target.

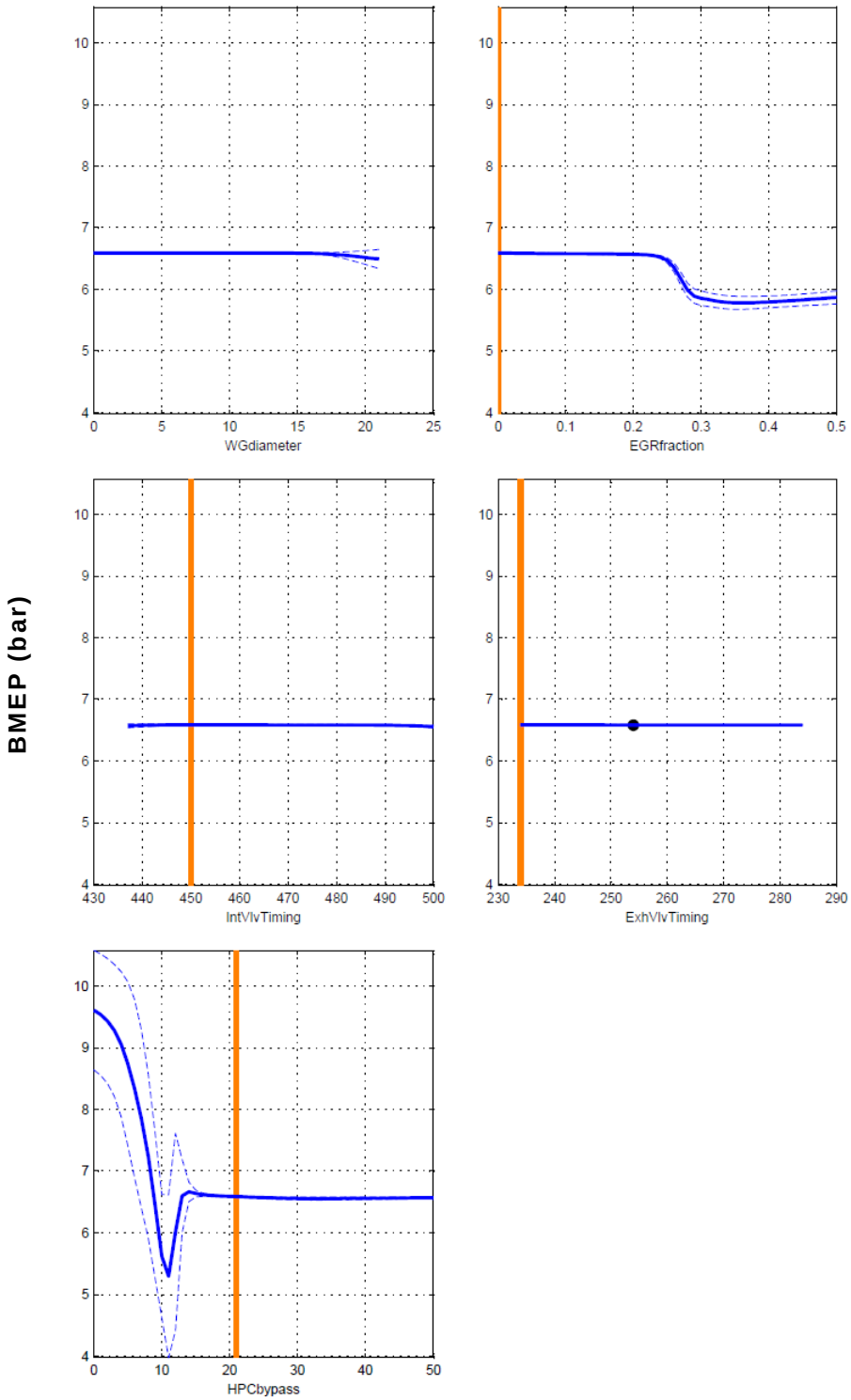

Figure 5.8 – Cross-section through SC engaged BMEP (bar) response model (at low EGR rate), showing effects of wastegate diameter (mm), target EGR rate, intake valve MOP (CAD ATDCF), exhaust valve MOP (CAD ATDCF), and supercharger bypass valve diameter (mm)

However, as Figure 5.8 shows (with the same combination of input values as Figure 5.7), with the increased EGR rate the BMEP target (in this case, 6.58 bar) can no longer be achieved. Thus there is clearly an upper limit to the practical level of EGR that can be used, which in part relates to the mass flow capabilities of the boosting system – as well as being limited by combustion stability and hydrocarbon emissions, as already discussed.

Figure 5.8 also demonstrates the difficulties in throttling and limiting intake mass air flow when the supercharger bypass diameter is reduced beyond a certain level (that is, with the supercharger engaged). This also greatly increases BSFC, as the supercharger is required to work harder (thus increasing parasitic power losses) as its throughput requirements ramp up. Throttle controller instability is evident when the supercharger bypass is reduced below around 20 mm, with unsteady and spiky BMEP behaviour and wide confidence bands – this corresponds to the threshold in the throttle response model. Also, as with the throttle response model, BMEP is unresponsive to wastegate diameter and valve timing (generally speaking).

At mid to high EGR rates (Figure 5.9), the instability threshold pertaining to throttling and the supercharger bypass diameter decreases as greater mass air flow is required to counteract the increased dilution. In fact, it is necessary to decrease the level of supercharger bypassing in order to maintain the target BMEP. Figure 5.9 also shows that wastegate diameter and valve timings do have an effect on BMEP, but only with certain combinations of the other parameters.

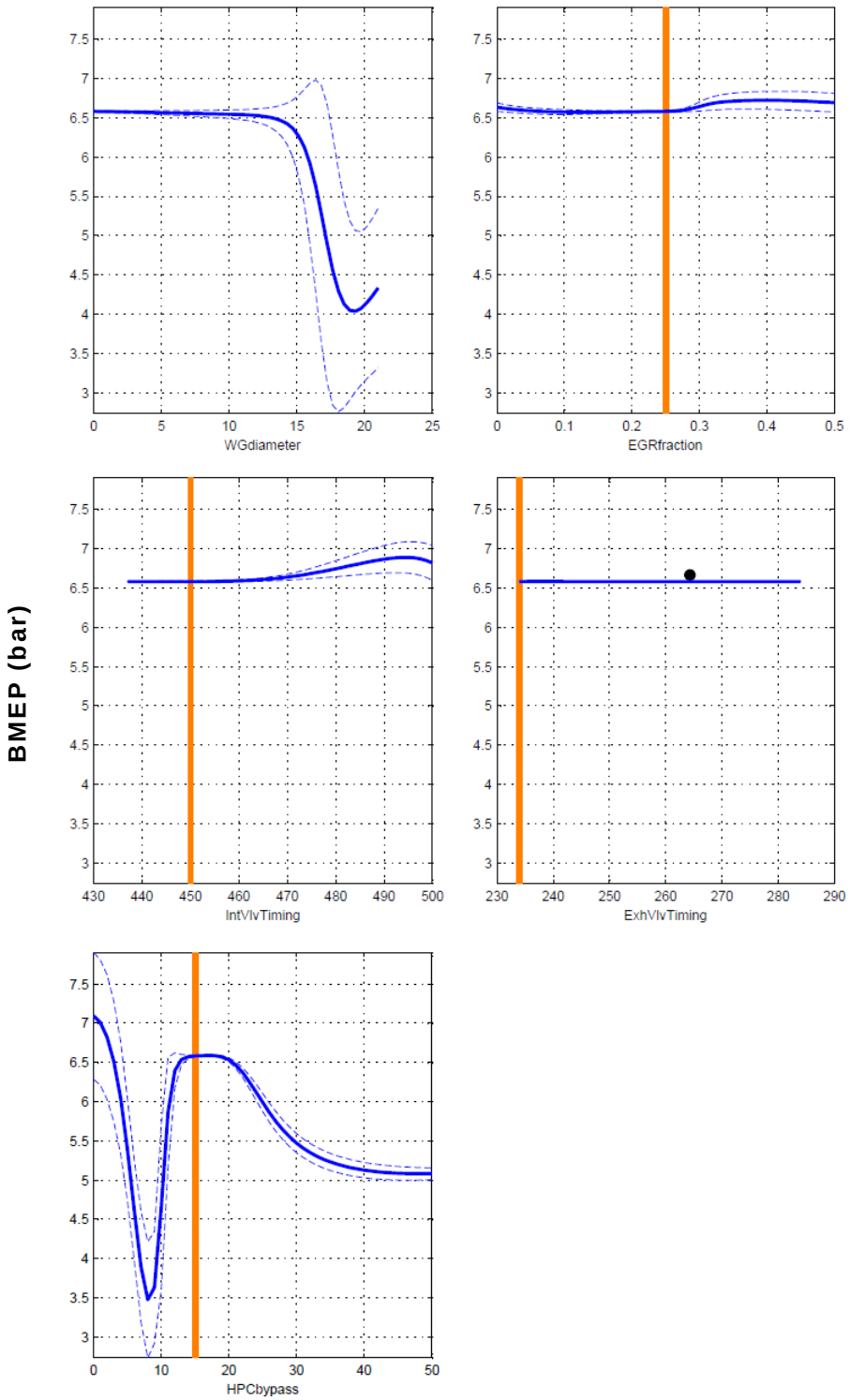

Figure 5.9 – Cross-section through SC engaged BMEP (bar) response model (at high EGR rate), showing effects of wastegate diameter (mm), target EGR rate, intake valve MOP (CAD ATDCF), exhaust valve MOP (CAD ATDCF), and supercharger bypass valve diameter (mm)

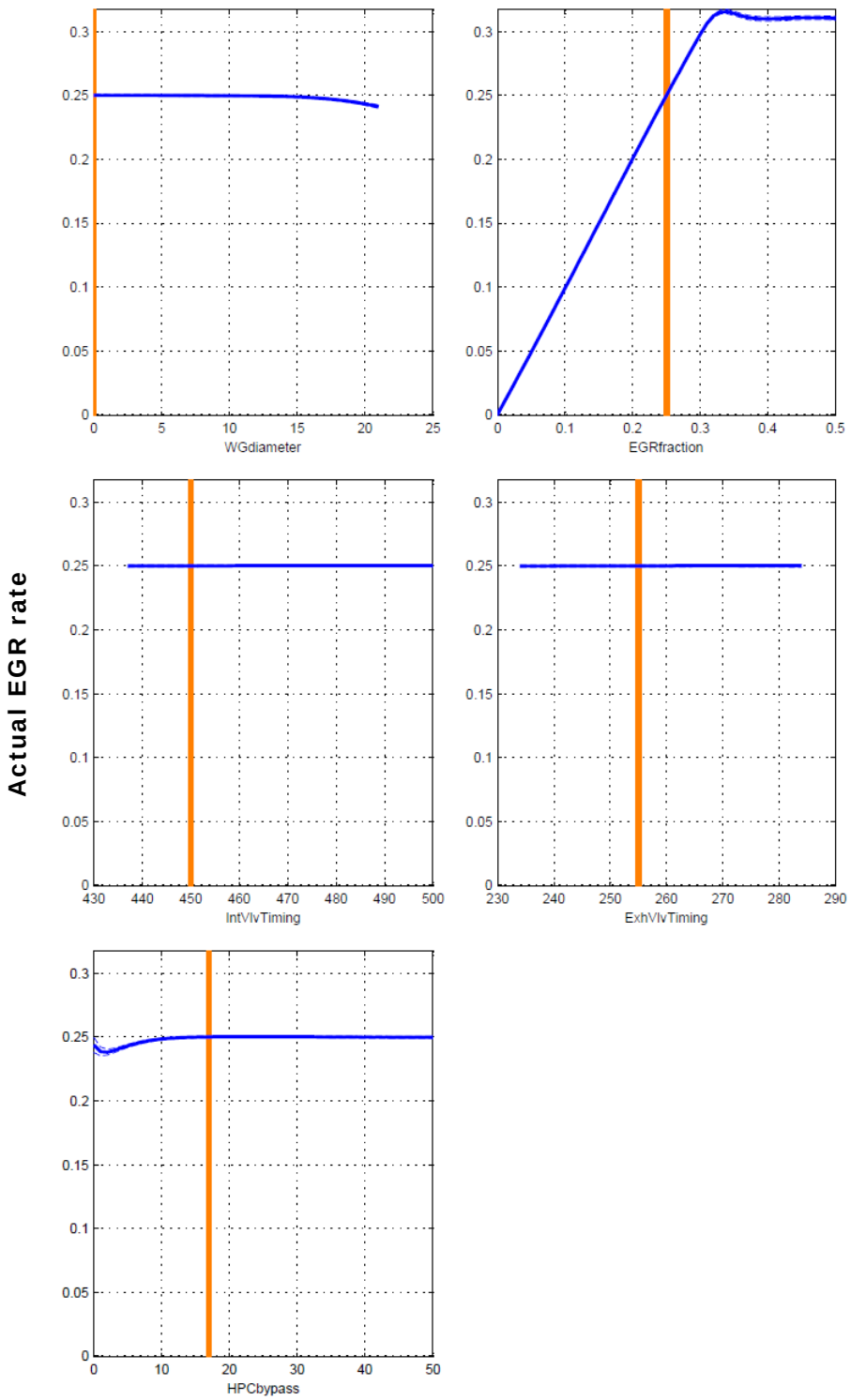

Figure 5.10 – Cross-section through SC engaged Actual EGR Rate response model, showing effects of wastegate diameter (mm), target EGR rate, intake valve MOP (CAD ATDCF), exhaust valve MOP (CAD ATDCF), and supercharger bypass valve diameter (mm)

Considering the response model of actual EGR rate (Figure 5.10), this output variable increases linearly with target EGR rate, as is to be expected. However, the

actual EGR rate is limited (primarily) by the driving pressure gradient from exhaust manifold to inlet manifold, and hence a plateau is reached, at just over 30%.

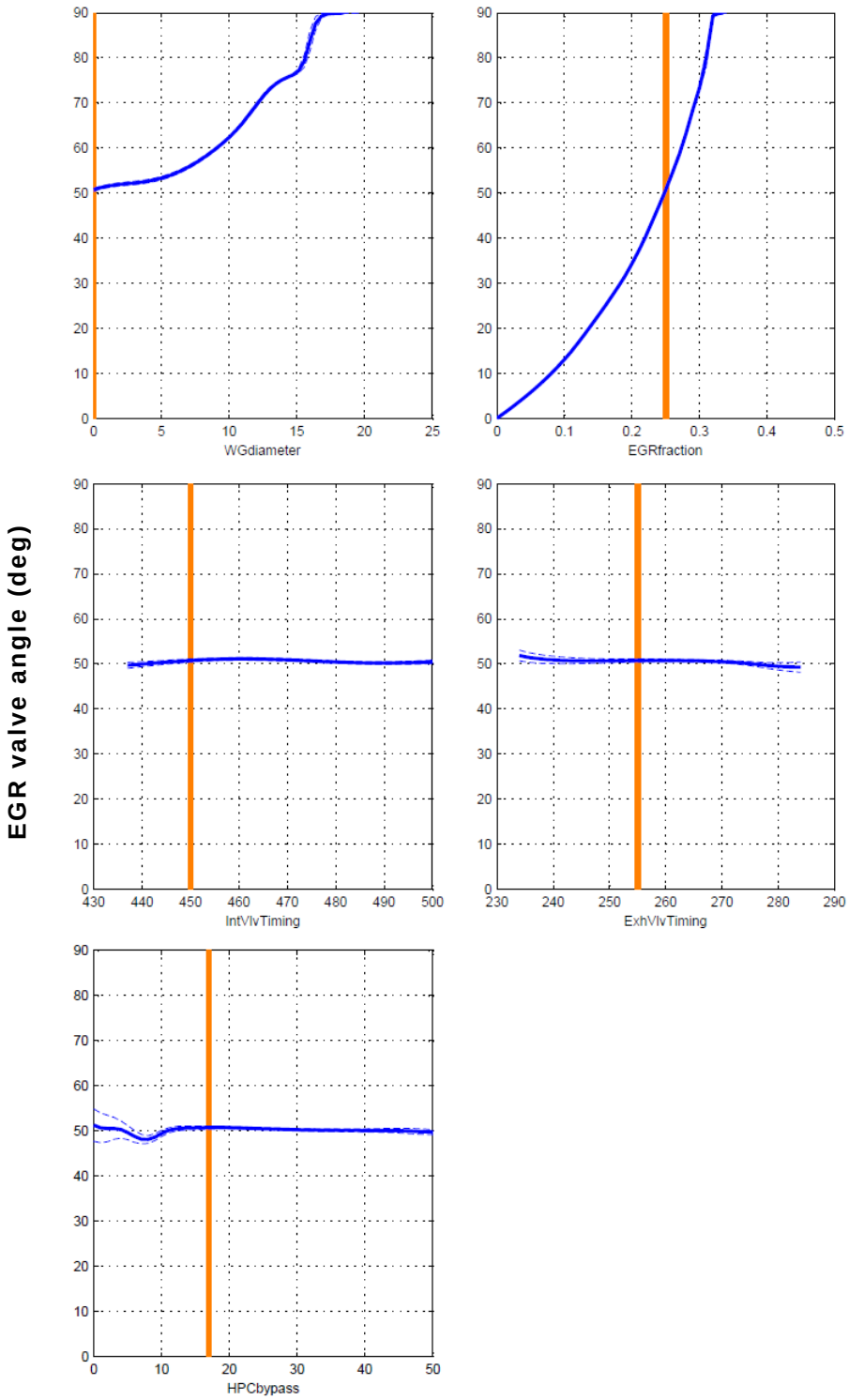

Figure 5.11 – Cross-section through SC engaged EGR Valve Angle (deg) response model, showing effects of wastegate diameter (mm), target EGR rate, intake valve MOP (CAD ATDCF), exhaust valve MOP (CAD ATDCF), and supercharger bypass valve diameter (mm)

This plateau in delivered EGR rate relates to the EGR valve being opened fully (Figure 5.11), and no further flow increases being possible. (The implications of this became clear in the subsequent optimisation process, as the EGR throttle valve could be set to fully open to effectively achieve 'maximum EGR'.) Also note that increasing the wastegate diameter has a corresponding effect on the EGR valve opening required to achieve the same EGR rate. This is due to the reduction in back-pressure resulting from increased turbine bypass flow through the wastegate effectively reducing the pressure gradient available to drive the EGR (since the EGR inlet is pre-turbine).

The response models discussed up to this point are for the supercharger engaged regime; the behaviour and trends of the response models of the supercharger disengaged regime are effectively simplified versions of these, without the effect of the supercharger bypass (or indeed the supercharger). Conversely, factoring in the variable drive ratio of the CVT-supercharger regime adds another layer of complexity to the response models. The responses most affected (of those response models considered) are BSFC, BMEP and throttle angle.

Firstly, considering the BSFC response model (Figure 5.12), as would be expected, increasing the drive ratio (i.e. speed) of the supercharger causes a corresponding increase in BSFC due to the increasing power consumption of the supercharger. The slightly uneven behaviour as the drive ratio is increased is due to other contributing factors, particularly the varying throttle angle attempting to maintain the target BMEP. As mentioned above with reference to the supercharger engaged regime, reducing the bypass diameter also increases BSFC, as increased throttling is required to limit mass air flow and BMEP, which results in associated losses. The reduction in BSFC as the wastegate is increasingly opened seems counter-intuitive; it is due to the reduced turbocharger speed and boost pressure resulting in a reduction in the level of throttling required to achieve the target BMEP, and this exceeds the benefits of energy recovery with the wastegate shut, as well as providing reduced back pressure. This is revealed more fully in Figure 5.13. A reduction in throttling losses is also the major contributing factor for the decreasing BSFC with increased EGR rate, again comparing Figure 5.12 and Figure 5.13.

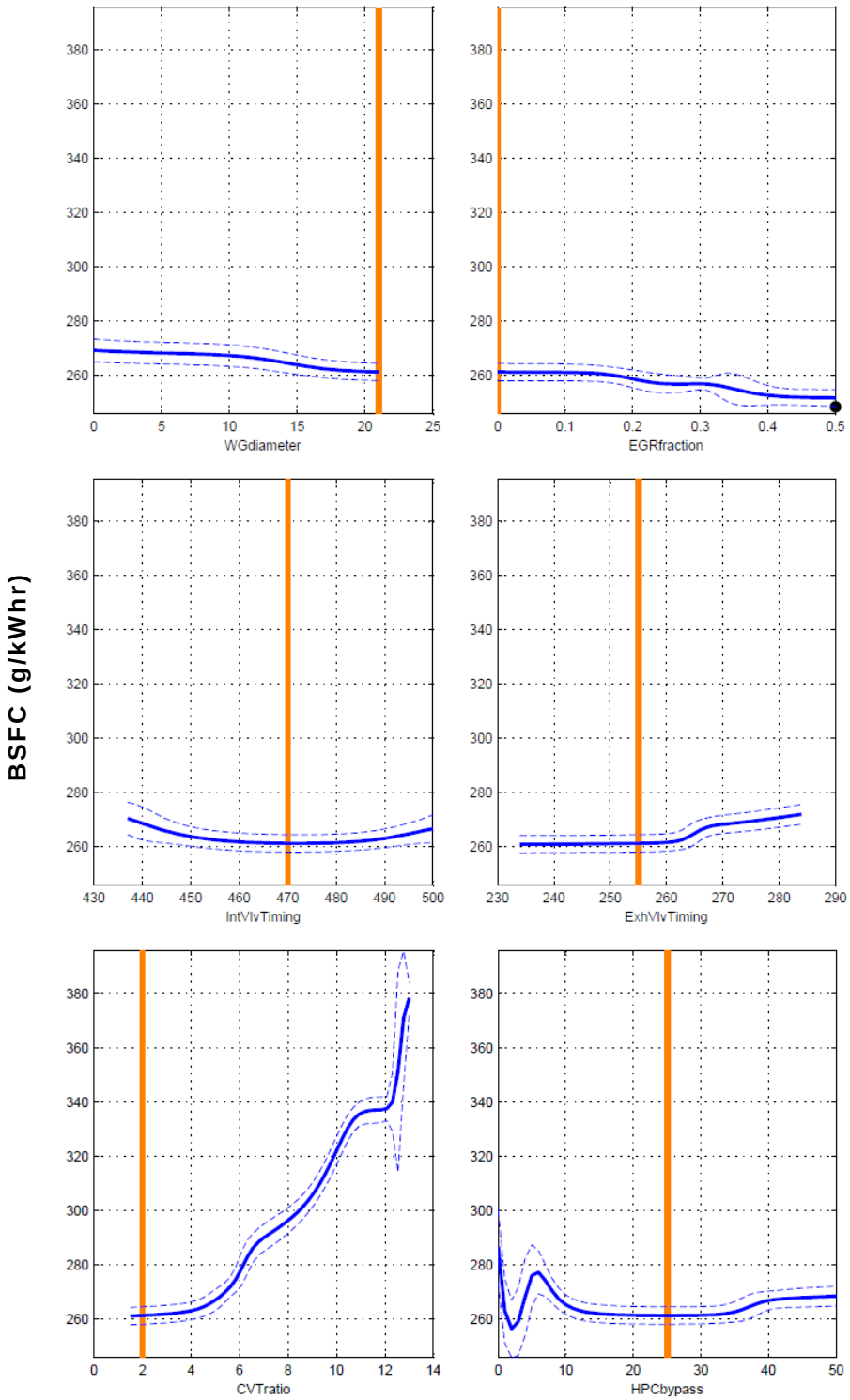

Figure 5.12 – Cross-section through SC CVT BSFC (g/kWhr) response model, showing effects of wastegate diameter (mm), target EGR rate, intake valve MOP (CAD ATDCF), exhaust valve MOP (CAD ATDCF), supercharger drive ratio, and supercharger bypass valve diameter (mm)

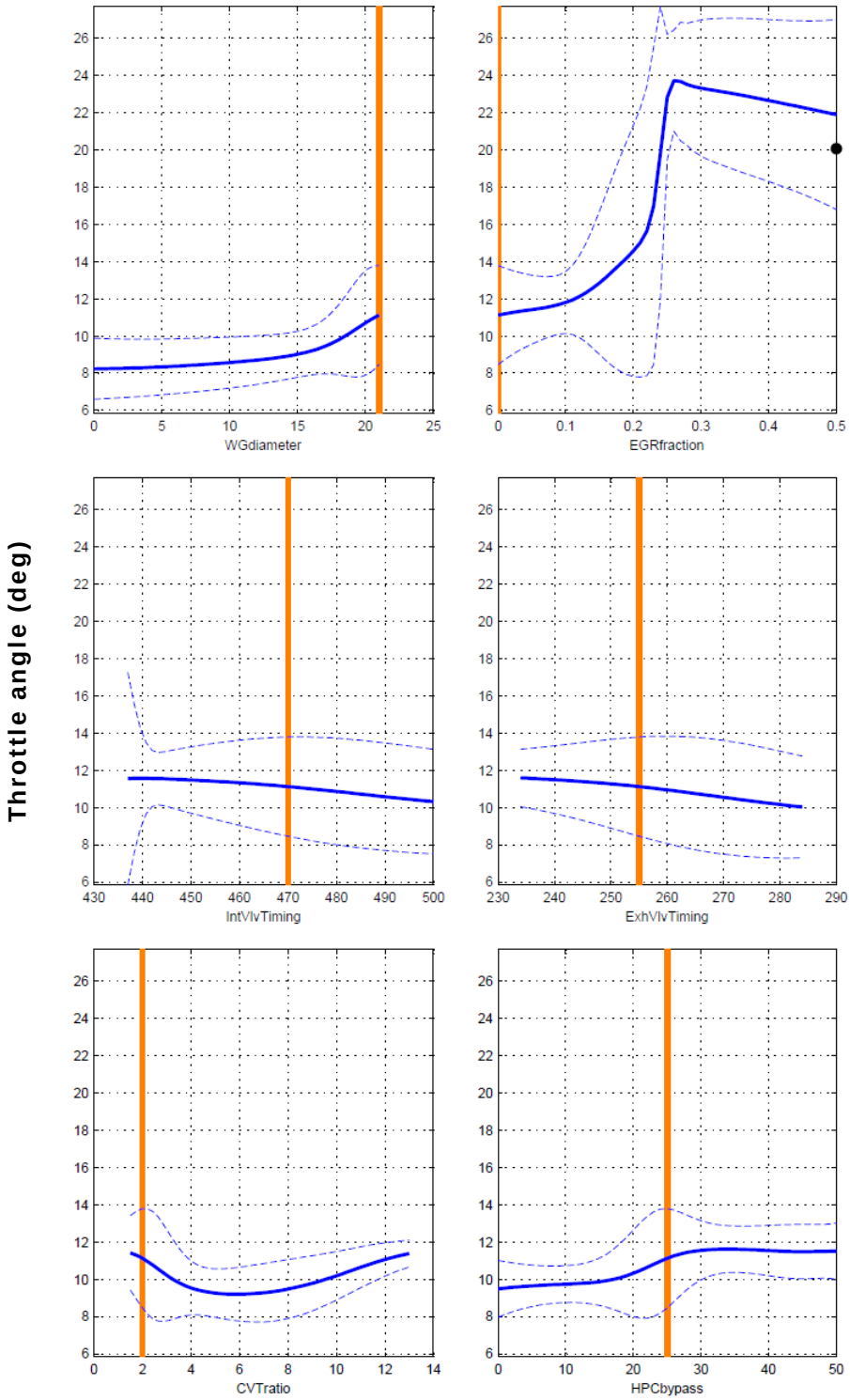

Figure 5.13 – Cross-section through SC CVT Throttle Angle (deg) response model, showing effects of wastegate diameter (mm), target EGR rate, intake valve MOP (CAD ATDCF), exhaust valve MOP (CAD ATDCF), supercharger drive ratio, and supercharger bypass valve diameter (mm)

The wide confidence bands of the throttle response model are a result of having to use a slightly 'loosely' fitted neural network model with the data in order to preserve realistic behaviour at the cost of some precision. This is mostly due to the instabilities and oscillation in the throttle controller output at some of the experimental set points causing anomalies in the data; although this mostly affects combinations of input parameters that would not be used in reality, it nevertheless has repercussions for the rest of the modelled design space as model fidelity cannot be varied across the design space. However, statistically speaking, the model is still well fitted to the data, as shown by the R^2 and RMSE values in Table 5.3. Also, the throttle values produced by the optimisation process were used only as a rough guideline for achieving the BMEP target in the subsequent transient simulations, and the throttle setting was fine-tuned accordingly in situ.

Results with excessively high BMEP or BSFC values were filtered out of the DoE data before processing the response models, since including these would have significantly distorted the results, requiring compromised response models to be fitted to avoid over-fitting and unrealistic behaviour (as typified by the throttle model here). Filtering in this way had consequences on particular regions of the BMEP and BSFC response models where these high values would have been expected to occur, such as at high supercharger drive ratios. For the BSFC response model this merely caused wide confidence bands and model uncertainty in these regions; however, this was not a problem since the focus of the optimisation was on regions of low BSFC anyway. In the case of the BMEP response model, since similar filtering of low BMEP values was not applied, the regions where high BMEP would have been expected showed inverse trends. This is demonstrated in Figure 5.14, where increasing the supercharger drive ratio (with other parameters constant) would have logically resulted in increased BMEP as the throttle controller would begin to struggle to limit the air mass flow and BMEP to the target value; in fact the reverse trend is shown, with BMEP rapidly dropping off at high drive ratios. Although this means that the response models are clearly inaccurate in these regions, it was considered not to be a problem, since BMEP values at either extreme outside the vicinity of the target Minimap value would have been avoided anyway, as with the regions of high BSFC.

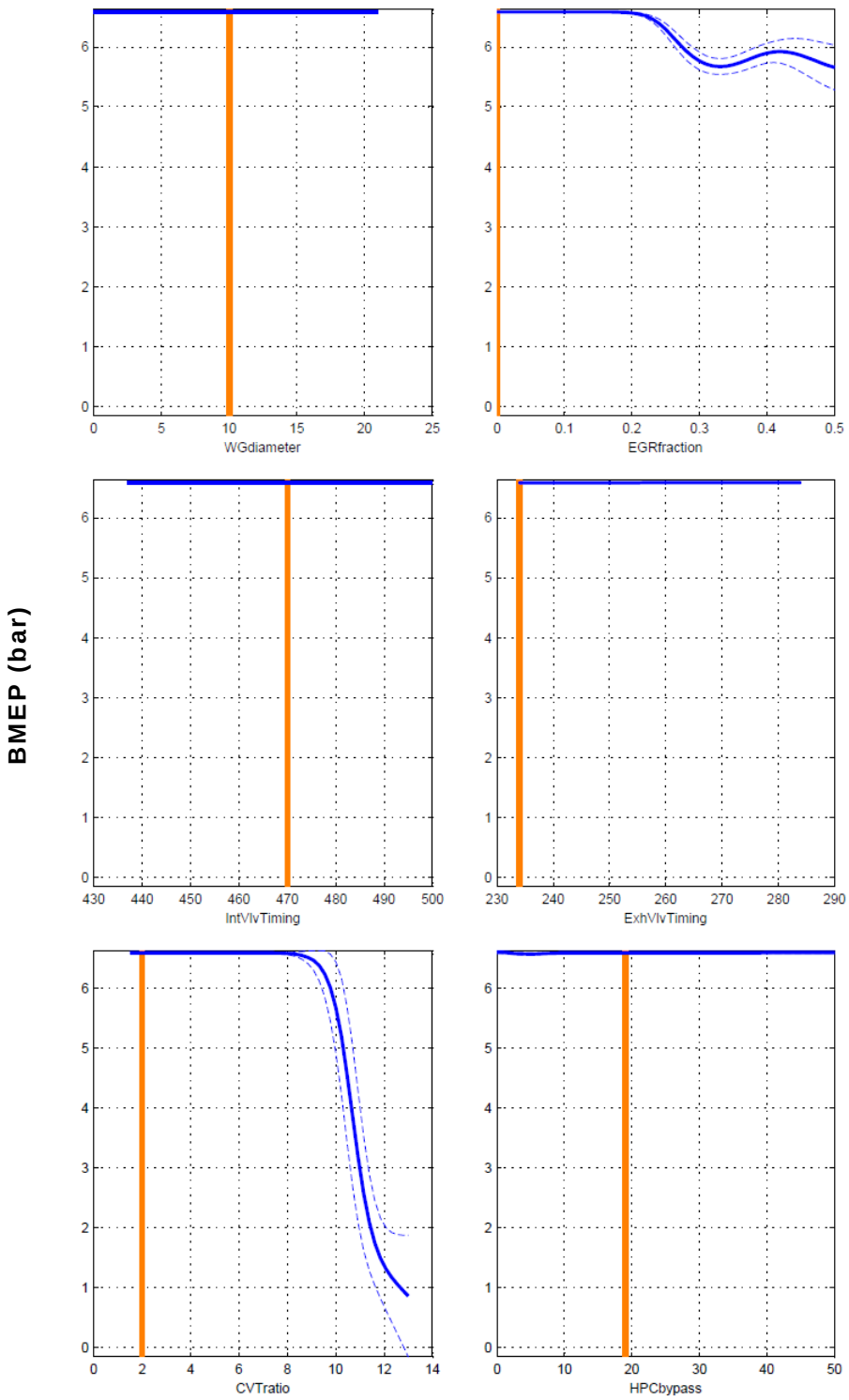

Figure 5.14 – Cross-section through SC CVT BMEP (bar) response model, showing effects of wastegate diameter (mm), target EGR rate, intake valve MOP (CAD ATDCF), exhaust valve MOP (CAD ATDCF), supercharger drive ratio, and supercharger bypass valve diameter (mm)

Overall, the response models that were fitted to the key variables showed logical trends and realistic behaviour in the regions of interest, as well as generally narrow

confidence bands in these regions. Where this was not the case, it was for non-critical variables – such as the throttle model for the CVT supercharger regime. It was concluded that the selected response models would be more than adequate for the following optimisation process.

5.2.2 Optimised Steady State Parameter Settings

With the supercharger disengaged, the best BSFC was found to be approximately 240 g/kWhr, which was achieved with a high EGR target (30% and above), and the wastegate diameter set to 15 mm. As Figure 5.15 shows, the low BSFC region extends across a range of wastegate diameters (~3-19 mm) at high EGR targets; however, with the wastegate open less than 15 mm the BMEP target was unattainable. EGR targets above 30% were also disregarded for the same reason, or the EGR throttle was already fully open. Intake valve timing was advanced 50 degrees (to 450 CAD), and exhaust valve timing retarded by 21 degrees (to 255 CAD), giving an overlap of 14 degrees.

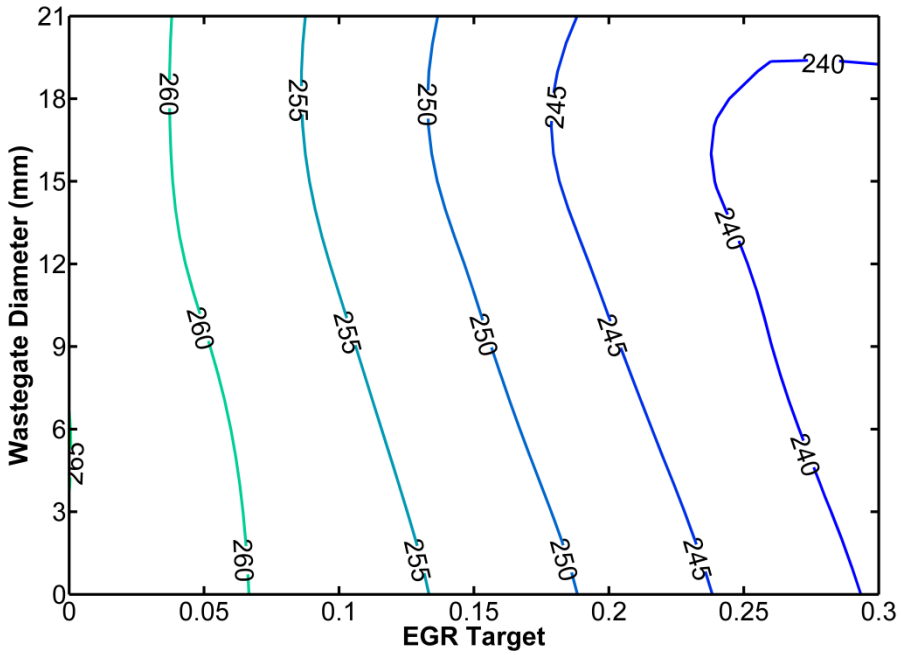

Figure 5.15 – Supercharger disengaged regime steady state parameter optimisation – contours of BSFC (in g/kWhr) for the trade-off between wastegate diameter and EGR target

Similarly, with the supercharger engaged, the best BSFC was obtained with a high EGR target (again, 30% and above) and this was only slightly higher than with the supercharger disengaged at around 245 g/kWhr. As Figure 5.16 shows, the wastegate was fully closed at this operating point, with the BSFC benefit being

derived from increased back pressure and, as a result, maximised EGR flow. As before, EGR targets above 40% were disregarded, as the EGR throttle was already fully open in this region. The supercharger bypass was partially open (17 mm diameter out of a maximum 50 mm) to allow some flow recirculation and reduce the supercharger power consumption, but wider openings caused the BMEP to drop below the target value. Intake valve timing was fully advanced (to 437 CAD), and exhaust valve timing retarded by 21 degrees (to 255 CAD), giving an overlap of 27 degrees.

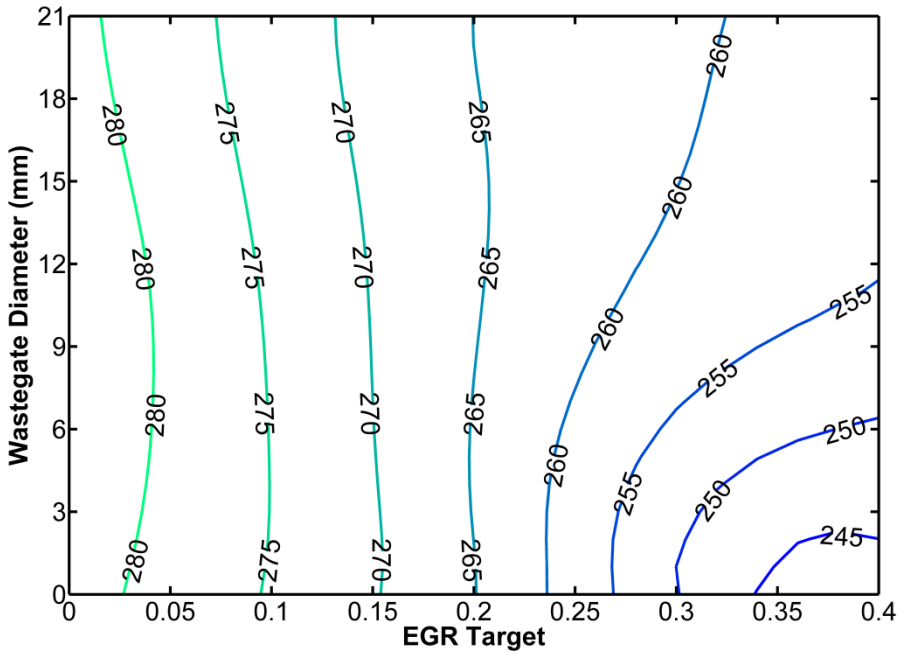

Figure 5.16 – Supercharger engaged regime steady state parameter optimisation – contours of BSFC (in g/kWhr) for the trade-off between wastegate diameter and EGR target

Considering the regime with the supercharger driven through a CVT, as would be expected, the drive ratio used had a major effect on overall efficiency, as shown in Figure 5.17. Consequently, a low drive ratio of 2:1 was chosen – lower than this gave no additional benefit. With this as a basis, a high EGR target again gave the best BSFC of approximately 251 g/kWhr, as shown in Figure 5.18, achieved with the wastegate fully open. By partially closing the wastegate, increased EGR flow could be achieved, resulting in equally good BSFC – as illustrated by the low BSFC region in Figure 5.18. However, adopting this strategy made the BMEP target difficult to attain and was therefore disregarded. For optimum operation, the supercharger bypass was partially open (16 mm diameter) again to allow some flow recirculation and reduce the supercharger power consumption. Intake valve timing was fully

advanced (to 437 CAD), and exhaust valve timing retarded by 36 degrees (to 270 CAD), giving a considerable amount of overlap of 42 degrees.

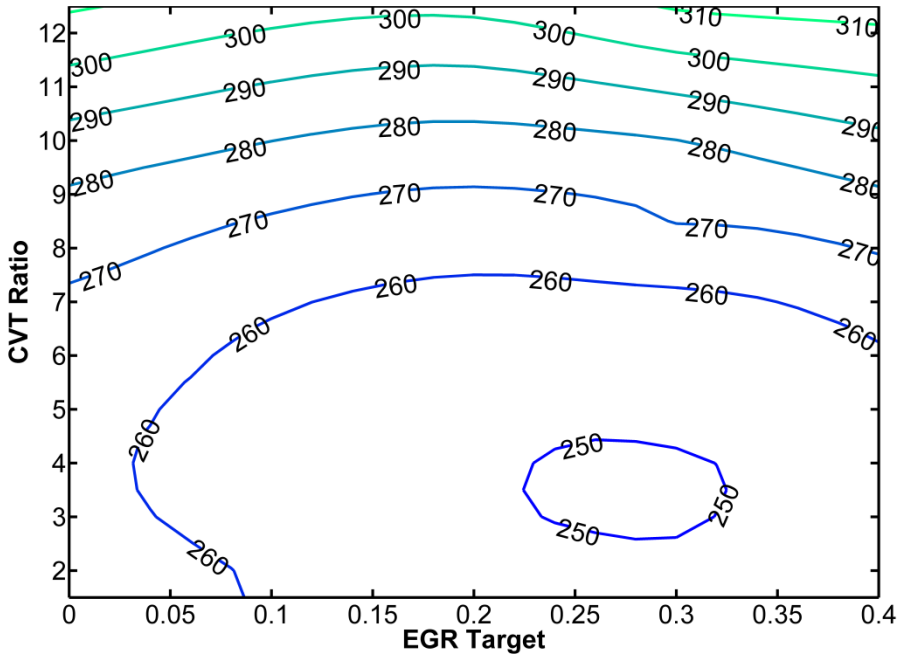

Figure 5.17 – CVT-driven supercharger regime steady state parameter optimisation – contours of BSFC (in g/kWhr) for the trade-off between CVT ratio and EGR target

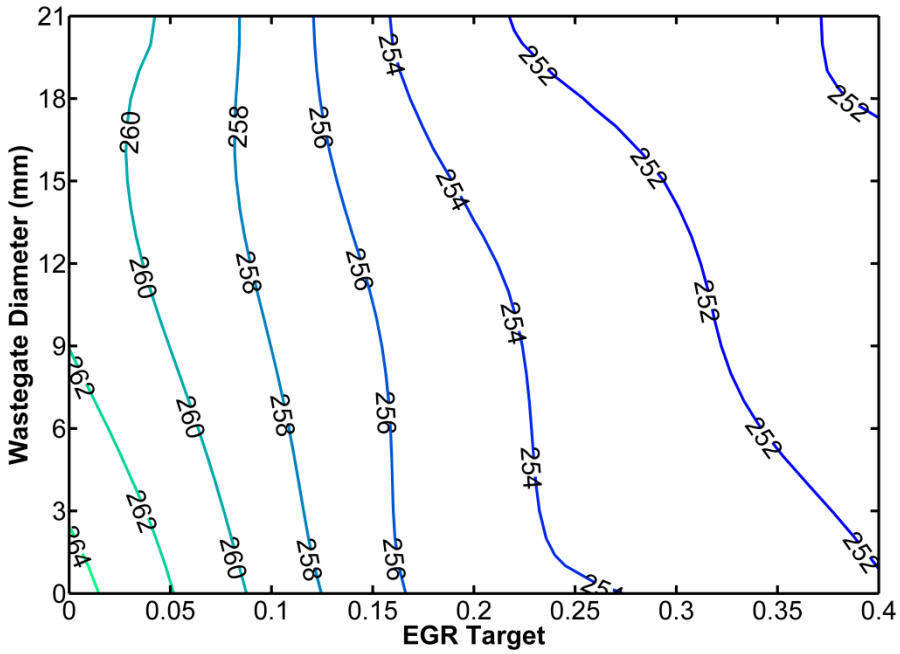

Figure 5.18 – CVT-driven supercharger regime steady state parameter optimisation – contours of BSFC (in g/kWhr) for the trade-off between wastegate diameter and EGR target (N.B. CVT ratio fixed at 2:1)

Across the different supercharger engagement regimes, the parameter that had the largest independent effect on BSFC was the EGR target – increasing the EGR target was found to cause an almost linear reduction in BSFC, as can be seen in Figure 5.15, Figure 5.16 and Figure 5.18. As the level of EGR used was also expected to have a significant effect on the resulting dynamic response, two 'optimum' steady state calibrations for each supercharger engagement regime were taken forward to be used in the transient simulations – zero EGR and maximum EGR (i.e. fully open EGR throttle). A summary of the parameter settings for the resulting six calibrations is given in Table 5.4; for reference, predicted BSFC and percentage BSFC reduction (compared with the baseline engine) are also included. (It is worth noting that even the best BSFC reduction (20%) is some way off the overall target of 35%.)

Table 5.4 – Optimised steady state parameter settings for Minimap point 3 (EGR and non-EGR settings)

Parameter	*SC disengaged*		*SC engaged*		*SC CVT*	
	EGR	*No EGR*	*EGR*	*No EGR*	*EGR*	*No EGR*
EGR throttle angle (deg)	90	0	90	0	90	0
Wastegate diameter (mm)	15	15	0	0	21	21
Intake valve MOP (CAD ATDCF)	450	437	437	443	437	470
Exhaust valve MOP (CAD ATDCF)	255	245	255	234	270	234
Valve overlap (deg)	14	17	27	0	42	0
SC bypass diameter (mm)	50	50	17	21	16	19
SC drive ratio	0	0	5.9	5.9	2	2
BSFC (g/kWhr)	*240*	*264*	*245*	*282*	*251*	*261*
Predicted BSFC reduction (%)	*20*	*12*	*18*	*6*	*16*	*13*

5.3 Transient Simulation Results

5.3.1 Comparison of Control Schemes

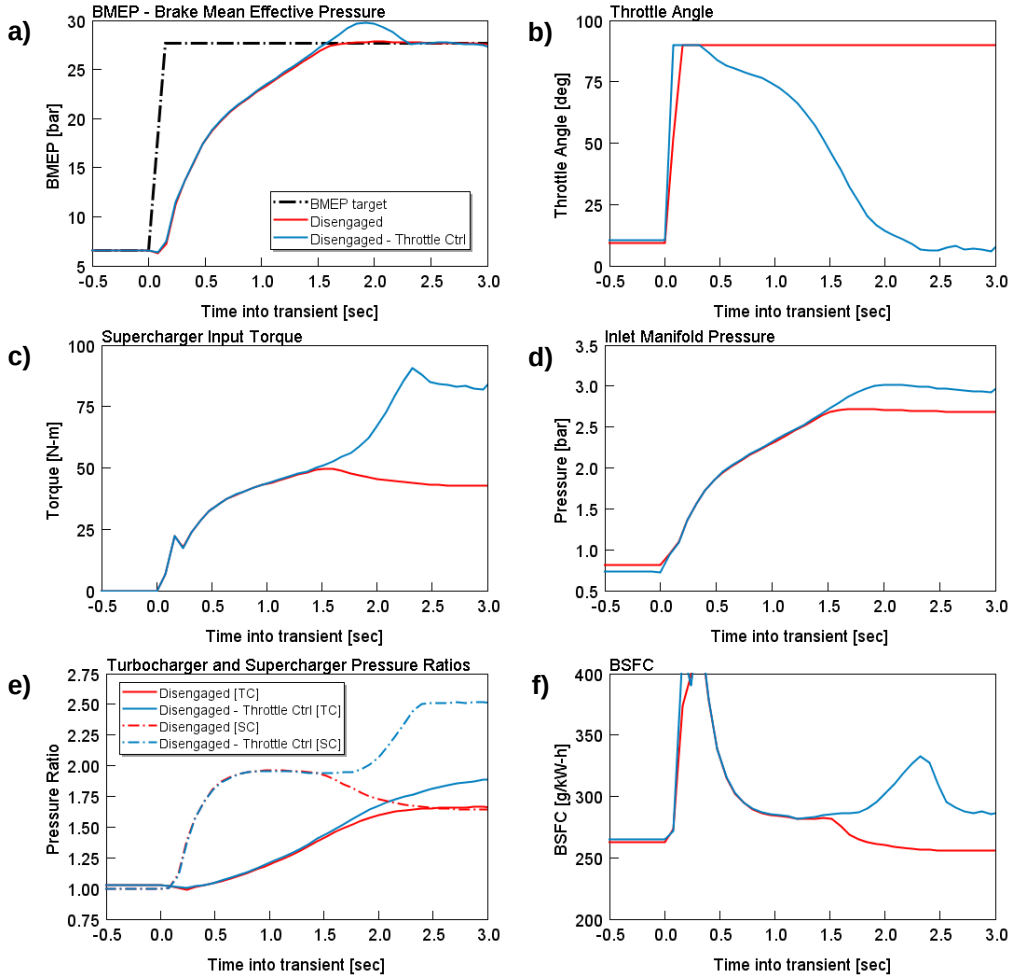

Figure 5.19 – Comparison of throttle control and supercharger bypass/turbocharger wastegate control – a) BMEP; b) Throttle angle; c) Supercharger input torque; d) Inlet manifold pressure; e) Turbocharger and supercharger pressure ratios; f) BSFC

A comparison of transient simulation results for the two control schemes described above (Section 5.1.6) are shown in Figure 5.19 (for the supercharger disengaged, no EGR operating point). As Figure 5.19a shows, the system with throttle control has pronounced overshoot (approximately 8%) when the target BMEP is achieved. Once the supercharger and turbocharger are both up to speed and producing significant pressure ratios (Figure 5.19e) the throttle has to be almost fully closed (6-10 degrees open) to maintain the target BMEP. This has the effect of wasting a considerable amount of energy, producing unnecessary intake pressure upstream of the throttle, with the supercharger input torque required increasing significantly, as

shown in Figure 5.19c. Consequently, BSFC at the BMEP target is poor, as displayed in Figure 5.19f. In contrast, the system with the throttle fixed fully open at the commencement of the tip-in, and with the supercharger bypass valve and turbocharger wastegate used to control MAF and thus BMEP, shows greatly improved transient behaviour and performance. BMEP overshoot is minimal and response time is on a par with the throttle-controlled system, as the red trace in Figure 5.19a shows. Pumping losses and supercharger work (Figure 5.19c) are greatly reduced by keeping the throttle fully open and recirculating the intake air using the supercharger bypass valve, resulting in greatly improved BSFC at the end of the transient – see Figure 5.19e. This improved control scheme was adopted and applied to the operating points listed in Table 5.4; the results are discussed below.

5.3.2 Supercharger Disengaged and Engaged Regimes

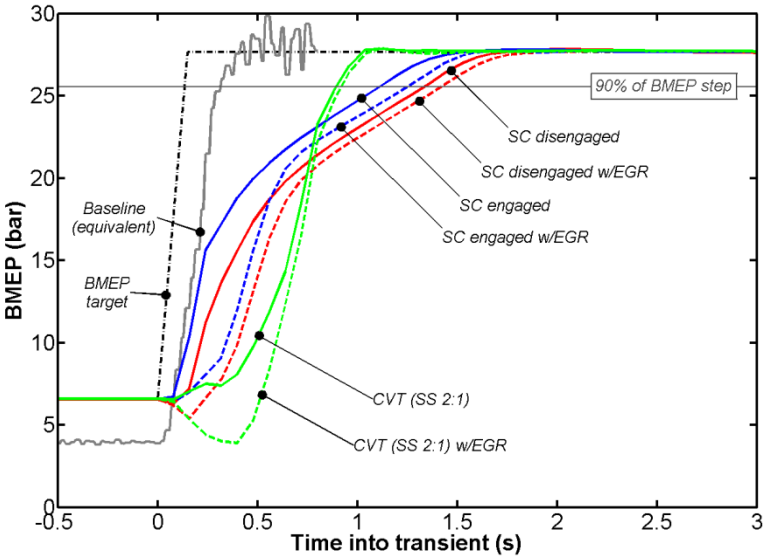

Figure 5.20 – Brake mean effective pressure (BMEP) response for tip-in simulations of supercharger (SC) engaged, supercharger disengaged, and CVT-driven supercharger regimes. For reference BMEP target, 90% of BMEP step demand, and equivalent BMEP for baseline experimental results are also shown

Figure 5.20 shows a comparison of BMEP response between the supercharger engaged and disengaged regimes, both with and without EGR. As would be expected, BMEP response is delayed by both the use of EGR and by having the supercharger disengaged at the beginning of the transient; these two components of delay are essentially independent, although there are some interactions. Comparing T90 times (that is, time taken to achieve 90% of the step demand in BMEP), the delay resulting from having the supercharger initially disengaged is around 0.2

seconds. The time lag related to the use of EGR is most pronounced in the first 0.6 seconds into the transient, at which point there is a marked dogleg in the BMEP responses; beyond this point the differences between the respective EGR and non-EGR settings are greatly reduced. Regarding the dogleg, there is also corresponding curvature in the non-EGR results, although much less pronounced. Without EGR, this dogleg phenomenon can be explained by the initial transient response being dominated by the supercharger performance (as shown in the pressure ratio traces in Figure 5.21 and Figure 5.22), and after the maximum supercharger pressure ratio is reached the remaining performance is dominated by the turbocharger accelerating up to the required speed and pressure ratio (Figure 5.22).

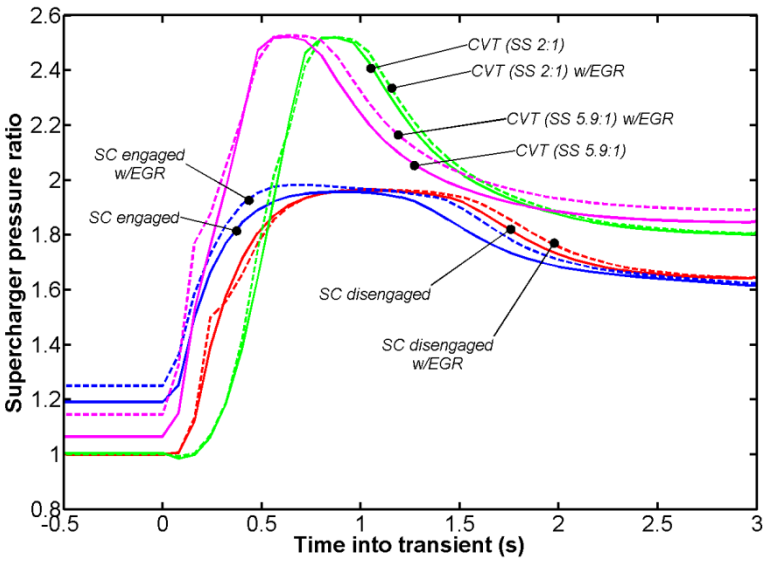

Figure 5.21 – Supercharger pressure ratio for tip-in simulations of supercharger engaged, supercharger disengaged, and CVT-driven supercharger regimes

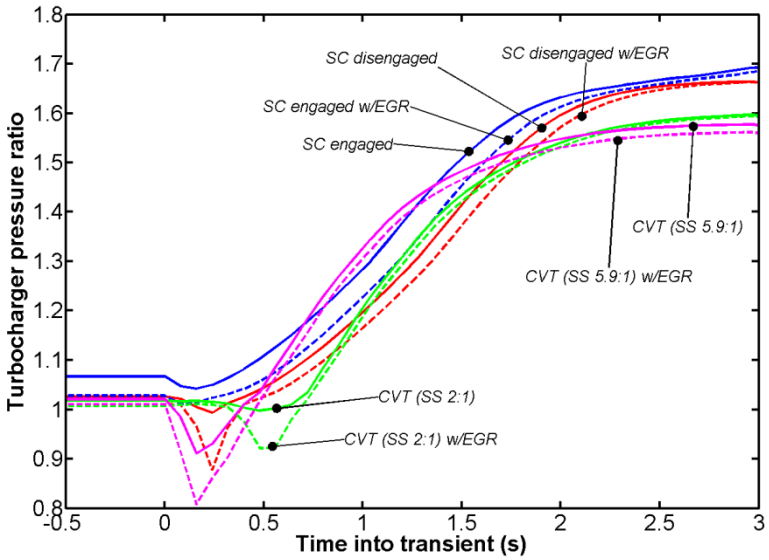

Figure 5.22 – Turbocharger compressor pressure ratio for tip-in simulations of supercharger engaged, supercharger disengaged, and CVT-driven supercharger regimes

With EGR, the dogleg is exaggerated by the time taken to clear the cylinders of residual exhaust gases happening concurrently with the supercharger acceleration. As Figure 5.23 shows, 0.6 seconds is needed to reduce in-cylinder EGR values to zero – with the presence of residual gases reducing the maximum achievable BMEP during the transient, in spite of comparable inlet manifold pressures as for the non-EGR settings (Figure 5.24).

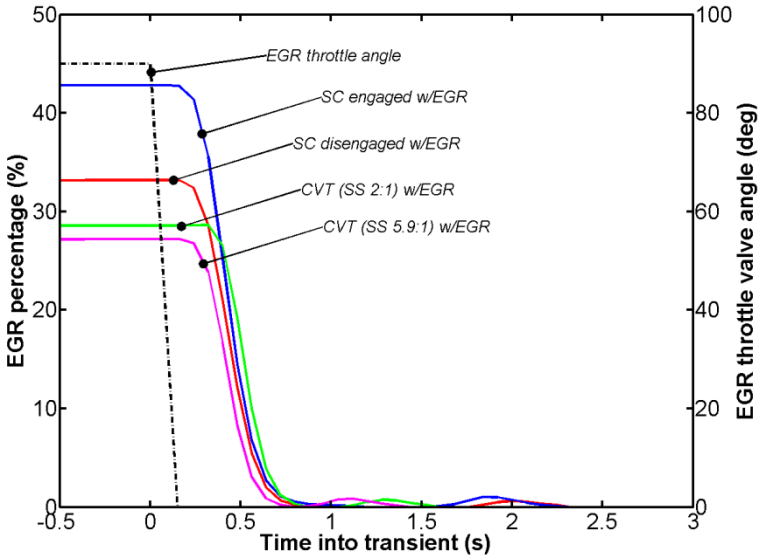

Figure 5.23 – In-cylinder EGR percentages for tip-in simulations of supercharger engaged, supercharger disengaged, and CVT-driven supercharger regimes (with EGR). For reference, EGR valve angle is also shown

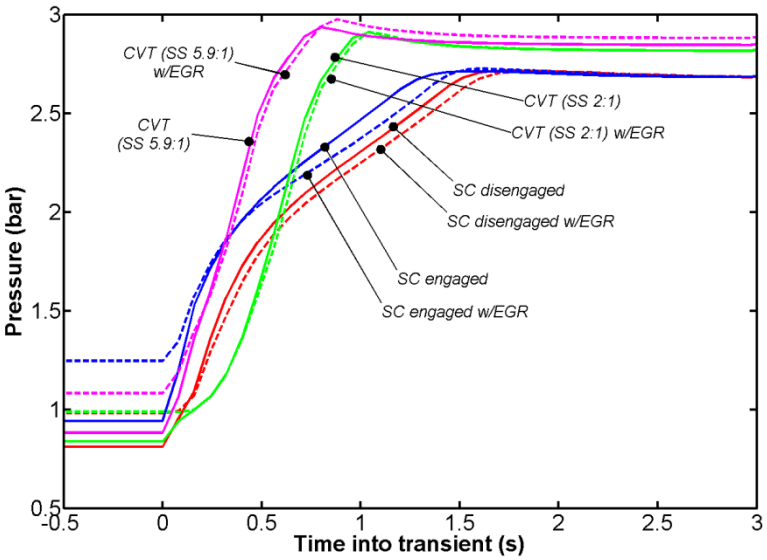

Figure 5.24 – Inlet manifold pressures for tip-in simulations of supercharger engaged, supercharger disengaged, and CVT-driven supercharger regimes

It is worth noting that, as Figure 5.23 shows, the simulations featured very high levels of EGR – up to 43%; in reality, lower values (<30%) would need to be used to retain combustion stability (which the simulations do not take into account) and to limit hydrocarbon emissions [29]. Another factor which must be accounted for is the effect of the EGR 'dead volume', since it can have a significant impact on turbocharger transient response. The EGR circuit as modelled was estimated based on the initial prototype engine design, and thus may have to change for reasons of production feasibility; the results given in Figure 5.20 should be interpreted accordingly.

Figure 5.20 also shows experimental tip-in data for the baseline V8 engine – the recorded torque data has been converted to show the equivalent BMEP that would need to be produced by the downsized engine. Even though the baseline engine starts from a lower initial BMEP (around 4 bar compared with 6.58 bar), it achieves the 90% BMEP value more than 70% sooner than the downsized engine simulations, at around 0.3 seconds, with virtually linear behaviour up to the target. With the supercharger engaged at the start of the tip-in and running without EGR, performance is on a par with the baseline up until the aforementioned dogleg in BMEP at around 15 bar, demonstrating the beneficial instantaneous response provided by the supercharger. Although a direct comparison cannot be drawn between the experimental and simulated results, it does help to provide some context for the computed performance of the downsized engine.

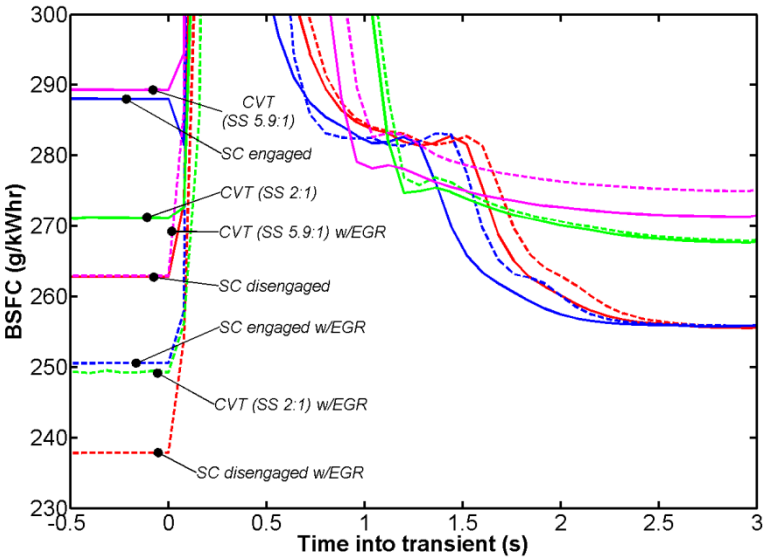

Figure 5.25 – Brake specific fuel consumption (BSFC) for tip-in simulations of supercharger engaged, supercharger disengaged, and CVT-driven supercharger regimes

The best simulated transient response also comes with a penalty in fuel efficiency. As Figure 5.25 shows, the best steady state (i.e. up to 0 seconds) BSFC results in the worst transient BMEP performance, and vice versa. (The steady state BSFC values reflect those obtained during the steady state optimisation procedure, shown in Table 5.4.) Further analysis of these results is discussed below in Section 5.3.4.

5.3.3 CVT-Driven Supercharger

Adding the CVT-driven supercharger regime to the comparison reveals that – with or without EGR – it achieves the 90% BMEP value some 20% sooner than the other supercharger engagement regimes, at approximately 0.9 seconds after the tip-in (Figure 5.20). Up until 0.75 seconds into the transient, however, the performance is in fact worse than the previously discussed supercharger regimes – below 0.5 seconds into the tip-in, it is significantly worse. In fact, the EGR operating condition shows a pronounced dip in BMEP at the start of the tip-in (to 4 bar, from the initial value of 6.58 bar), taking 0.5 seconds to recover and begin increasing beyond the initial steady state level; once recovered, a steeper rise in BMEP seems to be exhibited than the system without EGR. As with the other supercharger regimes, this initial difference between EGR and non-EGR settings is due to the time taken clearing the intake system and cylinders of the residual EGR gases (see Figure 5.23); once cleared, since the manifold pressure is already the same as the non-EGR system (Figure 5.24), and with the intake gases now 100% fresh air, the fuelling can quickly increase to catch up with the non-EGR system. The remainder

of the initial performance deficit between the CVT and supercharger engaged regimes is down to the torque required to accelerate the supercharger – as with the supercharger disengaged regime, discussed above. However, the magnitude of this torque is much greater, as Figure 5.26 shows. The supercharger is accelerated from its steady state speed (3000 rpm) up to a maximum of around 14000 rpm, compared with the previous maximum of 8850 rpm, and this is combined with the added inertia of the CVT and its accompanying mechanical efficiency reduction.

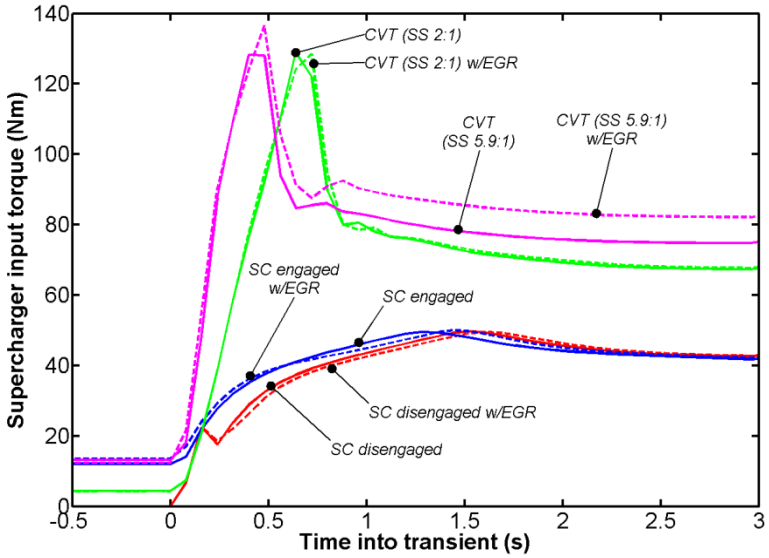

Figure 5.26 – Supercharger input torques for tip-in simulations of supercharger engaged, supercharger disengaged, and CVT-driven supercharger regimes

At the end of the transient, the BSFC of the CVT-driven supercharger scheme is worse than that of the previous configurations, due to the supercharger producing a larger share of the overall boost pressure – see Figure 5.21 and Figure 5.25. As the target BMEP is achieved earlier, the turbocharger has less time to accelerate before the wastegate is opened, resulting in lower turbocharger speed and higher supercharger speed. Increased steady state parasitic losses are an outcome of the higher supercharger speed that is required, meaning that a higher manifold pressure is needed to produce the same BMEP – see Figure 5.24 and Figure 5.26. This issue could be rectified with a more sophisticated controller calibration for the full load steady state conditions, bringing the BSFC in line with the other supercharger regimes; for the purposes of this investigation the current set up is sufficient, however, as the initial steady state and dynamic performance is the focus.

Overall, it is fair to say that the optimised steady state settings for the CVT-driven supercharger regime resulted in fairly poor dynamic performance in the tip-in simulations. As this can largely be attributed to the low initial supercharger drive ratio used an alternative setup was considered, using a higher steady state drive ratio of 5.9:1 – in line with the other supercharger regimes. Dynamic performance was greatly improved using this arrangement, reaching the 90% BMEP value some 40% sooner than the original supercharger engagement regimes, and 25% sooner than with an initial drive ratio of 2:1, at approximately 0.7 seconds after the tip-in (Figure 5.27). The almost-linear nature of the BMEP trace is also similar to that of the equivalent baseline experimental data discussed earlier – though with the response time doubled.

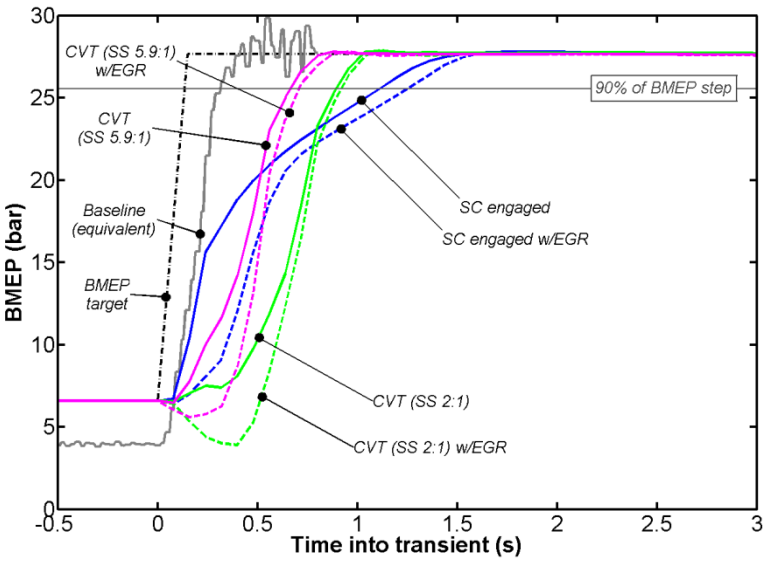

Figure 5.27 – Brake mean effective pressure (BMEP) response for tip-in simulations of supercharger (SC) engaged and CVT-driven supercharger regimes, showing the effect of initial steady state CVT ratio. For reference BMEP target, 90% of BMEP step demand, and equivalent BMEP for baseline experimental results are also shown

Nevertheless, the previously listed disadvantages of the CVT-driven supercharger configuration have not been totally eradicated. For instance, up until 0.5 seconds into the tip-in the BMEP produced remains inferior to that of the supercharger engaged regime (for the same reasons as mentioned above – the vastly increased torque required to accelerate and keep the supercharger at high speed, as shown in Figure 5.26). With EGR, a slight dip in BMEP below the initial steady state level is still exhibited for the first 0.4 seconds – although it is significantly better than the former CVT-supercharger setup (Figure 5.27). The final steady state BSFC also

suffers from the same problem as before (Figure 5.25), resulting from the supercharger taking a larger proportion of the boosting work than necessary (Figure 5.21) – but again this could be solved with better controller calibration. Furthermore, the improved dynamic performance comes at the expense of worsened initial BSFC compared with using a steady state CVT ratio of 2:1 (with or without EGR), as shown in Figure 5.25.

Considering the transient operating points on the turbocharger compressor map (Figure 5.28 – non-EGR data only plotted, for clarity), all of the simulations inhabit the bottom left region of low pressure ratio and low mass flow. Since this is where the map data is most extrapolated, this adds a layer of uncertainty about the reliability of the modelling predictions. However, the corresponding operating points on the supercharger map are more central, giving more confidence (Figure 5.29).

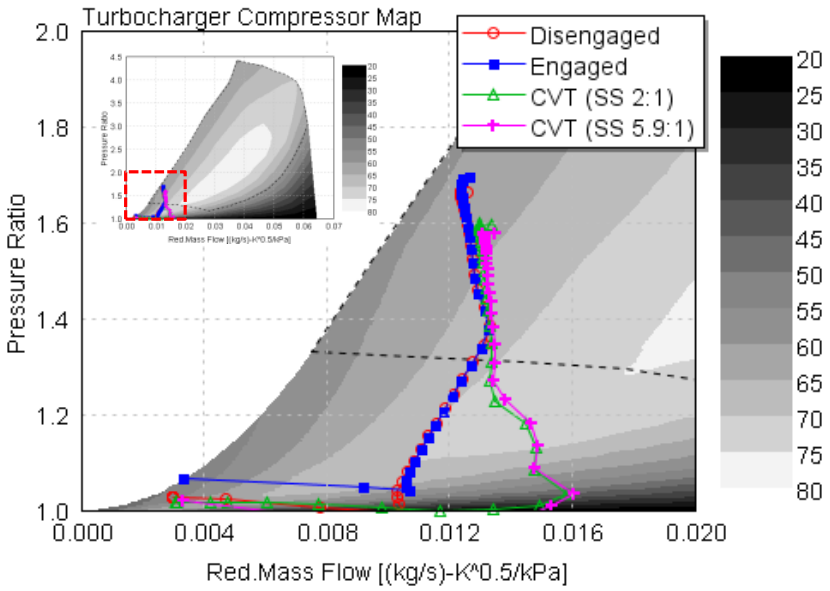

Figure 5.28 – Turbocharger compressor map with transient operating points (showing non-EGR data only, for clarity). Shaded contours show compressor isentropic efficiency (%). Horizontal axis is the reduced mass flow parameter $\frac{\dot{m}\sqrt{T_{inlet}}}{P_{inlet}}$, which is independent of inlet conditions (i.e. temperature and pressure)

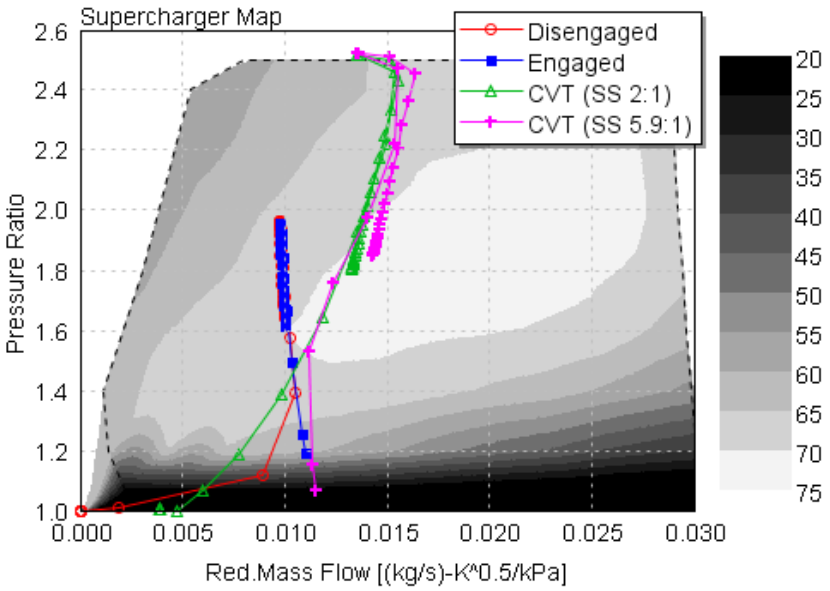

Figure 5.29 – Supercharger compressor map with transient operating points (showing non-EGR data only, for clarity). Shaded contours show compressor isentropic efficiency (%). Horizontal axis is the reduced mass flow parameter $\frac{\dot{m}\sqrt{T_{inlet}}}{P_{inlet}}$, which is independent of inlet conditions (i.e. temperature and pressure)

5.3.4 Rise Time Analysis

The complex nature of the simulation results necessitates a multifaceted approach for performance evaluation. As well as the relatively straightforward appraisal of the BMEP performance discussed above, rise time measurements and driveability assessment techniques were used. Firstly, considering the T10 values (that is, time taken to achieve 10% of the step demand in BMEP) of the various simulations against their respective initial steady state BSFC values, the supercharger engaged non-EGR regime clearly has the fastest initial response (Figure 5.30), but practically the worst BSFC; conversely, the supercharger engaged EGR regime has the best BSFC, but a significantly worse T10 time. A Pareto optimal front can be drawn using this data (the black dashed line in Figure 5.30), to show where the highest Pareto efficiency is achieved. In this case there is a roughly linear inversely proportional relationship between steady state BSFC and initial transient response, and the non-CVT supercharger regimes can be considered the most Pareto-efficient (i.e. closest to or on the Pareto optimal front). On the other hand, the CVT-supercharger points could not be shifted closer to the Pareto optimal front without sacrificing either steady state BSFC or T10 time. Considering the EGR and non-EGR points of any given supercharger regime shows a clear trade-off between steady state BSFC and

initial transient response – the same inversely proportional trend as displayed in the Pareto optimal front is visible in each case. The same can also be said of the initial supercharger speed (i.e. CVT ratio) of the equivalent CVT simulations, or having the supercharger engaged (for the non-CVT simulations) – improved transient response comes at the cost of worse efficiency. Each of these conclusions is consistent with those made in the previous sections but do not reveal the full picture of the respective performances; further complementary analysis is required.

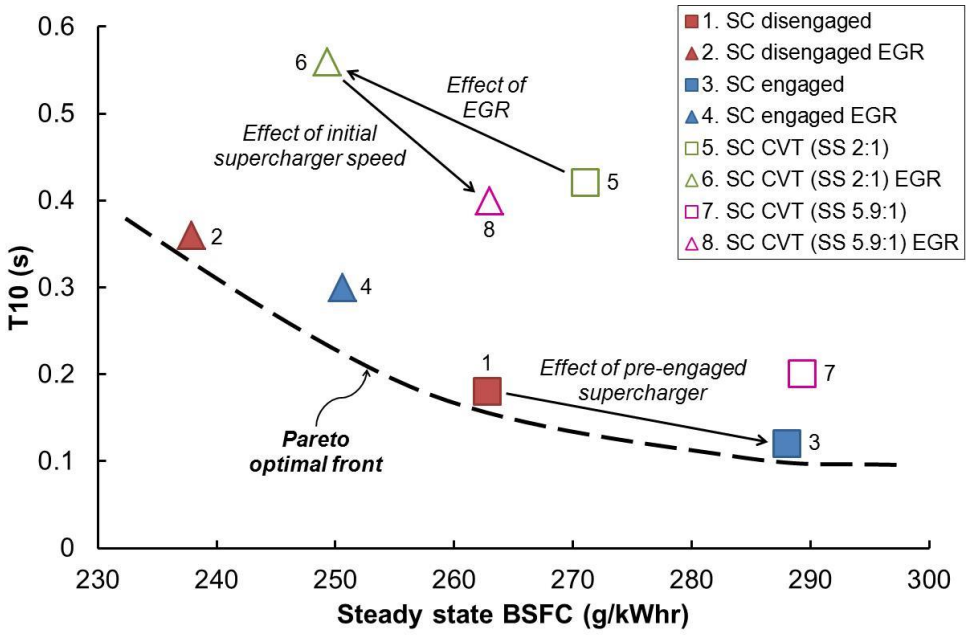

Figure 5.30 – Rise time analysis – T10 (time to achieve 10% of the step demand in BMEP) against initial steady state BSFC

An assessment of the corresponding T90 times (i.e. time to achieve 90% of the BMEP step demand) essentially shows a complete reversal (Figure 5.31), with the CVT-supercharger regimes the most Pareto-efficient – in terms of T90 time at least. The supercharger disengaged EGR point also features on the Pareto optimal front, but with a greatly increased T90 time and only slightly reduced BSFC (compared with the 2:1 CVT-supercharger with EGR condition). Again there is an interesting relationship between the EGR and non-EGR points of each supercharger engagement regime; using EGR gives a significant reduction in initial BSFC (8-13%), but approximately the same T90 time is achieved with or without EGR. As discussed previously, however, initial transient response deteriorates when using EGR. In terms of absolute Pareto-efficiency for T90 time versus BSFC, the two CVT-supercharger settings with EGR appear supreme.

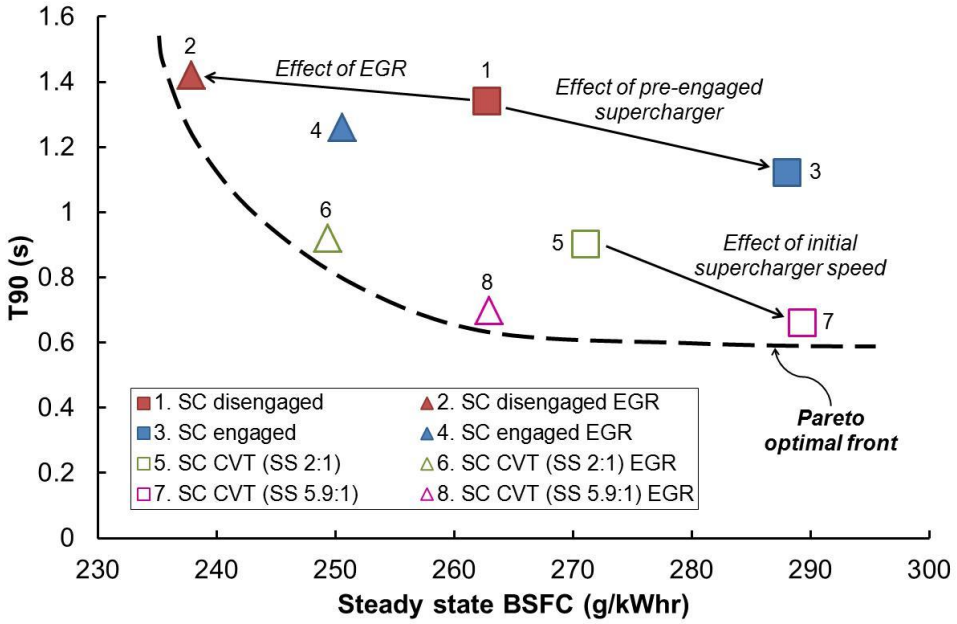

Figure 5.31 – Rise time analysis – T90 (time to achieve 90% of the step demand in BMEP) against initial steady state BSFC

Figure 5.32 shows the T10-T90 values (i.e. time taken to go from 10% to 90% of the BMEP step demand) for each of the simulations. A similar trend as to the T90 times (Figure 5.31) is displayed, but here the advantage of the CVT-supercharger regimes compared with those with fixed drive ratio is particularly clear – the T10-T90 times of the former are around 60% lower. A similar relationship between the EGR and non-EGR points of each supercharger engagement regime is also displayed (Figure 5.32); using EGR gives a significant reduction in initial BSFC (8-13%), accompanied by a comparable T10-T90 time (if anything, slightly lower). As mentioned previously, the EGR rates used in these simulations are higher than would be used in reality; however, the trends shown in these graphs can be interpreted as vectors (Figure 5.30, Figure 5.31, Figure 5.32), and thus reducing the level of EGR would simply shift the operating point along the vector towards the corresponding non-EGR result.

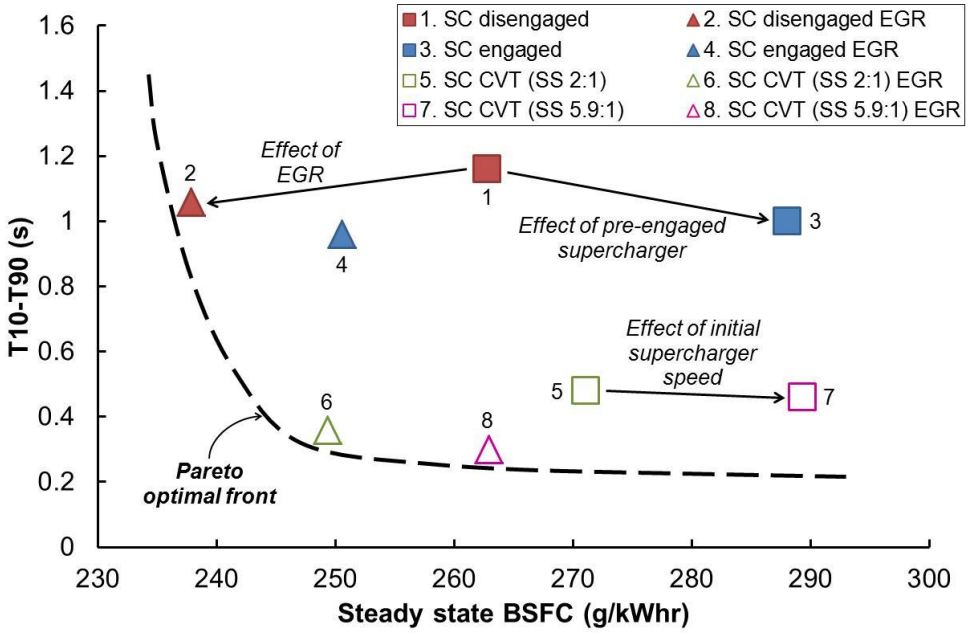

Figure 5.32 – Rise time analysis – T10-T90 (time taken to go from 10% to 90% of the BMEP step demand) against initial steady state BSFC

Taking the T90 and T10-T90 metrics in isolation, the CVT-supercharger regimes with EGR are clearly the most Pareto-efficient, providing the best balance between BSFC and dynamic performance; but again, this must interpreted in the context of the initial time to BMEP fluctuation (T10 times, Figure 5.30), where the CVT-supercharger regimes faired significantly worse. The performance appraisal may benefit from additional driveability assessments.

5.3.5 Driveability Analysis

As Pickering and Brace [105] state, 'driveability is by its nature a subjective rating', and is hence difficult to quantify. Studies have been performed into the correlation between subjective assessments and objective measurements of vehicle behaviour [106][107][108][109]; with regards to tip-in performance and assessment of launch feel, List and Schoeggl [106] and Wicke et al. [108] have identified delay time, acceleration, and jerk (defined as a measure of initial rate of change of acceleration) as key metrics for these correlations. These studies were based on in-vehicle tests, as opposed to fixed speed tip-in simulations in the current investigation, and hence the conclusions pertaining to acceleration and jerk are inapplicable. Also, time delay was defined as the time between change in pedal demand and first change in vehicle acceleration [108]; however, it is expected that likening this to the delay in engine response to the BMEP demand in the simulations will give at least an

indication of the driveability of the different boosting configurations when mounted in a vehicle. On this basis, the findings of Wicke et al. [108] that a delay time of less than around 350 ms is necessary to achieve a good subjective driveability rating can be applied as a criterion for the simulations in this investigation. Thus, considering the percentage increase in BMEP at this key period during the tip-in (Figure 5.33), with the possible exception of the supercharger engaged and disengaged regimes, the configurations with EGR provide inadequate performance; the supercharger engaged regime without EGR is clearly the best from a driveability point of view, with some competition from the supercharger disengaged and CVT-supercharger (with 5.9:1 steady state ratio) regimes.

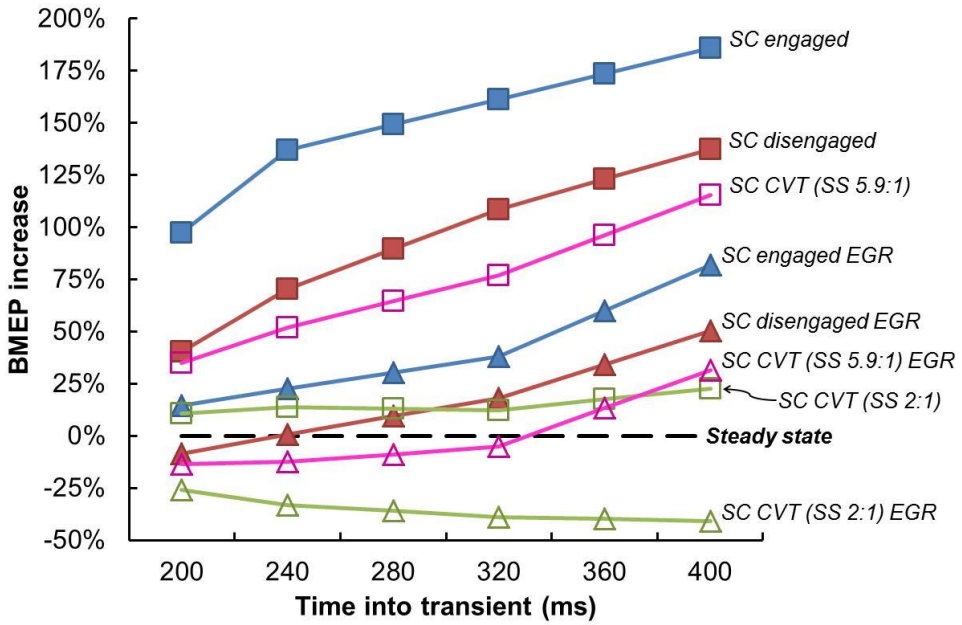

Figure 5.33 – Driveability analysis – percentage BMEP increase at key times during tip-in transient

Plotting these results against the respective steady state BSFC values gives another perspective (Figure 5.34) – highlighting the relative inefficiency of the SC engaged and CVT-supercharger regimes, and bringing to the fore the balance between driveability and efficiency provided by the supercharger disengaged regime. These conclusions must of course be made tentatively; the applicability of the delay time driveability criterion to fixed speed simulations and the assumed immediate response of controllers and parameter changes in the model necessitate caution. However, the relative merits of the different configurations are fairly clear.

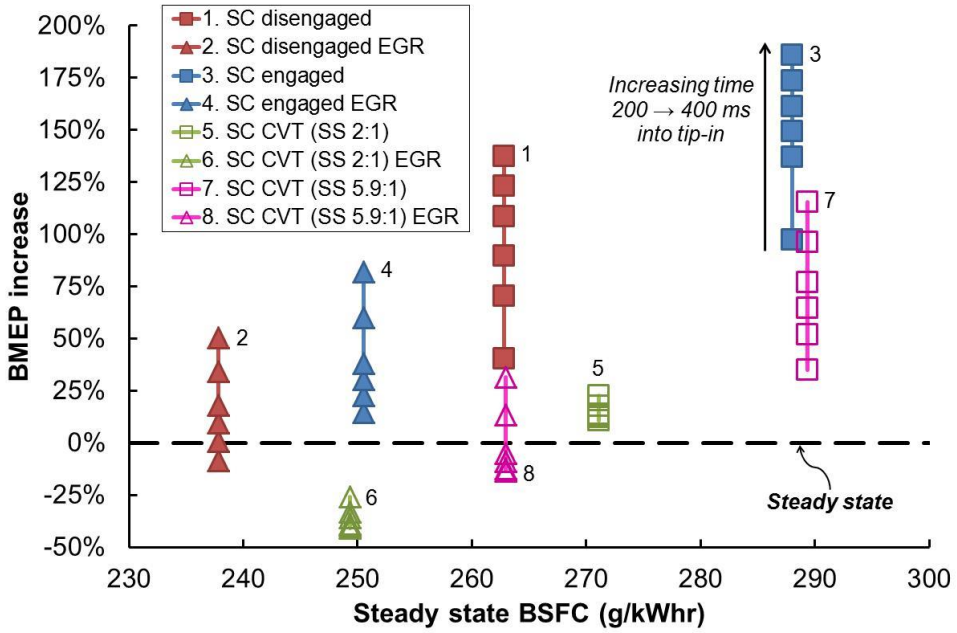

Figure 5.34 – Driveability analysis – percentage BMEP increase at key times during tip-in transient against initial steady state BSFC

Another aspect of driveability that has not been explored is the manner of engaging and accelerating the supercharger. As mentioned in Section 5.1.5, for these investigations supercharger clutch engagement was represented by a ramping up of supercharger speed over a 0.15 second period – in reality this may be unacceptable from a driveability standpoint and the degree of clutch slip may have to be increased. This would warrant further investigation.

5.4 Results at Additional Minimap Points

The entire design of experiment, parameter optimisation, and transient simulation process was completed for a further two Minimap points in order to assess the performance of the three supercharging engagement regimes from different speed and load starting points. Minimap points 14 and 9 were selected for investigation – 1250 rpm, 60 Nm (3.77 bar BMEP for the downsized engine), and 1000 rpm, 80 Nm (5.02 bar BMEP) respectively (see Table 4.2 and Figure 5.1). The same experimental test plan was used as for the establishing investigation at Minimap point 3, since the same ranges of the input parameters were applicable. The resulting response models were of comparable quality to those produced and analysed previously, and, in general, similar trends were exhibited. Table 5.5 and Table 5.6 summarise the subsequent optimised parameter settings for the two new Minimap points.

Table 5.5 – Optimised steady state parameter settings for Minimap point 14 (EGR and non-EGR settings). N.B. for SC CVT, figures outside and inside brackets represent drive ratios of 2 and 5.9 respectively

Parameter	*SC disengaged*		*SC engaged*		*SC CVT*	
	EGR	*No EGR*	*EGR*	*No EGR*	*EGR*	*No EGR*
EGR throttle angle (deg)	90	0	90	0	90	0
Wastegate diameter (mm)	0	0	7	5	0 (0)	0 (0)
Intake valve MOP (CAD ATDCF)	437	437	437	437	437 (437)	437 (437)
Exhaust valve MOP (CAD ATDCF)	273	284	284	284	264 (278)	268 (284)
Valve overlap (deg)	45	56	56	56	36 (50)	40 (56)
SC bypass diameter (mm)	50	50	22	24	10 (23)	11 (22)
SC drive ratio	0	0	5.9	5.9	2 (5.9)	2 (5.9)
BSFC (g/kWhr)	*269*	*305*	*290*	*340*	*270 (296)*	*311 (339)*
Predicted BSFC reduction (%)	*31*	*22*	*26*	*13*	*31 (24)*	*21 (13)*

Table 5.6 – Optimised steady state parameter settings for Minimap point 9 (EGR and non-EGR settings). N.B. for SC CVT, figures outside and inside brackets represent drive ratios of 2 and 5.9 respectively

Parameter	*SC disengaged*		*SC engaged*		*SC CVT*	
	EGR	*No EGR*	*EGR*	*No EGR*	*EGR*	*No EGR*
EGR throttle angle (deg)	90	0	90	0	90	0
Wastegate diameter (mm)	4	19	0	21	0 (0)	21 (21)
Intake valve MOP (CAD ATDCF)	437	437	437	437	437 (437)	437 (437)
Exhaust valve MOP (CAD ATDCF)	280	284	284	284	284 (284)	284 (284)
Valve overlap (deg)	52	56	56	56	56 (56)	56 (56)
SC bypass diameter (mm)	50	50	25	19	16 (20)	14 (21)
SC drive ratio	0	0	5.9	5.9	2 (5.9)	2 (5.9)
BSFC (g/kWhr)	*256*	*288*	*273*	*296*	*260 (275)*	*287 (310)*
Predicted BSFC reduction (%)	*24*	*14*	*19*	*12*	*23 (18)*	*15 (8)*

Compared with the previous optimisation results, high levels of overlap in the inlet and exhaust valve timings were found to be beneficial across all the operating regimes for both new Minimap points, in order to maximise cylinder 'scavenging' – utilising the positive pressure gradient from intake to exhaust to clear the cylinder of residuals as much as possible. For the Minimap point 9, the predicted BSFC reductions (compared with the baseline engine) were marginally higher than for the operating point previously considered, at up to 24% (Table 5.6); whereas for Minimap point 14, a greater than 30% reduction was predicted to be achievable (Table 5.5). This is due to the fuel efficiency benefits of downsizing increasing as required engine load decreases (N.B. torque requirement at Minimap 3 > Minimap 9 > Minimap 14). These findings suggest that the Ultraboost project target of 35% fuel consumption reduction across the NEDC may be feasible, once the relative Minimap point weightings and significant regions of engine idle time are taken into account.

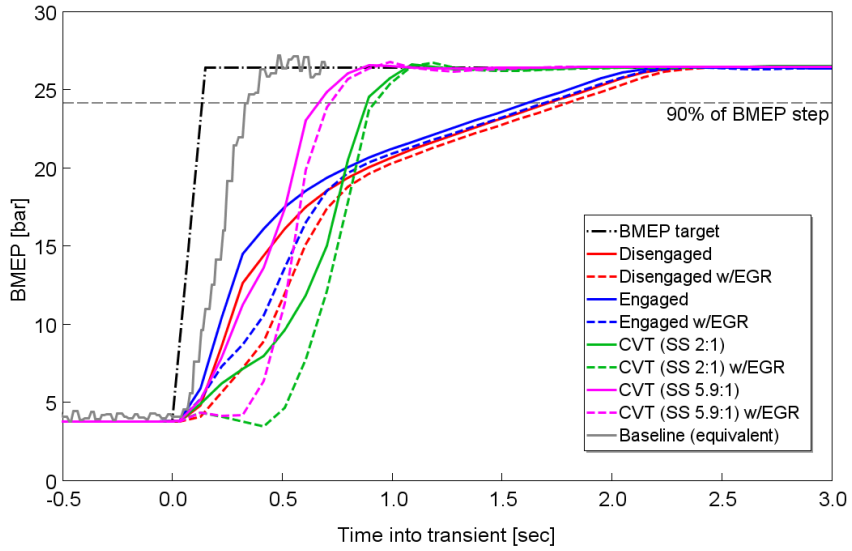

Figure 5.35 – Minimap 14 (1250 rpm, 60 Nm) BMEP response for tip-in simulations of supercharger (SC) engaged, supercharger disengaged, and CVT-driven supercharger regimes (from two different steady state CVT ratios). For reference BMEP target, 90% of BMEP step demand, and equivalent BMEP for baseline experimental results are also shown

As before, fixed speed tip-in transient simulations were conducted from the starting points of the optimised parameter settings of the various supercharger regimes. Considering the BMEP response from Minimap 14 (Figure 5.35), the profiles of the supercharger engaged and disengaged regimes approximately reflect those seen at Minimap 3 (Figure 5.20). The delay in T90 response time relating to the supercharger disengagement at the start of the transient is roughly half that of before, at around 0.1 seconds. This is due to the slower turbocharger acceleration dominating the overall response to a greater degree than before, as illustrated by the shallower gradient of the response curves beyond the dogleg (at around the 0.3 to 0.6 second mark). This, in turn, is a result of the lower exhaust mass flow and energy available to overcome the turbocharger inertia at this reduced engine speed (1250 rpm, compared with the previous 1500 rpm). This is demonstrated further at the 1000 rpm Minimap 9 point – see Figure 5.36. In this instance, the difference between supercharger engaged and disengaged regimes, as well as the effect of EGR, are largely insignificant compared with the sluggishness of the turbocharger performance.

The delay pertaining to the use of EGR is also still evident at both new Minimap points; however, the severity of the delay appears to depend on initial engine load, with the lowest load point (Minimap 14) being most significantly affected (Figure

5.35). Clearly there are complex interactions occurring, as this does not simply depend on the time taken to clear the cylinders of residual exhaust gases, for Minimap 9 takes the greatest time to do this – compare Figure 5.37, Figure 5.38 and Figure 5.23.

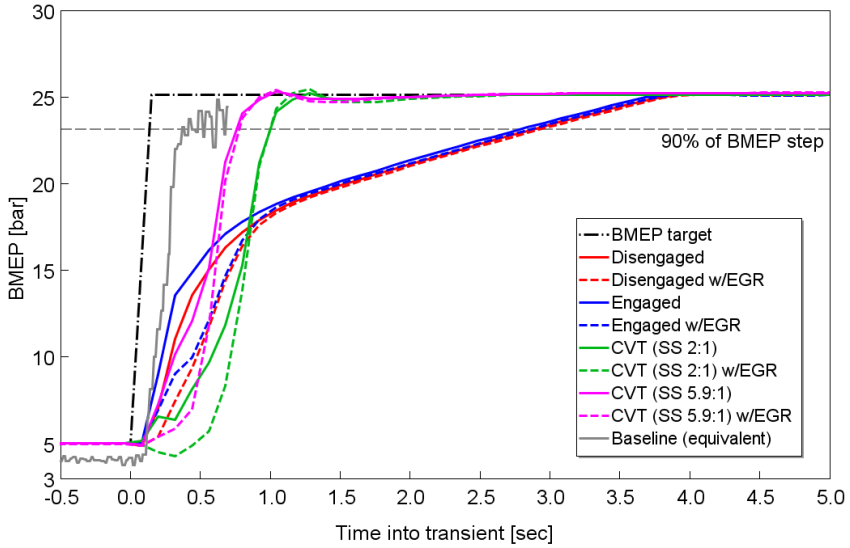

Figure 5.36 – Minimap 9 (1000 rpm, 80 Nm) BMEP response for tip-in simulations of supercharger (SC) engaged, supercharger disengaged, and CVT-driven supercharger regimes (from two different steady state CVT ratios). For reference BMEP target, 90% of BMEP step demand, and equivalent BMEP for baseline experimental results are also shown

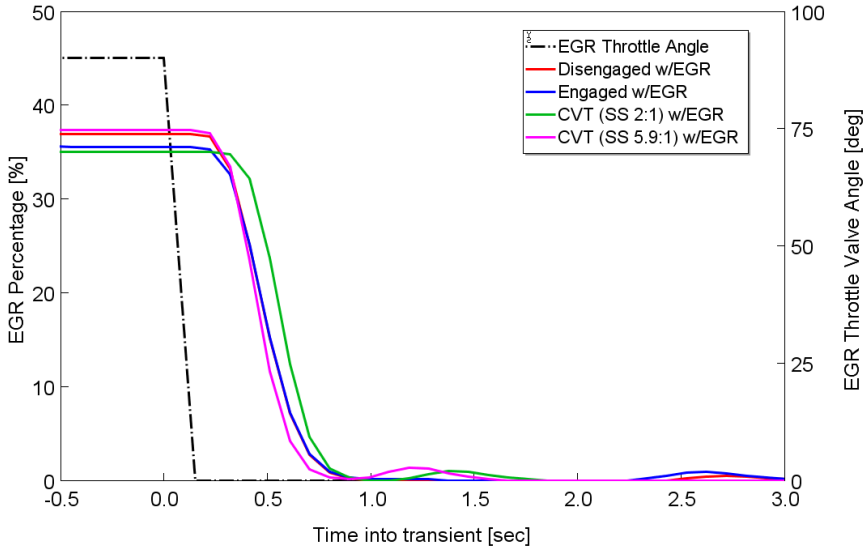

Figure 5.37 – Minimap 14 (1250 rpm, 60 Nm) in-cylinder EGR percentages for tip-in simulations of supercharger engaged, supercharger disengaged, and CVT-driven supercharger regimes (with EGR). For reference, EGR valve angle is also shown

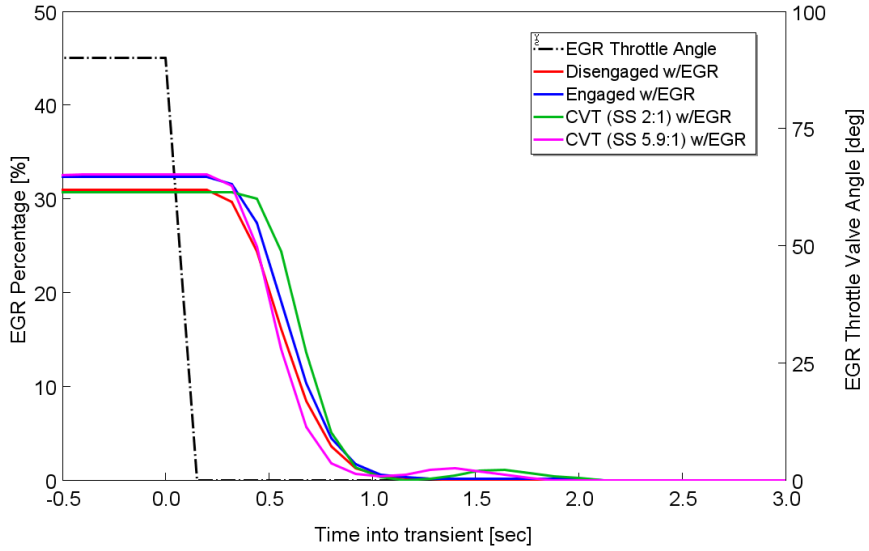

Figure 5.38 – Minimap 9 (1000 rpm, 80 Nm) in-cylinder EGR percentages for tip-in simulations of supercharger engaged, supercharger disengaged, and CVT-driven supercharger regimes (with EGR). For reference, EGR valve angle is also shown

The advantage of the CVT-driven supercharger in terms of BMEP response is made even clearer at these lower engine speed points (Figure 5.35 and Figure 5.36). Starting from an initial CVT ratio of 2:1, it achieves the 90% BMEP value around 45% sooner than the other supercharger engagement regimes (at around 0.9 seconds) at Minimap point 14, and some 65% sooner (at approximately 1 second) at Minimap point 9. However, as before, the significant torque required to accelerate the supercharger (see Figure 5.26) results in a performance deficit in the initial stages of the tip-in compared with the supercharger engaged regimes – although the gap closes with decreasing engine speed. Increasing the initial CVT ratio to 5.9:1 improves the BMEP response even further, reducing the T90 times to around 0.7 seconds and 0.8 seconds for Minimap 14 and Minimap 9 respectively (60% and 70% sooner than the corresponding supercharger engaged regimes). However, even these greatly improved response times still lag some way behind the performance of the naturally aspirated baseline engine – as before, experimental torque response data for the baseline engine has been converted to the equivalent BMEP that would need to be produced by the downsized engine, shown in Figure 5.35 and Figure 5.36. Also, the best transient response is again at the expense of the highest initial steady state BSFC (Figure 5.39), and therefore the lowest potential fuel consumption reduction compared with the baseline engine (Table 5.5 and Table 5.6).

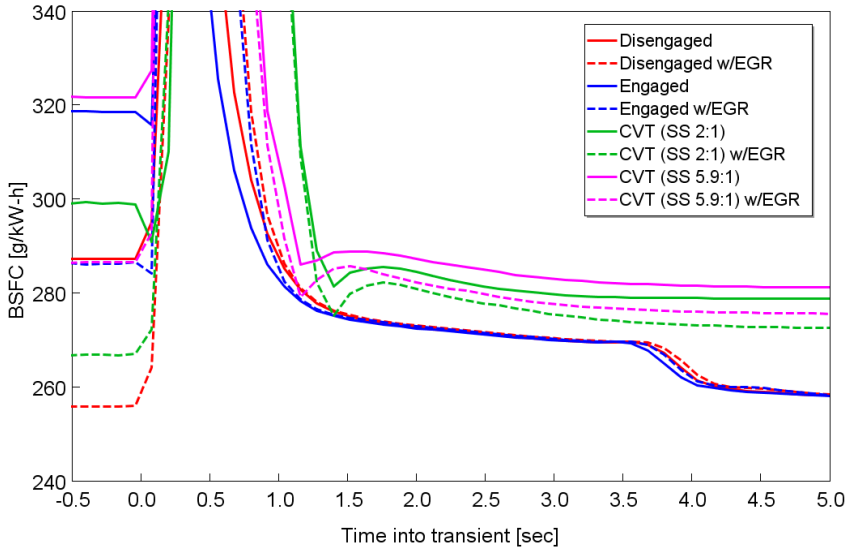

Figure 5.39 – Minimap 9 (1000 rpm, 80 Nm) brake specific fuel consumption (BSFC) for tip-in simulations of supercharger engaged, supercharger disengaged, and CVT-driven supercharger regimes

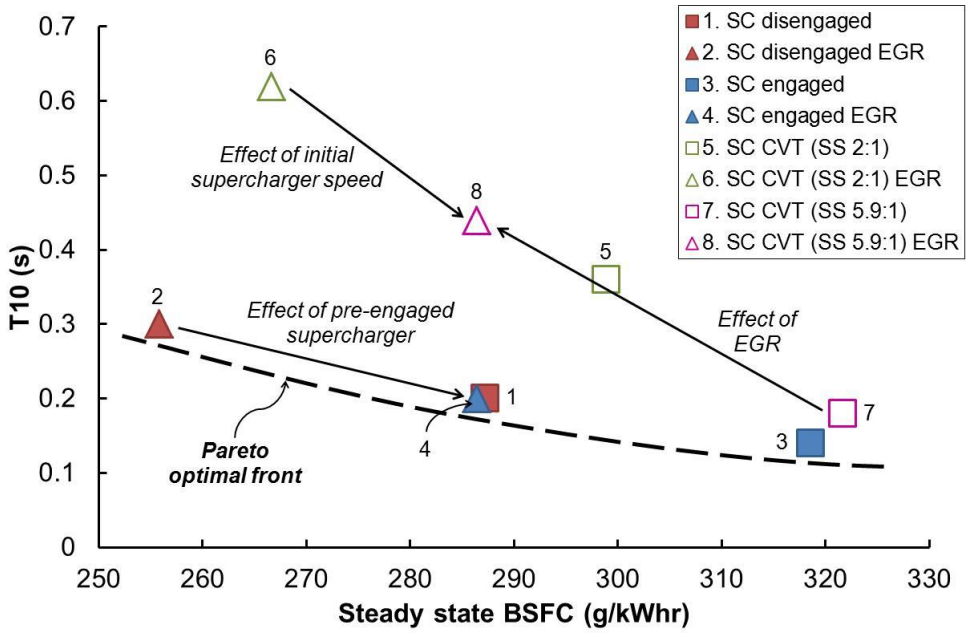

Figure 5.40 – Minimap 9 (1000 rpm, 80 Nm) rise time analysis – T10 (time to achieve 10% of the step demand in BMEP) against initial steady state BSFC

Considering the T10 times of the various simulations against their respective initial steady state BSFC values, for Minimap point 9 (Figure 5.40), the trade-off between the two factors is clear – improved transient response comes at the cost of worse efficiency. The Pareto optimal front fitted to the data displays a much shallower and flatter profile than for the corresponding data for Minimap point 3 (Figure 5.30). This

suggests that there is less to be gained in terms of initial response by having the supercharger engaged compared with the BSFC penalty incurred, and there is an approximately linear inverse relationship between the two variables. The non-CVT supercharger regimes are still the most Pareto-efficient, and the CVT-supercharger points still require either steady state BSFC or T10 time to be sacrificed in order to be shifted closer to the Pareto optimal front.

Assessing the T90 times in a similar way shows the points reversed (Figure 5.41). The CVT-supercharger regimes are now the most Pareto-efficient, as with Minimap point 3 (Figure 5.31), but the performance gap between them and the non-CVT regimes has been greatly increased compared with before. Again there is an interesting relationship between the EGR and non-EGR points of each supercharger engagement regime; using EGR gives a significant reduction in initial BSFC (around 10%), but approximately the same T90 time is achieved with or without EGR. As discussed previously, however, initial transient response deteriorates when using EGR. In terms of absolute Pareto-efficiency for T90 time versus BSFC, the two CVT-supercharger settings with EGR appear to be the best.

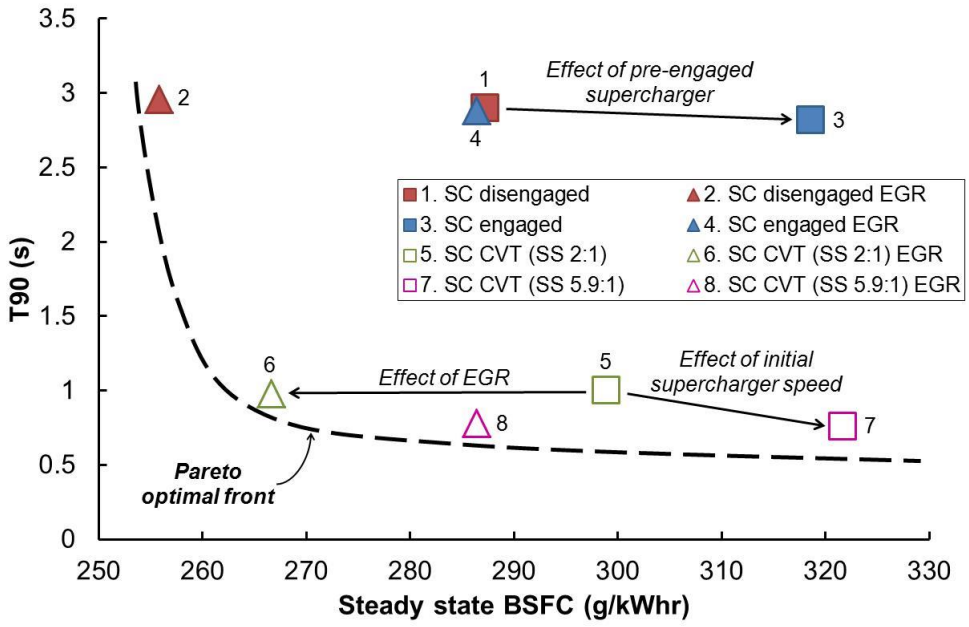

Figure 5.41 – Minimap 9 (1000 rpm, 80 Nm) rise time analysis – T90 (time to achieve 90% of the step demand in BMEP) against initial steady state BSFC

Plotting the T10-T90 values for Minimap point 9, a similar trend is displayed as for T90 times, but the performance gap between the CVT-supercharger regimes and

those with a fixed drive ratio has increased further still (Figure 5.42). Taking the T90 and T10-T90 metrics in isolation, the CVT-supercharger regimes with EGR are clearly the most Pareto-efficient, providing the best balance between BSFC and dynamic performance; but again, this must be interpreted in the context of the initial time to BMEP fluctuation (T10 times, Figure 5.40), where the CVT-supercharger regimes faired significantly worse.

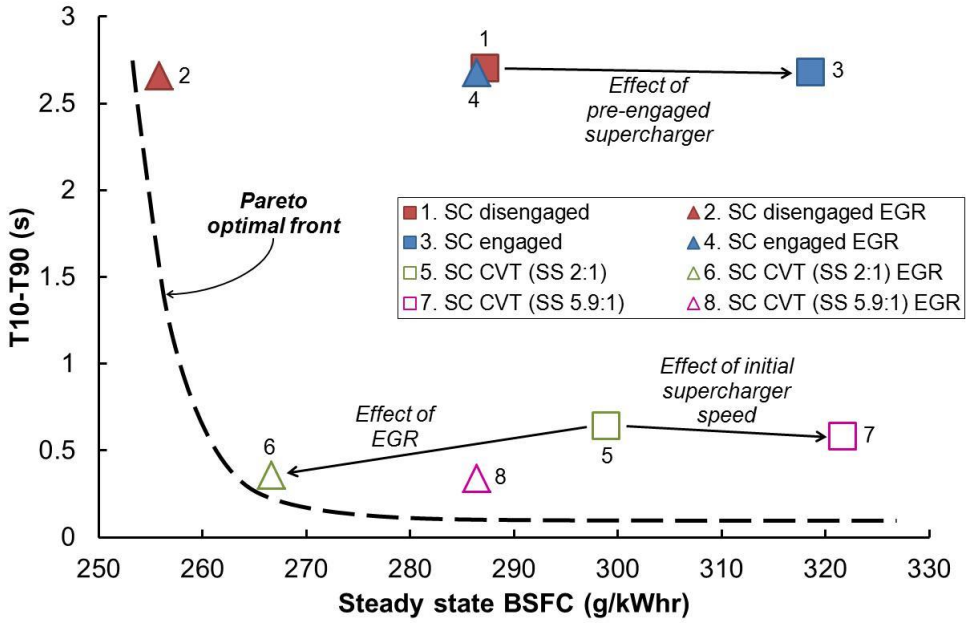

Figure 5.42 – Minimap 9 (1000 rpm, 80 Nm) rise time analysis – T10-T90 (time taken to go from 10% to 90% of the BMEP step demand) against initial steady state BSFC

Methods of quantifying subjective driveability were discussed in Section 5.3.5, and a criterion for delay time less than 350 ms was set forth as necessary for achieving a good subjective rating. Again, considering the percentage increase in BMEP at this key period during the tip-in (Figure 5.43), the supercharger engaged regime without EGR is clearly the best from a driveability point of view, but the supercharger disengaged and CVT-supercharger (with 5.9:1 steady state ratio) regimes are also competitive.

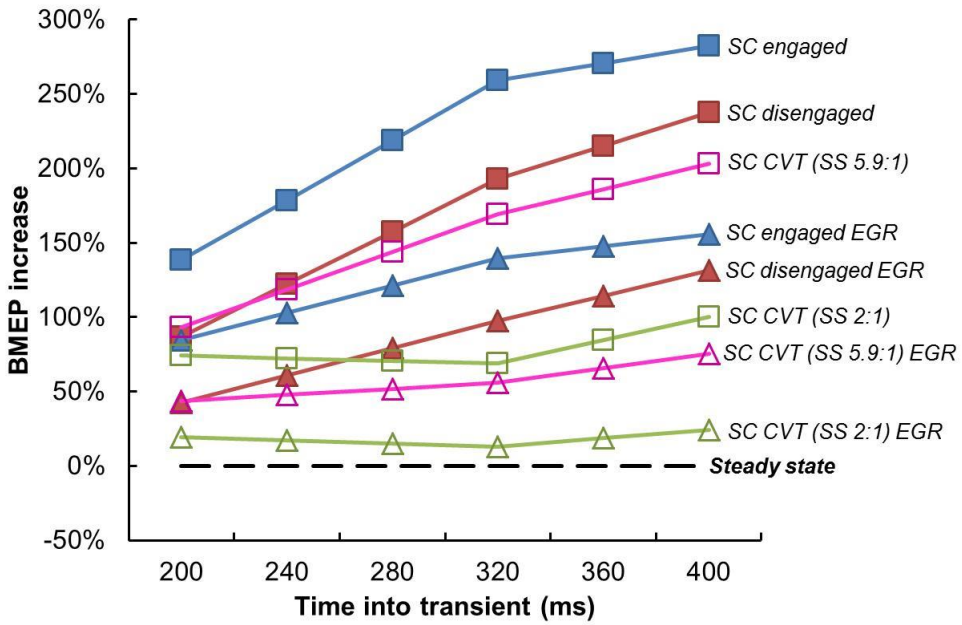

Figure 5.43 – Minimap 9 (1000 rpm, 80 Nm) driveability analysis – percentage BMEP increase at key times during tip-in transient

Note that for all these metrics (BSFC against T10, T90, and T10-T90) the trends of the intermediate Minimap point 14 essentially fall between those of Minimap point 3 and Minimap point 9, suggesting a strong dependence upon engine speed. Overall, although it is not absolutely clear which configuration and supercharger regime is best, the CVT-driven supercharger does make an increasingly strong proposition at lower engine speeds and loads, providing a greater range of control and performance flexibility over the standard fixed drive ratio supercharger arrangement.

5.5 Conclusions

The trade-off between steady state part load fuel efficiency and resulting tip-in performance has been investigated for a highly boosted downsized gasoline engine. Since the engine uses a fixed geometry turbocharger (with external wastegate) in a sequential series arrangement with a positive displacement supercharger, three different supercharger engagement regimes were considered: with the supercharger disengaged and bypassed; with the supercharger engaged with a fixed drive ratio; with the supercharger engaged using a variable ratio (i.e. through a CVT). Focussing on an operating point of 1500 rpm and 104 Nm (equivalent to 6.58 bar BMEP), design of experiments and optimisation techniques were used to find the best settings for the various engine control parameters. Of these parameters, target EGR rate was found to have the largest independent effect on BSFC – increasing the EGR target was found to cause an almost linear reduction in BSFC. However, it was expected that the level of residual gases present would have a large effect on tip-in performance; hence for each supercharger engagement regime, two modes of operation (zero EGR and maximum achievable EGR) were taken forward for evaluation in the transient simulations.

Dynamic performance was simulated in a GT-Power/Matlab Simulink co-simulation environment in order to utilise the more sophisticated dynamic control structures available within Simulink. Using each of the six part load calibrations, a fixed speed tip-in transient was performed, demanding full load (438 Nm, 27.7 bar BMEP) with the step taking place over 0.15 seconds. A control scheme was developed whereby the throttle was set to fully open at the start of the tip-in and engine air flow and load were controlled by the supercharger bypass valve and turbocharger wastegate; this was shown to be vastly superior – both in terms of fuel efficiency and transient behaviour (i.e. overshoot and stability) – to setting the latter two parameters to fully closed and using the throttle alone to control engine load. Evaluating the dynamic performance of the different operating regimes was a complex process; even ignoring steady state BSFC, none of the calibrations was entirely superior to the others. Compared with experimental data for the baseline engine, none of the downsized configurations were able to achieve equivalent performance. Initial response was best with the supercharger engaged, but the total time to reach the BMEP target was poor; conversely, the CVT-supercharger set up (with the same steady state drive ratio) achieved the BMEP target much sooner, but sacrificed initial

BMEP response in the process. As anticipated, settings with EGR showed worse performance – particularly in the initial response period – but compensated with reduced (by 8-13%) steady state BSFC. Driveability metrics were also considered, which indicated that the supercharger engaged arrangement (without EGR) would likely result in the greatest subjective rating – at the cost of the worst BSFC.

The entire design of experiment, parameter optimisation, and transient simulation process was completed for a further two Minimap points in order to assess the performance of the three supercharging engagement regimes from different speed and load starting points. Minimap points 14 and 9 were selected for investigation – 1250 rpm, 60 Nm (3.77 bar BMEP for the downsized engine), and 1000 rpm, 80 Nm (5.02 bar BMEP) respectively. In general, the performance trends were similar to the initial Minimap point, but performance of the CVT-driven supercharger did become more advantageous at these lower engine speeds and loads.

In summary, the trade-off situation was found to be more complex than first anticipated; identifying the best overall balance of steady state efficiency and dynamic performance requires a subjective assessment. However, the CVT does provide the best potential for dynamic response combined with satisfactory fuel economy – there would be scope to improve fuel economy further by initially disengaging the CVT-supercharger, at the expense of marginally reduced transient performance. Perhaps the most suitable solution would be to have multiple user-selectable calibrations, such as ‘economy’ and ‘sport’ modes used on many modern vehicles.

5.5.1 Further Work

Based on the boosting configurations and control schemes established in this chapter, vehicle acceleration simulations will be developed in the following chapter to enable more extensive driveability and performance analysis.

Chapter 6 Vehicle Model: In-Gear Acceleration Simulations

This chapter gives details of a vehicle model which was constructed to simulate the performance of the Ultraboost target vehicle. Logged empirical data of in-gear 'sawtooth' accelerations were used to calibrate a baseline model; this model was subsequently modified to incorporate the Ultraboost downsized engine. Simulations were performed from the respective starting points of the three supercharger engagement regimes described in Chapter 5, and the results are compared with the baseline.

6.1 Methodology

6.1.1 Empirical In-Gear Acceleration Data

In-gear acceleration data was obtained of the Ultraboost target vehicle – a luxury sports utility vehicle currently fitted with a naturally aspirated 5.0 litre V8 engine. The data was in the form of 'sawtooth' profile accelerations – accelerating from rest to a given speed, followed by a series of tip-outs and tip-ins between 0 and 100% pedal demand. Important ECU channels – such as vehicle and engine speeds, torque, and pedal demand – were recorded at a minimum 10Hz sample rate. A typical vehicle speed recording (with corresponding pedal demand) is shown in Figure 6.1.

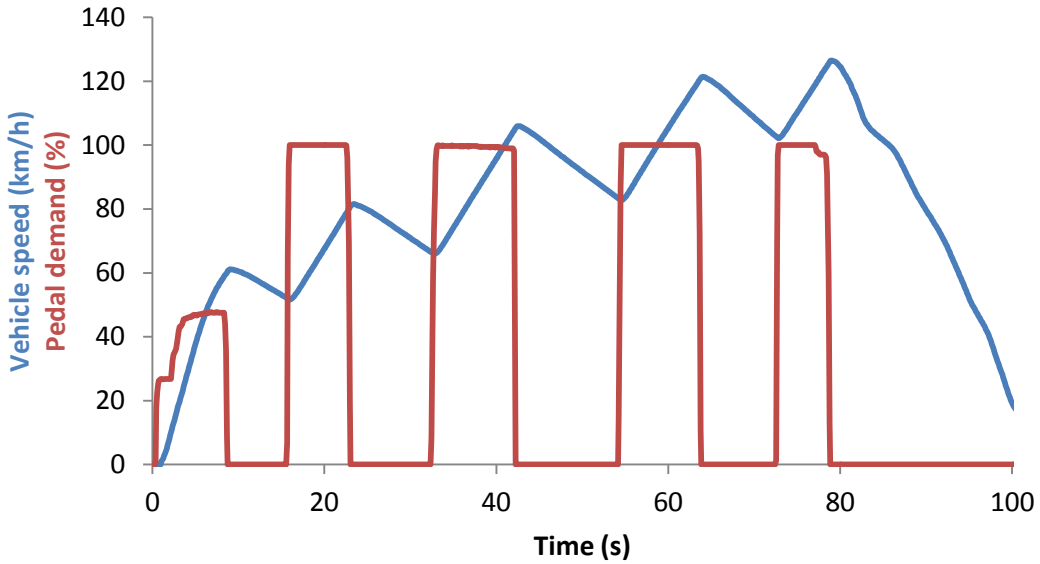

Figure 6.1 – Example 'sawtooth' acceleration profile

Since actual vehicle acceleration was not included with the data, this was calculated based on logged vehicle speed and the time step:

$$Acceleration, a_n = \frac{v_n - v_{n-1}}{t_n - t_{n-1}}$$

Equation 6.1

Data recorded in higher gears (5th and 6th gears from the 8-speed transmission) were chosen for investigation, to provide adequate durations for each period of acceleration. This was to allow sufficient time for the simulation to run; otherwise, the period of greatest interest at the beginning of the transient would be compressed and it would be difficult to distinguish between the different models and modes of

operation. Individual tip-in acceleration events in the particularly relevant lower end of the engine speed range were then extracted from the total dataset for analysis and simulation. In this way, three discrete accelerations were selected:

- 6th gear, 50→85 km/h (engine speed: 1300→2100 rpm) over approximately 8 seconds;
- 6th gear, 65→105 km/h (engine speed: 1650→2600 rpm) over approximately 9 seconds;
- 5th gear, 50→85 km/h (engine speed: 1600→2700 rpm) over approximately 6 seconds.

6.1.2 Baseline Vehicle Model

A vehicle model was constructed in GT-Power, a schematic of which is shown in Figure 6.2. Details of the individual components used in the model are given in Table 6.1. Inertias for the engine and various driveline components were scaled up from values of a typical C-segment passenger car; mechanical efficiency values were also assumed. All other vehicle and transmission attribute values reflect those of the target vehicle.

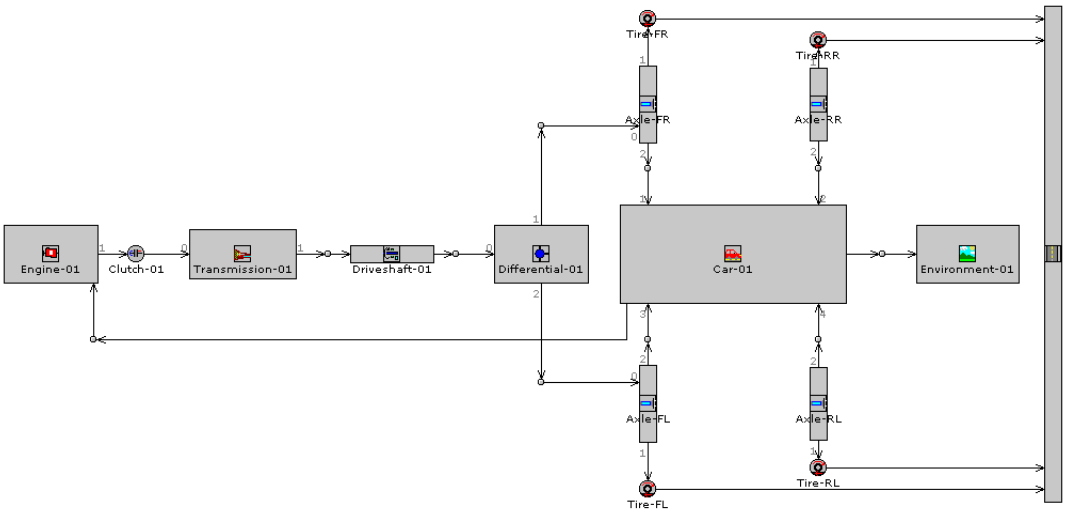

Figure 6.2 – Vehicle model schematic for the baseline engine

Table 6.1 – Baseline vehicle model component details

Component	*Attribute*	*Value*	
Vehicle	Mass	2500 kg	
	Frontal area	3.11 m^2	
	Drag coefficient	0.356	
	Wheelbase	2.88 m	
Engine	Inertia	0.4 kgm^2	
Transmission	Transmission ratios	1^{st}	4.714
		2^{nd}	3.143
		3^{rd}	2.106
		4^{th}	1.667
		5^{th}	1.285
		6^{th}	1
		7^{th}	0.839
		8^{th}	0.667
	Mechanical efficiency	97%	
	Input / output shaft inertias	0.06 kgm^2	
Driveshaft	Inertia	0.02 kgm^2	
Differential	Final drive ratio	3.55	
	Mechanical efficiency	97%	
	Input / output shaft inertias	0.02 kgm^2	
Axle	Inertia	0.2 kgm^2	
Tyre	Rolling radius	380 mm	
	Rolling resistance factor	0.025	
Environment	Ambient pressure	1 bar	
	Ambient temperature	25°C	

Engine performance was characterised using a BMEP map (for engine speed and throttle position) and a corresponding FMEP map (for engine speed and BMEP). The FMEP map was based on motored friction test data of the baseline engine installed in the engine test facilities described in Chapter 4. For the BMEP map, BMEP at WOT was from the known torque curve (shown in Figure 4.1a); at partial throttle openings BMEP was extrapolated based on the equivalent percentage

reductions of a naturally aspirated gasoline engine BMEP map provided in the GT-Power software tutorial materials (for example, BMEP at half throttle and 1000 rpm was 46% of the corresponding WOT value; at 6000 rpm and half throttle, BMEP was 37% of WOT). Since the model would only be using partial throttle openings for very short periods during the simulations, this approach was considered adequate. The resulting BMEP map is shown in Figure 6.3.

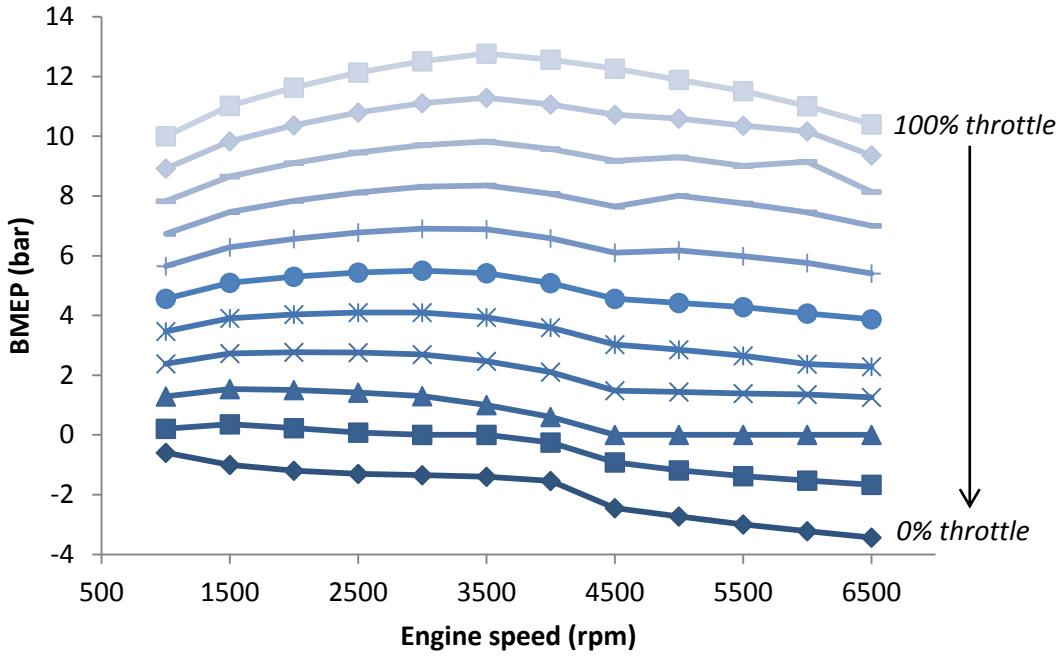

Figure 6.3 – Baseline engine BMEP map used in the vehicle model

A simple transient profile for throttle position was used as the control mechanism for the model. This baseline vehicle model was then run for the acceleration cases mentioned above. The results were compared with the empirical data, and attributes such as engine braking (i.e. BMEP at small or zero throttle openings), rolling resistance, and inertias were adjusted to calibrate the model.

6.1.3 Integration of the Ultraboost Engine

The complete engine model developed and described in Chapter 4 and Chapter 5 was imported into the vehicle model to replace the baseline engine for the three respective supercharger engagement regimes. The downsized engine was adapted to run based on a prescribed load torque, rather than the speed control of the previous simulations for which it was used. Engine inertia was assumed to be 0.25 kgm^2, based on the value of another 2.0 litre gasoline engine. Once again, the GT-

Power model was set up in co-simulation with Matlab Simulink in order to utilise the broader range of control structures that can be created in Simulink. (For a comprehensive description of the model set-up, see Section 5.1.6, the majority of which remains applicable.) The Simulink model from the previous transient simulations was adapted for the new vehicle simulations, with the only significant modifications being to the BMEP and intake manifold pressure target lookup tables, changing to engine speed as the input rather than simply using the simulation time as before. This was to ensure WOT throttle performance was achieved where possible during the transient.

As before, the simulation was set to run for four seconds prior to the tip-in to allow the model to achieve an initial steady state. However, unlike the constant part-load BMEP of the previous simulations, in this instance the vehicle was decelerating under engine braking (closed throttle) in this initial period in order to reproduce the sawtooth profile. Hence, the fuel injection control system was adapted to run at an extremely lean AFR of 250 (approx. lambda 17) in the initial four second period – this reflects the closed-throttle lambda values of the empirical data. The turbocharger wastegate and supercharger bypass valve were also set to fully open (apart from the supercharger disengaged regime, where the supercharger bypass valve was fully closed) to minimise BMEP and thus aid engine braking. At the start of the tip-in, the duration of the 'step' in throttle position and other engine control parameters was increased to 0.3 seconds (from the previous 0.15 seconds) to be consistent with the delay seen in the empirical data. During the transient the supercharger bypass valve and turbocharger wastegate were again used as the load control mechanism, with the throttle set to fully open.

One particular outcome of running at closed throttle in the initial period was that the simulations running EGR produced the same results as the equivalent non-EGR configurations, since negligible EGR flow is produced under these conditions. Hence, only non-EGR simulation results are considered below.

6.2 Simulation Results

6.2.1 Baseline Model Calibration

Figure 6.4 shows the baseline vehicle model results for the 6th gear acceleration from 50 to 85 km/h compared with the equivalent empirical data. The simulated vehicle speed trace clearly fits the data very well, throughout both the closed throttle and WOT sections of the transient. This suggests that the inertias, rolling resistance, and engine braking aspects of the model as a whole are reasonably accurate (the values of these attributes were calibrated to fit the model to the data), as well as the engine performance itself. Likewise, the engine speed trace matches the data well, although the slight torque converter slip displayed in the first 0.4 seconds of the tip-in is not included in the model. The acceleration data fluctuates to some degree (due to noise in the recorded vehicle speed channel from which it is calculated), but the simulation fits well to an approximate average of the data.

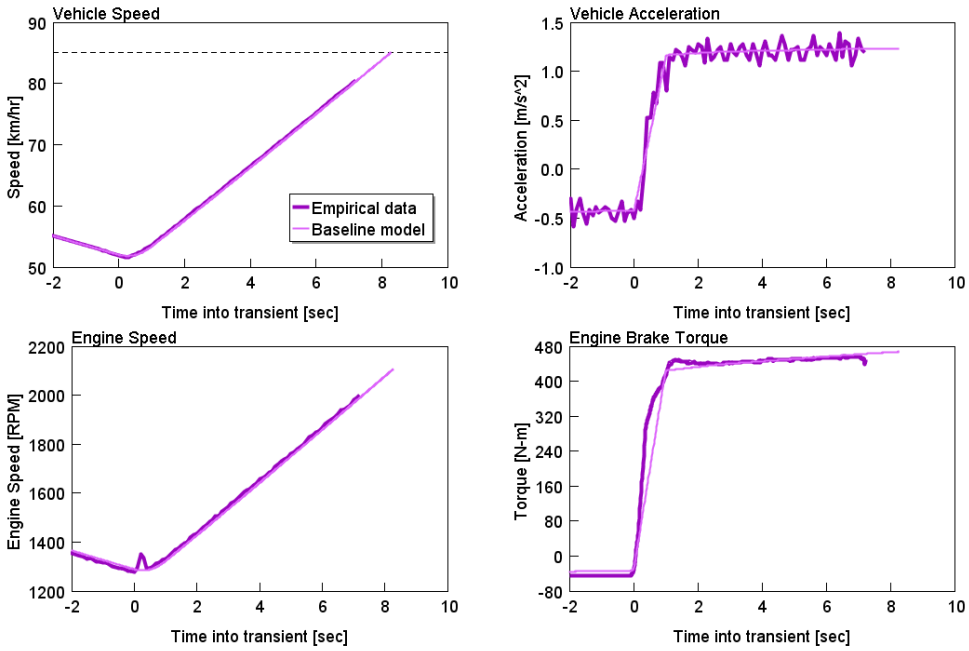

Figure 6.4 – Comparison of baseline vehicle model and empirical data for 6th gear acceleration (50→85 km/h) – a) vehicle speed; b) vehicle acceleration; c) engine speed; d) engine brake torque

The modelled engine torque gives an acceptable fit to the recorded data. The effect of the temporarily increased engine speed due to the aforementioned torque converter slip (as well as some transient fuelling effects) is shown in the margin

between the modelled and empirical data in the initial stages of the transient. The model also produces somewhat reduced engine braking in comparison with the empirical data (~25% less), but as already discussed with regards to the vehicle speed trace, the overall vehicle drag is representative.

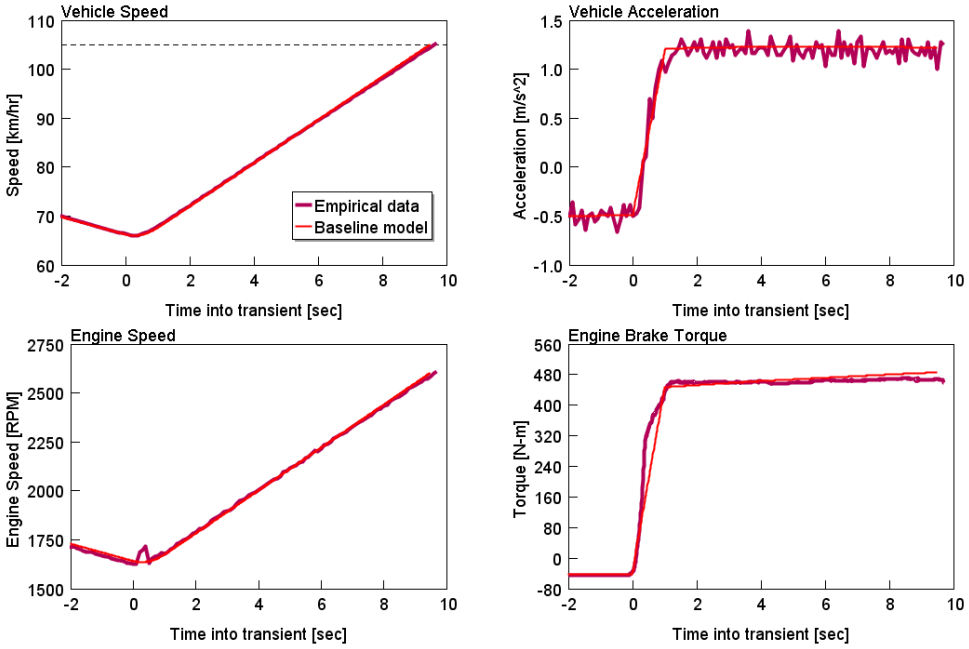

Figure 6.5 – Comparison of baseline vehicle model and empirical data for 6th gear acceleration (65→105 km/h) – a) vehicle speed; b) vehicle acceleration; c) engine speed; d) engine brake torque

Considering the equivalent results for the 6th gear acceleration from 65 to 105 km/h, again the model fits very well to the empirical data, as Figure 6.5 shows. In this case, engine braking (i.e. negative torque prior to the tip-in) is better matched than before; this certainly has no detrimental effect, as the overall accuracy of vehicle speed and engine speed traces in the initial period of deceleration remains. After two seconds into the transient the modelled engine torque increases at a higher rate than the logged data. This is reflected in a marginally higher rate of acceleration in the model, which, although difficult to discern from the noisy acceleration data, is visible in the vehicle and engine speed traces (particularly after the six second mark). However, these differences are only marginal, and the overall fit to the data is acceptable.

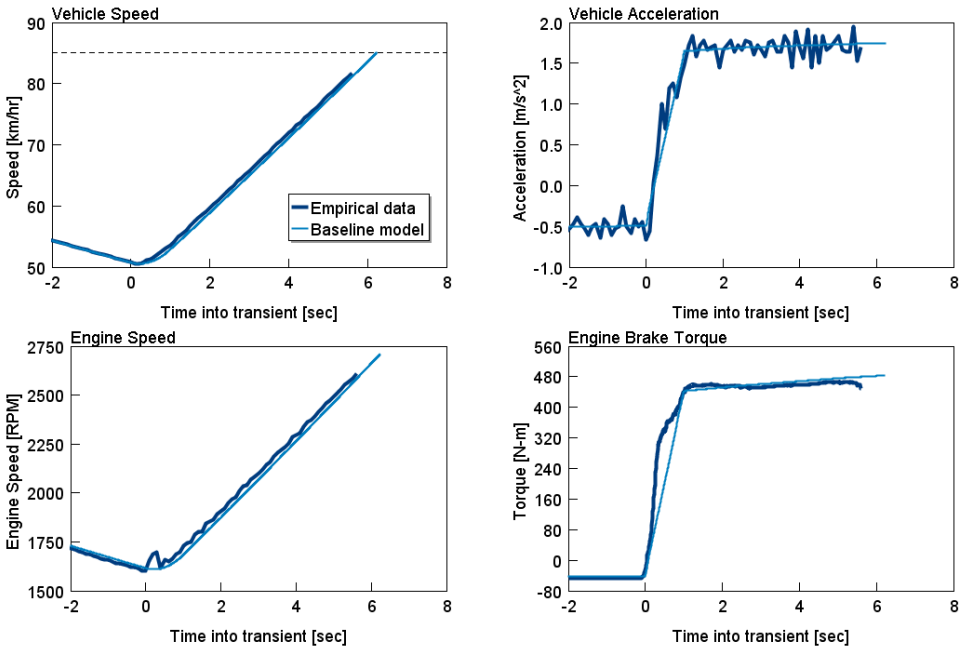

Figure 6.6 – Comparison of baseline vehicle model and empirical data for 5th gear acceleration (50→85 km/h) – a) vehicle speed; b) vehicle acceleration; c) engine speed; d) engine brake torque

The results for the 5th gear acceleration from 50 to 85 km/h are shown in Figure 6.6. On the whole, the fit of the model results to the data is again fairly good. There is a noticeable lag in modelled response at the start of the tip-in in this case, indicated clearly by the gap between the engine speed traces. However, ignoring this lag, the rate of acceleration is consistent with the logged data; and since the same behaviour will also be carried across to the vehicle models with the downsized engine, this was not considered to be a problem for the subsequent comparative performance investigation.

To summarise this section, the baseline vehicle model was considered to be more than adequate as a basis for the Ultraboost vehicle acceleration simulations.

6.2.2 Ultraboost Vehicle Acceleration Results

Figure 6.7 shows the simulation results for the 6th gear acceleration from 50 to 85 km/h for each of the supercharger engagement regimes previously investigated; as before, for the CVT-supercharger, initial drive ratios of 2:1 and 5.9:1 are both considered. As would be expected, the supercharger disengaged regime produces the worst performance, as the delay in clutching-in and then accelerating the supercharger result in a corresponding delay in engine torque produced (Figure

6.7d). The supercharger engaged regime and the CVT-supercharger starting from the higher drive ratio achieve the target vehicle speed at almost the same time; but, (as with the tip-ins previously considered in Chapter 5) the way they achieve the result differs considerably. The supercharger engaged regime produces a larger initial torque (and acceleration), but once the supercharger has achieved its maximum pressure ratio, the remaining performance is dependent on the slow turbocharger response – hence the doglegged torque curve. On the other hand, the model with CVT-supercharger has a delayed torque response, as significantly more torque is required to accelerate the supercharger up to high speeds; the pay-off is achieving peak torque much sooner, as it is no longer dependent on turbocharger performance. Perhaps unsurprisingly, the performance of the CVT-supercharger model starting from the lower initial drive ratio falls somewhere between higher ratio CVT-supercharger and supercharger disengaged regimes. These trends largely reflect those exhibited in the previous fixed speed tip-ins considered in Chapter 5.

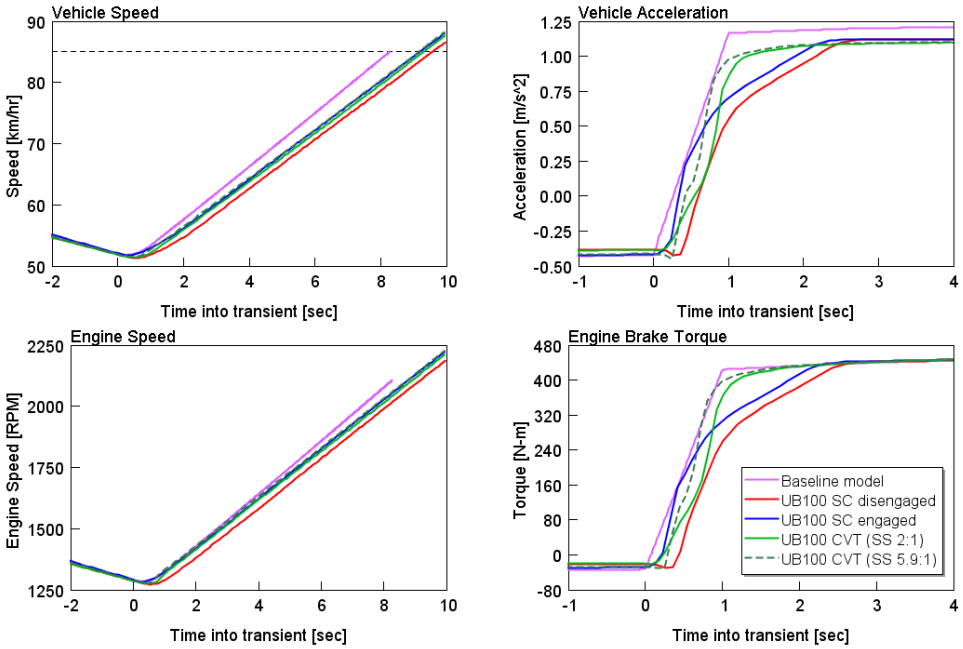

Figure 6.7 – Vehicle acceleration simulation results for 6th gear acceleration (50→85 km/h) – a) vehicle speed; b) vehicle acceleration; c) engine speed; d) engine brake torque (zoomed-in time scale for acceleration and torque)

Considering the time taken by each of the models to achieve the target vehicle speed, times varied between 9.2 and 9.6 seconds (CVT-supercharger with 5.9:1 initial ratio and supercharger disengaged regimes, respectively), compared with the baseline of 8.3 seconds. Converting these times to percentages with respect to the

baseline, this range represents an 11% to 16% lag – as represented by the left-hand dataset in Figure 6.8.

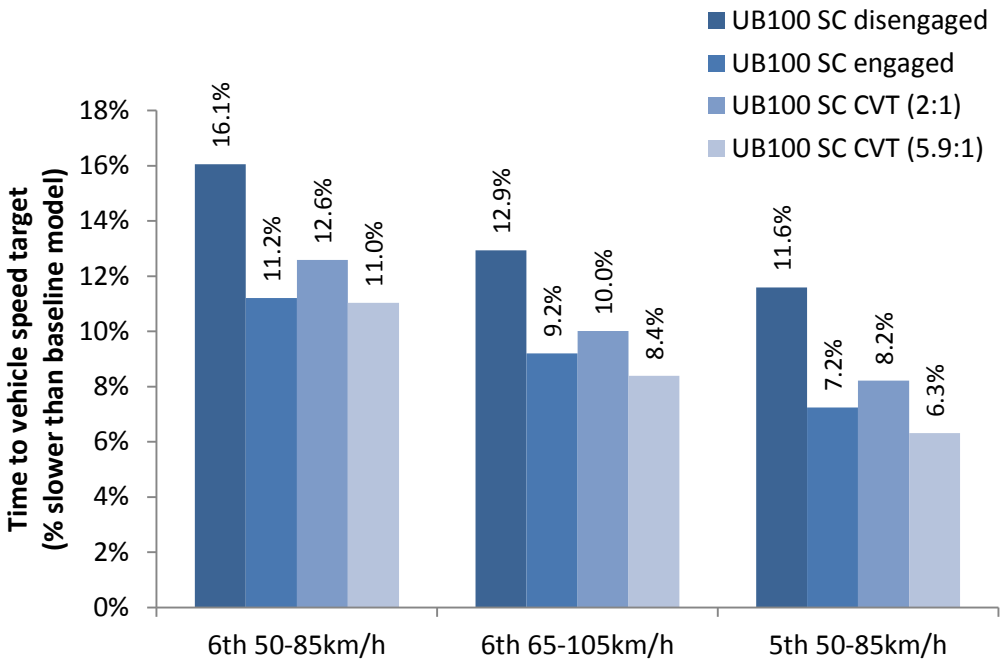

Figure 6.8 – Summary of vehicle acceleration results – delay to reach vehicle speed target of various downsized engine configurations compared with baseline model

The trends identified in the results for the 6th gear acceleration reviewed above are also evident in the additional accelerations (6th gear 65→105 km/h, and 5th gear 50→85 km/h), as can be seen in Figure 6.9 and Figure 6.10. However, as a result of the higher engine speeds from which these tip-ins commence, peak torque was attained earlier for all of the supercharger engagement regimes (Figure 6.9d and Figure 6.10d, compared with Figure 6.7d). This in turn resulted in reduced delays in achieving the respective target vehicle speeds – as shown in Figure 6.8. Nevertheless, the hierarchy of performance remained the same for each of the acceleration cases – the supercharger disengaged regime producing the worst response, and the CVT-supercharger with 5.9:1 initial drive ratio the best.

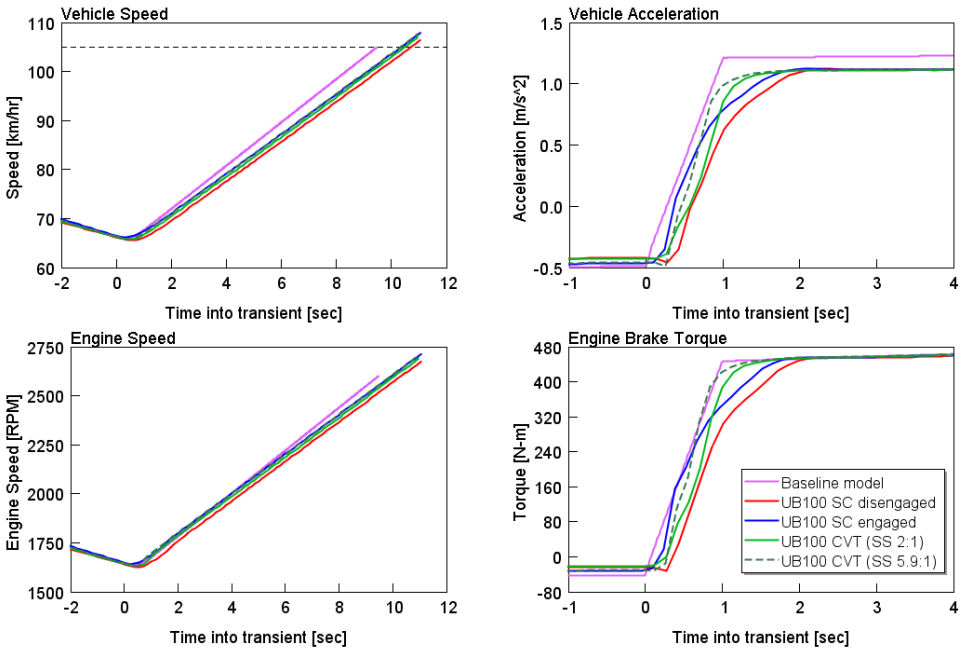

Figure 6.9 – Vehicle acceleration simulation results for 6th gear acceleration (65→105 km/h) – a) vehicle speed; b) vehicle acceleration; c) engine speed; d) engine brake torque (zoomed-in time scale for acceleration and torque)

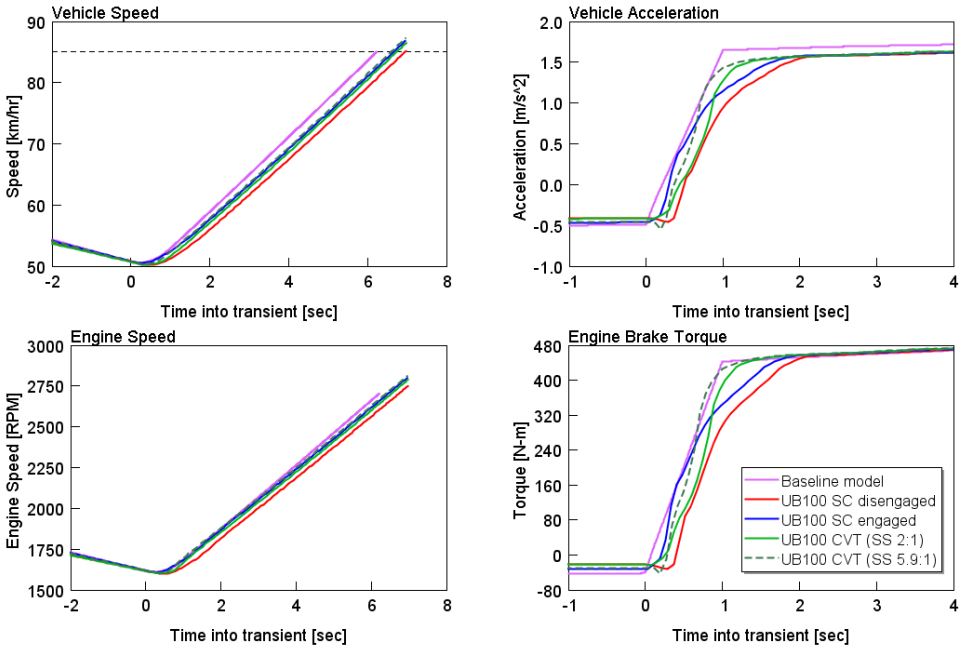

Figure 6.10 – Vehicle acceleration simulation results for 5th gear acceleration (50→85 km/h) – a) vehicle speed; b) vehicle acceleration; c) engine speed; d) engine brake torque (zoomed-in time scale for acceleration and torque)

In order to improve overall acceleration performance, there could be potential to incorporate a temporary 'over-boost' function into the control scheme for the

downsized engine – temporarily allowing higher boost pressure than the normal WOT conditions, thus increasing engine output over the baseline torque curve. Although the boosting system already operates at 2.7-3 bar absolute manifold pressure during the accelerations, it may be feasible to exceed this for short periods. This is particularly applicable to the CVT-supercharger arrangement, where normal peak torque is achieved early on during the transients, and turbocharger performance especially is limited to prevent excess boost pressure. The normal fixed supercharger drive ratio set-up would be less suitable for including this over-boost function, as peak torque (and thus the boost limit) is reached significantly later during the transients, especially at lower engine speeds.

Although fuel efficiency has not been included in the present analysis, it can be assumed that similar trends as exhibited in the tip-ins performed in Chapter 5 would also apply in these cases. Hence, the engagement regimes that produced the fastest response times (i.e. supercharger engaged and CVT-supercharger with high initial drive ratio) would be at the expense of fuel efficiency. As previously suggested, the best solution may be to have multiple calibrations available to be selected by the end user; to this end, it can be argued that the CVT-supercharger would provide the greatest flexibility for calibration for different combinations of fuel economy and performance.

6.3 Conclusions

A vehicle model was constructed based on the Ultraboost target vehicle, for the purpose of simulating in-gear accelerations. Empirical data was used to accurately calibrate and also validate the model. Three distinct tip-in acceleration events were then selected from the logged data for simulation and analysis: 6th gear, 50 to 85 km/h; 6th gear, 65 to 105 km/h; 5th gear, 50 to 85 km/h. The vehicle model was subsequently modified to incorporate the Ultraboost downsized engine model, and these acceleration events were then simulated for the three supercharger engagement regimes previously established in Chapter 5: with the supercharger disengaged at the start of the tip-in and then clutched-in; with the supercharger engaged; and with the supercharger drive through a variable transmission (i.e. CVT), at both low and high initial drive ratios. (Only non-EGR calibrations were assessed, due to the throttle being closed in the initial period prior to the tip-ins.)

Similar torque response trends as seen in Chapter 5 were again exhibited for the different supercharger engagement regimes, producing a consistent hierarchy of performance and results across the different acceleration cases. The CVT-supercharger with high initial drive ratio and the supercharger engaged regimes produced the best performance, with the lowest delay times to the respective vehicle speed targets (compared with the baseline model). However, it is expected that this performance would be at the cost of fuel efficiency – in accordance with the relationships shown in Chapter 5. Again, it is suggested that the CVT-supercharger provides the best flexibility for calibration and compromise between performance and fuel efficiency, perhaps to incorporate different user-selectable modes (such as ‘economy’ and ‘sport’ modes). There may even be potential to include an ‘over-boost’ facility, allowing boost pressure to temporarily exceed normal steady state limits in order to improve transient performance. This is particularly applicable to the CVT-supercharger set-up, where the boost limit is reached at an early stage during the transients, and as a consequence the development of turbocharger boost is especially restricted.

Chapter 7 Overall Conclusions

The final conclusions of this thesis are discussed with reference to the project objectives laid out in Chapter 1.

1. *To undertake an extensive review of current literature and research on the subject of engine boosting and exhaust energy recovery systems in the area of downsizing for passenger car engines; to consider how developing CVT technology may be applied to this field in order to maximise fuel efficiency, and thereby reduce emissions of CO2 and other pollutants.*

Chapter 2 presented a literature review on the subject of engine downsizing for passenger car engines. Focus was particularly placed on different pressure charging ('boosting') systems and their developments. The following factors were established as critical for a pressure charged and downsized engine to be effective:

- Increased specific power;
- Transient performance as close to a naturally aspirated characteristic as possible;
- Improved part load BSFC.

Various turbocharging systems and configurations were considered, including VGTs and several arrangements with multiple turbochargers. Compared with conventional turbocharging, most of these systems offered improved specific engine power and fuel efficiency, and faster transient response. Nevertheless, a number of authors maintain that the low speed torque and transient response of such systems is ultimately limited by the available exhaust gas energy, and these problems are compounded in highly boosted (i.e. highly downsized) applications [12][21][35][67]. Mechanical supercharging avoids both of these drawbacks, but is considerably less efficient than turbocharging due to the parasitic power losses incurred. Proponents of supercharging, however, argue that it provides positive pumping work, whereas

turbocharging incurs pumping losses due to the exhaust backpressure caused by the turbine – thus turbocharging is not 'free' energy recovery [50][51].

Combined charging systems, featuring both a declutchable supercharger and a turbocharger, were found to offer the transient response and low speed torque of supercharging with the overall efficiency and part load flexibility of turbocharging. Driving the supercharger through a CVT would offer greater flexibility of operation.

Electrical boosting systems – namely electrically driven compressors (EDCs) and electrically assisted turbochargers (EATs) – were also explored. Combined charging systems involving an electrically driven compressor in place of the mechanical supercharger have been investigated by some authors, yielding similar performance benefits. It was proposed, however, that a mechanical arrangement has significant advantages over electrical boosting systems, as the latter are generally limited by issues such as electrical heating and battery depletion, or require upgrading of the standard vehicle electrical architecture.

A number of turbocompounding arrangements, both mechanical and electrical, were considered. The general consensus of the authors is that turbocompounding is viable only for applications which operate consistently at high load [76], as the potential for energy recovery at low speed and load is minimal. Correspondingly, Baines [32] asserts that turbocompounding 'is not really suitable for application to passenger car engines, for example, which spend most of their time at part load'.

In line with the criteria listed above, a combined charging system with the supercharger driven through a CVT was the arrangement selected for further investigation.

2. *To conduct extensive simulations of the chosen system to assess it against three key performance criteria for downsized engines: Low-speed torque; Part-load fuel efficiency; Transient performance.*

Chapter 3 presents results of an initial investigation into the potential for augmentation of the low speed torque of a VGT-equipped high speed diesel engine by employing the chosen compound charging system (a combination of CVT driven supercharger and fixed geometry turbocharger). Peak torque was somewhat

increased, but more importantly up to 90% of the peak value was available at 1000 rpm, compared with 50% for the baseline engine. Fixed speed tip-in performance (at low engine speeds) was also greatly improved over the baseline. Rated power, however, was unchanged, mainly due to the inefficient turbomachinery used in the simulations.

In Chapter 4 shifts the focus to gasoline engines, introducing the Ultraboost project and its downsizing objectives – replacing a 5.0 litre naturally aspirated V8 with a 2.0 litre in-line four cylinder highly boosted engine. The Ultraboost engine features a combined charging system: a fixed geometry turbocharger in a sequential series arrangement with a positive displacement supercharger; the supercharger can be declutched and bypassed depending on engine speed and load. The overall aim of this particular downsizing project is a 35% reduction in fuel consumption (and corresponding reduction in CO_2) over the New European Drive Cycle (NEDC).

Chapter 5 gives details of a co-simulation based investigation into the trade-off between steady state part load fuel efficiency and resulting tip-in transient response for the Ultraboost engine. Three separate supercharger engagement regimes were investigated for part load operation – defined as: with the supercharger disengaged and bypassed; with the supercharger engaged with a fixed drive ratio; with the supercharger engaged using a variable ratio (i.e. through a CVT). Three distinct part load operating points were chosen for investigation (each representing a significant portion of the NEDC); for each point, design of experiments and optimisation techniques were used to find the best settings for the various engine control parameters. Of these parameters, target EGR rate was found to have the largest independent effect on BSFC – increasing the EGR target was found to cause an almost linear reduction in BSFC. However, it was expected that the level of residual gases present would have a large effect on tip-in performance; hence for each supercharger engagement regime, two modes of operation (zero EGR and maximum achievable EGR) were taken forward for evaluation in the transient simulations.

Using each of the six part load calibrations, a fixed speed tip-in transient was performed, demanding full load with the step taking place over 0.15 seconds. For this, a control scheme was developed whereby the throttle was set to fully open at the start of the tip-in and engine air flow and load were controlled by the

supercharger bypass valve and turbocharger wastegate. As anticipated, settings with EGR showed worse performance – particularly in the initial response period – but compensated with reduced steady state BSFC. On the whole, the trade-off situation was found to be more complex than first anticipated; identifying the best overall balance of steady state efficiency and dynamic performance required a subjective assessment. However, the CVT did provide the best potential for dynamic response combined with satisfactory fuel economy. Perhaps the most suitable solution would be to have multiple user-selectable calibrations, such as 'economy' and 'sport' modes used on many modern vehicles.

In Chapter 6 a vehicle model was developed based on the Ultraboost target vehicle, for the purpose of simulating in-gear accelerations. Three distinct tip-in acceleration events were selected simulation, using as a starting point the three supercharger engagement regimes previously established in Chapter 5. Similar torque response trends as seen in Chapter 5 were again exhibited for the different supercharger engagement regimes, producing a consistent hierarchy of performance and results across the different acceleration cases. The CVT-supercharger with high initial drive ratio and the supercharger engaged regimes produced the best performance, with the lowest delay times to the respective vehicle speed targets (compared with the baseline model). However, it is expected that this performance would be at the cost of fuel efficiency – in accordance with the relationships shown in Chapter 5. Again, it is suggested that the CVT-supercharger provides the best flexibility for calibration and compromise between performance and fuel efficiency, perhaps to incorporate different user-selectable modes (such as 'economy' and 'sport' modes). There may even be potential to include an 'over-boost' facility, allowing boost pressure to temporarily exceed normal steady state limits in order to improve transient performance. This is particularly applicable to the CVT-supercharger set-up, where the boost limit is reached at an early stage during the transients, and as a consequence the development of turbocharger boost is especially restricted.

3. *To evaluate model validity and simulation accuracy against relevant empirical data, where this was possible.*

In Chapter 4 details are given of the engine testing facilities at the University of Bath and the instrumentation and data acquisition methods used to collect performance data from a prototype of the Ultraboost engine. The GT-Power model of the

Ultraboost engine was then compared with and validated against this empirically recorded data. For the three part load operating points considered, simulation results generally closely matched the empirical data for the significant bulk flow parameters that were assessed – such as torque, air mass flow rate, and intake and exhaust pressures and temperatures. The exceptions to this were the tendency of the model to over-predict the required intake manifold pressure, and under-predict the resulting BSFC. However, these discrepancies were within acceptable margins of error, and were taken into account in interpreting subsequent simulation results. For the full load points that were compared, torque, air mass flow, and fuel flow results showed a generally adequate fit, but intake and exhaust manifold pressures were significantly over-predicted in simulation. Comparing cylinder pressure data revealed that this was due to the assumptions made in defining the combustion model producing conservative results, in terms of both timing and magnitude of peak cylinder pressures. This was in contrast to the tendency of the model to under-predict BSFC. Again, these trends were taken into account in the analysis and interpreting of subsequent simulation results.

In Chapter 6 logged empirical data of in-gear ‘sawtooth’ accelerations were used to accurately calibrate and validate the baseline vehicle model. Three distinct tip-in acceleration events which were selected from the logged data for simulation and analysis were used in this process.

7.1 Suggestions for Further Work

Suggestions of projects that would merit further investigation based on the results presented in this thesis:

- The initial diesel engine investigation described in Chapter 3 could be extended to consider commercially available turbomachinery, with the intention of increasing power density. This would allow equivalent comparison with larger, more powerful diesel engines that are currently available, and thus part load fuel efficiency benefits related to using this novel boosting system could also be assessed.

- Engine testing with the actual boosting hardware installed on the Ultraboost engine, rather than using the CAHU, would improve the opportunities for model calibration. The boosting hardware would also allow representative transient tests to be performed, enabling validation of the transient tip-in simulations considered in Chapter 5 and Chapter 6.

- The combustion model used for the Ultraboost simulations (discussed in Chapter 4) could be improved based on the data obtained from the engine testing work. This would increase confidence in the engine model as a whole, and the simulation results produced.

- A significant step forward would be to produce a prototype of the CVT-supercharger, either using a centrifugal compressor as in Chapter 3 or a positive displacement supercharger as used on the Ultraboost project (Chapter 4 to Chapter 6). Since the CVT specification has largely been kept arbitrary throughout this research, the different CVT options that are available (such as listed in Chapter 3) should be explored. Control schemes and packaging considerations could be investigated, as well as the financial implications of adopting this technology. A prototype would also provide major opportunities for performance testing and validation of the results of this research.

- The influence of clutch slip while engaging the supercharger, with particular consideration for its impact on vehicle driveability.

References

[1] **ECOpoint Inc.** *European Union Emissions Standards for Cars and Light Trucks* [online], 2012. Available from: http://www.dieselnet.com/standards/eu/ld.php [Accessed 17 May 2013].

[2] **HM Government.** *Vehicle tax rate tables – Cars registered on or after 1 March 2001* [online], 2013. Available from: https://www.gov.uk/vehicle-tax-rate-tables [Accessed 17 May 2013].

[3] **European Commission.** *Setting emission performance standards for new passenger cars as part of the Community's integrated approach to reduce CO2 emissions from light-duty vehicles*. Regulation (EC) No 443/2009, 2009.

[4] **United States Environmental Protection Agency.** *EPA and NHTSA Finalize Historic National Program to Reduce Greenhouse Gases and Improve Fuel Economy for Cars and Trucks*. Regulatory Announcement EPA-420-F-10-014, 2010.

[5] **European Communities.** *Commission proposal to limit the CO2 emissions from cars to help fight climate change, reduce fuel costs and increase European competitiveness.* EUROPA press release IP/07/1965, 2007.

[6] **Ronning, J.J.** and **Grant, G.L.** Global Hybrid Electric Vehicle Markets and Missions. SAE paper 1999-01-2946, 1999.

[7] **Brockbank, C.** and **Greenwood, C.** Fuel Economy Benefits of a Flywheel & CVT Based Mechanical Hybrid for City Bus and Commercial Vehicle Applications. SAE paper 2009-01-2868.

[8] **Kepner, R.P.** Hydraulic Power Assist – A Demonstration of Hydraulic Hybrid Vehicle Regenerative Braking in a Road Vehicle Application. SAE paper 2002-01-3128, 2002.

[9] **Nissan Motor Company.** *Nissan Unveils "Leaf" – The World's First Electric Car Designed for Affordability and Real-World Requirements* [online], 2009. Available from: http://www.nissan-global.com/EN/NEWS/2009/_STORY/090802-02-e.html [Accessed 7 February 2011].

[10] **Truckenbrodt, A.** Fuel Cell Vehicles for Future Car Concepts. SAE paper 2004-21-0081, 2004.

[11] **Aoyama, T., Iiyama, A., Shinohara, K., Kamegaya, S., Yamamoto, S.** and **Ban, Y.** Status of FCV Development at Nissan and Future Issues. SAE paper 2008-01-0423, 2008.

[12] **Hancock, R., Fraser, N., Jeremy, M., Sykes, R.** and **Blaxill, H.** A New 3 Cylinder 1.2l Advanced Downsizing Technology Demonstrator Engine. SAE paper 2008-01-0611, 2008.

[13] **Whitworth, B.** Doppelgänger. *Automotive Engineer*, May 2006, pp. 37-38 (Professional Engineering Publishing, London).

[14] **Luttermann, C.** and **Mährle, W.** BMW High Precision Fuel Injection in Conjunction with Twin-Turbo Technology: a Combination for Maximum Dynamic and High Fuel Efficiency. SAE paper 2007-01-1560, 2007.

[15] **Ford Motor Company.** *New High Efficiency Four-Cylinder Ford Ecoboost Engine Family Debuts at Frankfurt* [online], 2009. Available from: http://media.ford.com/news/newhighefficiencyfourcylinderfordecoboostenginefamilydebutsatfrankfurt.htm [Accessed 11 January 2011].

[16] **Mercedes-AMG GmbH.** *The AMG 5.5-Liter V8 Biturbo* [online], 2010. Available from: http://www.mercedes-amg.com/#/157v8 [Accessed 11 January 2011].

[17] **The Automotive Council.** *Automotive Technology Roadmaps* [online], 2013. Available from: http://www.automotivecouncil.co.uk/2013/09/automotive-technology-roadmaps/ [Accessed 14 November 2013].

[18] **Thirouard, M., Mendez, S., Pacaud, P., Chmielarczyk, V., Ambrazas, D, Garsi, C., Lavoisier, F.** and **Barbeau, B.** Potential to Improve Specific Power Using Very High Injection Pressure in HSDI Diesel Engines. SAE paper 2009-01-1524, 2009.

[19] **Petitjean, D., Bernardini, L., Middlemass, C.** and **Shahed, S.M.** Advanced Gasoline Engine Turbocharging Technology for Fuel Economy Improvements. SAE paper 2004-01-0988, 2004.

[20] **Kleeberg, H., Tomazic, D., Lang, O.** and **Habermann, K.** Future Potential and Development Methods for High Output Turbocharged Direct Injected Gasoline Engines. SAE paper 2006-01-0046, 2006.

[21] **Wijetunge, R., Criddle, M., Dixon, J.** and **Morris, G.** Comparative Performance of Boosting Systems for a High Output, Small Capacity Diesel Engine. STA paper F2004F195, 2004.

[22] **Chadwell, C.J.** and **Walls, M.** Analysis of a SuperTurbocharged Downsized Engine Using 1-D CFD Simulation. SAE paper 2010-01-1231, 2010.

[23] **Turner, J.W.G., Pearson, R.J.** and **Kenchington, S.A.** Concepts for improved fuel economy from gasoline engines. *International Journal of Engine Research*, 2005, **6**(2), 137-157.

[24] **Alfa Romeo.** *Alfa Romeo Technology Innovation: 1750i 200 bhp Turbo Petrol Engine* [online], 2010. Available from: http://www.alfaromeo.co.uk/uk/cmsen/models/alfa_159/pages/alfa-159-motori.aspx?outputXml=true&CustomResponse=WebCrawler [Accessed 14 January 2011].

[25] **Fiat Powertrain Technologies S.p.A.** *MultiAir: The Ultimate Air Management Strategy* [online], 2009. Available from: http://www.fptmultiair.com/flash_multiair_eng/Cartella%20Stampa%20ENG%20def%20_3_.pdf [Accessed 14 January 2011].

[26] **King, J., Schmidt, L., Stokes, J., Seabrook, J., Nor, F.** and **Sahadan, S.** Multiple injection and boosting benefits for improved fuel consumption on a Spray Guided Direct Injection gasoline engine. In *FISITA 2012 World Automotive Congress*, Beijing, China, 27-30 November 2012, paper F2012-A01-041 (FISITA, UK).

[27] **Roberts, M.** Benefits and Challenges of Variable Compression Ratio (VCR). SAE paper 2003-01-0398, 2003.

[28] **Kleeberg, H., Tomazic, D., Dohmen, J., Wittek, K.** and **Balazs, A.** Increasing Efficiency in Gasoline Powertrains with a Two-Stage Variable Compression Ratio (VCR) System. SAE paper 2013-01-0288, 2013.

[29] **Heywood, J.B.** *Internal Combustion Engine Fundamentals*, 1988 (McGraw-Hill, New York).

[30] **Watson, N.** and **Janota, M.S.** *Turbocharging the Internal Combustion Engine*, 1982 (Macmillan Publishers Ltd, Basingstoke).

[31] **Stobart, R.** and **Weerasinghe, R.** Heat Recovery and Bottoming Cycles for SI and CI Engines – A Perspective. SAE paper 2006-01-0662, 2006.

[32] **Baines, N.C.** *Fundamentals of Turbocharging*, 2005 (Concepts NREC, Vermont).

[33] **Arnold, S.** Single Sequential Turbocharger: A New Boosting Concept for Ultra-Low Emission Diesel Engines. SAE paper 2008-01-0298, 2008.

[34] **Schmitz, T., Holloh, K., Juergens, R.** and **Fleckenstein, G.** Potential of Additional Supercharging for Commercial Vehicle Engines. SAE paper 942268, 1994.

[35] **Matsura, Y., Nakazawa, N., Kobayashi, Y., Ogita, H.** and **Kawatani, T.** Effects of Various Methods for Improving Vehicle Startability and Transient Response of Turbocharged Diesel Trucks. SAE paper 920044, 1992.

[36] **Timoney, S.G.** A Review of Ideas for Improving Transient Response in Vehicle Diesel Engines. SAE paper 860454, 1986.

[37] **Hishikawa, A., Okazaki, Y.** and **Busch, P.** Developments of variable area radial turbines for small turbochargers. SAE paper 880120, 1988.

[38] **Kawamoto, A., Takahashi, Y., Koike, T.** and **Nakamura, F.** Variable Geometry System Turbocharger for Passenger Car Diesel Engine. SAE paper 2001-01-0273, 2001.

[39] **Hawley, J.G., Wallace, F.J., Cox, A., Horrocks, R.W.** and **Bird, G.L.** Variable geometry turbocharging for lower emissions and improved torque characteristics. *Proceedings of the Institution of Mechanical Engineers, Part D: Journal of Automobile Engineering*, 1999, **213**(2), 145-159.

[40] **Pflüger, F.** Regulated two-stage turbocharging – KKK's new charging system for commercial diesel engines. In Sixth International Conference on *Turbocharging and Air Management Systems*, London, UK, 3-5 November 1998, paper C554/035/98, pp. 127-141 (Professional Engineering Publishing, London).

[41] **Saulnier, S.** and **Guilain, S.** Computational Study of Diesel Engine Downsizing Using Two-Stage Turbocharging. SAE paper 2004-01-0929, 2004.

[42] **Luttermann, C.** and **Mährle, W.** BMW High Precision Fuel Injection in Conjunction with Twin-Turbo Technology: a Combination for Maximum Dynamic and High Fuel Efficiency. SAE paper 2007-01-1560, 2007.

[43] **Sommerhoff, F.A.** Analysis of a twin turbocharger and a single turbocharger concept on a HSDI V6 diesel engine applying engine cycle simulation. In Seventh International Conference on *Turbochargers and Turbocharging*, London, UK, 14-15 May 2002, paper C602/033/2002, pp. 235-245 (Professional Engineering Publishing, London).

[44] **Tashima, S., Taqdokoro, T., Okimoto, H.** and **Niwa, Y.** Development of Sequential Twin Turbo System for Rotary Engine. SAE paper 910624, 1991.

[45] **Brüstle, C., Wagner, J., Tran Van, K.** and **Burk, K.** Turbocharging techniques for sports car engines. In Fourth International Conference on *Turbocharging and Turbochargers*, London, UK, 22-24 May 1990, paper C405/055, pp. 317-328 (Professional Engineering Publishing, London).

[46] **Gyarmathy, G.** How does the Comprex pressure wave supercharger work? SAE paper 830234, 1983.

[47] **Schwarzbauer, G.E.** Turbocharging of tractor engines with exhaust gas turbochargers and the BBC-Comprex. In International Conference on *Turbocharging and Turbochargers*, London, UK, 18-20 April 1978, paper C69/78, pp. 161-164 (Professional Engineering Publishing, London).

[48] **Summerauer, I., Spinnler, F., Mayer, A.** and **Hafner, A.** A comparative study of the acceleration performance of a truck diesel engine with exhaust-gas turbocharger and with pressure-wave supercharger Comprex. In International Conference on *Turbocharging and Turbochargers*, London, UK, 18-20 April 1978, paper C70/78, pp. 165-173 (Professional Engineering Publishing, London).

[49] **Wallace, F.J.** and **Aldis, C.A.** Comprex supercharging versus turbocharging of a large truck diesel engine. In Second International Conference on *Turbocharging and Turbochargers*, London, UK, 26-28 April 1982, paper C39/82, pp. 89-99 (Professional Engineering Publishing, London).

[50] **Bhinder, F.S.** Supercharging Compressors – Problems and Potential of the Various Alternatives. SAE paper 840243, 1984.

[51] **Stone, R.** Exploitation of Full-Toroidal CVT Technology to a Centrifugal Supercharger for Radical Engine Downsizing Applications. In Ninth International Symposium on *Innovative Automotive Transmissions and Hybrid & Electric Drives*, Berlin, Germany, 29 November – 2 December 2010, (Car Training Institute, Düsseldorf).

[52] **Stone, C.R.** The efficiency of Roots compressors and compressors with fixed internal compression. *Proceedings of the Institution of Mechanical Engineers, Part A: Power and Process Engineering*, 1988, **202**(A3), 199-205.

[53] **Eaton Corporation.** *TVS Roots-Type Superchargers*, [online], 2011. Available from: http://www.eaton.com/EatonCom/ProductsServices/PerformanceProducts/Products/Superchargers/TVS/index.htm [Accessed 25 January 2011].

[54] **Hori, M., Ikeya, N., Takabe, S.** and **Miyagi, Y.** Examinations of a Lysholm Compressor's performance and the engine performance supercharged by the Lysholm Compressor. In Sixth International Conference on *Turbocharging and Air Management Systems*, London, UK, 3-5 November 1998, paper C554/019/98, pp. 115-126 (Professional Engineering Publishing, London).

[55] **Joyce, M.J.** Jaguar's supercharged 6-cylinder engine. In Fifth International Conference on *Turbocharging and Turbochargers*, London, UK, 7-9 June 1994, paper C484/055/94, pp. 127-137 (Professional Engineering Publishing, London).

[56] **Stone, R.** *Introduction to Internal Combustion Engines*, 3rd ed., 1999 (Macmillan, Basingstoke).

[57] **Richter, H.** and **Hemmerlein, N.** Experiences with supercharging the Porsche 944 engine. In Fourth International Conference on *Turbocharging and Turbochargers*, London, UK, 22-24 May 1990, paper C405/057, pp. 283-287 (Professional Engineering Publishing, London).

[58] **Rotrex A/S.** *Performance Vehicles*, [online], 2011. Available from: http://www.rotrex.com/Home/OEM_Applications/Automotive/Supercars_and_Performance_Vehicles.aspx [Accessed 26 January 2011].

[59] **Tomita, T., Ikeya, N., Ishihara, D., Kondoh, N.** and **Ohkita, A.** Hybrid Charging System for Heavy Duty Diesel Engines. SAE paper 910419, 1991.

[60] **Volkswagen.** *TSI: Maximum power with minimum consumption*, [online], 2011. Available from: http://www.volkswagen.co.uk/technology/petrol/tsi [Accessed 28 January 2011].

[61] **Cantore, G., Mattarelli, E.** and **Fontanesi, S.** A New Concept of Supercharging Applied to High Speed DI Diesel Engines. SAE paper 2001-01-2485, 2001.

[62] **Mattarelli, E.** Comparison among different 2-Stage Supercharging systems for HSDI Diesel engines. In Ninth International Conference on *Engines and Vehicles*, Naples, Italy, 14-17 September 2009, paper 2009-24-0072 (Consiglio Nazionale delle Richerche, Naples).

[63] **Controlled Power Technologies Ltd.** *VTES: Giving the Environment a Boost*, [online], 2011. Available from: http://www.cpowert.com/products/vtes.htm [Accessed 1 February 2011].

[64] **Pallotti, P., Torella, E., New, J., Criddle, M.** and **Brown, J.** Application of an Electric Boosting System to a Small, Four-Cylinder S.I. Engine. SAE paper 2003-32-0039, 2003.

[65] **Katrašnik, T., Rodman, S., Trenc, T., Hribernik, A.** and **Medica, V.** Improvement of the Dynamic Characteristic of an Automotive Engine by a Turbocharger Assisted by an Electric Motor. *Transactions of the ASME, Journal of Engineering for Gas Turbines and Power*, 2003, **125**(2), 590-595.

[66] **Panting, J., Pullen, K.R.** and **Martinez-Botas, R.F.** Turbocharger motor–generator for improvement of transient performance in an internal combustion engine. *Proceedings of the Institution of Mechanical Engineers, Part D: Journal of Automobile Engineering*, 2001, **215**(3), 369-383.

[67] **Fieweger, K., Paffrath, H.** and **Schorn, N.** Drivability assessment of an HSDI Diesel engine with electrically assisted boosting systems. In Seventh International Conference on *Turbochargers and Turbocharging*, London, UK, 14-15 May 2002, paper C602/009/2002, pp. 283-293 (Professional Engineering Publishing, London).

[68] **Brockbank, C.** Application of a Variable Drive to Supercharger & Turbo Compounder Applications. SAE paper 2009-01-1465.

[69] **VanDyne, E., Brinks, B.T., Riley, M.B.** and **Brown, J.W.** *Super-Turbocharger Having a High Speed Traction Drive and a Continuously Variable Transmission*. US patent application US 2010/01999666 A1, 12 August 2010.

[70] **Wallace, F.J.** Operating characteristics of compound engine schemes for traction purposes based on opposed piston two-stroke engines and differential gearing. *Proceedings of the Institution of Mechanical Engineers*, 1963, **177**(2), 64-85.

[71] **Wallace, F.J., Tarabad, M.** and **Howard, D.** The differential compound engine – a new integrated engine transmission system concept for heavy vehicles. *Proceedings of the Institution of Mechanical Engineers, Part A: Power and Process Engineering*, 1983, **197**, 209-218.

[72] **Wallace, F.J.** On-road performance of two alternative engine transmission systems for heavy vehicles. In Fourth International Conference on *Turbocharging and Turbochargers*, London, UK, 22-24 May 1990, paper C405/038, pp. 99-112 (Professional Engineering Publishing, London).

[73] **Patterson, A.T.C., Tett, R.J.** and **McGuire, J.** Exhaust Heat Recovery using Electro-Turbogenerators. SAE paper 2009-01-1604, 2009.

[74] **Cummins Turbo Technologies.** *Turbocompound System* [online], 2011. Available from: http://www.holset.co.uk/mainsite/files/2_5_1_3-turbocompound%20system.php [Accessed 8 February 2011].

[75] **Walsham, B.E.** Alternative turbocharger systems for the automotive diesel engine. In Fourth International Conference on *Turbocharging and Turbochargers*, London, UK, 22-24 May 1990, paper C405/036, pp. 39-50 (Professional Engineering Publishing, London).

[76] **Wallace, F.J.** The ultimate performance potential of compounded diesel engines for heavy vehicles. In Sixth International Conference on *Turbocharging and Air Management Systems*, London, UK, 3-5 November 1998, paper C554/015/98, pp. 253-268 (Professional Engineering Publishing, London).

[77] **Hopmann, U.** and **Algrain, M.C.** Diesel Engine Electric Turbo Compound Technology. SAE paper 2003-01-2294, 2003.

[78] **Millo, F., Mallamo, F., Pautasso, E.** and **Ganio Mego, G.** The Potential of Electric Exhaust Gas Turbocharging for HD Diesel Engines. SAE paper 2006-01-0437, 2006.

[79] **Hountalas, D.T., Katsanos, C.O.** and **Lamaris, V.T.** Recovering Energy from the Diesel Engine Exhaust Using Mechanical and Electrical Turbocompounding. SAE paper 2007-01-1563, 2007.

[80] **Aeristech Ltd.** *Aeristech: Breakthrough Technology*, [online], 2010. Available from: http://www.aeristech.co.uk/news/test-news3 [Accessed 1 February 2011].

[81] **Odaka, M., Koike, N., Hijikata, Y.** and **Miyajima, T.** Energy Regeneration of Heavy Duty Diesel Powered Vehicles. SAE paper 980891, 1998.

[82] **Hussain, Q.E., Brigham, D.R.** and **Maranville, C.W.** Thermoelectric Exhaust Heat Recovery for Hybrid Vehicles. SAE paper 2009-01-1327, 2009.

[83] **Arias, D.A., Shedd, T.A.** and **Jester, R.K.** Theoretical Analysis of Waste Heat Recovery from an Internal Combustion Engine in a Hybrid Vehicle. SAE paper 2006-01-1605, 2006.

[84] **Teng, H., Regner, G.** and **Cowland, C.** Achieving High Engine Efficiency for Heavy-Duty Diesel Engines by Waste Heat Recovery Using Supercritical Organic-Fluid Rankine Cycle. SAE paper 2006-01-3522, 2006.

[85] **Ringler, J., Seifert, M., Guyotot, V.** and **Hübner, W.** Rankine Cycle for Waste Heat Recovery of IC Engines. SAE paper 2009-01-0174, 2009.

[86] **Teng, H., Regner, G.** and **Cowland, C.** Waste Heat Recovery of Heavy-Duty Diesel Engines by Organic Rankine Cycle Part I: Hybrid Energy System of Diesel and Rankine Engines. SAE paper 2007-01-0537, 2007.

[87] **Endo, T., Kawajiri, S., Kojima, Y., Takahashi, K., Baba, T., Ibaraki, S., Takahashi, T.** and **Shinohara, M.** Study on Maximizing Exergy in Automotive Engines. SAE paper, 2007-01-0257, 2007.

[88] **Akehurst, S.** and **Piddock, M.** A Multiple Factor Simulation and Emulation Approach to Investigate Advanced Air Handling Systems for Future Diesel Engines. SAE paper 2008-01-0297, 2008.

[89] **Ricardo Software.** *Ricardo WAVE 7.2 – Engine Manual*, 2006.

[90] **The Mathworks, Inc.** *Model-Based Calibration Toolbox™ Model Browser User's Guide*. USA: The MathWorks, Inc, 2009.

[91] **Maiboom, A., Tauzia, X., Rahman Shah, S.** and **Hétet, J.** Experimental Study of an LP EGR System on an Automotive Diesel Engine, compared to HP EGR with respect to PM and NOx Emissions and Specific Fuel Consumption. In Ninth International Conference on *Engines and Vehicles*, Naples, Italy, 14-17 September 2009, paper 2009-24-0138 (Consiglio Nazionale delle Richerche, Naples).

[92] **Beatrice, C., Bertoli, C., Del Giacomo, N.** and **Guido, C.** Experimental Investigation of the Benefits of Cooled and Extra-cooled Low-Pressure EGR on a Light Duty Diesel Engine Performance. In Ninth International Conference on *Engines and Vehicles*, Naples, Italy, 14-17 September 2009, paper 2009-24-0126 (Consiglio Nazionale delle Richerche, Naples).

[93] **Akehurst, S., Parker, D. A.** and **Schaaf, S.** CVT Rolling Traction Drives – A Review of Research Into Their Design, Functionality, and Modelling. *Transactions of the ASME, Journal of Mechanical Design*, 2006, **128**(5), 1165-1176.

[94] **Akehurst, S., Brace, C.J., Vaughan, N.D., Milner, P.** and **Hosoi, Y.** Performance Investigations of a Novel Rolling Traction CVT. SAE paper 2001-01-0874, 2001.

[95] **Akehurst, S., Parker, D.A.** and **Schaaf, S.** Dynamic Modelling of the Milner Continuously Variable Transmission – The Basic Kinematics. *Transactions of the ASME, Journal of Mechanical Design*, 2007, **129**(11), 1170-1178.

[96] **Lee, A.P., Newall, J., Ono, Y.** and **Hoshino, T.** Developing the Durability of a Dual-Cavity Full-Toroidal IVT Variator. SAE paper 2002-01-0587, 2002.

[97] **Tanaka, H., Toyoda, N., Machida, H.** and **Imanishi, T.** Development of a 6 Power-Roller Half-Toroidal CVT – Mechanism and Efficiency. In *International Continuously Variable and Hybrid Transmission Congress*, California, 23-25 September 2004, paper 04CVT-36.

[98] **Akehurst, S.** Investigating the loss mechanisms associated with a pushing metal V-belt CVT. PhD thesis, University of Bath, Bath, 2001.

[99] **Akehurst, S.**, **Moyers, J.**, **Hunt, A.** and **Schaaf, S**. Development of a design tool for modelling and optimisation of the Milner CVT. In JSME International Conference on *Motion and Power Transmission*, Japan, 13-15 May 2009.

[100] **Akehurst, S.** Optimizing the Design of a Milner CVT Using Simulation Based Design of Experiments. In *SAE 2009 World Congress*, Detroit, Michigan, 20-23 April 2009.

[101] **Carey, C., McAllister, M., Sandford, M., Richardson, S., Pierson, S., Darnton, N., Bredda, S., Akehurst, S., Brace, C., Turner, J., Pearson, R., Luard, N., Martinez-Botas, R., Copeland, C., Lewis, M.** and **Fernandes, J.** Extreme engine downsizing. In International Conference on *Innovations in Fuel Economy and Sustainable Road Transport*, Pune, India, 8-9 November 2011 (Professional Engineering Publishing, London).

[102] **Copeland, C., Martinez-Botas, R., Turner, J., Pearson, R., Luard, N., Carey, C., Richardson, S., Di Martino, P.** and **Chobola, P.** Boost System Selection for a Heavily Downsized Spark Ignition Prototype Engine. In Tenth International Conference on *Turbochargers and Turbocharging*, London, UK, 15-16 May 2012 (Professional Engineering Publishing, London).

[103] **Salamon, C., McAllister, M., Robinson, R., Richardson, S., Martinez-Botas, R., Romagnoli, A., Copeland, C.** and **Turner, J.** Improving fuel economy by 35% through combined turbo and supercharging on a spark ignition engine. In *21st Aachen Colloquium on Automobile and Engine Technology*, Aachen, Germany, 8-10 October 2012 (Institute for Automotive Engineering, Aachen).

[104] **Gamma Technologies Inc.** *GT-POWER Engine Simulation Software* [online], 2012. Available from: http://www.gtisoft.com/applications/a_Engine_Performance.php [Accessed 13 December 2012].

[105] **Pickering, S.G.** and **Brace, C.J.** Automated data processing and metric generation for driveability analysis. *Proceedings of the Institution of Mechanical Engineers, Part D: Journal of Automobile Engineering*, 2007, **221**(4), 429-441.

[106] **List, H.O.** and **Schoeggl, P.** Objective Evaluation of Vehicle Driveability. SAE paper 980204, 1998.

[107] **Dorey, R.E.** and **Holmes, C.B.** Vehicle Driveability - Its Characterisation and Measurement. SAE paper 1999-01-0949, 1999.

[108] **Wicke, V., Brace, C.J.** and **Vaughan, N.D.** The Potential for Simulation of Driveability of CVT Vehicles. SAE paper 2000-01-0830, 2000.

[109] **Dorey, R.E.** and **Martin, E.J.** Vehicle Driveability - The Development of an Objective Methodology. SAE paper 2000-01-1326, 2000.

Appendix 1: Journal Paper based on Chapter 3

Rose, A.T.J.M., Akehurst, S. and **Brace, C.J.** Modelling the performance of a continuously variable supercharger drive system. *Proceedings of the Institution of Mechanical Engineers, Part D: Journal of Automobile Engineering*, 2011, **225**(10), 1399-1414.

Appendix 2: Journal Paper based on Chapters 4 & 5

Rose, A.T.J.M., Akehurst, S. and **Brace, C.J.** Investigation into the trade-off between the part-load fuel efficiency and the transient response for a highly boosted downsized gasoline engine with a supercharger driven through a continuously variable transmission. *Proceedings of the Institution of Mechanical Engineers, Part D: Journal of Automobile Engineering*, 2013, **227**(12), 1674-1686.